GENERAL ANESTHESIA: FROM THEORY TO EXPERIMENTS

EDITED BY: Axel Hutt and Anthony G. Hudetz

PUBLISHED IN: Frontiers in Systems Neuroscience

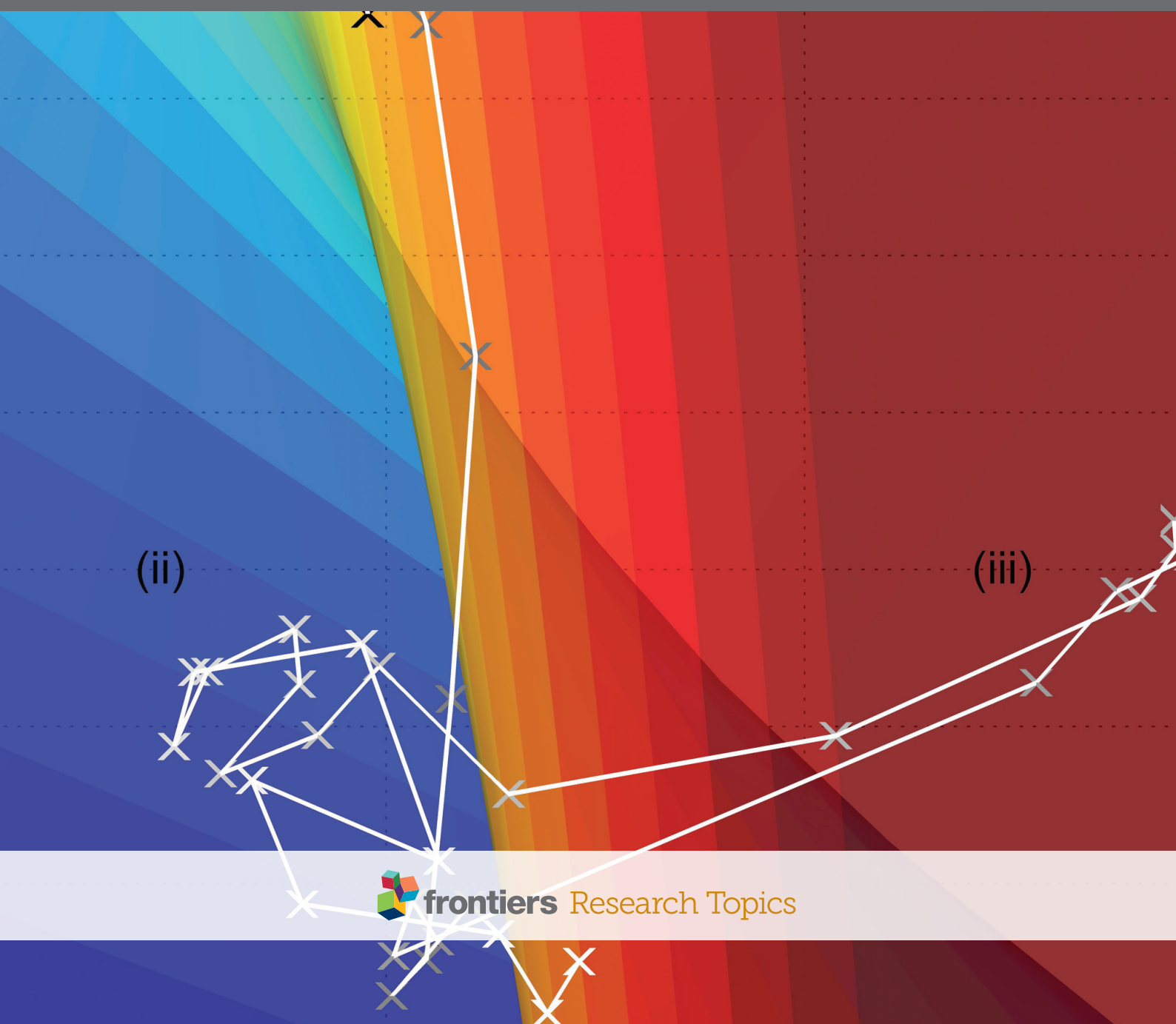

frontiers Research Topics

frontiers

ISSN 1664-8714
ISBN 978-2-88919-749-1
DOI 10.3389/978-2-88919-749-1

About Frontiers

Frontiers is more than just an open-access publisher of scholarly articles: it is a pioneering approach to the world of academia, radically improving the way scholarly research is managed. The grand vision of Frontiers is a world where all people have an equal opportunity to seek, share and generate knowledge. Frontiers provides immediate and permanent online open access to all its publications, but this alone is not enough to realize our grand goals.

Frontiers Journal Series

The Frontiers Journal Series is a multi-tier and interdisciplinary set of open-access, online journals, promising a paradigm shift from the current review, selection and dissemination processes in academic publishing. All Frontiers journals are driven by researchers for researchers; therefore, they constitute a service to the scholarly community. At the same time, the Frontiers Journal Series operates on a revolutionary invention, the tiered publishing system, initially addressing specific communities of scholars, and gradually climbing up to broader public understanding, thus serving the interests of the lay society, too.

Dedication to Quality

Each Frontiers article is a landmark of the highest quality, thanks to genuinely collaborative interactions between authors and review editors, who include some of the world's best academicians. Research must be certified by peers before entering a stream of knowledge that may eventually reach the public - and shape society; therefore, Frontiers only applies the most rigorous and unbiased reviews.

Frontiers revolutionizes research publishing by freely delivering the most outstanding research, evaluated with no bias from both the academic and social point of view.

By applying the most advanced information technologies, Frontiers is catapulting scholarly publishing into a new generation.

What are Frontiers Research Topics?

Frontiers Research Topics are very popular trademarks of the Frontiers Journals Series: they are collections of at least ten articles, all centered on a particular subject. With their unique mix of varied contributions from Original Research to Review Articles, Frontiers Research Topics unify the most influential researchers, the latest key findings and historical advances in a hot research area! Find out more on how to host your own Frontiers Research Topic or contribute to one as an author by contacting the Frontiers Editorial Office: **researchtopics@frontiersin.org**

GENERAL ANESTHESIA: FROM THEORY TO EXPERIMENTS

Topic Editors:
Axel Hutt, Inria Nancy, France; CNRS, Loria, UMR no. 7503, France; Univeristy of Lorraine, UMR no. 7503, France
Anthony G. Hudetz, University of Michigan, USA

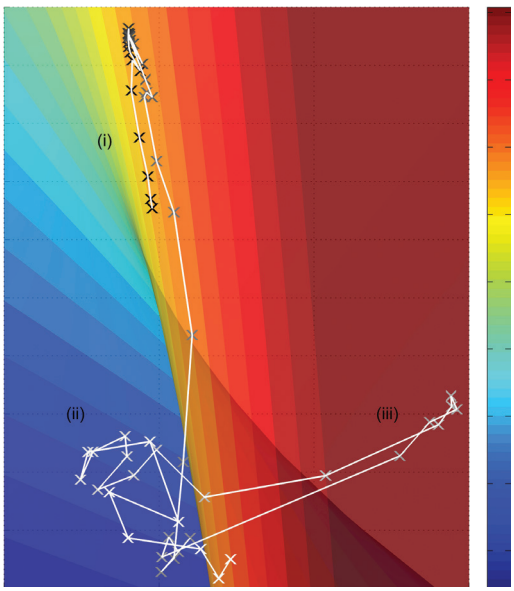

Projection of experimental EEG data onto model phase plane illustrating the emergence from unconsciousness to consciousness. Taken from Hight et al., Front. Syst. Neurosci. 8 : 148 (2015).

General anesthesia is a standard medical procedure in todays' hospital practice. Although in most cases the administration of anesthetics does not affect severely the patients health, side effects of anesthesia are well-known, such as nausea or cognitive impairment. Moreover 1-2 out of 1000 patients under surgery report a partial wake up from anesthesia during the operation. The reason for such a partial lack of control of depth of anesthesia is that medical procedures are highly optimized based on experience but the neural dynamics during general anesthesia is far from being understood. One reason for this lack of understanding is both the complex neural interactions of neurons on different spatial and temporal scales and the poorly understood action of anesthetics on neural populations. For instance, anesthetic agents act on synaptic receptors on a microscopic scale essentially evoking a macroscopic change of population activity, such as Local Field Potentials, EEG/MEG or resulting change of cerebral blood flow. This population effect then triggers the loss of consciousness in patients.

This Research Topic aims to address recent theoretical and experimental advances in the field. The theoretical and experimental studies represent a good overview over the current state of research in the field and provides a deeper insight into the underlying neural mechanisms. Each article in the issue focusses on a specific current research topic in general anesthesia research and several articles introduce to the topic in a pedagogical way. The issue covers various types of anaesthesia and the most important topics in the field, such as (but not limited to) recent advances in theoretical models and states of consciousness reflected in experimental data, the connectivity changes observed during anesthesia or effects of specific drugs on brain activity. The introduction style of the papers facilitates the reader to understand the background of the research aspect and even allows readers not familiar with general anesthesia research to enter the research domain. Hence the Research Topic aims to provide on one hand an overview of the current state of the art and on the other hand a good starting point for new researchers in the field.

Citation: Hutt, A., Hudetz, A. G., eds. (2016). General Anesthesia: From Theory to Experiments. Lausanne: Frontiers Media. doi: 10.3389/978-2-88919-749-1

Table of Contents

frontiers in Systems Neuroscience

EDITORIAL
published: 22 July 2015
doi: 10.3389/fnsys.2015.00105

Editorial: General anesthesia: from theory to experiments

Axel Hutt[1,2,3]* *and Anthony G. Hudetz*[4]

[1] Team Neurosys, INRIA, Villers-les-Nancy, France, [2] Team Neurosys, Centre National de la Recherche Scientifique, LORIA, UMR No. 7503, Villers-les-Nancy, France, [3] Team Neurosys, University of Lorraine, LORIA, UMR No. 7503, Villers-les-Nancy, France, [4] Department of Anesthesiology, Medical College of Wisconsin, Milwaukee, WI, USA

Keywords: consciousness, functional connectivity, coherence, EEG, fMRI, burst-suppression

General anesthesia is a standard and safe medical procedure performed in thousands of patients every day; therefore, it may come to many as a surprise that the ultimate neurobiological mechanisms responsible of the anesthetics' beneficial effect—that they suppress the patient's conscious awareness, is far from understood. One reason for this lack of understanding is that complex interactions of neurons occur on different spatial and temporal scales and the action of anesthetics on neural populations is poorly understood. Consequently, there is a need to bridge the knowledge of how anesthetic agents act on synaptic receptors on a microscopic scale to macroscopic changes in neuronal population activity as well as to higher order integrative processes that are more directly linked to the state of consciousness. The 10 contributions compiled in this research topic (ebook) intend to help solving this problem by exploring and adding to the current state of knowledge at various levels of brain complexity.

The first chapter by Mashour (2014) presents an authoritative review of the currently most influential theory of how chemically diverse general anesthetics on higher order processes may disrupt consciousness. The formerly favored "bottom-up" mechanisms of anesthetic action focusing on subcortical arousal centers and ascending thalamocortical information transfer are contrasted with the more recent cortical "top-down" explanations that are inherent to conscious perception and appear to be the preferential target of anesthetic modulation. Substantial electrophysiological and neuroimaging evidence from animal and human investigations supports the top-down mechanisms as a causally sufficient explanation for anesthetic-induced unconsciousness.

Raz et al. (2014) provides new support to this idea from their study of the effect of isoflurane on top-down vs. bottom-up neuronal pathways in rat auditory cortex during sensory and thalamic stimulation. By laminar recordings of local field potentials in the auditory cortex *in vivo*, they show that at hypnotic dose of isoflurane, bottom-up responses to auditory tone stimuli are enhanced, whereas top-down responses to visual flash stimuli are reduced. Consistent results were obtained in rodent brain slices, where cross-modal cortico-cortical descending pathways were suppressed far greater than specific thalamo-cortical afferents, supporting the preferential disruption of top-down connectivity at an anesthetic concentration associated with unconsciousness.

In the next chapter, Blain-Moraes et al. (2014) moves this idea to humans by demonstrating in surgical patients that anesthetic-invariant electroencephalographic effects occur in cortical top-down connectivity. Specifically, ketamine, a primarily non-GABAergic anesthetic drug, is found to suppress fronto-parietal functional and directional connectivity (measured by coherence and phase lag index), similar to that produced by propofol, a primarily GABAergic drug. Unlike propofol however, ketamine fails to augment frontal alpha power and coherence. The measured connectivity changes in the alpha band are therefore consistent markers of unconsciousness induced by both GABAergic and non-GABAergic anesthetics.

Moving on to deeper anesthetic levels, Kenny et al. (2014) explore anesthetic agent-dependent effects on burst-suppression patterns in rats. Burst suppression is a stereotypic pattern of

OPEN ACCESS

Edited and reviewed by:
Maria V. Sanchez-Vives, ICREA-IDIBAPS, Spain

***Correspondence:**
Axel Hutt, axel.hutt@inria.fr

Received: *24 April 2015*
Accepted: *10 July 2015*
Published: *22 July 2015*

Citation:
Hutt A and Hudetz AG (2015) Editorial: General anesthesia: from theory to experiments. Front. Syst. Neurosci. 9:105. doi: 10.3389/fnsys.2015.00105

alternating periods of electroencephalographic activity and inactivity that occurs in pathological states and in deep anesthesia, well beyond the threshold for loss of consciousness. After reviewing the presumed mechanism of generation, methods of quantification, and clinical application of burst-suppression, the authors demonstrate significant differences in the duration, amplitude, and power of burst-suppression patterns induced by two common general anesthetics, sevoflurane, and propofol suggesting that the neuronal circuits involved in burst-suppression generation may differ among different anesthetics.

By virtue of the similarity of anesthetic-induced loss of consciousness to the one experienced in sleep, anesthetic, and sleep research typically borrow analysis methods and neural processing concepts from each other. MacIver and Bland (2014) have compared frontal cortical and hippocampal micro-EEG signals under isoflurane anesthesia and during sleep by a chaos analysis. The shape of chaotic attractors of cortical frontal micro-EEG flattens in the anesthetic state compared to the awake state. In addition, delta-activity under isoflurane anesthesia exhibits a different chaotic attractor shape than NREM-sleep frontal EEG. The chaotic analysis demonstrates the power of nonlinear analysis methods revealing signal features beyond the frequency content.

In addition to the analysis of experimental data, theoretical models might provide deeper insight into the underlying neural mechanisms during general anesthesia. Hight et al. (2014) have modeled experimental EEG data obtained in individual human subjects during emergence from anesthesia to wakefulness by a neurophysiological model. This projection allows one to visualize the signal evolution in time and indicates differences between subjects. The study reveals an archetypical emergence pattern and non-archetypical evolution patterns which are all different from the archetypical emergence patterns. In addition to this classification, for all patients, a general neuronal hyperpolarization (increased resting membrane conductivity and reduced excitatory connection strength) appears to precede the return to consciousness.

The work by Hudetz et al. (2014) focuses on large-scale mechanisms combining human fMRI data and computer simulation to explore the diversity of brain connectivity patterns as a determinant of the state of consciousness. Implementing a spin-glass model with site interactions probabilistically defined by long-range functional connectivity, they predict the formation of metastable brain states whose repertoire is a function of cortical activation. The state repertoire is maximal at an optimal activation level corresponding to the conscious state. It is diminished in anesthesia (low activation) and seizure (high activation) suggesting a common mechanism for unconsciousness through a reduction of the brain's state repertoire.

To understand brain network interactions before and after loss of consciousness, the study of phase coherence provides valuable insights. Wang et al. (2014) have combined a detailed phase coherence study of experimental scalp EEG in the sub-delta frequency range with a theoretical model study. They have revealed a drop of phase coherence between electrode pairs in frontal, occipital, and fronto-occipital pairs. Conversely, the authors have revealed increased phase coherence between temporal and frontal, temporal, and occipital regions and temporal regions on left and right side. Theoretical model results confirm these findings and indicate a compensatory mechanism of sub-delta activity between a fronto-occipital and temporal region subsystem.

Anesthetic agents are known to affect various neural receptor types. They modify neural functions and inter-neuron interactions on the microscopic scale, consequently neural populations and eventually macroscopic electromagnetic activity, such as EEG/MEG/fMRI, and the behavior of subjects. To understand this bridge over multiple scales, Hashemi et al. (2014) have worked out a theoretical thalamo-cortical model demonstrating how GABAergic extra-synaptic receptors on a microscopic scale affect EEG on the macroscopic scale under propofol anesthesia. It turns out that cortical and thalamic anesthetic action on GABAergic extra-synaptic receptors contribute to the generation of delta-activity pointing out their importance.

In addition to action on extra-synaptic receptors, some anesthetics are known to desensitize synaptic receptors and may deplete synaptic vesicles. Bojak et al. (2014) hypothesize that these anesthetic actions contribute primarily to burst suppression. In a theoretical spatially extended cortical model assuming isoflurane action, they reveal spatially heterogeneous burst suppression patterns propagating in the cortex. This work provides an additional possible mechanism for burst suppression.

References

Blain-Moraes, S., Lee, U., Ku, S., Noh, G., and Mashour, G. A. (2014). Electroencephalographic effects of ketamine on power, cross-frequency coupling, and connectivity in the alpha bandwidth. *Front. Syst. Neurosci.* 8:114. doi: 10.3389/fnsys.2014.00114

Bojak, I., Stoyanov, Z. V., and Liley, D. (2014). Emergence of spatially heterogeneous burst suppression in a neural field model of electrocortical activity. *Front. Syst. Neurosci.* 9:18. doi: 10.3389/fnsys.2015.00018

Hashemi, M., Hutt, A., and Sleigh, J. W. (2014). Anesthetic action on extra-synaptic receptors: effects in neural population models of EEG activity. *Front. Syst. Neurosci.* 8:232. doi: 10.3389/fnsys.2014.00232

Hight, D. F., Dadok, V. M., Szeri, A. J., Garcia, P. S., Voss, L., and Sleigh, J. W. (2014). Emergence from general anesthesia and the sleep-manifold. *Front. Syst. Neurosci.* 8:148. doi: 10.3389/fnsys.2014.00148

Hudetz, A. G., Humphries, C. J., and Binder, J. R. (2014). Spin-glass model predicts metastable brain states that diminish in anesthesia. *Front. Syst. Neurosci.* 8:234. doi: 10.3389/fnsys.2014.00234

Kenny, J. D., Westover, M. B., Ching, S., Brown, E. N., and Solt, K. (2014). Propofol and sevoflurane induce distinct burst suppression patterns in rats. *Front. Syst. Neurosci.* 8:237. doi: 10.3389/fnsys.2014.00237

MacIver, B., and Bland, B. H. (2014). Chaos analysis of EEG during isoflurane-induced loss of righting in rats. *Front. Syst. Neurosci.* 8:203. doi: 10.3389/fnsys.2014.00203

Mashour, G. A. (2014). Top-down mechanisms of anesthetic-induced unconsciousness. *Front. Syst. Neurosci.* 8:115. doi: 10.3389/fnsys.2014.00115

Raz, A., Grady, S. M., Krause, B. M., Uhlrich, D. J., Manning, K. A., and Banks, M. I. (2014). Preferential effect of isoflurane on top-down vs. bottom-up pathways in sensory cortex. *Front. Syst. Neurosci.* 8:191. doi: 10.3389/fnsys.2014.00191

Wang, K., Steyn-Ross, M. L., Steyn-Ross, D. A., Wilson, M. T., and Sleigh, J. W. (2014). EEG slow-wave coherence changes in propofol-induced general anesthesia: experiment and theory. *Front. Syst. Neurosci.* 8:215. doi: 10.3389/fnsys.2014.00215

Conflict of Interest Statement: The authors declare that the research was conducted in the absence of any commercial or financial relationships that could be construed as a potential conflict of interest.

frontiers in
SYSTEMS NEUROSCIENCE

REVIEW ARTICLE
published: 23 June 2014
doi: 10.3389/fnsys.2014.00115

Top-down mechanisms of anesthetic-induced unconsciousness

George A. Mashour*

Neuroscience Graduate Program, Department of Anesthesiology, Center for Consciousness Science, University of Michigan Medical School, Ann Arbor, MI, USA

Edited by:
Anthony G. Hudetz, Medical College of Wisconsin, USA

Reviewed by:
Preston E. Garraghty, Indiana University, USA
Jamie Sleigh, University of Auckland, New Zealand

****Correspondence:***
George A. Mashour, Neuroscience Graduate Program, Department of Anesthesiology, Center for Consciousness Science, University of Michigan Medical School, 1500 East Medical Center Drive, 1H247 University Hospital/SPC-5048, Ann Arbor, MI 48109-5048, USA
e-mail: gmashour@umich.edu

The question of how structurally and pharmacologically diverse general anesthetics disrupt consciousness has persisted since the nineteenth century. There has traditionally been a significant focus on "bottom-up" mechanisms of anesthetic action, in terms of sensory processing, arousal systems, and structural scales. However, recent evidence suggests that the neural mechanisms of anesthetic-induced unconsciousness may involve a "top-down" process, which parallels current perspectives on the neurobiology of conscious experience itself. This article considers various arguments for top-down mechanisms of anesthetic-induced unconsciousness, with a focus on sensory processing and sleep-wake networks. Furthermore, recent theoretical work is discussed to highlight the possibility that top-down explanations may be causally sufficient, even assuming critical bottom-up events.

Keywords: consciousness, anesthesia, anesthetic mechanisms, ketamine, propofol, sleep

INTRODUCTION AND TERMINOLOGY

The mechanism by which structurally and pharmacologically diverse general anesthetics can render an individual unconscious has remained incompletely understood since 1846. One of the current controversies in the systems neuroscience approach to this question relates to the primacy of top-down vs. bottom-up mechanisms of anesthetic-induced unconsciousness. In the context of this article, the term "bottom-up" has three different meanings, which will always be explicit. The first meaning of "bottom-up" relates to a neurocognitive hierarchy of *sensory processing*, which might be best illustrated by considering the neural processing involved in visual consciousness. After retinal stimulation, visual information is transmitted to the lateral geniculate nucleus in the thalamus followed by transmission to the primary visual cortex (V1) in the occipital lobe. Visual processing thereafter follows two "streams" that flow dorsally to the prefrontal cortex and ventrally to the temporal lobe. Thus, visual information is received by peripheral sensors and transmitted in a bottom-up way to the thalamus, primary sensory cortex, higher modal processing areas, and multimodal association cortex. The second meaning of "bottom-up" relates to *arousal pathways*. From the pons to the midbrain to diencephalic structures such as the hypothalamus, a variety of subcortical nuclei project to and arouse the cortex through the actions of distinct neurotransmitters. This represents a bottom-up pathway from subcortical wake-promoting nuclei to the cortex, sometimes with a synaptic relay in the thalamus. The third meaning of "bottom-up" relates to processes that occur from smaller to larger structural scales, e.g., from the molecular, to the cellular, to the neuroanatomical, to the network level of the brain. These three meanings of "bottom-up"—referring to *sensory*, *arousal*, and *structural* hierarchies—all have relevance to understanding the mechanism of anesthetic-induced unconsciousness.

In the context of this article, the term "anesthetic-induced unconsciousness" refers to an unconscious cognitive state that is just below the threshold of normal conscious perception of the environment, with the further stipulation that the subject is not being exposed to a noxious stimulus (e.g., surgery). As an example, consider a human volunteer receiving an infusion of the intravenous anesthetic propofol that is titrated to higher concentrations until she can no longer follow verbal commands—this loss of responsiveness would be used as the (admittedly imperfect) surrogate of anesthetic-induced unconsciousness. It should be noted clearly that anesthetic-induced unconsciousness is not equivalent to surgical anesthesia, because a noxious stimulus such as a scalpel cutting through skin could easily reverse the unconscious state in our hypothetical volunteer. Anesthetic-induced unconsciousness may not be sufficient for surgical intervention and is therefore not necessarily equivalent to our clinical conception of general anesthesia.

WHY BOTTOM-UP FRAMEWORKS OF ANESTHETIC-INDUCED UNCONSCIOUSNESS HAVE BEEN DOMINANT

There are several reasons why bottom-up approaches to anesthetic-induced unconsciousness have dominated the field. With respect to the sensory or arousal hierarchy, consciousness has often been deconstructed into wakefulness (an active cortex, open eyes) and awareness (subjective experience). Our understanding of wakefulness and brain arousal as mediated by subcortical structures like the ascending reticular activating

system dates back some 65 years to the work of Moruzzi and Magoun (1949). Similarly, the association of consciousness with processing at the level of the primary sensory cortex remained dominant until some 20 years ago when Crick and Koch formally questioned whether visual consciousness was correlated with activity in V1 (Crick and Koch, 1995). For more than a decade, the "thalamic switch" hypothesis of anesthetic-induced unconsciousness—which is characterized by the blockade of sensory information from thalamus to primary sensory cortex—has been highly influential (Alkire et al., 2000). Thus, the long-standing viewpoint of consciousness and anesthesia as linked to subcortical arousal and primary sensory processes is significantly more entrenched than the relatively recent perspective of consciousness as a higher-order experiential process generated by network communication across association cortices. With respect to structural scales, there is a general scientific tendency to think of the term "mechanism" as a bottom-up process in which actions at the molecular or "micro" level lead to causal events that result in changes at the "macro" level. From this perspective, macro-level explanations merely supervene on micro-level explanations (Hoel et al., 2013). This is also true in the history of research into anesthetic-induced unconsciousness. Since 1847, there have been a series of micro-level approaches to anesthetic mechanism, including effects on lipids (1847 through the mid-1980s; for review of early theories see Perouansky, 2012) and proteins (mid-1980s until the present; Franks and Lieb, 1984). Thus, the targets of general anesthetics have traditionally been molecular, the foundational level of a bottom-up structural hierarchy.

The 1990s was an important era in anesthetic mechanisms research for four reasons. First, it became clear that there was a neuroanatomical segregation of the major therapeutic endpoints of general anesthesia, with immobility mediated in the spinal cord vs. unconsciousness and amnesia mediated in the brain (Antognini and Schwartz, 1993; Rampil, 1994). Second, the first neuroimaging studies of general anesthesia were conducted, pointing to regional differences in anesthetic action rather than global brain suppression (Alkire et al., 1995). Third, specific anesthetic binding sites on neurotransmitter receptors (most notably, the gamma-aminobutyric acid [GABA] receptor) were identified (Mihic et al., 1997). Fourth, it was first suggested that general anesthetics might suppress consciousness through actions on the subcortical nuclei that evolved to control sleep-wake states (Lydic and Biebuyck, 1994), a decidedly systems neuroscience approach. At least two of these developments—effects of anesthetics on neurotransmitter receptors and sleep-wake nuclei—are explicitly bottom-up approaches to anesthetic mechanisms. The focus on the molecular mediators of anesthetic action represents a bottom-up explanation from the perspective of structural scales and the "shared circuits" hypothesis of sleep and anesthesia represents a bottom-up explanation in terms of arousal systems. Both have received considerable attention and enjoy significant empirical support. The goal of the present article is not to argue that anesthetics have no effects on molecular targets or subcortical structures such as sleep-wake nuclei, but rather to counterbalance the tendency to think of anesthetic mechanisms as a fundamentally or exclusively bottom-up process. There are now several compelling lines of evidence to suggest that consciousness and anesthetic-induced unconsciousness in humans are higher-order processes and that, in principle, macro-level mechanisms can be causally sufficient to explain such emergent phenomena.

ARGUMENTS SUPPORTING TOP-DOWN MECHANISMS OF ANESTHETIC-INDUCED UNCONSCIOUSNESS

CONSCIOUSNESS AND ANESTHETIC-INDUCED UNCONSCIOUSNESS ARE ASSOCIATED WITH MULTIMODAL ASSOCIATION CORTEX RATHER THAN PRIMARY SENSORY CORTEX

A reasonable approach to understanding the mechanism of anesthetic-induced unconsciousness would be to consider the neurobiological underpinnings of conscious experience itself. As noted, consciousness is sometimes reduced to the dissociable processes of wakefulness and awareness. Importantly, wakefulness is neither sufficient nor even necessary for conscious experience. Dreaming is an example of how consciousness can occur in the absence of wakefulness (demonstrating a lack of necessity) and the vegetative state is an example of a presumably unconscious state despite evidence of wakefulness (demonstrating a lack of sufficiency) (Laureys, 2005). In terms of awareness, evidence is accumulating that conscious experience does not correlate with processing at the level of the primary sensory cortex. Numerous studies using contrastive analysis, in which a sensory stimulus is delivered at threshold and then brain activation patterns are "contrasted," suggest that primary sensory processing is not sufficient for conscious perception of a stimulus (for review see Dehaene and Changeux, 2011). Consciousness is, however, associated with widespread activation of multimodal cortical networks, including frontal, posterior parietal, and temporal areas (**Figure 1**). To summarize, neither arousal from subcortical structures nor activity of primary sensory cortex is sufficient for consciousness; processing in more distributed networks of association cortex appears to correlate best with conscious experience. It is also worth noting that many current and major theories of consciousness—including global neuronal workspace theory (Dehaene and Changeux, 2011), integrated information theory (Tononi, 2012), predictive coding (Clark, 2013), representationalism (Lau and Rosenthal, 2011)—consider some form of top-down or network-level process to be critical for consciousness.

Just because consciousness is associated with activation of more extended cortical networks does not necessitate that anesthetic-induced unconsciousness is as well. It is entirely possible that general anesthetics could block the transmission of information from the periphery, inhibit arousal centers, block thalamic relay of information to the primary sensory cortex, or disrupt primary sensory processing. However, neuroimaging data suggest that anesthetic-induced unconsciousness is associated with deactivation of more extended frontal-parietal networks, while primary sensory networks remain relatively intact (Boveroux et al., 2010; Bonhomme et al., 2012) (**Figure 2**). This is mirrored somewhat in the thalamus by preferential disruption of "non-specific" thalamic nuclei, which are thought to play more of an integrative role for cortical computation rather than a processing station for sensory information (Liu et al., 2013). Again, it is important to note that these findings may relate specifically to

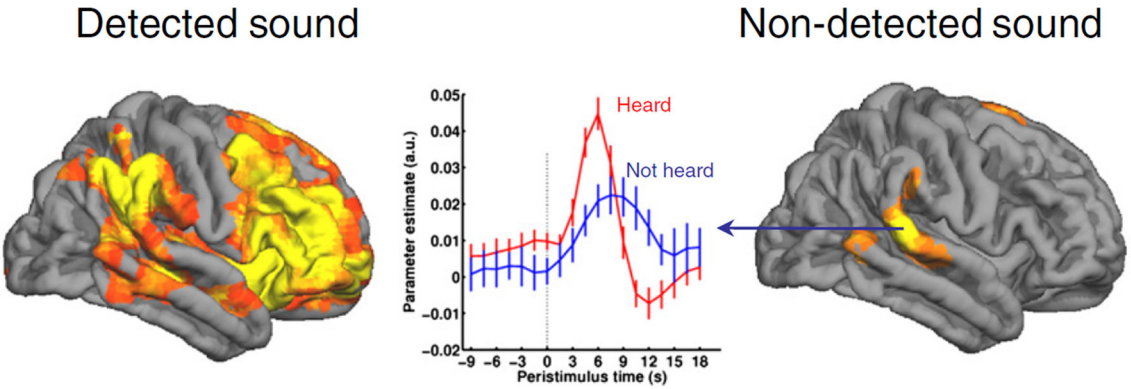

FIGURE 1 | Consciousness is not correlated with activation of primary sensory cortex. This example of contrastive analysis demonstrates activation of primary auditory cortex even in the absence of conscious perception. By contrast, detection of the auditory stimulus is correlated with activation of a widespread network prominently involving frontal-parietal networks. Reproduced from Dehaene and Changeux (2011), Neuron, with permission.

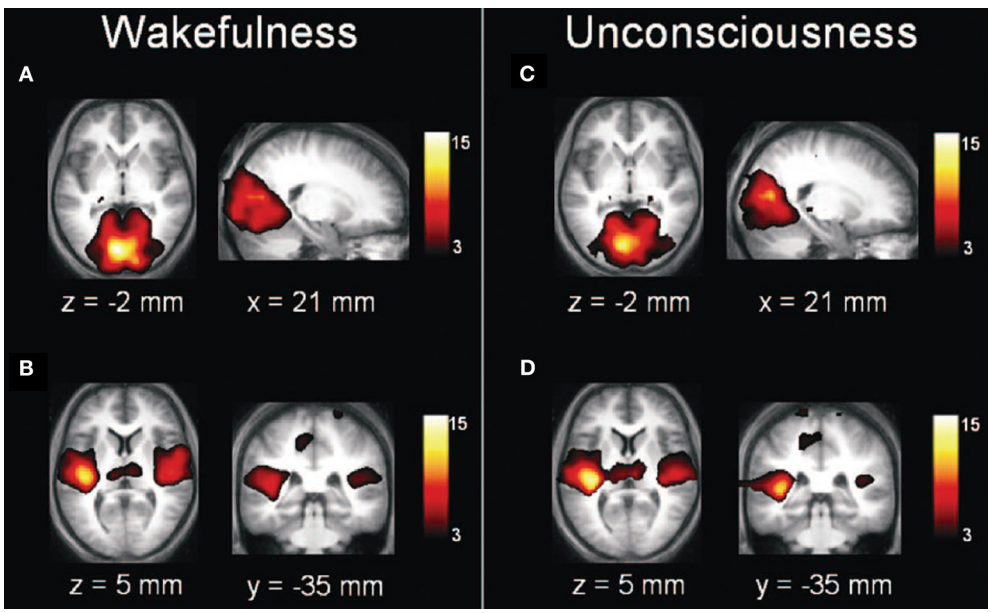

FIGURE 2 | Anesthetic-induced unconsciousness is not correlated with inactivation of primary sensory cortex. Transverse and sagittal sections of primary visual **(A,C)** and auditory **(B,D)** cortices during wakefulness **(A,B)** and propofol-induced unconsciousness **(C,D)**; note the relative preservation across states. Reproduced from Boveroux et al. (2010), Anesthesiology, with permission.

anesthetic-induced unconsciousness, the topic of interest, rather than surgical anesthesia. It is clear that higher concentrations of general anesthetics beyond those required for loss of responsiveness in a resting state can suppress primary sensory cortex (Ni Mhuircheartaigh et al., 2013) and at yet higher concentrations can cause more global suppression.

CONSCIOUSNESS AND ANESTHETIC-INDUCED UNCONSCIOUSNESS ARE ASSOCIATED WITH LATE EVOKED POTENTIALS RATHER THAN EARLY ONES

The neuroanatomical substrates of consciousness and anesthetic-induced unconsciousness give us a sense of the "where" of consciousness or anesthesia but also have implications for the "when" of consciousness or anesthesia. Studies using event-related potentials suggest that conscious experience is correlated with longer-latency potentials rather than early potentials (Del Cul et al., 2007) (**Figure 3**). Not surprisingly, evoked-potential data mirror the neuroanatomical structures of interest: early potentials reflect more primary processing, while later potentials reflect more integrative activity beyond the primary sensory cortex (e.g., V1) or higher-order modality-specific processing areas (e.g., V2 and beyond). Likewise, studies of anesthetic-induced unconsciousness have revealed that longer-latency visual evoked potentials are suppressed in a clear dose-dependent manner, while early potentials remain unperturbed (Hudetz et al., 2009) (**Figure 4**). These longer-latency potentials likely reflect, in

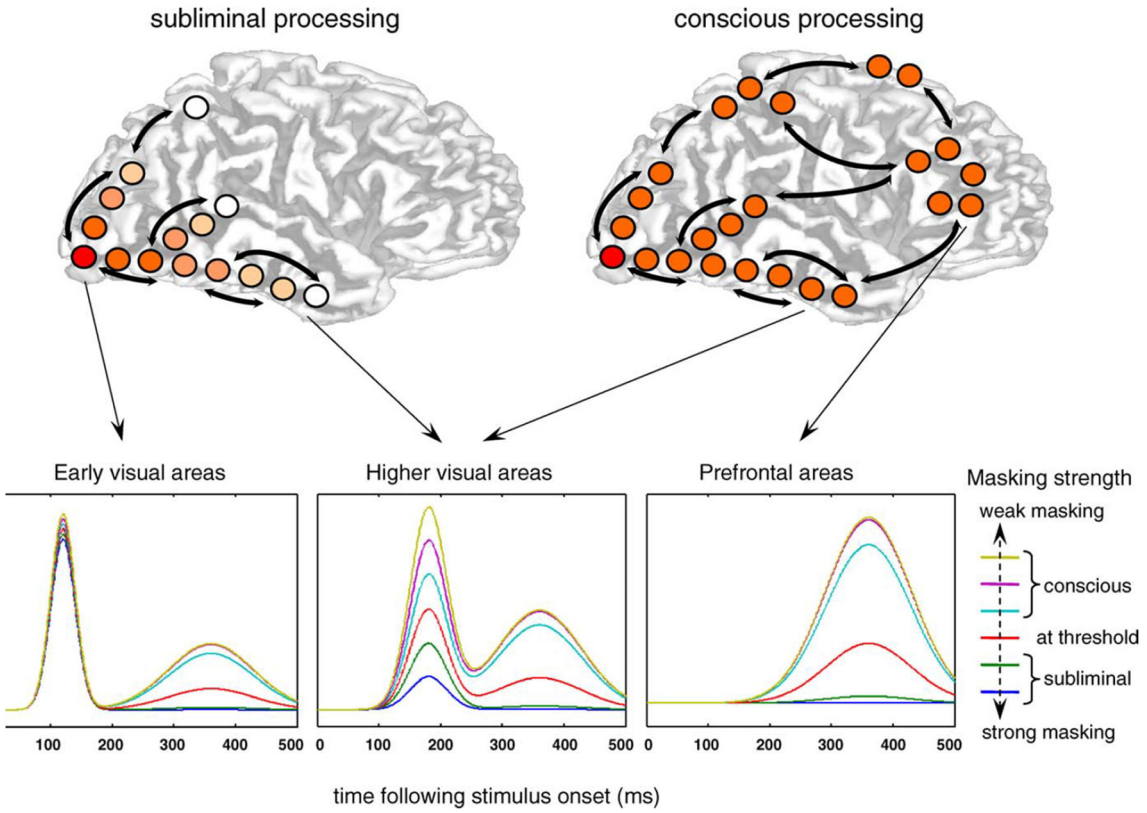

FIGURE 3 | Consciousness is not correlated with early event-related potentials. This electrophysiological study of visual processing concluded that early event-related potentials (reflecting more primary sensory processing) are not correlated with conscious perception. Top-down processing from prefrontal cortex was more closely associated with consciousness. Reproduced from Del Cul et al. (2007), PLoS Biology, with permission.

part, reentrant processing from anterior to posterior structures, which appear to be preferentially suppressed in association with anesthetic-induced unconsciousness in rats exposed to visual flash stimuli (Imas et al., 2005). It is difficult to see how anesthetics can act in a bottom-up manner in terms of a sensory hierarchy if visual information is still able to be transmitted through the thalamus to the primary cortex and forward through the dorsal stream, with only reentrant processing in the anterior-to-posterior (i.e., top-down) direction affected.

The observation that late cortical potentials are preferentially inhibited by general anesthetics is routine in the clinical practice of neuroanesthesiology, the subspecialty of anesthesiology that focuses on the perioperative care of neurosurgical patients. During both intracranial and spinal procedures, the use of sensory-evoked potentials to monitor neural function is common. In the case of somatosensory evoked potentials—reflecting a pathway from the peripheral stimulation source, to synapses in the medulla, thalamus, primary somatosensory cortex, and multimodal cortex—there is a clear dose-dependent reduction of amplitude and increase of latency. Importantly, late potentials are the first to be suppressed, while subcortically-derived and primary-sensory-related potentials are more robust (Banoub et al., 2003). The preferential susceptibility of late potentials to the effects of general anesthetics is especially evident when considering brainstem auditory evoked potentials. This complex, polysynaptic pathway of early auditory processing is virtually unperturbed by even supratherapeutic concentrations of anesthetics (Manninen et al., 1985). The sensitivity of late cortical potentials—reflecting processing beyond the sensory cortex—to the effects of anesthetics and the remarkable resilience of brainstem potentials make it difficult to argue that bottom-up sensory processes are being disabled, leading to dysfunction of higher-order systems.

ANESTHETIC-INDUCED UNCONSCIOUSNESS IS NOT DEPENDENT ON KEY SUBCORTICAL SLEEP-WAKE NUCLEI

A variety of anesthetics has been shown to metabolically activate sleep-promoting nuclei and metabolically inhibit wake-promoting nuclei. More recently, the inhaled anesthetic isoflurane has been shown to activate directly the sleep-promoting neurons within ventrolateral preoptic nucleus (VLPO), a key sleep-promoting region in the hypothalamus (Moore et al., 2012). It is remarkable that this general anesthetic—which typically depresses neuronal function—activates neurons that are specifically active during sleep. From the systems-neuroscience perspective, it is not difficult to conceive of how anesthetic-mediated unconsciousness could be a primarily bottom-up process from the perspective of arousal pathways. Sleep is well known to be generated by subcortical structures in the brainstem and diencephalon, with resultant changes in levels of cortical activity and

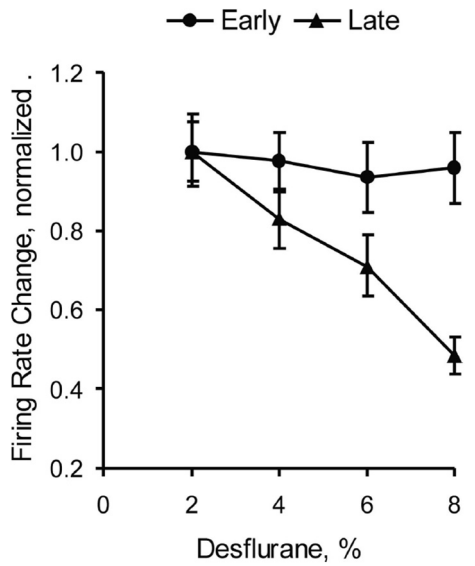

FIGURE 4 | Anesthetic-induced unconsciousness is not correlated with effects on early evoked potentials. This study of visual evoked potentials in rats demonstrates a clear dose-dependent effect of the inhaled anesthetic desflurane on long-latency potentials, with sparing of early potentials reflecting processing in primary visual cortex. Reproduced from Hudetz et al. (2009), Anesthesiology, with permission.

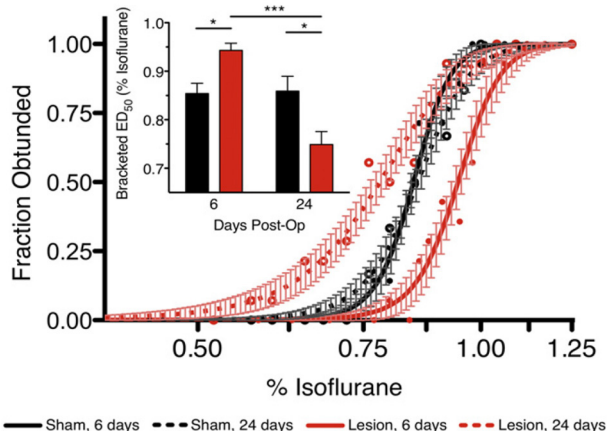

FIGURE 5 | Ventrolateral preoptic nucleus is not necessary for anesthetic-induced unconsciousness. Lesions of the ventrolateral preoptic nucleus reveal an acute effect of resistance but a chronic effect of hypersensitivity to the inhaled anesthetic isoflurane. Reproduced from Moore et al. (2012), Current Biology, with permission. $^{*}p < 0.05$; $^{***}p < 0.001$.

consciousness (Saper et al., 2005). If, indeed, there are shared circuits for sleep and anesthesia—as a number of studies would suggest—then it stands to reason that anesthetic-induced unconsciousness must follow a similar bottom-up path.

Although the shared-circuits hypothesis has shown promise, the evidence is far from conclusive. Both intravenous and inhaled anesthetics have been shown to metabolically activate VLPO (Nelson et al., 2002; Moore et al., 2012), which would suggest that VLPO is a key mediator of anesthetic-induced unconsciousness and would lead to the prediction that lesions of the VLPO would eliminate or attenuate the ability of an anesthetic to induce unconsciousness. However, lesions of the VLPO have only an acute effect in conferring partial resistance to inhaled anesthetics. Two studies have demonstrated that, with prolonged insomnia in the absence of a functioning VLPO, animals ultimately become hypersensitive to the effects of anesthetics (Eikermann et al., 2011; Moore et al., 2012) (**Figure 5**). VLPO is therefore neither sufficient nor necessary for anesthetic-induced unconsciousness. Furthermore, the anesthetic ketamine appears to suppress VLPO activation despite its hypnotic effects (Lu et al., 2008). Collectively, these data suggest that an activated VLPO does not play a critical role in anesthetic-induced unconsciousness.

An alternative bottom-up mechanism of anesthetic-induced unconsciousness that could be mediated through sleep-wake circuitry is the inhibition of subcortical arousal centers by general anesthetics. However, key arousal nuclei have been shown to have a limited role in anesthetic mechanisms. For example, orexinergic neurons in the hypothalamus do not appear to play a role in anesthetic-induced unconsciousness; rather, they modulate the emergence from general anesthesia (Kelz et al., 2008). Histaminergic neurons in the tuberomammillary nucleus (also in the hypothalamus) have been thought to play a role in anesthetic-induced unconsciousness (Luo and Leung, 2011), but recent data bring the behavioral relevance of this nucleus into question (Zecharia et al., 2012). Suppression of brainstem structures such as the locus coeruleus may mediate anesthetic-induced unconsciousness, since mutant mice lacking dopamine-B-hydroxylase (which is required to synthesize norepinephrine in the locus coeruleus) are more sensitive to anesthetics (Hu et al., 2012). However, ketamine appears to *activate* the locus coeruleus in association with its hypnotic effects (Lu et al., 2008) and is dependent, in part, on noradrenergic neurotransmission (Kushikata et al., 2011). Although this list is certainly not exhaustive, it should be clear that inhibition of a number of key arousal nuclei in the brainstem and diencephalon does not appear to be necessary for anesthetic-induced unconsciousness.

The asymmetric role of some arousal nuclei in the process of induction and emergence suggests that the two processes are not mirror images of one another. Recently, a series of elegant studies has provided strong support for the hypothesis that there is a distinct neurobiology of induction and emergence that accounts for the observation of anesthetic hysteresis (Friedman et al., 2010; Joiner et al., 2013). Hysteresis implies that the process of "coming out" of a state is not simply the reverse process of "going in." In this context hysteresis is manifested as different anesthetic concentrations for induction of and emergence from general anesthesia: higher concentrations are associated with loss of consciousness compared with recovery of consciousness. Why should this be the case? Evidence suggests that there is a barrier to state transitions, termed neural inertia, which may be mediated by sleep systems (Joiner et al., 2013). Neural inertia could explain hysteresis, but it also has implications for the mechanism of anesthetic-induced unconsciousness. Consider: higher concentrations of anesthetic

are associated with induction compared to emergence, with sleep networks accounting for the fact that an organism needs less anesthetic to stay anesthetized than to become anesthetized (Friedman et al., 2010). However, this implies that *sleep networks only play a functional role after anesthetic-induced unconsciousness has already occurred*. Therefore, one implication of neural inertia is that sleep-related processes do not play a critical role in the induction of unconsciousness but rather are active during maintenance of unconsciousness.

SEDATIVE-HYPNOTIC EFFECTS OF MULTIPLE CLASSES OF ANESTHETICS CAN BE EXPLAINED BY A TOP-DOWN BUT NOT BOTTOM-UP PROCESS

In the nineteenth century, an anesthesiologist could walk into an operating room and use (for example) ether, chloroform or nitrous oxide to induce unconsciousness or, at the very least, a state in which the patient had lost "connected consciousness" of the environment (Sanders et al., 2012). We could argue over whether the state induced by ether was precisely the same state as that induced by chloroform, but we would likely agree that the same *functional* outcome had been achieved. In the twenty-first century, an anesthesiologist can walk into an operating room and use (for example) propofol, ketamine, or sevoflurane to induce unconsciousness. It is likely that the state induced by ketamine is quite different than the state induced by propofol, but again a similar functional outcome would be achieved: the patient would not be responding to commands or other environmental stimuli, the patient would be deemed unconscious based on this loss of responsiveness (not universally true, but usually so), and the clinician could therefore start with the business of the day. Although I have framed this in rather practical terms, it is this similar functional outcome that motivates the inclusion of these structurally and pharmacologically diverse drugs in the class of general anesthetics. The relatively fungible nature of these drugs in inducing unconsciousness is also at the core of the anesthetic mechanisms problem: what is the common property that allows us to use these highly diverse anesthetics in a very similar way?

It has not yet been possible to identify a single and common bottom-up process that parallels the common functional outcome resulting from the use of propofol, ketamine, and sevoflurane (representatives of the three major classes of general anesthetics). It is ketamine, in particular, that is generally problematic. Unlike propofol, sevoflurane and many other general anesthetics in current use, ketamine fails to (1) act primarily through GABA receptors (Antkowiak, 1999; Salmi et al., 2005; Zhou et al., 2013), (2) activate sleep-promoting nuclei (as noted above) (Lu et al., 2008), (3) metabolically depress the thalamus (Langsjo et al., 2005), or (4) depress fast activity of the electroencephalogram (Lee et al., 2013). In other words, ketamine [and, to some extent, nitrous oxide (Jevtovic-Todorovic et al., 1998)] fails to conform to virtually all bottom-up frameworks of anesthetic mechanisms: molecular, neuroanatomical, systems neuroscience, and even the relatively macroscopic neurophysiologic approach. By contrast, the top-down approach to ketamine-induced unconsciousness has successfully identified a common neural correlate of unconsciousness induced by propofol, ketamine, and sevoflurane that could have been predicted based on the neurobiology of consciousness (Lee et al., 2013) (**Figure 6**). Loss of effective connectivity from the frontal cortex to more posterior cortices has been consistently observed with all three drugs, suggesting inhibition of reentrant processing as a candidate for the common mediator of anesthetic effects on consciousness (Ku et al., 2011; Jordan et al., 2013). Furthermore, this loss of top-down information processing was selective, because feedforward processing (from posterior parietal to frontal area) appeared preserved. These data are supported by earlier animal studies, as well as more recent studies in humans showing a disruption of cortical communication by various anesthetic drugs (Ferrarelli et al., 2010; Casali et al., 2013). Importantly, this approach reveals parallels with pathological states of unconsciousness (Boly et al., 2011). Although loss of reentrant processing (also referred to as feedback, recurrent, reafferent, or reverberant processing) is currently only correlated with anesthetic-induced and pathological unconsciousness, it is has strong mechanistic implications given its proposed role in consciousness itself (Dehaene and Changeux, 2011). By contrast, no single bottom-up correlate or candidate mechanism of anesthetic-induced unconsciousness across all major classes of anesthetics has been identified or empirically supported.

The association of cortical network events with anesthetic-induced unconsciousness may not be compelling because it is possible that they are simply following the mechanistic parade rather than leading it. We know that modulation of sleep-wake neurons can result in dramatic changes of cortical networks, but can modulation of cortical neurons have a widespread effect? The answer appears to be *yes*. It has been demonstrated that activation of a *single* cortical neuron can lead to transitions in global brain states and produce measurable changes in behavior (Brecht et al., 2004; Houweling and Brecht, 2008; Li et al., 2009), supporting the possibility that even small cortical areas affected by general anesthetics can be instrumental in behavioral and brain state transitions.

MACRO CAUSATION CAN SUPERSEDE MICRO CAUSATION

One straightforward and plausible way of explaining top-down mechanisms of anesthetic-induced unconsciousness would be that the activity or dynamics of the cortical networks mediating awareness are more susceptible to the effects of general anesthetics than subcortical nuclei mediating sleep-wake states. Demonstrating a more significant contribution—or perhaps an earlier contribution—to unconsciousness by disruption of higher-order cortical processes vs. subcortical or lower-order cortical processes would help resolve the question of top-down vs. bottom-up mechanisms within a sensory or arousal hierarchy. A robust quantitative theory of cortical dynamics will be critical for this line of investigation. However, one might still make the reasonable claim that cortical disruption is not really the true mechanism because it can still be reduced to the underlying molecular mechanisms of anesthetic binding to neurotransmitter receptors or ion channels (i.e., some bottom-up event on a structural scale). It has previously been suggested that it might be helpful to divide anesthetic mechanisms into root and proximate causes, where diverse root causes at the molecular level might be

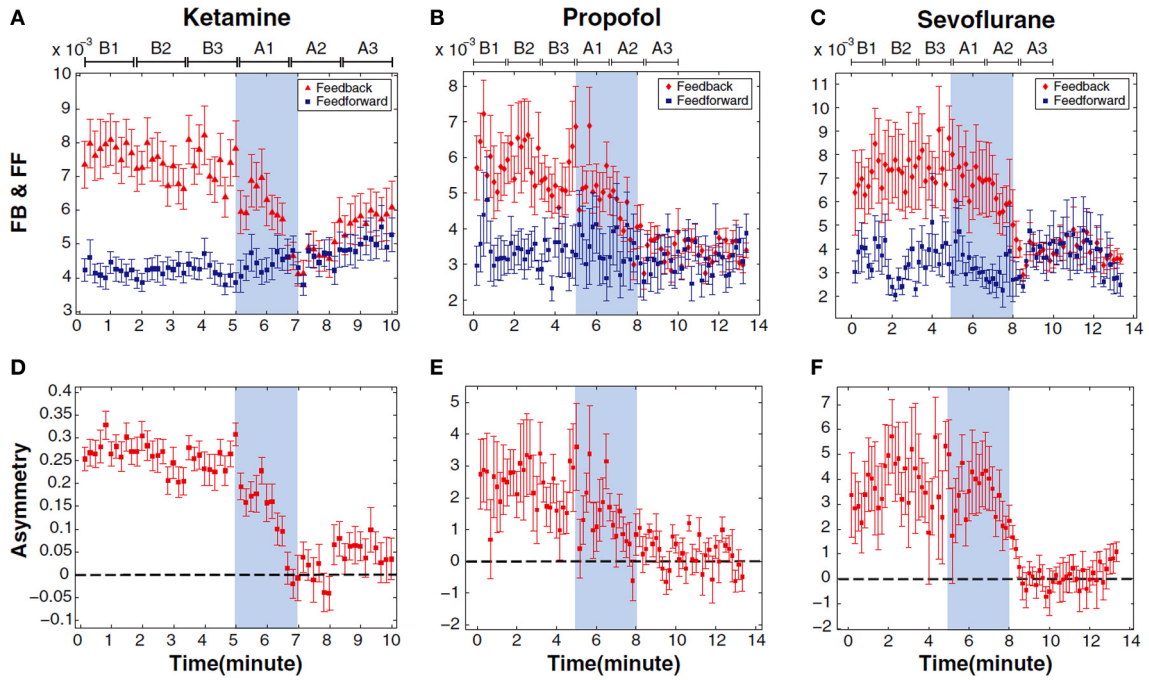

FIGURE 6 | Inhibition of top-down connectivity is a common correlate of anesthetic-induced unconsciousness across three distinct classes of general anesthetics. This figure depicts frontal-to-parietal (feedback) and parietal-to-frontal (feedforward) connectivity before, during and after anesthetic-induced unconsciousness in surgical patients **(A–C)**. Lower panels **(D–F)** show asymmetry of directional connectivity, with positive values representing feedback dominance and negative values representing feedforward dominance. Connectivity was measured using electroencephalography and symbolic transfer entropy, which is rooted in information theory. Blue shaded area represents induction of anesthesia; the period before induction is baseline consciousness and the period after is anesthetic-induced unconsciousness. Each state is separated into three substates of Baseline (B1–B3) and Anesthetized (A1–A3) conditions; the timescale is different because patients receiving ketamine were studied using a different protocol than patients receiving propofol and sevoflurane. FB, Feedback; FF, Feedforward. Reproduced from Lee et al. (2013), Anesthesiology, with permission.

translated across scales to a common proximate cause at the level of cortical information processing (Mashour, 2013). This would lead to a bottom-up framework with individual micro-causes converging on a single macro-level causality. From this perspective, the macro cause would simply supervene on the micro cause. In other words, once the micro level is fixed (e.g., binding of propofol to the $GABA_A$ receptor), so too is the macro level—and therefore the underlying micro event has done all of the real causal work.

Recent theoretical efforts have shown that macro-level processes might trump micro-level processes when it comes to true causation. It has been demonstrated in a simulation that a true emergent event can occur in which the macro-level causation contains more effective information than the micro-level causation (Hoel et al., 2013). In other words, *the macro level is actually doing more of the causal work than the micro level.* This suggests the possibility of macro-level *supersedence* in addition to the usual assumption of macro-level *supervenience.* Applying this principle to anesthetic-induced unconsciousness, it is therefore possible that observations at the top-down/macro-level may contain more effective information than the micro-level and thus causally supersede molecular events such as anesthetic binding. This would not imply that anesthetic binding is irrelevant to anesthetic-induced unconsciousness, but rather that it might not add further information to a macro-causal explanation. It is important to note that there is currently no evidence that this is the case. However, it is now at least conceivable that there could be a single causal explanation of anesthetic-induced unconsciousness at the macro level (e.g., cortical dynamics) that is not enhanced by the addition of micro-level information (e.g., molecular binding).

DISCUSSION

Traditionally, various bottom-up molecular mechanisms have been proposed to explain anesthetic-induced unconsciousness, including disruption of the lipid bilayer and modulation of protein-based neurotransmitter receptors or ion channels. From the neurocognitive perspective, bottom-up explanations of anesthetic-induced unconsciousness have focused on subcortical nuclei that mediate the sleep-wake cycle or early cortical areas that mediate sensory processing. There is growing evidence, however, that general anesthetics disrupt higher-order cognitive processes and that networks of association cortex may be particularly susceptible to anesthetic effects; this evidence parallels current thinking in the science of consciousness. Thus, top-down mechanisms of anesthetic-induced unconsciousness warrant serious consideration. It is possible that the observed changes in the cortex are not simply signatures of lower-order anesthetic actions,

but rather that direct modulation of cortical dynamics may be the mechanism of unconsciousness. Furthermore, it is now at least conceivable that such an explanatory framework could represent a sole macro-level causation that supersedes any bottom-up or even molecular description.

Intellectual bias is difficult to escape and thus it is probably better to disclose such bias rather than having it function as a "hidden variable" that shapes the discourse in a covert way. As an anesthesiologist and clinical researcher, my work has focused on the problem of intraoperative awareness with explicit recall and the possibility of brain monitoring techniques that are rooted in the neuroscience of consciousness. As such, the cortex—which is more accessible to study and monitoring in the operating room setting—has been a focus. As a neuroscientist and consciousness researcher, my focus is on the network-level interactions that most current theories deem to be critical for experiential processing. Such clinical and scientific predilections clearly influence my perspective. As such, in this article I have focused on arguments supporting the top-down approach—the reader is encouraged to explore the considerable evidence for alternative perspectives and to draw his or her own conclusions. It is also important to note that bottom-up and top-down perspectives need not be mutually exclusive. This is especially relevant for the higher-order thalamic nuclei, which primarily receive cortical input and are intimately involved in cortical function.

One point deserves emphasis before succumbing to the temptation of disregarding top-down causation on the basis of its inconsistency with the known effects of general anesthetics across species (Crowder, 2008). General anesthetics can stop single-cell organisms, fruit flies, and worms in their tracks… so who needs a cortical network for a satisfactory explanation of anesthetic mechanism? First, it is important to note that the anesthetic endpoint in these model systems is movement alone. Although one could rightfully argue that all endpoints relate to some kind of motor response, the endpoint of impaired movement in *Drosophila* or *C. elegans* cannot necessarily be regarded as a surrogate for impaired perception (van Swinderen, 2006; van Swinderen et al., 1999). It is therefore not even clear that the term "anesthetic-induced unconsciousness" applies here as it would for *Homo sapiens*. Second, as species evolve, so too do the networks governing their behavior and the mechanisms by which behavioral state transitions occur. For example, if we were investigating the mechanism of movement in humans, we might consider the motor cortex and supplementary motor area as starting points. It would be absurd to claim that the motor cortex could not be involved in the primary mechanism of movement in humans based on the arguments that worms move, but worms do not have a motor cortex. Similarly, it would be absurd to claim that higher-order cortical processes cannot be causally central to the mechanisms of anesthetic-induced unconsciousness in humans simply because worms or other species do not exhibit higher-order cortical processes.

CONCLUSION

The mechanism of anesthetic-induced unconsciousness is a fundamental question in both anesthesiology and neuroscience, with links to the neurobiology of consciousness itself. An emerging body of evidence suggests that both consciousness (in the experiential sense of the word) and anesthetic-induced unconsciousness are mediated by higher-order processes in the brain. Top-down approaches to anesthetic mechanisms may therefore provide critical insight to both the scientific understanding and clinical practice of anesthesiology.

FUNDING

Dr. Mashour is supported by grant RO1 GM098578 from the National Institutes of Health (Bethesda, MD), the James S. McDonnell Foundation (St. Louis, MO), and Cerephex Corporation (Los Altos, CA).

REFERENCES

Alkire, M. T., Haier, R. J., Barker, S. J., Shah, N. K., Wu, J. C., and Kao, Y. J. (1995). Cerebral metabolism during propofol anesthesia in humans studied with positron emission tomography. *Anesthesiology* 82, 393–403. doi: 10.1097/00000542-199502000-00010

Alkire, M. T., Haier, R. J., and Fallon, J. H. (2000). Toward a unified theory of narcosis: brain imaging evidence for a thalamocortical switch as the neurophysiologic basis of anesthetic-induced unconsciousness. *Conscious. Cogn.* 9, 370–386. doi: 10.1006/ccog.1999.0423

Antkowiak, B. (1999). Different actions of general anesthetics on the firing patterns of neocortical neurons mediated by the GABA(A) receptor. *Anesthesiology* 91, 500–511.

Antognini, J. F., and Schwartz, K. (1993). Exaggerated anesthetic requirements in the preferentially anesthetized brain. *Anesthesiology* 79, 1244–1249. doi: 10.1097/00000542-199312000-00015

Banoub, M., Tetzlaff, J. E., and Schubert, A. (2003). Pharmacologic and physiologic influences affecting sensory evoked potentials: implications for perioperative monitoring. *Anesthesiology* 99, 716–737. doi: 10.1097/00000542-200309000-00029

Boly, M., Garrido, M. I., Gosseries, O., Bruno, M. A., Boveroux, P., Schnakers, C., et al. (2011). Preserved feedforward but impaired top-down processes in the vegetative state. *Science* 332, 858–862. doi: 10.1126/science.1202043

Bonhomme, V., Boveroux, P., Brichant, J. F., Laureys, S., and Boly, M. (2012). Neural correlates of consciousness during general anesthesia using functional magnetic resonance imaging (fMRI). *Arch. Ital. Biol.* 150, 155–163. doi: 10.4449/aib.v150i2.1242

Boveroux, P., Vanhaudenhuyse, A., Bruno, M. A., Noirhomme, Q., Lauwick, S., Luxen, A., et al. (2010). Breakdown of within- and between-network resting state functional magnetic resonance imaging connectivity during propofol-induced loss of consciousness. *Anesthesiology* 113, 1038–1053. doi: 10.1097/ALN.0b013e3181f697f5

Brecht, M., Schneider, M., Sakmann, B., and Margrie, T. W. (2004). Whisker movements evoked by stimulation of single pyramidal cells in rat motor cortex. *Nature* 427, 704–710. doi: 10.1038/nature02266

Casali, A. G., Gosseries, O., Rosanova, M., Boly, M., Sarasso, S., Casali, K. R., et al. (2013). A theoretically based index of consciousness independent of sensory processing and behavior. *Sci. Transl. Med.* 5, 198ra105. doi: 10.1126/scitranslmed.3006294

Clark, A. (2013). Whatever next? Predictive brains, situated agents, and the future of cognitive science. *Behav. Brain Sci.* 36, 181–204. doi: 10.1017/s0140525x12000477

Crick, F., and Koch, C. (1995). Are we aware of neural activity in primary visual cortex? *Nature* 375, 121–123. doi: 10.1038/375121a0

Crowder, C. M. (2008). Does natural selection explain the universal response of metazoans to volatile anesthetics? *Anesth. Analg.* 107, 862–863. doi: 10.1213/ane.0b013e31817d866a

Dehaene, S., and Changeux, J. P. (2011). Experimental and theoretical approaches to conscious processing. *Neuron* 70, 200–227. doi: 10.1016/j.neuron.2011.03.018

Del Cul, A., Baillet, S., and Dehaene, S. (2007). Brain dynamics underlying the nonlinear threshold for access to consciousness. *PLoS Biol.* 5:e260. doi: 10.1371/journal.pbio.0050260

Eikermann, M., Vetrivelan, R., Grosse-Sundrup, M., Henry, M. E., Hoffmann, U., Yokota, S., et al. (2011). The ventrolateral preoptic nucleus is not required for isoflurane general anesthesia. *Brain Res.* 1426, 30–37. doi: 10.1016/j.brainres.2011.10.018

Ferrarelli, F., Massimini, M., Sarasso, S., Casali, A., Riedner, B. A., Angelini, G., et al. (2010). Breakdown in cortical effective connectivity during midazolam-induced loss of consciousness. *Proc. Natl. Acad. Sci. U.S.A.* 107, 2681–2686. doi: 10.1073/pnas.0913008107

Franks, N. P., and Lieb, W. R. (1984). Do general anaesthetics act by competitive binding to specific receptors? *Nature* 310, 599–601.

Friedman, E. B., Sun, Y., Moore, J. T., Hung, H. T., Meng, Q. C., Perera, P., et al. (2010). A conserved behavioral state barrier impedes transitions between anesthetic-induced unconsciousness and wakefulness: evidence for neural inertia. *PLoS ONE* 5:e11903. doi: 10.1371/journal.pone.0011903

Hoel, E. P., Albantakis, L., and Tononi, G. (2013). Quantifying causal emergence shows that macro can beat micro. *Proc. Natl. Acad. Sci. U.S.A.* 110, 19790–19795. doi: 10.1073/pnas.1314922110

Houweling, A. R., and Brecht, M. (2008). Behavioural report of single neuron stimulation in somatosensory cortex. *Nature* 451, 65–68. doi: 10.1038/nature06447

Hu, F. Y., Hanna, G. M., Han, W., Mardini, F., Thomas, S. A., Wyner, A. J., et al. (2012). Hypnotic hypersensitivity to volatile anesthetics and dexmedetomidine in dopamine beta-hydroxylase knockout mice. *Anesthesiology* 117, 1006–1017. doi: 10.1097/ALN.0b013e3182700ab9

Hudetz, A. G., Vizuete, J. A., and Imas, O. A. (2009). Desflurane selectively suppresses long-latency cortical neuronal response to flash in the rat. *Anesthesiology* 111, 231–239. doi: 10.1097/ALN.0b013e3181ab671e

Imas, O. A., Ropella, K. M., Ward, B. D., Wood, J. D., and Hudetz, A. G. (2005). Volatile anesthetics disrupt frontal-posterior recurrent information transfer at gamma frequencies in rat. *Neurosci. Lett.* 387, 145–150. doi: 10.1016/j.neulet.2005.06.018

Jevtovic-Todorovic, V., Todorovic, S. M., Mennerick, S., Powell, S., Dikranian, K., Benshoff, N., et al. (1998). Nitrous oxide (laughing gas) is an NMDA antagonist, neuroprotectant and neurotoxin. *Nat. Med.* 4, 460–463. doi: 10.1038/nm0498-460

Joiner, W. J., Friedman, E. B., Hung, H. T., Koh, K., Sowcik, M., Sehgal, A., et al. (2013). Genetic and anatomical basis of the barrier separating wakefulness and anesthetic-induced unresponsiveness. *PLoS Genet.* 9:e1003605. doi: 10.1371/journal.pgen.1003605

Jordan, D., Ilg, R., Riedl, V., Schorer, A., Grimberg, S., Neufang, S., et al. (2013). Simultaneous electroencephalographic and functional magnetic resonance imaging indicate impaired cortical top-down processing in association with anesthetic-induced unconsciousness. *Anesthesiology* 119, 1031–1042. doi: 10.1097/ALN.0b013e3182a7ca92

Kelz, M. B., Sun, Y., Chen, J., Cheng Meng, Q., Moore, J. T., Veasey, S. C., et al. (2008). An essential role for orexins in emergence from general anesthesia. *Proc. Natl. Acad. Sci. U.S.A.* 105, 1309–1314. doi: 10.1073/pnas.0707146105

Ku, S. W., Lee, U., Noh, G. J., Jun, I. G., and Mashour, G. A. (2011). Preferential inhibition of frontal-to-parietal feedback connectivity is a neurophysiologic correlate of general anesthesia in surgical patients. *PLoS ONE* 6:e25155. doi: 10.1371/journal.pone.0025155

Kushikata, T., Yoshida, H., Kudo, M., Kudo, T., Kudo, T., and Hirota, K. (2011). Role of coerulean noradrenergic neurones in general anaesthesia in rats. *Br. J. Anaesth.* 107, 924–929. doi: 10.1093/bja/aer303

Langsjo, J. W., Maksimow, A., Salmi, E., Kaista, K., Aalto, S., Oikonen, V., et al. (2005). S-ketamine anesthesia increases cerebral blood flow in excess of the metabolic needs in humans. *Anesthesiology* 103, 258–268. doi: 10.1097/00000542-200508000-00008

Lau, H., and Rosenthal, D. (2011). Empirical support for higher-order theories of conscious awareness. *Trends Cogn. Sci.* 15, 365–373. doi: 10.1016/j.tics.2011.05.009

Laureys, S. (2005). The neural correlate of (un)awareness: lessons from the vegetative state. *Trends Cogn. Sci.* 9, 556–559. doi: 10.1016/j.tics.2005.10.010

Lee, U., Ku, S., Noh, G., Baek, S., Choi, B., and Mashour, G. A. (2013). Disruption of frontal-parietal communication by ketamine, propofol, and sevoflurane. *Anesthesiology* 118, 1264–1275. doi: 10.1097/ALN.0b013e31829103f5

Li, C. Y., Poo, M. M., and Dan, Y. (2009). Burst spiking of a single cortical neuron modifies global brain state. *Science* 324, 643–646. doi: 10.1126/science.1169957

Liu, X., Lauer, K. K., Ward, B. D., Li, S. J., and Hudetz, A., G. (2013). Differential effects of deep sedation with propofol on the specific and nonspecific thalamocortical systems: a functional magnetic resonance imaging study. *Anesthesiology* 118, 59–69. doi: 10.1097/ALN.0b013e318277a801

Lu, J., Nelson, L. E., Franks, N., Maze, M., Chamberlin, N. L., and Saper, C. B. (2008). Role of endogenous sleep-wake and analgesic systems in anesthesia. *J. Comp. Neurol.* 508, 648–662. doi: 10.1002/cne.21685

Luo, T., and Leung, L. S. (2011). Involvement of tuberomamillary histaminergic neurons in isoflurane anesthesia. *Anesthesiology* 115, 36–43. doi: 10.1097/ALN.0b013e3182207655

Lydic, R., and Biebuyck, J. F. (1994). Sleep neurobiology: relevance for mechanistic studies of anaesthesia. *Br. J. Anaesth.* 72, 506–508. doi: 10.1093/bja/72.5.506

Manninen, P. H., Lam, A. M., and Nicholas, J. F. (1985). The effects of isoflurane and isoflurane-nitrous oxide anesthesia on brainstem auditory evoked potentials in humans. *Anesth. Analg.* 64, 43–47. doi: 10.1213/00000539-198501000-00009

Mashour, G. A. (2013). Cognitive unbinding: a neuroscientific paradigm of general anesthesia and related states of unconsciousness. *Neurosci. Biobehav. Rev.* 37, 2751–2759. doi: 10.1016/j.neubiorev.2013.09.009

Mihic, S. J., Ye, Q., Wick, M. J., Koltchine, V. V., Krasowski, M. D., Finn, S. E., et al. (1997). Sites of alcohol and volatile anaesthetic action on GABA(A) and glycine receptors. *Nature* 389, 385–389. doi: 10.1038/38738

Moore, J. T., Chen, J., Han, B., Meng, Q. C., Veasey, S. C., Beck, S. G., et al. (2012). Direct activation of sleep-promoting VLPO neurons by volatile anesthetics contributes to anesthetic hypnosis. *Curr. Biol.* 22, 2008–2016. doi: 10.1016/j.cub.2012.08.042

Moruzzi, G., and Magoun, H. W. (1949). Brain stem reticular formation and activation of the EEG. *Electroencephalogr. Clin. Neurophysiol.* 1, 455–473. doi: 10.1016/0013-4694(49)90219-9

Nelson, L. E., Guo, T. Z., Lu, J., Saper, C. B., Franks, N. P., and Maze, M. (2002). The sedative component of anesthesia is mediated by GABA(A) receptors in an endogenous sleep pathway. *Nat. Neurosci.* 5, 979–984. doi: 10.1038/nn913

Ni Mhuircheartaigh, R., Warnaby, C., Rogers, R., Jbabdi, S., and Tracey, I. (2013). Slow-wave activity saturation and thalamocortical isolation during propofol anesthesia in humans. *Sci. Transl. Med.* 5, 208ra148. doi: 10.1126/scitranslmed.3006007

Perouansky, M. (2012). The quest for a unified model of anesthetic action: a century in Claude Bernard's shadow. *Anesthesiology* 117, 465–474. doi: 10.1097/ALN.0b013e318264492e

Rampil, I. J. (1994). Anesthetic potency is not altered after hypothermic spinal cord transection in rats. *Anesthesiology* 80, 606–610. doi: 10.1097/00000542-199403000-00017

Salmi, E., Langsjo, J. W., Aalto, S., Nagren, K., Metsahonkala, L., Kaisti, K. K., et al. (2005). Subanesthetic ketamine does not affect 11C-flumazenil binding in humans. *Anesth. Analg.* 101, 722–725. doi: 10.1213/01.ane.0000156951.83242.8d

Sanders, R. D., Tononi, G., Laureys, S., and Sleigh, J. W. (2012). Unresponsiveness not equal unconsciousness. *Anesthesiology* 116, 946–959. doi: 10.1097/ALN.0b013e318249d0a7

Saper, C. B., Scammell, T. E., and Lu, J. (2005). Hypothalamic regulation of sleep and circadian rhythms. *Nature* 437, 1257–1263. doi: 10.1038/nature04284

Tononi, G. (2012). Integrated information theory of consciousness: an updated account. *Arch. Ital. Biol.* 150, 293–329.

van Swinderen, B. (2006). A succession of anesthetic endpoints in the Drosophila brain. *J. Neurobiol.* 66, 1195–1211. doi: 10.1002/neu.20300

van Swinderen, B., Saifee, O., Shebester, L., Roberson, R., Nonet, M. L., and Crowder, C. M. (1999). A neomorphic syntaxin mutation blocks volatile-anesthetic action in *Caenorhabditis elegans*. *Proc. Natl. Acad. Sci. U.S.A.* 96, 2479–2484. doi: 10.1073/pnas.96.5.2479

Zecharia, A. Y., Yu, X., Gotz, T., Ye, Z., Carr, D. R., Wulff, P., et al. (2012). GABAergic inhibition of histaminergic neurons regulates active waking but not the sleep-wake switch or propofol-induced loss of consciousness. *J. Neurosci.* 32, 13062–13075. doi: 10.1523/jneurosci.2931-12.2012

Zhou, C., Douglas, J. E., Kumar, N. N., Shu, S., Bayliss, D. A., and Chen, X. (2013). Forebrain HCN1 channels contribute to hypnotic actions of ketamine. *Anesthesiology* 118, 785–795. doi: 10.1097/ALN.0b013e31828 7b7c8

Conflict of Interest Statement: Dr. Mashour holds a patent (pending) through the University of Michigan on directional/effective connectivity as a method of assessing consciousness (Application No.: 13/804,706, Filed March 14, 2013, "System and Method to Assess Causal Signaling in the Brain during States of Consciousness").

Received: 25 April 2014; accepted: 27 May 2014; published online: 23 June 2014.
Citation: Mashour GA (2014) Top-down mechanisms of anesthetic-induced unconsciousness. Front. Syst. Neurosci. ***8****:115. doi: 10.3389/fnsys.2014.00115*
This article was submitted to the journal Frontiers in Systems Neuroscience.

frontiers in
SYSTEMS NEUROSCIENCE

ORIGINAL RESEARCH ARTICLE
published: 07 October 2014
doi: 10.3389/fnsys.2014.00191

Preferential effect of isoflurane on top-down vs. bottom-up pathways in sensory cortex

Aeyal Raz[1,2]*, Sean M. Grady[1], Bryan M. Krause[3], Daniel J. Uhlrich[4], Karen A. Manning[4] and Matthew I. Banks[1,4]

[1] *Department of Anesthesiology, School of Medicine and Public Health, University of Wisconsin, Madison, WI, USA*
[2] *Department of Anesthesiology, Rabin Medical Center, Petah-Tikva, Israel, Affiliated with Sackler School of Medicine, Tel Aviv University, Tel Aviv, Israel*
[3] *Neuroscience Training Program, University of Wisconsin, Madison, WI, USA*
[4] *Department of Neuroscience, University of Wisconsin, Madison, WI, USA*

Edited by:
Anthony G. Hudetz, Medical College of Wisconsin, USA

Reviewed by:
Bruce MacIver, Stanford University School of Medicine, USA
George Mashour, University of Michigan Medical School, USA
Flavio Frohlich, University of North Carolina - Chapel Hill, USA

****Correspondence:***
Aeyal Raz, Department of Anesthesiology, University of Wisconsin, 1300 University Avenue, Room 4625, Madison, WI 53706, USA
e-mail: raz@wisc.edu

The mechanism of loss of consciousness (LOC) under anesthesia is unknown. Because consciousness depends on activity in the cortico-thalamic network, anesthetic actions on this network are likely critical for LOC. Competing theories stress the importance of anesthetic actions on bottom-up "core" thalamo-cortical (TC) vs. top-down cortico-cortical (CC) and matrix TC connections. We tested these models using laminar recordings in rat auditory cortex *in vivo* and murine brain slices. We selectively activated bottom-up vs. top-down afferent pathways using sensory stimuli *in vivo* and electrical stimulation in brain slices, and compared effects of isoflurane on responses evoked via the two pathways. Auditory stimuli *in vivo* and core TC afferent stimulation in brain slices evoked short latency current sinks in middle layers, consistent with activation of core TC afferents. By contrast, visual stimuli *in vivo* and stimulation of CC and matrix TC afferents in brain slices evoked responses mainly in superficial and deep layers, consistent with projection patterns of top-down afferents that carry visual information to auditory cortex. Responses to auditory stimuli *in vivo* and core TC afferents in brain slices were significantly less affected by isoflurane compared to responses triggered by visual stimuli *in vivo* and CC/matrix TC afferents in slices. At a just-hypnotic dose *in vivo*, auditory responses were enhanced by isoflurane, whereas visual responses were dramatically reduced. At a comparable concentration in slices, isoflurane suppressed both core TC and CC/matrix TC responses, but the effect on the latter responses was far greater than on core TC responses, indicating that at least part of the differential effects observed *in vivo* were due to local actions of isoflurane in auditory cortex. These data support a model in which disruption of top-down connectivity contributes to anesthesia-induced LOC, and have implications for understanding the neural basis of consciousness.

Keywords: cortical column, anesthesia, auditory evoked response, neocortex, multimodal integration, current source density

INTRODUCTION

Although in widespread use for >150 years, how anesthetics cause loss of consciousness (LOC) remains one of the great unsolved mysteries in biomedical science. Elucidating these mechanisms would benefit patient care in terms of improved monitoring and more selective anesthetic agents, and would provide insight into neural mechanisms of consciousness. Indeed, in recent years, research in the fields of anesthetic mechanisms and the neural basis of consciousness have begun to converge (Mashour, 2006; Alkire et al., 2008b; Shushruth, 2013).

We have extensive knowledge of the molecular targets and behavioral effects of anesthetic agents (Antkowiak, 2001; Rudolph and Antkowiak, 2004; Franks, 2008). Much less is known about how anesthetics act at the level of cortical circuits. Previous studies focused on the dramatic reduction in cortical activity observed at surgical anesthetic doses (Schwender et al., 1993a), and imaging and electrophysiological studies in thalamus suggested that anesthetics suppress ascending information flow into cortex (Ries and Puil, 1999; Alkire et al., 2000; Schroter et al., 2012). Because TC information transfer has been hypothesized as the key mediator for consciousness (Llinas et al., 1998), these observations formed the basis of the *thalamic switch hypothesis* of anesthetic-induced LOC (Alkire et al., 2000). However, studies have also shown that suppression of cortical sensory responses by anesthetics can be unrelated to awareness (Dueck et al., 2005; Kerssens et al., 2005; Plourde et al., 2006), that sensory evoked responses can even be enhanced dramatically under anesthesia compared to waking conditions (Imas et al., 2005b), and that anesthetics selectively suppress "matrix" thalamic nuclei, which provide largely modulatory TC input, compared to "core" thalamic nuclei, which provide largely driving TC input (Jones, 1998; Liu et al., 2013; Saalmann, 2014). Thus, evidence suggests that during anesthesia-induced

LOC, as during sleep, external sensory stimuli activate cortex but fail to become incorporated into the hierarchical processing stream (Liu et al., 2011; Hobson and Friston, 2012). These data have motivated an alternative hypothesis, which we call here the *cortico-thalamic network disruption hypothesis* that emphasizes anesthetic effects on CC connectivity and information processing. This hypothesis derives from two related theories. The first, the *information integration theory of consciousness*, proposes that consciousness relies on the dense interconnectivity within the TC network and the vast number of possible network states (Tononi, 2004). According to this hypothesis, anesthetics act across wide areas of cortex to reduce the repertoire of network states (i.e., information) and connectivity (i.e., integration) (Alkire et al., 2008b). In the other, the *cognitive unbinding hypothesis*, anesthetics disrupt the cortical integration of sensory information to prevent a unified percept of the external world (Mashour, 2013).

Specific ideas about which connections are targeted under the *cortico-thalamic network disruption hypothesis* have emerged recently, based on predictive coding models of neocortex. These models posit comparisons of observed, bottom-up sensory information with top-down predictions based on memory and context, all simultaneously at multiple hierarchical processing stages (Grossberg and Versace, 2008; Bar, 2009; George and Hawkins, 2009; Bastos et al., 2012). Processes such as priming, context, expectation, and attention influence responses to sensory stimuli (Warren, 1970; Haist et al., 2001; Alain and Izenberg, 2003; Alain, 2007; Davis and Johnsrude, 2007; Fritz et al., 2007; Todorovic et al., 2011; Chennu et al., 2013; Kok et al., 2013), likely via modulation of infra- and supragranular pyramidal cells due to the concentration of descending CC and "matrix" TC (see below) inputs to these layers (Zeki and Shipp, 1988; Felleman and Van Essen, 1991; Cauller, 1995). This comparison or integration of bottom-up and top-down information streams is postulated to be a critical component of sensory awareness, and its disruption is thought to represent a common mechanism for LOC in natural and clinically relevant conditions. Thus, several lines of evidence suggest that LOC due to anesthesia and slow wave sleep and in patients in vegetative states is caused by suppressed CC connectivity and thus disruption of this integrative process. During midazolam-induced LOC and during slow-wave sleep, local cortical responses to transcranial magnetic stimulation are enhanced locally but the spread of activity due to CC interactions is reduced (Massimini et al., 2005; Ferrarelli et al., 2010). Furthermore, under a variety of anesthetic regimes, long range descending CC connectivity is preferentially suppressed (Imas et al., 2005a; Peltier et al., 2005; Alkire, 2008; Lee et al., 2009, 2013a,b; Ku et al., 2011; Liu et al., 2011; Schrouff et al., 2011; Boly et al., 2012; Jordan et al., 2013; Blain-Moraes et al., 2014; Mashour, 2014). Similar results demonstrating selective loss of descending CC connectivity were demonstrated in vegetative states as well (Boly et al., 2011). Finally, general anesthetics eliminate contextual modulation of responses in primary visual cortex that are likely mediated by top-down connections, but leave bottom-up responses intact (Lamme et al., 1998) and suppress integration of local receptive field information (Pack et al., 2001). However, in none of these studies were effects of anesthetics on bottom-up vs. top-down projections tested directly. Many of these studies are based on EEG methods, which are unable to measure thalamic activity, leaving the thalamic involvement in this process as a theoretical consideration rather than actual measurement. Even fMRI studies often lack the spatial resolution to differentiate between anesthetic effects on core vs. matrix thalamic nuclei.

Sensory cortex in general, and auditory cortex specifically, is a useful system to test these competing hypotheses about anesthesia-induced LOC (Imas et al., 2004; Banks, 2010; Liu et al., 2011). This area is relevant to clinical monitoring of anesthesia depth (Drummond, 2000) and for evaluating modulation of sensory information received by the brain. It is possible to activate selectively different projection pathways. Ascending (bottom-up) afferents from ventral medial geniculate (MGv; "core TC afferents") terminate with highest density in layers 3 and 4 of auditory cortex (Scheel, 1988; Roger and Arnault, 1989; Romanski and Ledoux, 1993; Winer et al., 1999; Polley et al., 2007; Storace et al., 2010; Smith et al., 2012), and their activation via acoustic stimuli *in vivo* leads to a stereotypical synaptic response in these layers (Kaur et al., 2005; Szymanski et al., 2009). Other inputs arising from descending CC afferents as well as other thalamic nuclei (e.g., medial division of MG; "matrix TC afferents") also provide large numbers of synaptic connections (Rockland and Virga, 1989; Salin et al., 1995; Budd, 1998) and are likely to modulate responses to ascending input (Sandell and Schiller, 1982) and regulate information transmission (Saalmann, 2014), in some cases driving columnar activity prior to or in the absence of ascending input (Cauller and Kulics, 1991; Mignard and Malpeli, 1991; Krupa et al., 2004). Although these descending CC and matrix TC afferents likely serve distinct functions, for simplicity and for the purposes of this study we will refer to these afferents as top-down due to their largely modulatory nature and the overlap in their projection patterns. These projections target preferentially layers 1, 2, 5, and 6 (Shi and Cassell, 1997; Kimura et al., 2004; Smith et al., 2012), and their activation will thus lead to a response pattern distinct from core TC afferents. We, and others, have shown that visual responses in auditory cortex are carried by descending cortical and matrix thalamic afferents (Budinger et al., 2006; Bizley et al., 2007; Smith et al., 2010; Banks et al., 2011), and thus visual stimuli will activate top-down pathways in auditory cortex *in vivo*. In brain slices, CC and matrix TC pathways can be activated directly by electrical stimulation.

In this paper, we used electrophysiological recordings from whole columns *in vivo* and *in vitro* and activated ascending thalamic and descending cortical pathways selectively to test the hypothesis of a differential effect of anesthetics on ascending vs. descending pathways.

MATERIALS AND METHODS

All procedures followed the NIH Guide for the Care and Use of Laboratory Animals and were in accordance with institutional guidelines.

IN VIVO EXPERIMENTS

Electrode implantation

Female Harlan Sprague Dawley ($n = 2$) or ACI ($n = 8$) rats (170–250 gm) were housed individually in transparent Plexiglas

cages in dedicated rooms (12:12 reversed light-dark cycle, on at 6 p.m., 23 ± 1°C; food and water *ad libitum*). Animals were chronically implanted under aseptic conditions with 1 × 16 single shank silicon electrode arrays (15 μm thick, 150 μm wide) with iridium recording sites (177 μm^2; 1.5 MΩ; Neuronexus Technologies, Ann Arbor, MI). Anesthesia was induced and maintained with isoflurane (1.5–2% in 50% O_2/50% room air). Meloxicam (1 mg/kg SQ) was administered during surgery to manage pain and swelling. Rats were kept on an infrared heating pad throughout surgery and recovery to maintain core temperature at 37 ± 0.5°C. Core auditory cortex was located stereotaxically (Doron et al., 2002; Polley et al., 2007) and electrode placement confirmed *post-hoc* histologically (see below). A craniotomy ∼2.5 mm^2 was made over left auditory cortex using a surgical drill and an ultra-fine burr bit and the dura dissected. The electrode was advanced at an angle normal to the surface of the brain until the most superficial recording site was embedded just below the pial surface. Ground and reference electrodes were attached to skull screws placed over the contralateral parietal cortex and over the cerebellum. The craniotomy was sealed with silicone elastomer (Kwik Sil, World Precision Instruments, Sarasota, FL) and the electrode array was fixed to the skull screws and the skull with dental acrylic. Connectors that served as mounting devices for head-mounted LEDs were fixed to the skull using dental acrylic. Animals were medicated postoperatively for pain (buprenorphine 0.05 mg/kg SQ and meloxicam 1 mg/kg SQ) and monitored daily for signs of discomfort and infection. The animals were allowed to recover for 1 week before their first recording session.

Electrophysiological recordings

Recordings were performed in a sound-proof chamber (Industrial Acoustics Company, Inc., Bronx, NY), inside which animals were placed in a home-made gas-tight acrylic enclosure (20 × 19 × 11 cm) that had gas inflow and outflow ports for administering and scavenging isoflurane and a gas sampling port for monitoring the isoflurane concentration using a commercial monitor (Multigas Monitor 602, Criticare Systems, Waukesha, WI). A heating pad was placed in the bottom of the enclosure to keep the animals warm during anesthesia application. A small speaker (TDT-ES1, Tucker Davis Technologies, Alachua, FL) was mounted inside the enclosure, oriented toward the animal. The speaker was calibrated using a microphone (#4016, ACO Pacific, Inc., Belmont, CA) placed approximately 4 cm from the speaker, and stimuli presented at approximately 20–80 dB SPL assuming the animal's head was this distance from the speaker. Since the animal was unrestrained, actual stimulus levels on each trial varied slightly. Speaker output varies by < ±10 dB SPL over the range 4–60 kHz. Free-field stimuli were applied using commercial software (Brainware, RPVDX, Tucker-Davis Technologies, Alachua, FL) and custom software written in Matlab. A 16 channel headstage (TDT RA16) on a flexible tether was plugged into an Omnetics connector on the animal's head. For all electrophysiological recordings, responses were bandpass-filtered at 2–7500 Hz, amplified 5000–10,000 ×, digitized at 24.414 kHz (TDT RZ5 or RX5) and collected using Brainware. Local field potentials (LFPs) were isolated offline by filtering at 1–300 Hz. Spiking activity was measured by filtering the raw data at 500–3000 Hz, but because the quality of these high frequency data was variable over time and from animal to animal, likely because of changes in electrode impedance (that fortunately did not affect recorded LFPs), these data were not analyzed further. In the first recording session, approximate best frequency (BF) of the recording site was determined by presenting pure tone stimuli (50 ms duration, 5 ms cosine windowed rise/fall times) at 11 frequencies logarithmically spaced from 4.2 to 64 kHz, at 20–80 dB SPL in 20 dB steps. The frequency at which the LFP was detectable at the lowest intensity presented was taken as the BF. On occasion additional frequencies and/or intensities were presented to resolve ambiguity.

Multiple recording sessions were obtained in each animal (range 1–6 sessions, median = 3). In most animals (9/10) a single isoflurane concentration (subhypnotic = 0.4%, just-hypnotic = 0.8–0.9%, or reliably hypnotic = 1.6%) was selected for every experimental day, and data was obtained at baseline, drug and recovery conditions. The just-hypnotic concentration was selected as that causing loss of righting reflex (LORR) in that animal on that particular day. Baseline recordings were obtained for approximately 60 min, after which isoflurane was applied in room air. After reaching the desired concentration, 15 min were allowed for the animal to equilibrate and the drug applied for an additional 15 min to obtain the responses in the drug condition. Finally, the isoflurane was turned off and responses recorded continuously for 60 min at 0% isoflurane. In one animal, we recorded only at the just-hypnotic dose, in another only at the just- and reliably hypnotic doses, and in one animal, the isoflurane concentration was increased in a step wise manner, allowing recording with multiple isoflurane doses in one recording session.

In these recording sessions, stimuli consisted of pure tones, LED flashes, and paired LED-tone stimuli (11 stimuli in all for each recording session, randomly interleaved). Five different tones (50 ms duration) were chosen for each session: three at 40 dB SPL at BF, 1/2BF, and 2xBF, and an additional two at 20 and 60 dB SPL at BF. The five tones were presented alone and in combination with 1 ms, 0.37 cd-s/m^2 LED flashes, with LED flashes preceding the tones at a stimulus onset asynchrony chosen to maximally align the visual and auditory responses, typically 65 ms. The eleventh stimulus in the set was the LED flash alone. LEDs were mounted on the head and positioned to be a constant 1 cm from the animal's eyes during the recording sessions. We note that the LED flash did not elicit any observable startle reflex in the animals. Animals were monitored via infrared video camera to ensure that their eyes remained open throughout the experiment, including when unconscious due to isoflurane. Responses to unilateral visual stimuli presented to the ipsilateral and contralateral eye were recorded, but as expected based on the known anatomy of the visual system in rats, ipsilateral stimuli were ineffective and not analyzed further.

Histological processing

Brain tissue was preserved histologically by means of previously described methods (Smith et al., 2010, 2012; Banks et al., 2011) to determine electrode track locations upon completion of *in vivo* recording experiments. In brief, rats were deeply

anesthetized with sodium pentobarbital (90 mg/kg i.p.) and perfused intracardially with phosphate-buffered saline followed by 300–500 ml of an aldehyde fixative solution in sodium phosphate buffer. Coronal tissue sections 60 μm thick were cut from the fixed brain, mounted serially on slides, stained with Cresyl Violet, and coverslipped. Electrode entry, tracks, and tip position in the brain were determined by examination of serial sections using light microscopy camera lucida techniques. Locations in the brain were identified initially using the terminology and atlas of Paxinos and Watson (2007). Refer to Smith et al. (2012) for a full description of cytological features used to aid in identification of auditory cortical areas. Electrode sites were then mapped to corresponding functionally-defined auditory areas (**Figure 1B**) described in Polley et al. (2007) based on the dorsal-ventral and rostral-caudal position of the site of electrode entry. Digitized light level photomicrographs were acquired with a Spot camera (Diagnostic Instruments, Sterling Heights, MI) mounted on a Nikon Eclipse E600 microscope and prepared using Adobe Photoshop (San Jose, CA).

BRAIN SLICE EXPERIMENTS

All reagents not specified below were obtained from Sigma-Aldrich (St. Louis, MO).

Brain slice preparation

Male B6CBAF1/J mice ($n = 17$ animals; median age = p38, range = p28–p98) were decapitated under isoflurane anesthesia, and the brains were extracted and immersed in modified artificial CSF [mACSF; composed of (in mM) 111 NaCl, 35 $NaHCO_3$, 20 HEPES, 1.8 KCl, 1.05 $CaCl_2$, 2.8 $MgSO_4$, 1.2 KH_2PO_4, and 10 glucose] at 0–4°C. HEPES was included to improve slice health and prevent edema (Macgregor et al., 2001). Two types of slices were used. Auditory TC brain slices (450 μm; $n = 10$) were prepared from the right hemisphere as previously described (Cruikshank et al., 2002; Verbny et al., 2006). To record responses in auditory cortex to stimulation in extrastriate visual cortex, we also prepared coronal slices (450 μm; $n = 7$) from both hemispheres using standard techniques, as described (Banks et al., 2011). In these latter slices, we observed that the most consistent responses to V2 stimulation were observed in slices cut ∼15° off the coronal plane, with the dorsal edge of the slice caudal to the ventral edge. Slices were maintained in mACSF saturated with 95% O_2/5% CO_2 at 24°C for >1 h before transfer to the recording chamber, which was perfused at 4–6 ml/min with ACSF [composed of (in mM) 111 NaCl, 35 $NaHCO_3$, 20 HEPES, 1.8 KCl, 2.1 $CaCl_2$, 1.4 $MgSO_4$, 1.2 KH_2PO_4, and 10 glucose] at 30–34°C. In TC slices, primary auditory cortex was identified based on its position relative to the hippocampus and strong responses to stimulation of thalamic afferents, as in previous studies (Verbny et al., 2006). In coronal slices, primary auditory and extrastriate visual cortex were identified based on their position relative to the rhinal sulcus, midline and hippocampus, as described (Banks et al., 2011). Cortical layers were identified by differences in cell density and based on distance from the pia, as in previous studies (Verbny et al., 2006; Banks et al., 2011). We further used the tissue appearance under bright field illumination to identify the approximate borders between cortical layers. Layers 4 had a relatively dark appearance compared to the light colored bands of layers 3, 5, and 6.

Electrophysiological recordings

LFPs were recorded using silicon multi-electrode arrays consisting of 16 shanks (15 μm thick, 100 μm spacing) each with one iridium recording site (A16; Neuronexus Technologies). Data were amplified (HS-16, Lynx8; Neuralynx, Bozeman, MT), low-pass filtered (10 kHz), digitized (20 kHz; DigiData 1322A; Molecular Devices, City, State), and recorded using pClamp version 9.2 (Molecular Devices). Afferents were activated using pairs of tungsten electrodes (0.1 MΩ, 75 μm diameter; FHC Inc., Bowdoin, ME) cemented together at tip separations of ∼50–200 μm. In coronal slices, stimuli were applied to layer 5 in V2 (see **Figure 6B**), as described (Banks et al., 2011). In TC slices, stimuli were applied to the superior thalamic radiation, just rostral to the hippocampus (Verbny et al., 2006), and to layer 1, ∼1 mm rostral to the recording site (see **Figure 6A**). Stimuli (100 μs, 50–200 μA) were applied using constant current stimulus isolation units (A365, World Precision Instruments, Sarasota, FL) and consisted of either single pulses or brief trains (4 pulses, 40 Hz). Throughout, we refer to the L1 and V2/L5 stimuli as corticocortical (CC) stimuli, but we note that the L1 stimulus could also activate matrix TC afferents.

Anesthetic application

Isoflurane (0.5%, 1%, and 2%; Novaplus; Abbott Labs, N. Chicago, IL) was bath applied to slices from a 500 ml Teflon gas sampling bags (Fisher Scientific International Inc., Hampton, NH; cat. No. 10-923-5). Isoflurane was prepared as an aqueous solution either from a saturated 95% O_2–5% CO_2 gas diluted to final concentration in 50% gas (95% O_2–5% CO_2) and 50% ACSF in the sampling bags on the day of the experiment, or by bubbling 95% O_2–5% CO_2 into ACSF via Isoflurane vaporizer and measuring the gas concentration at the fluid surface with an anesthetic gas monitor (Poet II Anesthesia Monitor, Criticare Systems Inc., Waukesha, WI). Final Isoflurane concentrations in the bags were verified by either gas chromatography measurements (Gow-Mac Series 580 FID Isothermal Gas Chromatograph, Gow-Mac Instrument Co., Lehigh Valley, PA) of samples from each bag, or by sampling the gas concentration in the gas phase of the bag with an anesthetic gas monitor (Poet II Anesthesia Monitor, Criticare Systems Inc., Waukesha, WI) after 15 min of equilibration during shaking of the solution ("The belly dancer," Stovall Life Sciences, Stovall, NC). Final anesthetic concentrations and electrophysiological results using the two methods were indistinguishable and were pooled in all analyses. Concentration measurements were used as covariates in statistical analysis of the data in **Figures 8C,D**.

DATA ANALYSIS

Neuronal data analysis

LFP responses to the different stimuli presented (both *in vivo* and in slices) were averaged for each channel triggered on the stimuli. Separate averaging was performed for each recording condition (control, isoflurane and recovery) in each recording session. To obtain steady state effects of isoflurane, LFPs were averaged only

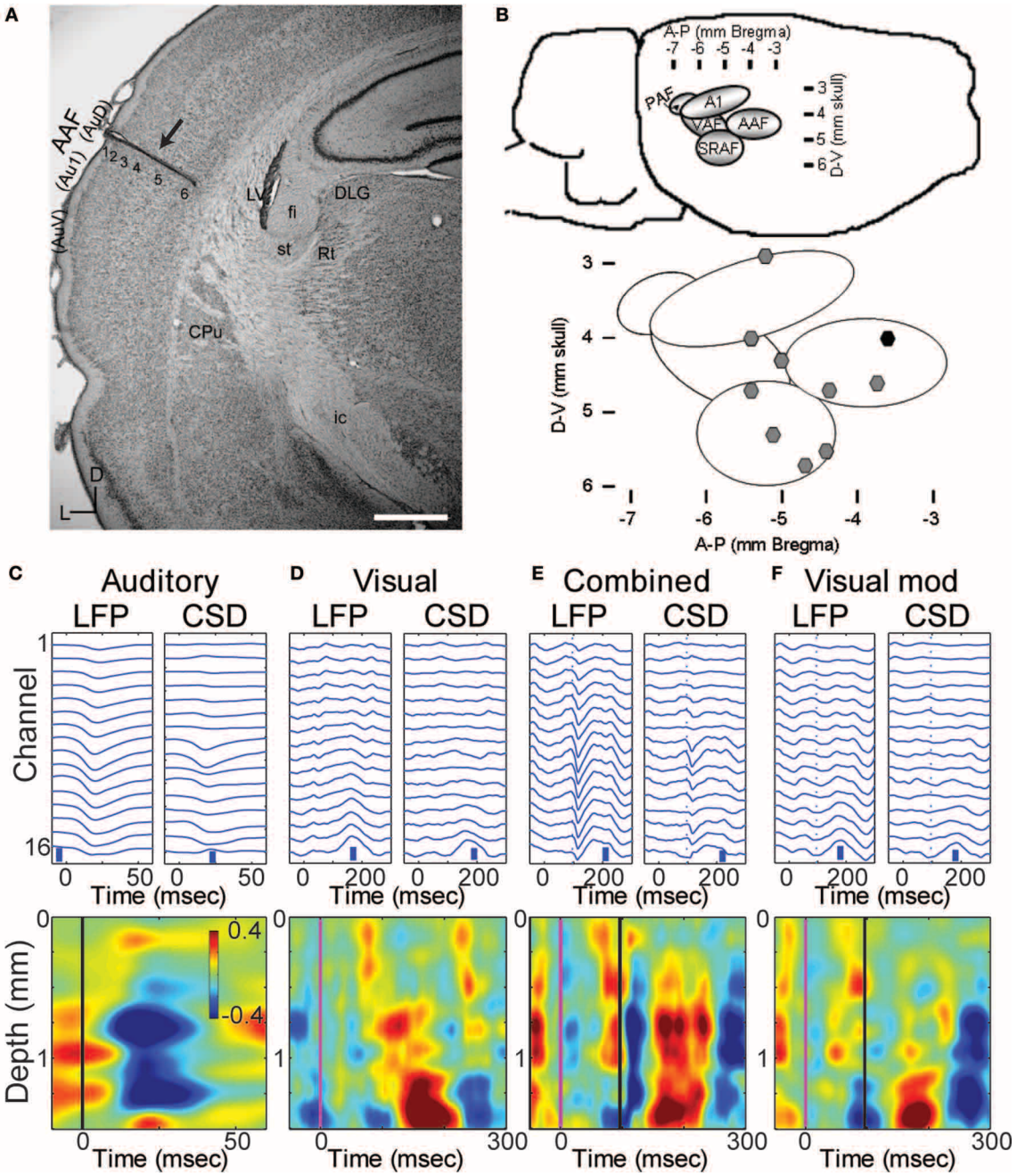

FIGURE 1 | Multichannel recordings of sensory responses from auditory cortex *in vivo*. **(A)** Photomicrograph of a section through auditory cortex of a chronically implanted rat. The electrode trace can be clearly seen in auditory cortex (*arrow*). Scale bar in *lower right* is 1 mm. **(B)** Location of implanted probes: a map with coordinates of the auditory areas on the rat's brain (*top*) and the location of the implanted electrodes used in the manuscript on the map (*black symbol*: probe in **A**). **(C–F)** LFPs and derived CSD traces (*top row*) and CSD contour plots (*bottom row*) in response to a 50 ms tone burst at best frequency (13.4 kHz, 40 dB SPL; **C;** tone onset at time zero), a 1 ms LED flash (**D;** flash onset at time 0), combined stimulation **(E)** of the LED flash (at time 0) and best-frequency tone (at 96 ms), and the calculated visual modulation of the auditory response (**F;** difference between the combined and auditory responses). In CSD contour plots, sinks are indicated by blue and cool colors. Units for color bars are $\mu A/mm^3$ throughout the manuscript. Scale bars (*vertical blue bars*) in top row of (**C–F**): 0.1 mV and 1 $\mu A/mm^3$. Vertical lines in bottom row of **(C)** mark stimulus onsets: *black,* auditory; *magenta,* visual. Most anatomical terminology adopted from Polley et al. (2007), except "Au1," "AuD," and "AuV," from Paxinos and Watson (2007). Cortical parcellation scheme in **(B)** adapted from Polley et al. (2007). Abbreviations: Au1, primary auditory cortex; AuV, secondary (ventral) auditory cortex; AuD, secondary (dorsal) auditory cortex; CPu, caudate putamen; LV, lateral ventricle; st, stria terminalis; fi, fimbria (hippocampus); Rt, reticular thalamic nucleus; ic, internal capsule; DLG, dorsal lateral geniculate nucleus; AAF, anterior auditory field; PAF, posterior auditory field; VAF, ventral auditory field; SRAF, suprarhinal auditory field.

following 15 min or more of the drug application *in vivo*. For animals in which we performed more than one recording session in a certain isoflurane concentration we averaged the LFP responses over the corresponding sessions.

Current source density (CSD) (Mitzdorf, 1985) of the averaged LFP responses were estimated using either the spline or delta inverse CSD method (Pettersen et al., 2006). Briefly, transmembrane currents flowing in neurons establish a time varying distribution of net current sources and sinks that constitutes a CSD distribution. These sources and sinks give rise to currents flowing in the extracellular space that are recorded as LFPs. Thus, the underlying CSD distribution can be calculated from LFP measurements, specifically by taking the second spatial derivative of the LFP measurements. Due to the relatively homogeneous geometry of neocortical tissue, when a linear electrode array is oriented perpendicularly to the cortical surface and LFPs are sampled at a fine enough spatial scale (inter-electrode spacing = 100 μm), the CSD distribution can be estimated using the standard solution technique as:

$$I_m = \frac{k * [\varphi(z + \Delta z) - 2\varphi(z) + \varphi(z - \Delta z)]}{\Delta z^2}$$

Where $\varphi(z)$ is the LFP measurement at depth z, Δz is the inter-electrode spacing, and k is a conductivity constant. Positive values of I_m correspond to net current sources, i.e., outward flowing current, and negative values correspond to net current sinks, i.e., inward flowing currents.

In order to determine the effect of anesthesia on the descending pathways, we calculated the difference between the response to a combined auditory + visual stimuli and the response to pure auditory stimuli for all five auditory stimuli presented in each experiment, then averaged the resulting five visual modulation responses (**Figure 1F**) and refer to it as the visual modulation response. This modulation response was nearly identical to the visual response alone, but because it could be derived from all five auditory stimuli presented, we recorded many more trials from which to calculate this response and it was often less noisy. Therefore, we used this visual modulation response for most analyses.

LFP responses *in vivo* were evaluated using the channel with the maximal peak response absolute value during the control period, and calculating the area under the peak response and above the significance line (average plus two standard deviation of the channel potential at rest). Response latency was calculated as the time from stimulus onset to 10% of the peak of the response.

Two types of measurements were derived from the CSD profile, one to measure the effect of isoflurane on the magnitude of the sink integral and one to measure the effect of isoflurane on the spatio-temporal response pattern. Response magnitude was calculated by first identifying the channel that displayed the maximal current sink within a pre-defined response window (*in vivo* auditory response: 10–100 ms post stimulus, search for maximum across all channels; *in vivo* visual modulation response: 20–300 ms after the visual stimulus, search for maximum across four deepest channels; slice TC and CC responses: 2–22 ms after the first stimulus in the 4 × 40 Hz train, search for maximum across all channels). Once the channel containing the peak CSD sink was identified, the CSD signal on this channel and the two channels immediately adjacent were thresholded (mean − 2 *SD*, computed over the pre-stimulus period) and integrated. To evaluate the effect of isoflurane on the spatio-temporal response pattern, the two-dimensional correlation coefficient of the CSD profile within the response window as defined above was calculated between the control (pre-drug) and drug and recovery conditions.

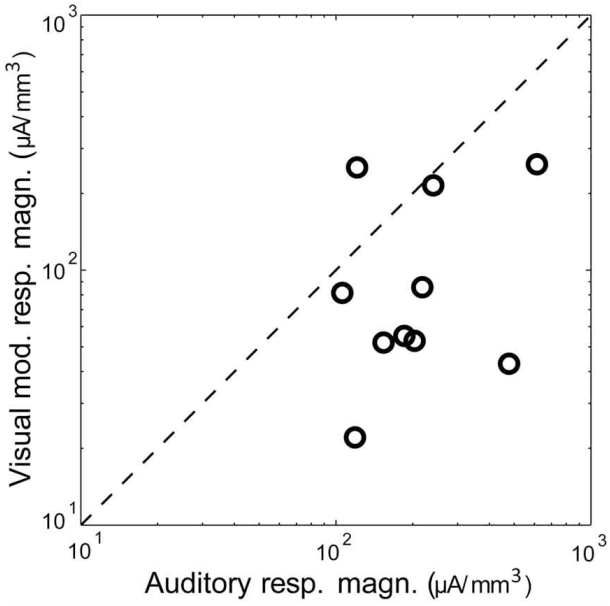

FIGURE 2 | Magnitude of auditory vs. visual modulation response. Shown is the magnitude (area under the significant peak, i.e., >mean + 2 *SD* of baseline) of the visual modulation response as a function of the auditory response in the same animal, recorded under control conditions. The diagonal is the identity line.

Statistical analysis

Statistical analyses were performed in SPSS (v22, IBM). To focus on the effects of isoflurane *per se* and not differences in response magnitude for different stimuli, the data were first normalized by dividing all the data across all conditions for each stimulus to the mean of the control data (across experiments) for that stimulus. For the *in vivo* LFP data of **Figure 4B** and the *in vivo* CSD sink data of **Figure 5C**, repeated measures analysis of variance ("GLM > Repeated Measures" in SPSS) was used to determine whether isoflurane had a differential effect on the auditory vs. visual modulation responses, with condition (control, drug, recovery) as the within-subjects factor and stimulus (auditory, visual) as the between-subjects factor. The reported ANOVA parameters (F statistic, *p*-value, and effect size) are on the condition * stimulus interaction term. The effect size presented is partial η^2, which ranges from 0 (i.e., no effect) to 1 and corresponds to the fraction of variance accounted for by this interaction after controlling for other sources of variability. Because for most animals the data were collected separately for each concentration of isoflurane, the analysis was run independently for each drug concentration and the significance level

was corrected for multiple comparisons to 0.017 (=0.05/3). For the cross correlation analysis of *in vivo* responses (**Figure 5D**), the control condition always has a value of 1, and thus we used paired Student's *t*-tests at each concentration, with the significance level corrected as above. For the brain slice data of **Figure 8**, experiments were typically conducted with five conditions (control, 0.5%, 1%, and 2% isoflurane, and recovery), but in 6 of 25 slices there were missing data points, either experiments in which only 1 or 2 of the isoflurane concentrations were tested ($n = 4$ slices) or experiments that terminated before recovery data could be obtained ($n = 2$ slices). These missing data points required a slightly different approach in SPSS, a linear mixed model analysis, to investigate the differential effect of isoflurane on TC vs. L1 and V2/L5 responses. Two approaches were used. For both approaches, because the results for the two CC stimuli were indistinguishable, these data were pooled and compared to TC responses. In the first, we analyzed the data using drug condition as a five level factor (**Figures 8A,B**), which allowed explicit comparisons at each isoflurane concentration by comparing the interaction term parameter estimates, i.e., the slopes on the fitted regression lines. As for the *in vivo* data, stimulus (TC, CC) was the between-subjects factor and the reported F statistic is on the condition * stimulus interaction term. In the second approach, we treated measured isoflurane concentration as a covariate (**Figures 8C,D**). Measured concentrations at nominal 0.5%, 1%, and 2% isoflurane for TC response data were 0.48 ± 0.035%, 1.0 ± 0.064%, and 2.0 ± 0.14% and for CC response data were 0.48 ± 0.068%, 0.99 ± 0.14%, and 2.0 ± 0.31%.

The LFP data of **Figure 4B**, and the sink integral data of **Figures 5C**, **8A** deviated significantly from normality (Kolmogorov–Smirnoff test, $p < 0.05$); log-transformation alleviated this problem, and the analysis was run on these log-transformed data. Zeros in the *in vivo* data (corresponding to cases where no significant sink was detected) were replaced by 10^{-3} for the statistical analysis only. The specific choice of this replacement value had no qualitative effect on the results of the analysis. No log transformation was necessary for the cross correlation data of **Figures 5D**, **8B**. Results are presented as mean ± *SD* for data that could be described by a normal distribution, and as median [1st quartile, 3rd quartile] for data that deviated significantly from normality.

RESULTS

IN VIVO ELECTROPHYSIOLOGY

The data presented here were obtained from 10 animals in which probes were localized to a primary auditory field (**Figures 1A,B**), probes penetrated at least to layer 5 (**Figure 1A**) and responses to both auditory and visual stimuli could be identified in the LFP (**Figure 1C**). Angles of entry were close to 0 degrees (i.e., normal to the surface) in both the dorsal-ventral and anterior-posterior dimension (mean ± *SD*: 3.5 ± 6.9° D-V, 2.5 ± 2.6° A-P).

Responses to auditory, visual, and bimodal stimuli

Pure tones at BF elicited large and well-timed LFP responses, which corresponded to a stereotypical CSD response profile (**Figure 1C**). Shortest latency of significant LFP responses (12.3 ± 2.2 ms) were observed in the middle layers (0.9 ± 0.3 mm), as expected for responses mediated by core TC afferents (Scheel, 1988; Roger and Arnault, 1989; Romanski and Ledoux, 1993; Winer et al., 1999; Polley et al., 2007; Storace et al., 2010; Smith et al., 2012). Brief, early sinks were also observed in the deepest layers, consistent with direct projections to layer 6 from the auditory thalamus (Huang and Winer, 2000; Smith et al., 2012), and consistent with previous reports (Szymanski et al., 2009; Constantinople and Bruno, 2013). Subsequent to these presumably monosynaptic TC sinks, activity spread to supra- and infragranular layers (**Figure 1C**).

Visual stimuli elicited long latency (∼50 ms), long lasting (∼250 ms) responses in primary auditory cortex, consistent with previous reports of multimodal responses in primary sensory cortex (Besle et al., 2009; Bizley and King, 2009; Doehrmann et al., 2010) (**Figure 1D**). Voltage amplitudes of visual responses were typically smaller than those of BF tones, but in some animals were comparable in size (**Figure 2**). CSD profiles typically had an alternating sink-source-sink pattern that was maximal in infragranular layers (**Figure 1D**). Visual stimuli presented before or simultaneous with auditory stimuli modulated auditory responses (**Figure 1E**). This modulation was mostly linear, and the visual modulation response, i.e., the difference between the paired and auditory alone responses (**Figure 1F**), was used for most subsequent analyses.

Effects of isoflurane on sensory responses in vivo

In order to determine isoflurane dose, we measured the minimal concentration required to achieve reliable LORR in 27 rats (including all the animals participating in this study). The LORR isoflurane dose was 0.86 ± 0.06%. We therefore used three isoflurane concentrations: sub-hypnotic (0.4%) in which the rats were active and responsive, just-hypnotic (0.8–0.9%) the dose in which LORR was obtained, and deep (surgical) anesthesia (1.6%).

Isoflurane had dose-dependent effects on ongoing activity in auditory cortex, but only modest effects on average evoked responses (**Figure 3A**). The most dramatic effect was burst-suppression (Hartikainen et al., 1995; Detsch et al., 2002), i.e., quiescence punctuated by spontaneous bursts, especially at 1.6% isoflurane (**Figure 3Aiv**). Spectral analysis of spontaneous activity showed enhancement of low frequency LFP components at lower doses of isoflurane and suppression of higher frequency components at 1.6% isoflurane (**Figure 3B**), as reported previously (Lukatch et al., 2005; Hudetz et al., 2011). Sensory stimuli also triggered burst responses that were indistinguishable from spontaneous bursts, as reported in visual cortex previously (Hudetz and Imas, 2007).

In **Figure 4A**, we show an example of the LFP responses to the auditory stimulus (left), combined stimulus (middle) and calculated visual modulation (right) under the different drug conditions recorded on one channel (1.4 mm depth). It can be seen that auditory LFP response are minimally affected by isoflurane whereas the visual modulation response is decreased. In order to quantify this effect we computed the response magnitude, defined as the area under the maximal peak of the LFP response for each animal (see Methods). As can be seen in the figure, the auditory response was mostly unchanged by sub-hypnotic dose, and increased by larger doses. The visual modulation

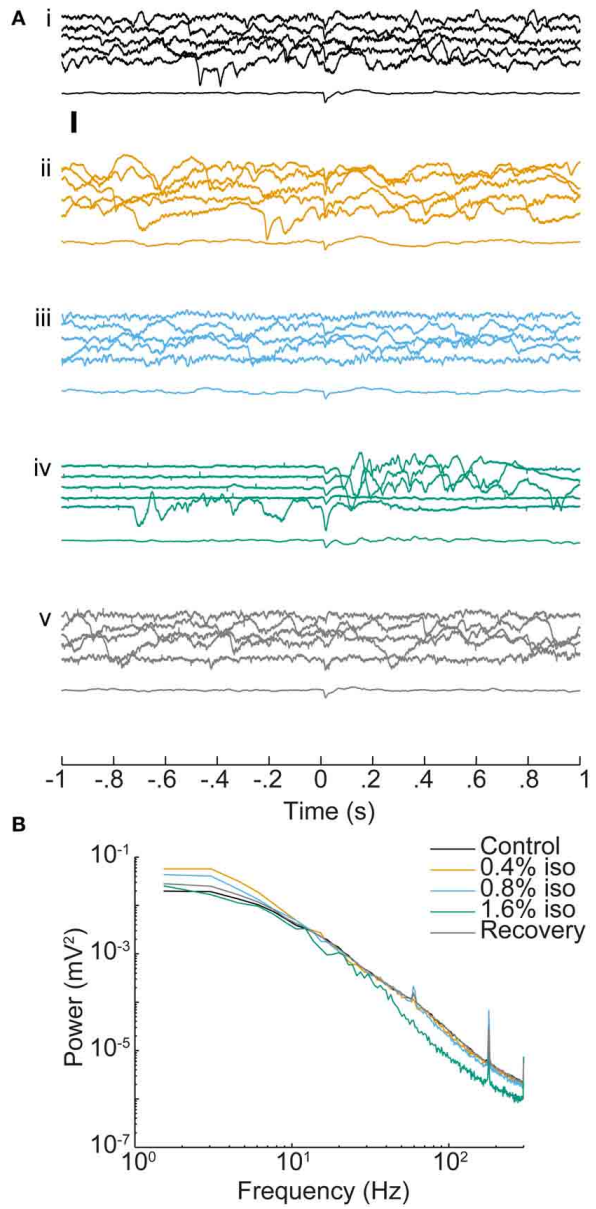

FIGURE 3 | Effect of isoflurane on spontaneous and sensory evoked responses in auditory cortex. (A) LFPs recorded from one electrode (depth = 1 mm) during control conditions **(i)**, under increasing doses of isoflurane (**ii–iv**) and during recovery **(v)**. In each set, the top five traces are consecutive single trial LFPs and the bottom trace is the average of 20 responses. Stimulus onset is at $t = 0$ and was a BF tone at 60 dB SPL. Note the appearance of burst-suppression at 1.6% isoflurane and the occurrence of both spontaneous and stimulus-evoked bursts. Scale bar: 1 mV. **(B)** Mean power spectra of pre-stimulus activity derived from the animal in **(A)**. Spectra are the average single trial spectra of 220 trials under each drug condition, and control and recovery traces are averaged across three experiments.

magnitude, on the other hand, decreased under sub-hypnotic and just-hypnotic doses. The effect on the magnitude of the auditory and the visual modulation responses (calculated separately at each concentration; **Figure 4B**) was significantly different at the sub-hypnotic and just-hypnotic isoflurane concentrations [0.4% iso: $F_{(2,\ 28)} = 7.32$, $p = 0.0105$, partial $\eta^2 = 0.343$; 0.8% iso: $F_{(2,\ 36)} = 8.71$, $p = 0.0114$, partial $\eta^2 = 0.326$; 1.6% iso: $F_{(2,\ 32)} = 1.63$, $p = 0.214$, partial $\eta^2 = 0.0926$; repeated measures ANOVA; see Methods]. *Post-hoc* tests for the sub-hypnotic and just-hypnotic cases showed significant differences between auditory and visual modulation responses for the drug condition but not the control or recovery conditions ($p = 0.0185$ and $p = 0.00278$ for 0.4% and 0.8–0.9%, respectively). The paradoxical increase at the highest concentration of isoflurane was due to late bursting activity elicited by the visual stimulus, as previously reported in visual cortex (Imas et al., 2004, 2005b). At this concentration, burst suppression was observed in the ongoing cortical activity, and sensory stimuli of both modalities often triggered burst responses. However, as visual stimuli triggered bursts more frequently than auditory stimuli, the response magnitude of the visual response increased to a greater extent in this condition.

The effects of isoflurane on CSD responses in auditory cortex were modality specific, with greater suppression of visual modulation responses at sub-hypnotic and just-hypnotic isoflurane concentrations (**Figure 5**). We used two measures to quantify the effect of isoflurane on CSD responses. First, to measure the effect of isoflurane on the magnitude of the response, we calculated the integral of the major current sink for each stimulus under control conditions (see Methods), and compared this measurement to the integral of the current sink at the same spatial location and time window under isoflurane and upon recovery. Second, to measure the effect of isoflurane on the spatio-temporal pattern of the response, we computed the averaged CSD responses under control conditions, and calculated the 2-dimensional correlation coefficient between this control response and the drug response ($C(ctrl,drug)$), within standardized response windows.

Using both measures, isoflurane had a greater effect on visual modulation compared to auditory responses (**Figures 5C,D**). Auditory responses were largely unaffected at 0.4% isoflurane (median ratio of drug to control [1st quartile, 3rd quartile]: 1.13 [0.317, 1.54]), and enhanced at 0.8% and 1.6% (1.84 [0.759, 3.53] and 1.91 [0.965, 8.66], respectively), whereas visual modulation responses were suppressed at 0.4% and 0.8% and enhanced at 1.6% (0.0245 [0.00, 0.622], 0.010 [0.00, 0.459] and 6.09 [3.41, 12.2], respectively). There was a significant difference in the effect of isoflurane on the sink area of visual modulation vs. auditory responses at 0.4% and 0.8 – 0.9%, but not at 1.6% isoflurane [**Figure 5C**; 0.4% iso: $F_{(2,\ 28)} = 6.22$, $p = 0.00583$, partial $\eta^2 = 0.308$; 0.8–0.9% iso: $F_{(2,\ 36)} = 7.96$, $p = 0.00553$, partial $\eta^2 = 0.307$; 1.6% iso: $F_{(2,\ 32)} = 1.04$, $p = 0.355$, partial $\eta^2 = 0.0610$; repeated measures ANOVA]. *Post-hoc* tests for the sub-hypnotic and just-hypnotic cases showed significant differences between the auditory and visual modulation responses for the drug condition but not the control or recovery conditions ($p = 0.00318$ and $p = 0.00912$ for 0.4% and 0.8–0.9%, respectively). Differential effects of isoflurane on auditory vs. visual modulation responses were also observed for the correlation coefficient, though the effect reached statistical significance only at the just-hypnotic concentration [**Figure 5D**; mean ± *SD C(ctrl,drug)* for 0.4% iso: aud, 0.64 ± 0.22; vis mod, 0.20 ± 0.29, $p = 0.0500$; for 0.8–0.9% iso: aud, 0.65 ± 0.11; vis, 0.054 ± 0.32, $p = 0.00122$; for 1.6%

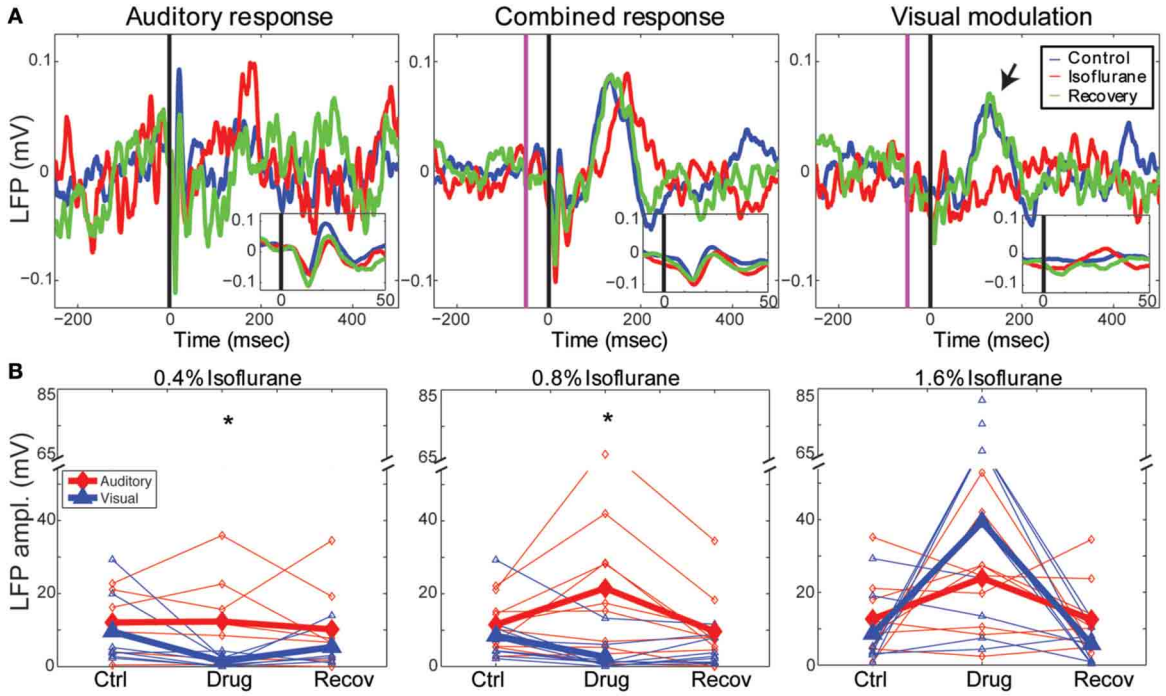

FIGURE 4 | Effects of isoflurane on auditory and visual responses. **(A)** Single channel LFP responses to a 50 ms best-frequency tone burst (17.4 kHz, 60 dB SPL) at $t = 0$ *(left)*, combined stimulation, i.e., 1 ms LED flash preceding the same tone burst by 65 ms *(middle)* and the calculated visual modulation response (difference between the combined response and the auditory; *right)*. *Blue*: control; *red*: 0.8% isoflurane; *green*: recovery. *Insets* show early response components on expanded time scale. Note visual modulation response component between $t = 100$ and 200 ms (*arrow*) that is suppressed by isoflurane. **(B)** Summary of drug effects across animals. Plotted are LFP magnitude (area under the peak LFP response) of auditory (blue) and modulation (red) responses under 0.4% (*left*), 0.8–0.9% (*middle*) and 1.6% isoflurane (*right*). *Open symbols*: individual animals; *closed symbols*: mean across animals. $^*p < 0.05$, repeated measures ANOVA.

iso: aud, 0.38 ± 0.31; vis mod, -0.26 ± 0.29, $p = 0.0192$; paired Student's t-tests]. As for the LFP data of **Figure 4B**, the paradoxical increase in sink magnitude at 1.6% isoflurane was due to long-latency bursting elicited by visual and auditory stimuli during burst suppression.

BRAIN SLICE ELECTROPHYSIOLOGY

We have shown that isoflurane suppresses visual modulation of auditory responses recorded in primary auditory cortex *in vivo* to a greater extent than auditory responses. This modality-specific effect could be due to selective and local effects on synapses in auditory cortex carrying visual (from higher-order cortical areas and non-specific thalamus) vs. auditory (specific thalamic) information. Alternatively, isoflurane could have a greater effect on the sources of visual vs. auditory input to auditory cortex, with these effects reflected indirectly in our recordings. To examine whether isoflurane can produce this effect at the level of the auditory cortex independently of the effects on upstream areas, we investigated the effects of isoflurane on TC and CC responses in auditory cortical brain slices (**Figure 6**).

CSD responses to TC, L1, and V2/L5 stimulation

We measured extracellular LFP responses in brain slices of auditory cortex to afferent stimulation using multi-channel electrode arrays in two different brain slice preparations. In TC slices ($n = 10$ slices) (Cruikshank et al., 2002; Verbny et al., 2006), we stimulated TC afferents and compared these responses to stimulation of CC afferents in L1 (**Figures 6A,C, 7A,B**). As we and others have shown previously (Cruikshank et al., 2002; Verbny et al., 2006), stimulation of the fiber pathway just rostral to the medial geniculate in auditory TC brain slices triggered short latency (2.3 ± 0.7 ms), presumably monosynaptic LFP responses that corresponded to current sinks in granular layers (**Figure 6C**). The spatial location of this short latency sink was similar to the initial current sink observed in middle layers *in vivo* in response to auditory stimuli.

To activate CC fibers, in 8 of these 10 TC slices we stimulated in layer 1 approximately 0.5–1 mm rostral to the recording site (**Figure 6A**). The spatial CSD profile of the responses to stimulation in layer 1 consisted of a short latency (5.9 ± 1.9 ms), presumably monosynaptic current sink. In most slices (7/8) this early sink was maximal in the supra-granular layers (4/8 in layer 1–2, 3/8 in layer 2–3; **Figure 7A**), consistent with the known anatomy of these fibers and with previous reports (Cauller and Connors, 1994). In one slice L1 stimulation elicited an early current sink in layer 5 (not shown). We note that the spatial profiles of these responses are distinct from the response to TC stimulation.

Responses were examined in coronal slices as well ($n = 7$ slices; **Figure 6B**), in which we were able to better isolate CC from the

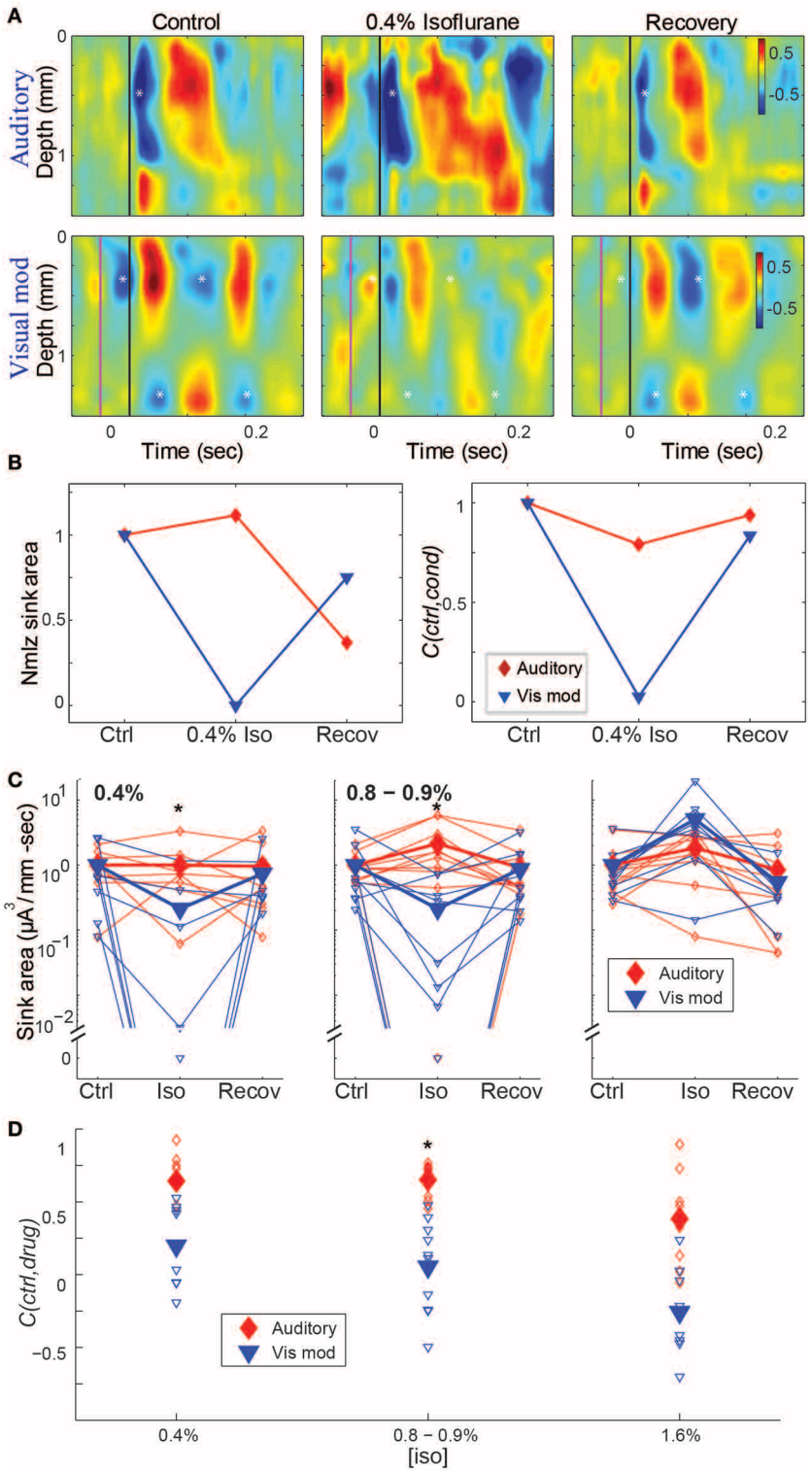

FIGURE 5 | Effect of isoflurane on spatiotemporal activity patterns in auditory cortex. (A) CSD profiles of responses recorded in one animal to an auditory stimulus (50 ms tone, 17.4 kHz, 40 dB SPL) alone (*top*) and visual modulation of the auditory response (*bottom*) recorded in room air (*left*), 0.4% isoflurane (*center*) and recovery (*right*). Note early auditory response component (*asterisk*) that is relatively unaffected by isoflurane, and alternating supra- and infragranular sinks during visual modulation response (*asterisks*) that are suppressed by isoflurane. In *center* and *right* panels, asterisks are plotted at the same relative positions as in *left* panel. **(B)** Normalized response magnitude (*left*; normalized to the average of the control values) and correlation coefficient between control and drug and recovery responses ($C(ctrl,cond)$) for the data in **(A)** (*red*: auditory; *blue*: visual modulation). **(C–D)** Summary across animals. Magnitude

(Continued)

FIGURE 5 | Continued
(C) and correlation coefficient **(D)** of the auditory (*red*) and visual modulation (*blue*) responses under different isoflurane concentrations. *Open symbols*: single animals; *filled symbols*: average across animals. $^*p < 0.05$, repeated measures ANOVA, in **(C)** and $p < 0.017$, paired Student's *t*-test, in **(D)**.

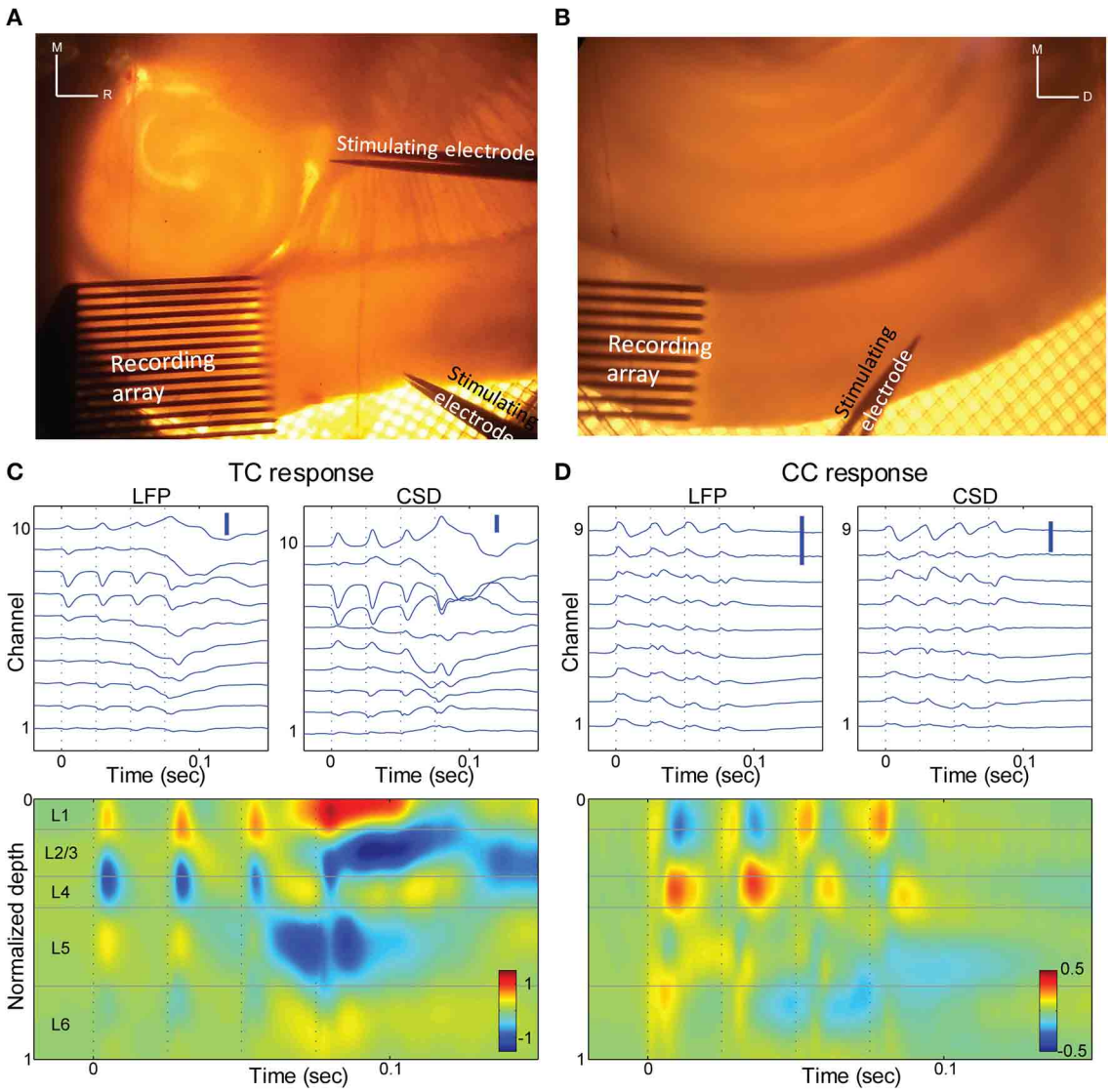

FIGURE 6 | Thalamo-cortical and cortico-cortical responses in brain slices. (A) Photomicrograph of a TC slice. Recording array is in auditory cortex, and stimulating electrodes are in the TC afferent bundle and in layer 1 of a proximal cortical region. For scale reference, inter-electrode spacing in the recording array is 100 μm. **(B)** Photomicrograph of a coronal slice. Recording array is in auditory cortex, and stimulating electrodes in upper layer 5 of area V2. **(C)** LFP responses at different depths (*top left*) and derived CSD (*top right; bottom*) in response to a train of 4 × 40 Hz stimuli of the TC fibers. Same slice as in **(A)**. Only electrodes that were in the cortex are shown and were used for further calculations. Scale bars 0.1 mV and 1 μA/mm^3. **(D)** Similar to **(C)**, but for stimulation of V2 in layer 5. Same slice as in **(B)** Scale bars 0.1 mV and 1 μA/mm^3.

non-specific TC fibers that also travel in L1. In this preparation, slices were prepared that preserved the descending CC projection from extrastriate visual cortex (V2) to primary auditory cortex, as previously described (Banks et al., 2011). To activate V2, we stimulated in L5, where descending projection cells are concentrated (Felleman and Van Essen, 1991). The CSD response profile to V2 stimulation was again distinct from the TC response profile, with prominent short-latency (5.2 ± 2.0 ms), presumably monosynaptic current sinks observed either in infragranular layers (4/7 slices) or in the superficial layers (3/7 slices) (**Figure 6D**), as for L1 stimulation in TC slices. The latencies of the early TC evoked sinks were shorter than those of the different CC responses ($p < 0.001$, unpaired Student's *t*-test for both TC to L1 and TC to V2 comparisons), whereas there was no significant difference

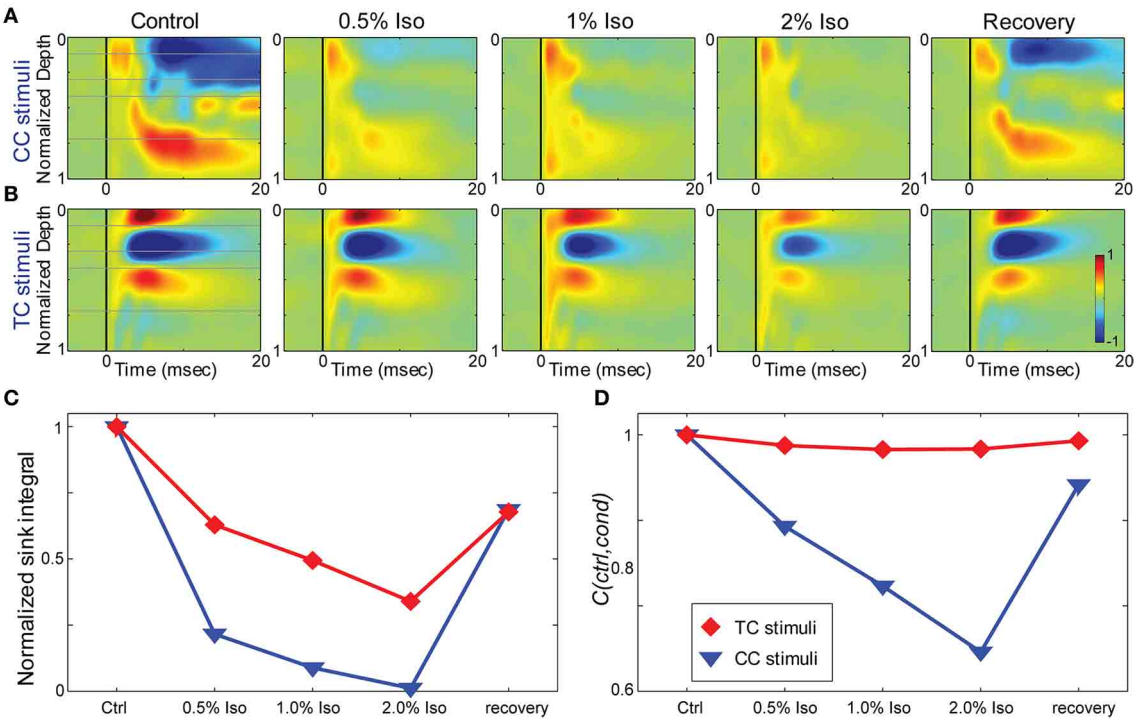

FIGURE 7 | Effects of isoflurane on synaptic responses in brain slices. **(A,B)** CSD response to a L1 stimulus **(A)** and TC stimulus **(B)** in the same TC slice under increasing isoflurane doses (left to right: control, 0.5%, 1%, 2% and recovery). **(C)** Magnitude of the response (area under the maximal sink in response to the first stimulus in the train, normalized to the average of the control and recovery responses) for the data in **(A)** (*blue*) and **(B)** (*red*). **(D)** Correlation coefficient between the control response and each drug condition for the data in **(A,B)**; color code as in **(C)**.

between the latencies of the two CC responses ($p = 0.497$, unpaired Student's *t*-test).

TC and CC afferent stimuli could also trigger longer latency polysynaptic activation of supra- and infragranular layers. This activity originated in layer 5 and often spread to more superficial layers (e.g., the late current sink in layer 5 at ∼0.055 s in **Figure 6C**, *bottom*), and appeared as all-or-none network bursts; shorter latencies to polysynaptic activity were observed with higher stimulation strength or the presence of multiple stimuli in a train. This polysynaptic activity has been observed previously in auditory, visual, and somatosensory brain slice preparations (Metherate and Cruikshank, 1999; Sanchez-Vives and McCormick, 2000; Cruikshank et al., 2002; Maclean et al., 2005; Watson et al., 2008; Rigas and Castro-Alamancos, 2009), where it has been shown to be non-epileptiform in nature and represent an *in vitro* correlate of UP states that occur *in vivo* (Sanchez-Vives and McCormick, 2000; Shu et al., 2003; Cunningham et al., 2006; Rigas and Castro-Alamancos, 2007).

Effects of isoflurane on electrophysiological responses in brain slices

To determine whether the effects of isoflurane observed *in vivo* could be accounted for by local effects of the drug in auditory cortex, we applied isoflurane dissolved in ACSF to brain slices and measured the effects on CSD responses to stimulation of TC and CC (L1 and V2/L5) pathways. Three concentrations of isoflurane were applied (0.5%, 1%, and 2%), corresponding approximately to the three concentrations employed *in vivo* after taking into account loss of isoflurane gas in the recording chamber (see Methods). Examples of the effect of isoflurane on short latency synaptic responses can be seen in **Figure 7**, which we focus on for all further analysis. Polysynaptic activity driven by both TC and CC stimuli were suppressed by isoflurane (not shown). Consistent with our observations *in vivo*, bath application of isoflurane suppressed short latency L1 and V2/L5 responses in brain slices to a greater extent than TC responses. As for the *in vivo* data, we measured the change in the response strength using the sink integral and the response pattern using the 2-D correlation coefficient. Although isoflurane reduced the magnitude of both TC and CC sink integrals, it had a significantly greater effect on CC responses compared to TC responses at 1% and 2% isoflurane (**Figures 8A,C**). Because the effects of isoflurane on L1 and V2/L5 responses were indistinguishable, we pooled these data and compared to the effects on TC responses. We found that the sink integral was suppressed by isoflurane to a greater extent at each concentration tested (TC vs. CC median ratio of drug to control [1st quartile, 3rd quartile] at 0.5% iso: 0.836 [0.656, 1.06] vs. 0.616 [0.379, 0.784]; 1% iso: 0.737 [0.521, 0.856] vs. 0.379 [0.248, 0.506]; 2% iso: 0.356 [0.312, 0.649] vs. 0.088 [0.0400, 0.281]). Statistical analysis using a linear mixed model (see Methods) to compare the effects of isoflurane on TC vs. CC responses found a significant effect overall using drug condition as a categorical factor [$F_{(4,\ 82.4)} = 9.07$, $p = 4.00\text{e-}6$], with significant differences in the interaction terms at 1% and 2% isoflurane

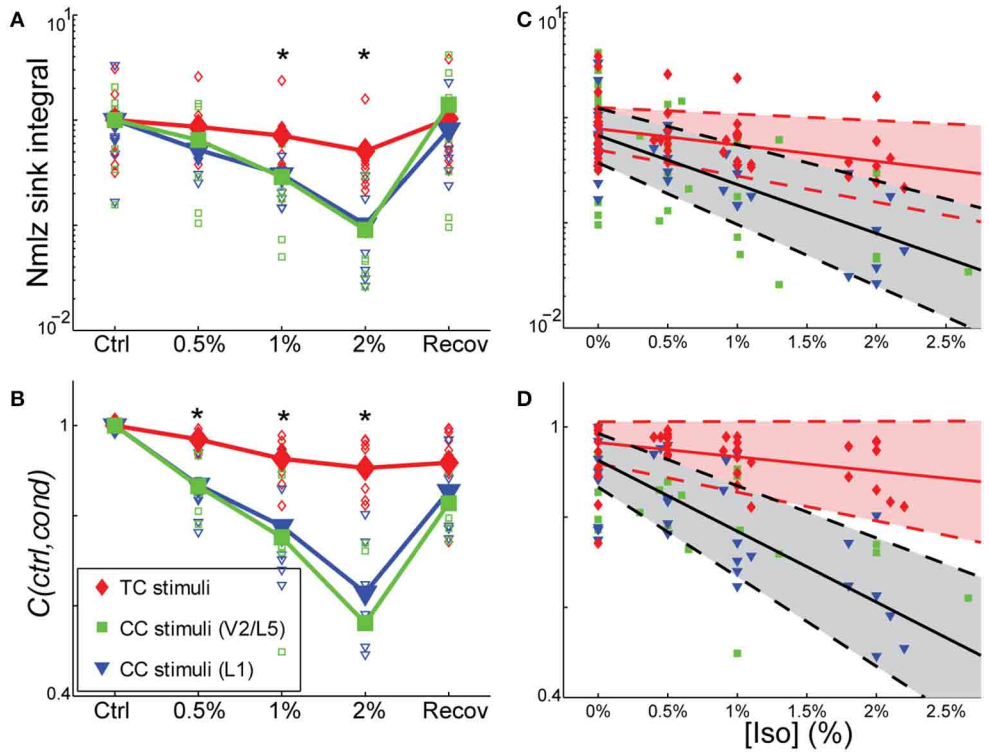

FIGURE 8 | Differential sensitivity of CC vs. TC pathways to isoflurane. **(A,B)** Effect of isoflurane on sink integral **(A)** and 2D-cross correlation **(B)** of responses to TC (*red*), V2\L5 (*blue*), and layer 1 (*green*) stimuli under increasing isoflurane concentrations (left to right: control, 0.5%, 1%, 2% and recovery). Open marks represent single slices and filled marks represent the average. **(C,D)**. Linear mixed model fits to sink integral **(C)** and 2D-cross correlation **(D)** of responses to TC and CC stimuli plotted as function of actual measured isoflurane concentration. Shaded areas (*red*: TC; *gray*: CC) represent 95% confidence bounds for the model fits. Note the similarity in the effects of isoflurane on responses to the two types of CC stimuli (obtained in two different slice preparations), whereas the TC response is much less affected. $^*p < 0.05$, repeated measures ANOVA.

[$t_{(-2.88)}$, $p = 5.023\text{e-}3$ and $t_{(-5.34)}$, $p = 8.17\text{e-}7$, respectively]. Similar results were obtained when measured isoflurane concentration was included as a covariate [instead of drug condition as a factor; $F_{(1,\ 88.7)} = 26.2$, $p = 2.00\text{e-}6$; slopes and 95% confidence intervals for the stimulus * [iso] terms were −0.155 [−0.248, −0.062] for TC and −0.465 [−0.580, −0.345] for CC]. Converting back from logarithmic units, this tells us that the slope of the iso effect on the TC response was about −30% change/unit % isoflurane, compared to a slope of >−65% change/unit % isoflurane for the CC response, i.e., a suppressive effect that is more than twice as strong for CC vs. TC responses.

Similar effects on the response pattern were observed by measuring the response window correlation coefficient, but in this case significant differences between effects on TC and CC responses were observed at all three concentrations of isoflurane (**Figures 8B,D**; mean ± *SD C(ctrl,drug)* for TC vs. CC at 0.5% iso: 0.97 ± 0.020 vs. 0.87 ± 0.069; 1% iso: 0.93 ± 0.050 vs. 0.77 ± 0.13; 2% iso: 0.91 ± 0.061 vs. 0.60 ± 0.15). Statistical analysis showed a significant effect overall using drug condition as a categorical factor [$F_{(4,\ 83.2)} = 19.2$, $p = 3.30\text{e-}11$], and significant effects at all three concentrations of isoflurane [effects on interaction term for 0.5% iso: $t_{(-2.97)}$, $p = 3.94\text{e-}3$; 1% iso: $t_{(-4.58)}$, $p = 1.6\text{e-}5$; 2% iso: $t_{(-8.30)}$, $p = 1.56\text{e-}12$]. Similar results were obtained when measured isoflurane concentration was included as a covariate [instead of drug condition as a factor; $F_{(1,\ 90.5)} = 36.5$, $p = 3.38\text{e-}8$; slopes and confidence intervals for the stimulus * [iso] terms were −0.0316 [−0.0637, 0.000545] for TC and −0.156 [−0.199, −0.115] for CC]. Thus, the slope of the iso effect on the TC response was about −7% change/unit % isoflurane, compared to a slope of >−30% change/unit % isoflurane for the CC response, i.e., an effect that is more than four times as strong for CC vs. TC responses.

Although the magnitude of CC responses was on average smaller than TC responses under control conditions, the larger magnitude of the TC response did not play a role in the differential effect of isoflurane. This can be seen in plots of the ratio of the response under each drug condition to the control response as a function of the control response magnitude (**Figure 9**). Larger effects of isoflurane would manifest as scatter plots with positive slopes; by contrast, in all cases the data exhibited significant negative slopes (not shown), indicating that stronger responses had a slight tendency to be more suppressed by isoflurane.

The observation that isoflurane decreases the magnitude of synaptic current sinks in brain slices suggests a local action of isoflurane on the TC network. Previous studies have demonstrated that volatile anesthetics can suppress synaptic responses

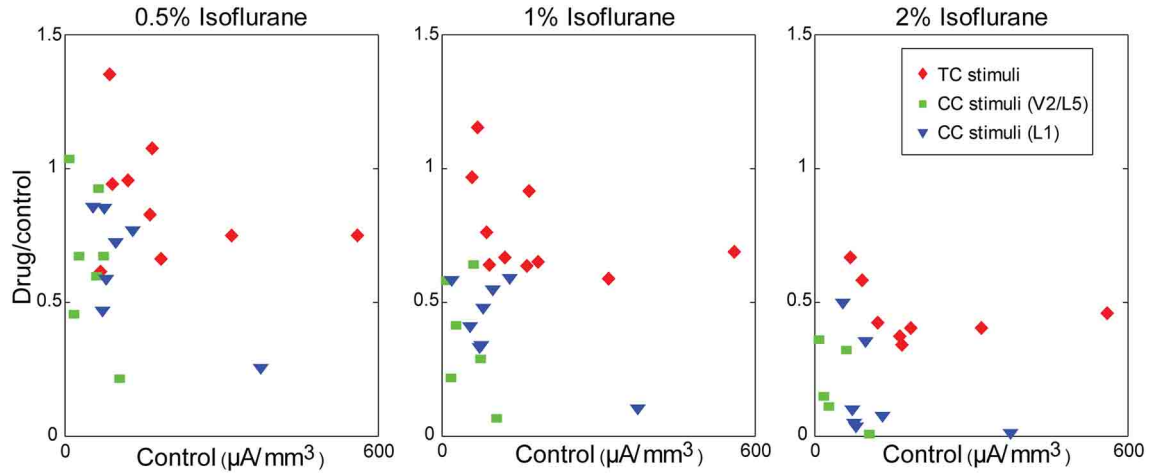

FIGURE 9 | Modulation of synaptic responses in slices by isoflurane is independent of control response magnitude. Ratio of the response in drug to the response in control, plotted as a function of the control response magnitude, at different isoflurane concentrations (left to right: 0.5%, 1%, 2%). Note the dose-dependency of the isoflurane effect (i.e., compare across panels), but that small responses within any given panel are not more affected by isoflurane than large responses.

by acting presynaptically to reduce neurotransmitter release (Perouansky et al., 1995; Maciver et al., 1996; Kirson et al., 1998). One possible mechanism for the differential effects of isoflurane observed here is greater sensitivity of CC synaptic terminals in supra- and infragranular layers to such suppressive effects compared to TC synaptic terminals in granular layers. We investigated this issue by evaluating effects of isoflurane on short-term plasticity of responses to TC, L1, and V2/L5 stimulation by presenting trains of stimuli at 40 Hz. Under control conditions, TC pathways exhibited short-term depression, whereas L1 and V2/L5 exhibited a wide range of plasticity including both facilitation and depression (**Figures 10A,B**—left column). The short-term plasticity in the L1 and V2/L5 responses was indistinguishable, and to examine the effect of isoflurane these data were pooled together. Interestingly, we observed that the isoflurane effect on short-term plasticity was minimal in both TC and CC pathways. Statistical analysis of the ratio of the fourth to first response in the 4 × 40 Hz train indicated no effect of drug condition [TC: $F_{(4,\ 28)} = 0.716$, $p = 0.428$, partial $\eta^2 = 0.093$; CC: $F_{(4,\ 36)} = 1.368$, $p = 0.280$, partial $\eta^2 = 0.132$; repeated measures ANOVA run separately for TC and CC stimuli, within-subjects factor = condition (control, 0.5%, 1%, 2%, recovery)]. These data suggest that changes in release probabilities as manifested in short-term plasticity (Del Castillo and Katz, 1954; Zucker, 1989) do not play a major role in the effects of isoflurane.

DISCUSSION

PATHWAY-SPECIFIC ACTIONS OF ISOFLURANE

We have shown that LFP responses in auditory cortex to visual vs. auditory and CC vs. TC inputs are differentially modulated by the general anesthetic isoflurane. We distinguished bottom-up responses to acoustic stimuli *in vivo*, driven largely by ascending thalamic input from MGv (based on the laminar profile of current sinks), as well as responses *in vitro* to direct stimulation of the TC fiber pathway, and compared these to "top-down" responses, such as responses to visual stimuli *in vivo*, driven largely by descending CC and matrix thalamic input, as well as CC responses *in vitro* to stimulation in V2/L5 and L1. Isoflurane suppressed visual and CC responses to a greater extent than auditory and TC responses in auditory cortex, consistent with reports of differential effects on bottom-up vs. top-down connectivity derived from EEG and imaging data in humans (Imas et al., 2005a; Peltier et al., 2005; Alkire, 2008; Lee et al., 2009, 2013b; Ku et al., 2011; Liu et al., 2011; Schrouff et al., 2011; Boly et al., 2012). Our observations *in vitro* indicate that the effects of isoflurane observed *in vivo* can be accounted for largely by local, pathway-specific actions of isoflurane in auditory cortex. Results were remarkably consistent between V2/L5 and L1 stimulation in the two different slice preparations investigated (**Figure 8**), suggesting that the observed suppression of synaptic responses generalizes across multiple CC pathways. One difference between the results *in vivo* and *in vitro* that merits further investigation was that we observed a greater suppressive effect of isoflurane on TC responses in brain slices compared to auditory responses *in vivo* (see below). Although responses to CC stimuli were in general smaller than those to TC stimuli at comparable stimulation intensity, the differential effect of isoflurane cannot be explained simply by the magnitude of the synaptic response, i.e., greater suppression of smaller responses, as we observed no relationship between the effect of isoflurane and the magnitude of the response under control conditions (**Figure 9**).

CSD RESPONSES UNDER CONTROL CONDITIONS

Within a cortical column, the laminar segregation of synaptic terminals arising from afferent fibers as well as intra-columnar connections results in specific spatio-temporal patterns of activity that vary with the input fiber pathway engaged (Felleman and Van Essen, 1991). Responses to acoustic stimuli and to stimulation of core TC fibers elicited current sinks with largest amplitude and shortest latency in middle layers (**Figure 1C**), consistent with

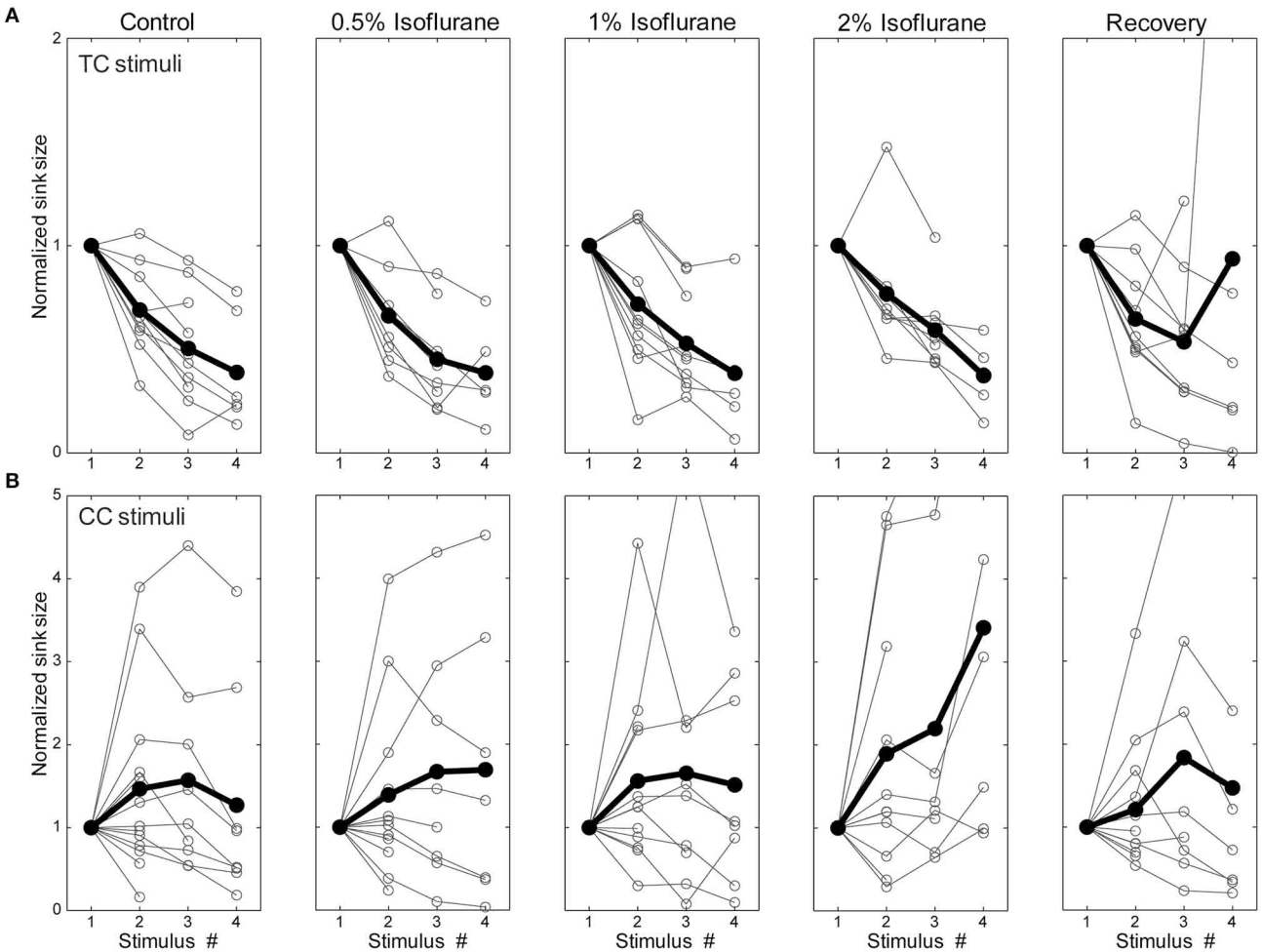

FIGURE 10 | Short-term plasticity was not changed by isoflurane. Synaptic current sink magnitude during a 4 × 40 Hz train normalized to the response to the first stimulus in the train under different isoflurane concentrations (left to right: control, 0.5%, 1%, 2%, and recovery) for TC **(A)** and CC **(B)** stimuli. Horizontal axis is the stimulus number within the train. Note that although trains of 4 stimuli were presented in all experiments, only sinks that differed significantly from baseline (i.e., >mean + 2 *SD*) are plotted in the figure. It can be seen that TC stimulation always displayed short-term depression whereas CC stimulation could display either depression or facilitation. However, isoflurane did not affect this short-term plasticity.

highest thalamic synaptic terminal density in granular layers 3 and 4 (Shi and Cassell, 1997; Huang and Winer, 2000; Smith et al., 2012). A secondary current sink of similar latency was sometimes observed in the deepest layers, consistent with the observed secondary projection of MGv to layer 6 (Smith et al., 2012). Similar CSD patterns have been observed previously in auditory cortex *in vivo* and *in vitro* (Cruikshank et al., 2002; Kaur et al., 2005; Lakatos et al., 2005; Szymanski et al., 2009).

In contrast to the CSD pattern elicited by TC stimulation, responses to CC stimuli were dominated by current sinks in either supra- (**Figures 6B**, **7A**) or infragranular (not shown) layers. This sink/source pattern was complementary to that elicited by TC stimulation, analogous to the complementary nature of TC vs. CC afferent terminal density patterns (Smith et al., 2010, 2012; Banks et al., 2011), and is consistent with these stimuli engaging different afferent fiber pathways. Complimentary activation patterns have been observed in auditory cortex for acoustic and non-acoustic sensory stimulation previously (Lakatos et al., 2007, 2009).

Several papers have indicated that visual stimuli and eye movements can elicit responses on their own or alter responses to auditory stimuli in auditory cortical areas including primary auditory cortex (Fu et al., 2004; Besle et al., 2009; Bizley and King, 2009). The anatomical projections carrying visual information to auditory cortex terminate with highest density in supra- and infragranular layers (Miller and Vogt, 1984; Budinger et al., 2006; Bizley et al., 2007; Smith et al., 2010) in a classically top-down/modulatory pattern (Felleman and Van Essen, 1991; Shi and Cassell, 1997; Kimura et al., 2004). Cortical descending projections are postulated to carry expectation- and memory-based predictive information to be integrated with ascending sensory information (Bar, 2009; Bastos et al., 2012). Recent experimental observations (Covic and Sherman, 2011; De Pasquale and Sherman, 2011) and theoretical considerations (Bastos et al.,

2012) suggest that these inputs may be both modulatory and driving. We found that the response to a combined auditory-visual stimuli was well-described by the linear sum of the two separate responses. Although some previous studies have shown super-additive effects of somatosensory and auditory inputs to auditory cortex (Ghazanfar et al., 2005; Lakatos et al., 2007), these effects were observed for near-threshold stimuli, whereas higher intensity stimuli, similar to what we employed in this study, were simply additive, as seen in our data (inverse effectiveness phenomenon).

Responses in slices were dominated by early, putatively monosynaptic current sinks that were of limited extent spatially and temporally, followed by late, burst responses reminiscent of UP state activity reported previously in cortical slices (Metherate and Cruikshank, 1999; Sanchez-Vives and McCormick, 2000; Cruikshank et al., 2002; Maclean et al., 2005; Watson et al., 2008; Rigas and Castro-Alamancos, 2009; Wester and Contreras, 2012). By contrast, CSD responses *in vivo* exhibited intermediate latency current sinks in supra- and infragranular layers and likely reflected polysynaptic sensory responses within the cortical column. Responses to visual sensory stimuli in auditory cortex *in vivo* and CC (V2/L5 and L1) stimulation in brain slices were less similar (compare **Figures 1D** and **6D**), in that the latency and duration of visual responses were much longer than V2/L1 responses in slices, and sinks *in vitro* were confined to either the supra- or infragranular layer (usually the former), whereas *in vivo* we observed an alternating sink/source pattern that was most pronounced in the infragranular layers, and often alternated between infra- and supragranular layers (**Figures 1D,F**). These differences are not unexpected given the different stimulation paradigms utilized. Visual stimuli *in vivo* evoke long-latency responses in auditory cortex (Bizley et al., 2007; Kayser et al., 2008; Schroeder et al., 2008) due to slow transduction in the retina as well as the circuitous synaptic pathway carrying visual information to auditory cortex. The accumulated jitter in the latencies of visual thalamic and cortical cells will distribute temporally responses *in vivo*. By contrast, in our slice experiments, electrical stimulation of L1 or V2/L5 fiber pathways synchronously activated cells and fibers with monosynaptic, short distance projections to auditory cortex, resulting in shorter latency, less dispersed responses.

We used two different species for our recordings *in vivo* and brain slices. The reason for this was a practical one. The TC slice preparation has only been described for mice, and thus rats are unsuitable for the brain slice experiments. However, for *in vivo* recordings we wished to have both the LED mount and the 16-channel connector cemented into the animal's headcap, and the skulls of mice did not provide sufficient surface area to achieve this easily whereas rats' skulls did. Besides for the broad similarities apparent in cortical anatomy and physiology (Ehret, 1997; Stiebler et al., 1997; Kaur et al., 2005), we have shown that one of the afferent pathways central to the current study, the projection from V2 to A1, exhibits remarkable similarity between the two species (Smith et al., 2010; Banks et al., 2011). However, it is possible that subtle differences in connectivity and response properties in the two species contributed to some of the differences between our results *in vivo* and in brain slices.

MODULATION OF RESPONSES BY ISOFLURANE

Several recent studies have emphasized the roles of brainstem and midbrain nuclei in acting as switches that control the arousal level and hypnotic effects of anesthetic agents (Devor and Zalkind, 2001; Nelson et al., 2002; Alkire et al., 2007; Langsjo et al., 2012; Solt et al., 2014), but there is overwhelming evidence that consciousness itself is a phenomenon of the cortico-thalamic network (Llinas et al., 1998; Crick and Koch, 2003; Tononi, 2004; Alkire et al., 2008b; Mashour, 2013). Anesthetic actions on nuclei involved in arousal and the sleep/wake cycle are likely to constitute on/off switches whose effects are mediated through actions in the cortico-thalamic network. The results presented here, as well as recent study demonstrating layer- and area-specific effects of anesthesia in cortex (Sellers et al., 2013), will aid in understanding mechanistically how actions in the cortico-thalamic network can mediate changes in consciousness.

Early studies on anesthetic modulation of cortical responses to auditory stimuli reported a reduction and slowing of field potentials recorded at the surface by several classes of anesthetic agents at surgical (i.e., higher than just-hypnotic) doses (Schwender et al., 1993b,c, 1994). These results indicated that the magnitude of mid-latency auditory evoked responses, which derive at least in part from activation of auditory cortex (Milner et al., 2014), could be used to predict the extent of verbal memory retention under anesthesia. Similar results have been obtained more recently in imaging studies in humans, which have shown general anesthetics suppress auditory cortical fMRI BOLD signals in response to musical or speech stimuli (Dueck et al., 2005; Kerssens et al., 2005; Plourde et al., 2006). Interestingly, decreased BOLD responses, and impaired memory, are observed even at sub-hypnotic doses, and thus may reflect effects on higher order cortical processing related to memory formation rather than stimulus identification *per se*. Consistent with this hypothesis, a more recent study reported that cortical responses to verbal stimuli are maintained in primary auditory cortex, but disrupted in higher order cortex, under deep propofol sedation (Liu et al., 2011).

In animal studies, in which primary sensory cortex can be targeted specifically and neuronal responses measured directly, it has long been known that sensory-evoked responses are maintained under anesthesia (Mountcastle et al., 1957; Hubel and Wiesel, 1959; Merzenich et al., 1975). For example, the tonotopic organization in auditory cortex appears to be preserved under a variety of anesthetic agents (Merzenich et al., 1975; Guo et al., 2012). Dose-dependent suppression by isoflurane of some, but not all, epidurally-recorded evoked responses has been observed (Santarelli et al., 2003), though in visual cortex high anesthetic doses have been reported to enhance LFP responses to sensory stimuli (Imas et al., 2005b). We observed similar enhanced response amplitude at the highest dose (1.6%) tested, which was sufficient to cause a burst-suppression spontaneous activity pattern (not shown) (Hartikainen et al., 1995). At this concentration, both auditory and visual stimuli could elicit burst responses that were stereotypical and likely reflected engagement of the same cortical circuitry underlying spontaneous bursts. At all concentrations tested, however, the magnitude and overall pattern of the response to auditory stimulation was relatively resistant to isoflurane (**Figures 4**, **5**). In brain slices, isoflurane suppressed early

current sinks in response to TC stimulation, though the effect was much more modest than for CC responses (**Figures 7**, **8**). It is possible that enhanced acoustic responses in the auditory periphery compensate *in vivo* for suppression of TC synaptic responses in cortex; alternatively, species differences may account for some of the differences between our results *in vivo* and in slices (see above).

Our results *in vivo* stand in contrast to the thalamic switch hypothesis (Alkire et al., 2000), in which anesthetics cause LOC by impairing information flow along the TC pathway. Several studies have reported suppressed activity in thalamus at clinically relevant doses, both *in vitro* and *in vivo* (Ries and Puil, 1999; Alkire et al., 2000; Alkire, 2008; Langsjo et al., 2012; Schroter et al., 2012), and thalamic micro-injections of GABAergic and cholinergic agonists can trigger loss and recovery of consciousness, respectively, in rats (Miller, 1992; Alkire et al., 2007). However, evidence suggests that anesthetics selectively target non-specific thalamic nuclei, leaving ascending sensory pathways intact (Liu et al., 2013), and, as for anesthetic effects on cortical activity, reductions in thalamic activity can occur even when LOC does not (Alkire et al., 2008a).

In contrast to relatively preserved signals in sensory cortex for stimuli of the primary modality and for core TC responses, we have shown that responses to stimuli of a secondary modality and CC responses are preferentially suppressed by isoflurane. These results are broadly supportive of a mechanism based on cortico-thalamic network disruption, derived from the information integration theory of consciousness and the cognitive unbinding hypothesis (Tononi, 2004; Mashour, 2013). We note that disruption of multimodal integration while leaving primary sensory pathways intact is a specific prediction of the latter model. Consistent with these results, multimodal interactions between auditory and visual cortex in humans under resting state conditions, presumably reflecting suppression of concurrent activity in the two regions that arises due to direct or indirect synaptic connections, are suppressed at hypnotic doses of propofol (Boveroux et al., 2010). Although this is the first direct observation of differential effects of anesthetics on sensory afferent pathways, these results are consistent with previous studies showing that anesthetics at hypnotic doses reduce effective connectivity between cortical areas, and especially descending connections (Ku et al., 2011; Schrouff et al., 2011; Lee et al., 2013b).

Interestingly, we observed that suppression of the visual response in auditory cortex *in vivo* reached a significant level even at sub-hypnotic doses of isoflurane. At these doses, the animal had intact righting reflex, but their overall behavior and behavioral responses to external stimuli were not assayed explicitly. The decreased response may be related to a gradual decrease in the consciousness level of the animal, or to a decreased level of sensory integration and awareness. Previous studies have shown that sub-hypnotic doses of volatile anesthetics can modulate neuronal activity (Antkowiak and Helfrichforster, 1998; Hentschke et al., 2005; Becker et al., 2012) as well as learning and a variety of behaviors (Cook et al., 1978; Dwyer et al., 1992; Alkire and Gorski, 2004; Burlingame et al., 2007). In predictive coding models, descending signals reflect memory traces engaged to predict observed responses throughout the cortical hierarchy (Rao and Ballard, 1999; Bar, 2009; Bastos et al., 2012; Wacongne et al., 2012). Evidence indicates that memory formation is extremely sensitive to anesthesia, with concentrations suppressing recall approximately one half those causing LOC (Alkire and Gorski, 2004; Perouansky et al., 2010). In humans, the incidence of recall under anesthesia is exceedingly low, estimated to occur in at most 0.1–0.2% of patients (Myles et al., 2004; Avidan et al., 2011). It is possible that this high sensitivity of memory to anesthesia is related to suppression of multimodal and CC responses (Newton et al., 1990; Alkire and Gorski, 2004).

There are a number of possible mechanisms for the differential effects of isoflurane on V2/L5 and L1 vs. core TC synaptic responses. First, isoflurane may act presynaptically, reducing neurotransmitter release in a synapse-specific way. There is precedence for this type of specificity, in that volatile agents have been shown to preferentially reduce synaptic release of glutamate compared to GABA (Perouansky et al., 1995; Maciver et al., 1996; Maciver, 1997; Kirson et al., 1998; Westphalen and Hemmings, 2006a,b; Peters et al., 2008). We note, however, that we were unable to detect evidence for a presynaptic mechanism based on paired pulse facilitation of TC, V2/L5, and L1 responses (**Figure 10**). Isoflurane could also affect axonal excitability, and thus sensitivity to electrical stimulation, which would not be manifest in changes in short-term plasticity. We did not observe fiber volley components in our recordings except at higher stimulus intensities than those employed here and thus we cannot exclude this possibility. However, fiber volleys in hippocampus have been shown to be insensitive to isoflurane except at extremely high concentrations (Winegar and Maciver, 2006). These observations suggest that the differential effect of isoflurane may rely on postsynaptic differences in synapse location, in which more distal synapses (V2/L5 and L1) will be more affected compared to more proximal synapses (core TC) due to anesthetic effects on postsynaptic membrane properties [e.g., potassium leak currents (Franks and Lieb, 1999; Patel et al., 1999; Putzke et al., 2007)].

FUNCTIONAL IMPLICATIONS

In predictive coding models of sensory processing, the nervous system compares at each moment in time the expectations about impending sensory input with what is actually observed (Hawkins and Blakeslee, 2005; Bar, 2009; Bastos et al., 2012). These expectations are based on memory and the statistical regularity of the physical world, and this integration of top-down and bottom-up information streams is postulated to be the critical step in sensory awareness. We have used sensory stimuli and electrical stimulation to activate selectively ascending and descending pathways to auditory cortex, and have demonstrated that descending pathways are preferentially suppressed by clinically relevant doses of the volatile anesthetic isoflurane. These data are thus consistent with the emerging model of how loss and recovery of consciousness occur under anesthesia, in which anesthetic agents preferentially suppressing top-down connections and thus interfering with predictive coding, and provide evidence that the integration of top-down and bottom-up signals is indeed a necessary component of consciousness. We note that the data presented here, although representing a direct test of the predictions of the

cognitive unbinding and information integration theories, are by themselves correlative in nature. In particular, although we used doses of isoflurane calibrated to be just-hypnotic, we did not assay the specific involvement of top-down projections in consciousness, test the role of their disruption in LOC, or assay sensory awareness or recall directly. Such direct tests await future studies in which level of consciousness can be measured simultaneously with measurements of top-down connectivity, and more importantly these top-down connections can be manipulated independently to investigate their causal role in loss and recovery of consciousness. For example, experiments in which opto- or pharmacogenetic methods are used to selectively inhibit, under awake conditions, or activate, under LOC, descending and matrix thalamic projections will allow us to more firmly establish a causal role for top-down connectivity in sensory awareness.

ACKNOWLEDGMENTS

Supported by National Institutes of Health (DC006013 to Matthew I. Banks; T32 GM007507 to Bryan M. Krause), a grant from the International Anesthesia Research Society (to Aeyal Raz), the UW-Madison Office of the Vice Chancellor for Research and Graduate Education, with funding from the Wisconsin Alumni Research Foundation (to Daniel J. Uhlrich), and the Department of Anesthesiology, School of Medicine and Public Health, University of Wisconsin, Madison, WI, USA. The authors thank Jane Sekulski and Anna Kowalkowski (Department of Neuroscience) for technical support on this project.

REFERENCES

Alain, C. (2007). Breaking the wave: effects of attention and learning on concurrent sound perception. *Hear. Res.* 229, 225–236. doi: 10.1016/j.heares.2007.01.011

Alain, C., and Izenberg, A. (2003). Effects of attentional load on auditory scene analysis. *J. Cogn. Neurosci.* 15, 1063–1073. doi: 10.1162/089892903770007443

Alkire, M. T. (2008). Loss of effective connectivity during general anesthesia. *Int. Anesthesiol. Clin.* 46, 55–73. doi: 10.1097/AIA.0b013e3181755dc6

Alkire, M. T., and Gorski, L. A. (2004). Relative amnesic potency of five inhalational anesthetics follows the Meyer-Overton rule. *Anesthesiology* 101, 417–429. doi: 10.1097/00000542-200408000-00023

Alkire, M. T., Gruver, R., Miller, J., McReynolds, J. R., Hahn, E. L., and Cahill, L. (2008a). Neuroimaging analysis of an anesthetic gas that blocks human emotional memory. *Proc. Natl. Acad. Sci. U.S.A.* 105, 1722–1727. doi: 10.1073/pnas.0711651105

Alkire, M. T., Haier, R. J., and Fallon, J. H. (2000). Toward a unified theory of narcosis: brain imaging evidence for a thalamocortical switch as the neurophysiologic basis of anesthetic- induced unconsciousness. *Conscious. Cogn.* 9, 370–386. doi: 10.1006/ccog.1999.0423

Alkire, M. T., Hudetz, A. G., and Tononi, G. (2008b). Consciousness and anesthesia. *Science* 322, 876–880. doi: 10.1126/science.1149213

Alkire, M. T., McReynolds, J. R., Hahn, E. L., and Trivedi, A. N. (2007). Thalamic microinjection of nicotine reverses sevoflurane-induced loss of righting reflex in the rat. *Anesthesiology* 107, 264–272. doi: 10.1097/01.anes.0000270741.33766.24

Antkowiak, B. (2001). How do general anaesthetics work? *Naturwissenschaften* 88, 201–213. doi: 10.1007/s001140100230

Antkowiak, B., and Helfrichforster, C. (1998). Effects of small concentrations of volatile anesthetics on action potential firing of neocortical neurons *in vitro*. *Anesthesiology* 88, 1592–1605. doi: 10.1097/00000542-199806000-00024

Avidan, M. S., Jacobsohn, E., Glick, D., Burnside, B. A., Zhang, L., Villafranca, A., et al. (2011). Prevention of intraoperative awareness in a high-risk surgical population. *N. Engl. J. Med.* 365, 591–600. doi: 10.1056/NEJMoa1100403

Banks, M. I. (2010). "Anesthetic modulation of auditory perception: linking cellular, circuit and behavioral effects," in *Suppressing the Mind: Anesthetic Modulation of Memory and Consciousness*, eds A. G. Hudetz and R. A. Pearce (New York, NY: Humana Press), 81–97.

Banks, M. I., Uhlrich, D. J., Smith, P. H., Krause, B. M., and Manning, K. A. (2011). Descending projections from extrastriate visual cortex modulate responses of cells in primary auditory cortex. *Cereb. Cortex* 21, 2620–2638. doi: 10.1093/cercor/bhr048

Bar, M. (2009). The proactive brain: memory for predictions. *Philos. Trans. R. Soc. Lond. B Biol. Sci.* 364, 1235–1243. doi: 10.1098/rstb.2008.0310

Bastos, A. M., Usrey, W. M., Adams, R. A., Mangun, G. R., Fries, P., and Friston, K. J. (2012). Canonical microcircuits for predictive coding. *Neuron* 76, 695–711. doi: 10.1016/j.neuron.2012.10.038

Becker, K., Eder, M., Ranft, A., Von Meyer, L., Zieglgansberger, W., Kochs, E., et al. (2012). Low dose isoflurane exerts opposing effects on neuronal network excitability in neocortex and hippocampus. *PLoS ONE* 7:e39346. doi: 10.1371/journal.pone.0039346

Besle, J., Bertrand, O., and Giard, M. H. (2009). Electrophysiological (EEG, sEEG, MEG) evidence for multiple audiovisual interactions in the human auditory cortex. *Hear. Res.* 258, 143–151. doi: 10.1016/j.heares.2009.06.016

Bizley, J. K., and King, A. J. (2009). Visual influences on ferret auditory cortex. *Hear. Res.* 258, 55–63. doi: 10.1016/j.heares.2009.06.017

Bizley, J. K., Nodal, F. R., Bajo, V. M., Nelken, I., and King, A. J. (2007). Physiological and anatomical evidence for multisensory interactions in auditory cortex. *Cereb. Cortex* 17, 2172–2189. doi: 10.1093/cercor/bhl128

Blain-Moraes, S., Lee, U., Ku, S., Noh, G., and Mashour, G. A. (2014). Electroencephalographic effects of ketamine on power, cross-frequency coupling, and connectivity in the alpha bandwidth. *Front. Syst. Neurosci.* 8:114. doi: 10.3389/fnsys.2014.00114

Boly, M., Garrido, M. I., Gosseries, O., Bruno, M. A., Boveroux, P., Schnakers, C., et al. (2011). Preserved feedforward but impaired top-down processes in the vegetative state. *Science* 332, 858–862. doi: 10.1126/science.1202043

Boly, M., Moran, R., Murphy, M., Boveroux, P., Bruno, M. A., Noirhomme, Q., et al. (2012). Connectivity changes underlying spectral EEG changes during propofol-induced loss of consciousness. *J. Neurosci.* 32, 7082–7090. doi: 10.1523/JNEUROSCI.3769-11.2012

Boveroux, P., Vanhaudenhuyse, A., Bruno, M. A., Noirhomme, Q., Lauwick, S., Luxen, A., et al. (2010). Breakdown of within- and between-network resting state functional magnetic resonance imaging connectivity during propofol-induced loss of consciousness. *Anesthesiology* 113, 1038–1053. doi: 10.1097/ALN.0b013e3181f697f5

Budd, J. M. (1998). Extrastriate feedback to primary visual cortex in primates: a quantitative analysis of connectivity. *Proc. Biol. Sci.* 265, 1037–1044. doi: 10.1098/rspb.1998.0396

Budinger, E., Heil, P., Hess, A., and Scheich, H. (2006). Multisensory processing via early cortical stages: connections of the primary auditory cortical field with other sensory systems. *Neuroscience* 143, 1065–1083. doi: 10.1016/j.neuroscience.2006.08.035

Burlingame, R. H., Shrestha, S., Rummel, M. R., and Banks, M. I. (2007). Subhypnotic doses of isoflurane impair auditory discrimination in rats. *Anesthesiology* 106, 754–762. doi: 10.1097/01.anes.0000264755.24264.68

Cauller, L. (1995). Layer I of primary sensory neocortex: where top-down converges upon bottom-up. *Behav. Brain Res.* 71, 163–170. doi: 10.1016/0166-4328(95)00032-1

Cauller, L. J., and Connors, B. W. (1994). Synaptic physiology of horizontal afferents to layer I in slices of rat SI neocortex. *J. Neurosci.* 14, 751–762.

Cauller, L. J., and Kulics, A. T. (1991). The neural basis of the behaviorally relevant component of the somatosensory-evoked potential in SI cortex of awake monkey evidence that backward cortical projections signal conscious touch sensation. *Exp. Brain Res.* 84, 607–619. doi: 10.1007/BF00230973

Chennu, S., Noreika, V., Gueorguiev, D., Blenkmann, A., Kochen, S., Ibanez, A., et al. (2013). Expectation and attention in hierarchical auditory prediction. *J. Neurosci.* 33, 11194–11205. doi: 10.1523/JNEUROSCI.0114-13.2013

Constantinople, C. M., and Bruno, R. M. (2013). Deep cortical layers are activated directly by thalamus. *Science* 340, 1591–1594. doi: 10.1126/science.1236425

Cook, T. L., Smith, M., Winter, P. M., Starkweather, J. A., and Eger, E. I. 3rd. (1978). Effect of subanesthetic concentration of enflurane and halothane on human behavior. *Anesth. Analg.* 57, 434–440.

Covic, E. N., and Sherman, S. M. (2011). Synaptic properties of connections between the primary and secondary auditory cortices in mice. *Cereb. Cortex* 21, 2425–2441. doi: 10.1093/cercor/bhr029

Crick, F., and Koch, C. (2003). A framework for consciousness. *Nat. Neurosci.* 6, 119–126. doi: 10.1038/nn0203-119

Cruikshank, S. J., Rose, H. J., and Metherate, R. (2002). Auditory thalamocortical synaptic transmission *in vitro*. *J. Neurophysiol.* 87, 361–384.

Cunningham, M. O., Pervouchine, D. D., Racca, C., Kopell, N. J., Davies, C. H., Jones, R. S., et al. (2006). Neuronal metabolism governs cortical network response state. *Proc. Natl. Acad. Sci. U.S.A.* 103, 5597–5601. doi: 10.1073/pnas.0600604103

Davis, M. H., and Johnsrude, I. S. (2007). Hearing speech sounds: top-down influences on the interface between audition and speech perception. *Hear. Res.* 229, 132–147. doi: 10.1016/j.heares.2007.01.014

Del Castillo, J., and Katz, B. (1954). Statistical Factors involved in neuromuscular facilitation and depression. *J. Physiol.* 124, 574–585.

De Pasquale, R., and Sherman, S. M. (2011). Synaptic properties of corticocortical connections between the primary and secondary visual cortical areas in the mouse. *J. Neurosci.* 31, 16494–16506. doi: 10.1523/JNEUROSCI.3664-11.2011

Detsch, O., Kochs, E., Siemers, M., Bromm, B., and Vahle-Hinz, C. (2002). Increased responsiveness of cortical neurons in contrast to thalamic neurons during isoflurane-induced EEG bursts in rats. *Neurosci. Lett.* 317, 9–12. doi: 10.1016/S0304-3940(01)02419-3

Devor, M., and Zalkind, V. (2001). Reversible analgesia, atonia, and loss of consciousness on bilateral intracerebral microinjection of pentobarbital. *Pain* 94, 101–112. doi: 10.1016/S0304-3959(01)00345-1

Doehrmann, O., Weigelt, S., Altmann, C. F., Kaiser, J., and Naumer, M. J. (2010). Audiovisual functional magnetic resonance imaging adaptation reveals multisensory integration effects in object-related sensory cortices. *J. Neurosci.* 30, 3370–3379. doi: 10.1523/JNEUROSCI.5074-09.2010

Doron, N. N., Ledoux, J. E., and Semple, M. N. (2002). Redefining the tonotopic core of rat auditory cortex: physiological evidence for a posterior field. *J. Comp. Neurol.* 453, 345–360. doi: 10.1002/cne.10412

Drummond, J. C. (2000). Monitoring depth of anesthesia: with emphasis on the application of the bispectral index and the middle latency auditory evoked response to the prevention of recall. *Anesthesiology* 93, 876–882. doi: 10.1097/00000542-200009000-00039

Dueck, M. H., Petzke, F., Gerbershagen, H. J., Paul, M., Hesselmann, V., Girnus, R., et al. (2005). Propofol attenuates responses of the auditory cortex to acoustic stimulation in a dose-dependent manner: a FMRI study. *Acta Anaesthesiol. Scand.* 49, 784–791. doi: 10.1111/j.1399-6576.2005.00703.x

Dwyer, R., Bennett, H. L., Eger, E. I., and Heilbron, D. (1992). Effects of isoflurane and nitrous oxide in subanesthetic concentrations on memory and responsiveness in volunteers. *Anesthesiology* 77, 888–898. doi: 10.1097/00000542-199211000-00009

Ehret, G. (1997). The auditory cortex. [Review] [132 refs]. *J. Comp. Physiol. A* 181, 547–557. doi: 10.1007/s003590050139

Felleman, D. J., and Van Essen, D. C. (1991). Distributed hierarchical processing in the primate cerebral cortex. *Cereb. Cortex* 1, 1–47. doi: 10.1093/cercor/1.1.1

Ferrarelli, F., Massimini, M., Sarasso, S., Casali, A., Riedner, B. A., Angelini, G., et al. (2010). Breakdown in cortical effective connectivity during midazolam-induced loss of consciousness. *Proc. Natl. Acad. Sci. U.S.A.* 107, 2681–2686. doi: 10.1073/pnas.0913008107

Franks, N. P. (2008). General anaesthesia: from molecular targets to neuronal pathways of sleep and arousal. *Nat. Rev. Neurosci.* 9, 370–386. doi: 10.1038/nrn2372

Franks, N. P., and Lieb, W. R. (1999). Background K+ channels: an important target for volatile anesthetics? *Nat. Neurosci.* 2, 395–396.

Fritz, J. B., Elhilali, M., and Shamma, S. A. (2007). Adaptive changes in cortical receptive fields induced by attention to complex sounds. *J. Neurophysiol.* 98, 2337–2346. doi: 10.1152/jn.00552.2007

Fu, K. M., Shah, A. S., O'connell, M. N., McGinnis, T., Eckholdt, H., Lakatos, P., et al. (2004). Timing and laminar profile of eye-position effects on auditory responses in primate auditory cortex. *J. Neurophysiol.* 92, 3522–3531. doi: 10.1152/jn.01228.2003

George, D., and Hawkins, J. (2009). Towards a mathematical theory of cortical micro-circuits. *PLoS Comput. Biol.* 5:e1000532. doi: 10.1371/journal.pcbi.1000532

Ghazanfar, A. A., Maier, J. X., Hoffman, K. L., and Logothetis, N. K. (2005). Multisensory integration of dynamic faces and voices in rhesus monkey auditory cortex. *J. Neurosci.* 25, 5004–5012. doi: 10.1523/JNEUROSCI.0799-05.2005

Grossberg, S., and Versace, M. (2008). Spikes, synchrony, and attentive learning by laminar thalamocortical circuits. *Brain Res.* 1218, 278–312. doi: 10.1016/j.brainres.2008.04.024

Guo, W., Chambers, A. R., Darrow, K. N., Hancock, K. E., Shinn-Cunningham, B. G., and Polley, D. B. (2012). Robustness of cortical topography across fields, laminae, anesthetic states, and neurophysiological signal types. *J. Neurosci.* 32, 9159–9172. doi: 10.1523/JNEUROSCI.0065-12.2012

Haist, F., Song, A. W., Wild, K., Faber, T. L., Popp, C. A., and Morris, R. D. (2001). Linking sight and sound: fMRI evidence of primary auditory cortex activation during visual word recognition. *Brain Lang.* 76, 340–350. doi: 10.1006/brln.2000.2433

Hartikainen, K. M., Rorarius, M., Perakyla, J. J., Laippala, P. J., and Jantti, V. (1995). Cortical reactivity during isoflurane burst-suppression anesthesia. *Anesth. Analg.* 81, 1223–1228.

Hawkins, J., and Blakeslee, S. (2005). *On Intelligence.* New York, NY: Henry Holt & Co.

Hentschke, H., Schwarz, C., and Antkowiak, B. (2005). Neocortex is the major target of sedative concentrations of volatile anaesthetics: strong depression of firing rates and increase of GABAA receptor-mediated inhibition. *Eur. J. Neurosci.* 21, 93–102. doi: 10.1111/j.1460-9568.2004.03843.x

Hobson, J. A., and Friston, K. J. (2012). Waking and dreaming consciousness: neurobiological and functional considerations. *Prog. Neurobiol.* 98, 82–98. doi: 10.1016/j.pneurobio.2012.05.003

Huang, C. L., and Winer, J. A. (2000). Auditory thalamocortical projections in the cat: laminar and areal patterns of input. *J. Comp. Neurol.* 427, 302–331. doi: 10.1002/1096-9861(20001113)427:2<302::AID-CNE10>3.0.CO;2-J

Hubel, D. H., and Wiesel, T. N. (1959). Receptive fields of single neurones in the cat's striate cortex. *J. Physiol.* 148, 574–591.

Hudetz, A. G., and Imas, O. A. (2007). Burst activation of the cerebral cortex by flash stimuli during isoflurane anesthesia in rats. *Anesthesiology* 107, 983–991. doi: 10.1097/01.anes.0000291471.80659.55

Hudetz, A. G., Vizuete, J. A., and Pillay, S. (2011). Differential effects of isoflurane on high-frequency and low-frequency gamma oscillations in the cerebral cortex and hippocampus in freely moving rats. *Anesthesiology* 114, 588–595. doi: 10.1097/ALN.0b013e31820ad3f9

Imas, O. A., Ropella, K. M., Ward, B. D., Wood, J. D., and Hudetz, A. G. (2005a). Volatile anesthetics disrupt frontal-posterior recurrent information transfer at gamma frequencies in rat. *Neurosci. Lett.* 387, 145–150. doi: 10.1016/j.neulet.2005.06.018

Imas, O. A., Ropella, K. M., Ward, B. D., Wood, J. D., and Hudetz, A. G. (2005b). Volatile anesthetics enhance flash-induced gamma oscillations in rat visual cortex. *Anesthesiology* 102, 937–947. doi: 10.1097/00000542-200505000-00012

Imas, O. A., Ropella, K. M., Wood, J. D., and Hudetz, A. G. (2004). Halothane augments event-related gamma oscillations in rat visual cortex. *Neuroscience* 123, 269–278. doi: 10.1016/j.neuroscience.2003.09.014

Jones, E. G. (1998). Viewpoint: the core and matrix of thalamic organization. *Neuroscience* 85, 331–345. doi: 10.1016/S0306-4522(97)00581-2

Jordan, D., Ilg, R., Riedl, V., Schorer, A., Grimberg, S., Neufang, S., et al. (2013). Simultaneous electroencephalographic and functional magnetic resonance imaging indicate impaired cortical top-down processing in association with anesthetic-induced unconsciousness. *Anesthesiology* 119, 1031–1042. doi: 10.1097/ALN.0b013e3182a7ca92

Kaur, S., Rose, H. J., Lazar, R., Liang, K., and Metherate, R. (2005). Spectral integration in primary auditory cortex: laminar processing of afferent input, *in vivo* and *in vitro*. *Neuroscience* 134, 1033–1045. doi: 10.1016/j.neuroscience.2005.04.052

Kayser, C., Petkov, C. I., and Logothetis, N. K. (2008). Visual modulation of neurons in auditory cortex. *Cereb. Cortex* 18, 1560–1574. doi: 10.1093/cercor/bhm187

Kerssens, C., Hamann, S., Peltier, S., Hu, X. P., Byas-Smith, M. G., and Sebel, P. S. (2005). Attenuated brain response to auditory word stimulation with sevoflurane: a functional magnetic resonance imaging study in humans. *Anesthesiology* 103, 11–19. doi: 10.1097/00000542-200507000-00006

Kimura, A., Donishi, T., Okamoto, K., and Tamai, Y. (2004). Efferent connections of "posterodorsal" auditory area in the rat cortex: implications for auditory spatial processing. *Neuroscience* 128, 399–419. doi: 10.1016/j.neuroscience.2004.07.010

Kirson, E. D., Yaari, Y., and Perouansky, M. (1998). Presynaptic and postsynaptic actions of halothane at glutamatergic synapses in the mouse hippocampus. *Br. J. Pharmacol.* 124, 1607–1614. doi: 10.1038/sj.bjp.0701996

Kok, P., Brouwer, G. J., Van Gerven, M. A., and De Lange, F. P. (2013). Prior expectations bias sensory representations in visual cortex. *J. Neurosci.* 33, 16275–16284. doi: 10.1523/JNEUROSCI.0742-13.2013

Krupa, D. J., Wiest, M. C., Shuler, M. G., Laubach, M., and Nicolelis, M. A. L. (2004). Layer-specific somatosensory cortical activation during active tactile discrimination. *Science* 304, 1989–1992. doi: 10.1126/science.1093318

Ku, S. W., Lee, U., Noh, G. J., Jun, I. G., and Mashour, G. A. (2011). Preferential inhibition of frontal-to-parietal feedback connectivity is a neurophysiologic correlate of general anesthesia in surgical patients. *PLoS ONE* 6:e25155. doi: 10.1371/journal.pone.0025155

Lakatos, P., Chen, C. M., O'connell, M. N., Mills, A., and Schroeder, C. E. (2007). Neuronal oscillations and multisensory interaction in primary auditory cortex. *Neuron* 53, 279–292. doi: 10.1016/j.neuron.2006.12.011

Lakatos, P., O'connell, M. N., Barczak, A., Mills, A., Javitt, D. C., and Schroeder, C. E. (2009). The leading sense: supramodal control of neurophysiological context by attention. *Neuron* 64, 419–430. doi: 10.1016/j.neuron.2009.10.014

Lakatos, P., Shah, A. S., Knuth, K. H., Ulbert, I., Karmos, G., and Schroeder, C. E. (2005). An oscillatory hierarchy controlling neuronal excitability and stimulus processing in the auditory cortex. *J. Neurophysiol.* 94, 1904–1911. doi: 10.1152/jn.00263.2005

Lamme, V. A. F., Zipser, K., and Spekreijse, H. (1998). Figure-ground activity in primary visual cortex is suppressed by anesthesia. *Proc. Natl. Acad. Sci. U.S.A.* 95, 3263–3268. doi: 10.1073/pnas.95.6.3263

Langsjo, J. W., Alkire, M. T., Kaskinoro, K., Hayama, H., Maksimow, A., Kaisti, K. K., et al. (2012). Returning from oblivion: imaging the neural core of consciousness. *J. Neurosci.* 32, 4935–4943. doi: 10.1523/JNEUROSCI.4962-11.2012

Lee, H., Mashour, G. A., Noh, G. J., Kim, S., and Lee, U. (2013a). Reconfiguration of network hub structure after propofol-induced unconsciousness. *Anesthesiology* 119, 1347–1359. doi: 10.1097/ALN.0b013e3182a8ec8c

Lee, U., Kim, S., Noh, G. J., Choi, B. M., Hwang, E., and Mashour, G. A. (2009). The directionality and functional organization of frontoparietal connectivity during consciousness and anesthesia in humans. *Conscious. Cogn.* 18, 1069–1078. doi: 10.1016/j.concog.2009.04.004

Lee, U., Ku, S., Noh, G., Baek, S., Choi, B., and Mashour, G. A. (2013b). Disruption of frontal-parietal communication by ketamine, propofol, and sevoflurane. *Anesthesiology* 118, 1264–1275. doi: 10.1097/ALN.0b013e31829103f5

Liu, X., Lauer, K. K., Ward, B. D., Li, S. J., and Hudetz, A. G. (2013). Differential effects of deep sedation with propofol on the specific and nonspecific thalamocortical systems: a functional magnetic resonance imaging study. *Anesthesiology* 118, 59–69. doi: 10.1097/ALN.0b013e318277a801

Liu, X., Lauer, K. K., Ward, B. D., Rao, S. M., Li, S. J., and Hudetz, A. G. (2011). Propofol disrupts functional interactions between sensory and high-order processing of auditory verbal memory. *Hum. Brain Mapp.* 33, 2487–2498. doi: 10.1002/hbm.21385

Llinas, R., Ribary, U., Contreras, D., and Pedroarena, C. (1998). The neuronal basis for consciousness. *Philos. Trans. R. Soc. Lond. B Biol. Sci.* 353, 1841–1849. doi: 10.1098/rstb.1998.0336

Lukatch, H. S., Kiddoo, C. E., and Maciver, M. B. (2005). Anesthetic-induced burst suppression EEG activity requires glutamate-mediated excitatory synaptic transmission. *Cereb. Cortex* 15, 1322–1331. doi: 10.1093/cercor/bhi015

Macgregor, D. G., Chesler, M., and Rice, M. E. (2001). HEPES prevents edema in rat brain slices. *Neurosci. Lett.* 303, 141–144. doi: 10.1016/S0304-3940(01)01690-1

Maciver, M. B. (1997). "General anesthetic actions on transmission at glutamate and gaba synapses," in *Anesthesia: Biologic Foundations*, eds T. L. Yaksh, C. Lynch, W. M. Zapol, M. Maze, J. F. Biebuyck and L. J. Saidman (Philadelphia: Lippincott-Raven Publishers), 277–286.

Maciver, M. B., Mikulec, A. A., Amagasu, S. M., and Monroe, F. A. (1996). Volatile anesthetics depress glutamate transmission via presynaptic actions. *Anesthesiology* 85, 823–834. doi: 10.1097/00000542-199610000-00018

Maclean, J. N., Watson, B. O., Aaron, G. B., and Yuste, R. (2005). Internal dynamics determine the cortical response to thalamic stimulation. *Neuron* 48, 811–823. doi: 10.1016/j.neuron.2005.09.035

Mashour, G. A. (2006). Integrating the science of consciousness and anesthesia. *Anesth. Analg.* 103, 975–982. doi: 10.1213/01.ane.0000232442.69757.4a

Mashour, G. A. (2013). Cognitive unbinding: a neuroscientific paradigm of general anesthesia and related states of unconsciousness. *Neurosci. Biobehav. Rev.* 37, 2751–2759. doi: 10.1016/j.neubiorev.2013.09.009

Mashour, G. A. (2014). Top-down mechanisms of anesthetic-induced unconsciousness. *Front. Syst. Neurosci.* 8:115. doi: 10.3389/fnsys.2014.00115

Massimini, M., Ferrarelli, F., Huber, R., Esser, S. K., Singh, H., and Tononi, G. (2005). Breakdown of cortical effective connectivity during sleep. *Science* 309, 2228–2232. doi: 10.1126/science.1117256

Merzenich, M. M., Knight, P. L., and Roth, G. L. (1975). Representation of cochlea within primary auditory cortex in the cat. *J. Neurophysiol.* 38, 231–249.

Metherate, R., and Cruikshank, S. J. (1999). Thalamocortical inputs trigger a propagating envelope of gamma-band activity in auditory cortex *in vitro*. *Exp. Brain Res.* 126, 160–174. doi: 10.1007/s002210050726

Mignard, M., and Malpeli, J. G. (1991). Paths of information flow through visual cortex. *Science* 251, 1249–1251. doi: 10.1126/science.1848727

Miller, J. W. (1992). The role of mesencephalic and thalamic arousal systems in experimental seizures. *Prog. Neurobiol.* 39, 155–178. doi: 10.1016/0301-0082(92)90009-4

Miller, M. W., and Vogt, B. A. (1984). Direct connections of rat visual cortex with sensory, motor, and association cortices. *J. Comp. Neurol.* 226, 184–202. doi: 10.1002/cne.902260204

Milner, R., Rusiniak, M., Lewandowska, M., Wolak, T., Ganc, M., Piatkowska-Janko, E., et al. (2014). Towards neural correlates of auditory stimulus processing: a simultaneous auditory evoked potentials and functional magnetic resonance study using an odd-ball paradigm. *Med. Sci. Monit.* 20, 35–46. doi: 10.12659/MSM.889712

Mitzdorf, U. (1985). Current source-density method and application in cat cerebral cortex: investigation of evoked potentials and EEG phenomena. *Physiol. Rev.* 65, 37–100.

Mountcastle, V. B., Davies, P. W., and Berman, A. L. (1957). Response properties of neurons of cat's somatic sensory cortex to peripheral stimuli. *J. Neurophysiol.* 20, 374–407.

Myles, P. S., Leslie, K., McNeil, J., Forbes, A., and Chan, M. T. (2004). Bispectral index monitoring to prevent awareness during anaesthesia: the B-Aware randomised controlled trial. *Lancet* 363, 1757–1763. doi: 10.1016/S0140-6736(04)16300-9

Nelson, L. E., Guo, T. Z., Lu, J., Saper, C. B., Franks, N. P., and Maze, M. (2002). The sedative component of anesthesia is mediated by GABA(A) receptors in an endogenous sleep pathway. *Nat. Neurosci.* 5, 979–984. doi: 10.1038/nn913

Newton, D. E., Thornton, C., Konieczko, K., Frith, C. D., Dore, C. J., Webster, N. R., et al. (1990). Levels of consciousness in volunteers breathing sub-MAC concentrations of isoflurane. *Br. J. Anaesth.* 65, 609–615. doi: 10.1093/bja/65.5.609

Pack, C. C., Berezovskii, V. K., and Born, R. T. (2001). Dynamic properties of neurons in cortical area MT in alert and anaesthetized macaque monkeys. *Nature* 414, 905–908. doi: 10.1038/414905a

Patel, A. J., Honore, E., Lesage, F., Fink, M., Romey, G., and Lazdunski, M. (1999). Inhalational anesthetics activate two-pore-domain background K+ channels. *Nat. Neurosci.* 2, 422–426. doi: 10.1038/8084

Paxinos, G., and Watson, C. (2007). *The Rat Brain in Stereotaxic Coordinates*. Burlington, VT: Elsevier.

Peltier, S. J., Kerssens, C., Hamann, S. B., Sebel, P. S., Byas-Smith, M., and Hu, X. (2005). Functional connectivity changes with concentration of sevoflurane anesthesia. *Neuroreport* 16, 285–288. doi: 10.1097/00001756-200502280-00017

Perouansky, M., Baranov, D., Salman, M., and Yaari, Y. (1995). Effects of halothane on glutamate receptor-mediated excitatory postsynaptic currents. A patch-clamp study in adult mouse hippocampal slices. *Anesthesiology* 83, 109–119. doi: 10.1097/00000542-199507000-00014

Perouansky, M., Rau, V., Ford, T., Oh, S. I., Perkins, M., Eger, E. I. 2nd., et al. (2010). Slowing of the hippocampal theta rhythm correlates with anesthetic-induced amnesia. *Anesthesiology* 113, 1299–1309. doi: 10.1097/ALN.0b013e3181f90ccc

Peters, J. H., McDougall, S. J., Mendelowitz, D., Koop, D. R., and Andresen, M. C. (2008). Isoflurane differentially modulates inhibitory and excitatory synaptic transmission to the solitary tract nucleus. *Anesthesiology* 108, 675–683. doi: 10.1097/ALN.0b013e318167af9a

Pettersen, K. H., Devor, A., Ulbert, I., Dale, A. M., and Einevoll, G. T. (2006). Current-source density estimation based on inversion of electrostatic forward

solution: effects of finite extent of neuronal activity and conductivity discontinuities. *J. Neurosci. Methods* 154, 116–133. doi: 10.1016/j.jneumeth.2005.12.005

Plourde, G., Belin, P., Chartrand, D., Fiset, P., Backman, S. B., Xie, G., et al. (2006). Cortical processing of complex auditory stimuli during alterations of consciousness with the general anesthetic propofol. *Anesthesiology* 104, 448–457. doi: 10.1097/00000542-200603000-00011

Polley, D. B., Read, H. L., Storace, D. A., and Merzenich, M. M. (2007). Multiparametric auditory receptive field organization across five cortical fields in the albino rat. *J. Neurophysiol.* 97, 3621–3638. doi: 10.1152/jn.01298.2006

Putzke, C., Hanley, P. J., Schlichthorl, G., Preisig-Muller, R., Rinne, S., Anetseder, M., et al. (2007). Differential effects of volatile and intravenous anesthetics on the activity of human TASK-1. *Am. J. Physiol. Cell Physiol.* 293, C1319–C1326. doi: 10.1152/ajpcell.00100.2007

Rao, R. P., and Ballard, D. H. (1999). Predictive coding in the visual cortex: a functional interpretation of some extra-classical receptive-field effects. *Nat. Neurosci.* 2, 79–87. doi: 10.1038/4580

Ries, C. R., and Puil, E. (1999). Mechanism of anesthesia revealed by shunting actions of isoflurane on thalamocortical neurons. *J. Neurophysiol.* 81, 1795–1801.

Rigas, P., and Castro-Alamancos, M. A. (2007). Thalamocortical Up states: differential effects of intrinsic and extrinsic cortical inputs on persistent activity. *J. Neurosci.* 27, 4261–4272. doi: 10.1523/JNEUROSCI.0003-07.2007

Rigas, P., and Castro-Alamancos, M. A. (2009). Impact of persistent cortical activity (up states) on intracortical and thalamocortical synaptic inputs. *J. Neurophysiol.* 102, 119–131. doi: 10.1152/jn.00126.2009

Rockland, K. S., and Virga, A. (1989). Terminal arbors of individual "feedback" axons projecting from area V2 to V1 in the macaque monkey: a study using immunohistochemistry of anterogradely transported Phaseolus vulgaris-leucoagglutinin. *J. Comp. Neurol.* 285, 54–72. doi: 10.1002/cne.902850106

Roger, M., and Arnault, P. (1989). Anatomical study of the connections of the primary auditory area in the rat. *J. Comp. Neurol.* 287, 339–356. doi: 10.1002/cne.902870306

Romanski, L. M., and Ledoux, J. E. (1993). Organization of rodent auditory cortex: anterograde transport of PHA-L from MGv to temporal neocortex. *Cereb. Cortex* 3, 499–514. doi: 10.1093/cercor/3.6.499

Rudolph, U., and Antkowiak, B. (2004). Molecular and neuronal substrates for general anaesthetics. *Nat. Rev. Neurosci.* 5, 709–720. doi: 10.1038/nrn1496

Saalmann, Y. B. (2014). Intralaminar and medial thalamic influence on cortical synchrony, information transmission and cognition. *Front. Syst. Neurosci.* 8:83. doi: 10.3389/fnsys.2014.00083

Salin, P. A., Kennedy, H., and Bullier, J. (1995). Spatial reciprocity of connections between areas 17 and 18 in the cat. *Can. J. Physiol. Pharmacol.* 73, 1339–1347. doi: 10.1139/y95-188

Sanchez-Vives, M. V., and McCormick, D. A. (2000). Cellular and network mechanisms of rhythmic recurrent activity in neocortex. *Nat. Neurosci.* 3, 1027–1034. doi: 10.1038/79848

Sandell, J. H., and Schiller, P. H. (1982). Effect of cooling area 18 on striate cortex cells in the squirrel monkey. *J. Neurophysiol.* 48, 38–48.

Santarelli, R., Arslan, E., Carraro, L., Conti, G., Capello, M., and Plourde, G. (2003). Effects of isoflurane on the auditory brainstem responses and middle latency responses of rats. *Acta Otolaryngol.* 123, 176–181. doi: 10.1080/0036554021000028108

Scheel, M. (1988). Topographic organization of the auditory thalamocortical system in the albino rat. *Anat. Embryol.* 179, 181–190. doi: 10.1007/BF00304700

Schroeder, C. E., Lakatos, P., Kajikawa, Y., Partan, S., and Puce, A. (2008). Neuronal oscillations and visual amplification of speech. *Trends Cogn. Sci.* 12, 106–113. doi: 10.1016/j.tics.2008.01.002

Schroter, M. S., Spoormaker, V. I., Schorer, A., Wohlschlager, A., Czisch, M., Kochs, E. F., et al. (2012). Spatiotemporal reconfiguration of large-scale brain functional networks during propofol-induced loss of consciousness. *J. Neurosci.* 32, 12832–12840. doi: 10.1523/JNEUROSCI.6046-11.2012

Schrouff, J., Perlbarg, V., Boly, M., Marrelec, G., Boveroux, P., Vanhaudenhuyse, A., et al. (2011). Brain functional integration decreases during propofol-induced loss of consciousness. *Neuroimage* 57, 198–205. doi: 10.1016/j.neuroimage.2011.04.020

Schwender, D., Kaiser, A., Klasing, S., Peter, K., and Poppel, E. (1994). Midlatency auditory evoked potentials and explicit and implicit memory in patients undergoing cardiac surgery. *Anesthesiology* 80, 493–501. doi: 10.1097/00000542-199403000-00004

Schwender, D., Klasing, S., Madler, C., Poppel, E., and Peter, K. (1993a). Depth of anesthesia. Midlatency auditory evoked potentials and cognitive function during general anesthesia. *Int. Anesthesiol. Clin.* 31, 89–106. doi: 10.1097/00004311-199331040-00009

Schwender, D., Klasing, S., Madler, C., Poppel, E., and Peter, K. (1993b). Effects of benzodiazepines on mid-latency auditory evoked potentials. *Can. J. Anaesth.* 40, 1148–1154. doi: 10.1007/BF03009604

Schwender, D., Klasing, S., Madler, C., Poppel, E., and Peter, K. (1993c). Mid-latency auditory evoked potentials during ketamine anaesthesia in humans. *Br. J. Anaesth.* 71, 629–632.

Sellers, K. K., Bennett, D. V., Hutt, A., and Frohlich, F. (2013). Anesthesia differentially modulates spontaneous network dynamics by cortical area and layer. *J. Neurophysiol.* 110, 2739–2751. doi: 10.1152/jn.00404.2013

Shi, C. J., and Cassell, M. D. (1997). Cortical, thalamic, and amygdaloid projections of rat temporal cortex. *J. Comp. Neurol.* 382, 153–175.

Shu, Y. S., Hasenstaub, A., Badoual, M., Bal, T., and McCormick, D. A. (2003). Barrages of synaptic activity control the gain and sensitivity of cortical neurons. *J. Neurosci.* 23, 10388–10401.

Shushruth, S. (2013). Exploring the neural basis of consciousness through Anesthesia. *J. Neurosci.* 33, 1757–1758. doi: 10.1523/JNEUROSCI.5215-12.2013

Smith, P. H., Manning, K. A., and Uhlrich, D. J. (2010). Evaluation of inputs to rat primary auditory cortex from the suprageniculate nucleus and extrastriate visual cortex. *J. Comp. Neurol.* 518, 3679–3700. doi: 10.1002/cne.22411

Smith, P. H., Uhlrich, D. J., Manning, K. A., and Banks, M. I. (2012). Thalamocortical projections to rat auditory cortex from the ventral and dorsal divisions of the medial geniculate nucleus. *J. Comp. Neurol.* 520, 34–51. doi: 10.1002/cne.22682

Solt, K., Van Dort, C. J., Chemali, J. J., Taylor, N. E., Kenny, J. D., and Brown, E. N. (2014). Electrical stimulation of the ventral tegmental area induces reanimation from general Anesthesia. *Anesthesiology* 121, 311–319. doi: 10.1097/ALN.0000000000000117

Stiebler, I., Neulist, R., Fichtel, I., and Ehret, G. (1997). The auditory cortex of the house mouse: left-right differences, tonotopic organization and quantitative analysis of frequency representation. *J. Comp. Physiol. A* 181, 559–571. doi: 10.1007/s003590050140

Storace, D. A., Higgins, N. C., and Read, H. L. (2010). Thalamic label patterns suggest primary and ventral auditory fields are distinct core regions. *J. Comp. Neurol.* 518, 1630–1646. doi: 10.1002/cne.22345

Szymanski, F. D., Garcia-Lazaro, J. A., and Schnupp, J. W. (2009). Current source density profiles of stimulus-specific adaptation in rat auditory cortex. *J. Neurophysiol.* 102, 1483–1490. doi: 10.1152/jn.00240.2009

Todorovic, A., Van Ede, F., Maris, E., and De Lange, F. P. (2011). Prior expectation mediates neural adaptation to repeated sounds in the auditory cortex: an MEG study. *J. Neurosci.* 31, 9118–9123. doi: 10.1523/JNEUROSCI.1425-11.2011

Tononi, G. (2004). An information integration theory of consciousness. *BMC Neurosci.* 5:42. doi: 10.1186/1471-2202-5-42

Verbny, Y. I., Erdelyi, F., Szabo, G., and Banks, M. I. (2006). Properties of a population of GABAergic cells in murine auditory cortex weakly excited by thalamic stimulation. *J. Neurophysiol.* 96, 3194–3208. doi: 10.1152/jn.00484.2006

Wacongne, C., Changeux, J. P., and Dehaene, S. (2012). A neuronal model of predictive coding accounting for the mismatch negativity. *J. Neurosci.* 32, 3665–3678. doi: 10.1523/JNEUROSCI.5003-11.2012

Warren, R. M. (1970). Perceptual restoration of missing speech sounds. *Science* 167, 392–393. doi: 10.1126/science.167.3917.392

Watson, B. O., Maclean, J. N., and Yuste, R. (2008). UP states protect ongoing cortical activity from thalamic inputs. *PLoS ONE* 3:e3971. doi: 10.1371/journal.pone.0003971

Wester, J. C., and Contreras, D. (2012). Columnar interactions determine horizontal propagation of recurrent network activity in neocortex. *J. Neurosci.* 32, 5454–5471. doi: 10.1523/JNEUROSCI.5006-11.2012

Westphalen, R. I., and Hemmings, H. C. Jr. (2006a). Volatile anesthetic effects on glutamate versus GABA release from isolated rat cortical nerve terminals: 4-aminopyridine-evoked release. *J. Pharmacol. Exp. Ther.* 316, 216–223. doi: 10.1124/jpet.105.090662

Westphalen, R. I., and Hemmings, H. C. Jr. (2006b). Volatile anesthetic effects on glutamate versus GABA release from isolated rat cortical nerve terminals: basal release. *J. Pharmacol. Exp. Ther.* 316, 208–215. doi: 10.1124/jpet.105.090647

Winegar, B. D., and Maciver, M. B. (2006). Isoflurane depresses hippocampal CA1 glutamate nerve terminals without inhibiting fiber volleys. *BMC Neurosci.* 7:5. doi: 10.1186/1471-2202-7-5

Winer, J. A., Sally, S. L., Larue, D. T., and Kelly, J. B. (1999). Origins of medial geniculate body projections to physiologically defined zones of rat primary auditory cortex. *Hear. Res.* 130, 42–61. doi: 10.1016/S0378-5955(98)00217-2

Zeki, S., and Shipp, S. (1988). The functional logic of cortical connections. *Nature* 335, 311–317. doi: 10.1038/335311a0

Zucker, R. S. (1989). Short-term synaptic plasticity. *Annu. Rev. Neurosci.* 12, 13–31. doi: 10.1146/annurev.ne.12.030189.000305

Conflict of Interest Statement: The authors declare that the research was conducted in the absence of any commercial or financial relationships that could be construed as a potential conflict of interest.

Received: 12 August 2014; accepted: 18 September 2014; published online: 07 October 2014.

Citation: Raz A, Grady SM, Krause BM, Uhlrich DJ, Manning KA and Banks MI (2014) Preferential effect of isoflurane on top-down vs. bottom-up pathways in sensory cortex. Front. Syst. Neurosci. ***8****:191. doi: 10.3389/fnsys.2014.00191*

This article was submitted to the journal Frontiers in Systems Neuroscience.

frontiers in
SYSTEMS NEUROSCIENCE

ORIGINAL RESEARCH ARTICLE
published: 01 July 2014
doi: 10.3389/fnsys.2014.00114

Electroencephalographic effects of ketamine on power, cross-frequency coupling, and connectivity in the alpha bandwidth

Stefanie Blain-Moraes[1], UnCheol Lee[1], SeungWoo Ku[2], GyuJeong Noh[2] and George A. Mashour[1,3]*

[1] *Department of Anesthesiology, Center for Consciousness Science, University of Michigan Medical School, Ann Arbor, MI, USA*
[2] *Department of Anesthesiology, Asan Medical Center, University of Ulsan College of Medicine, Seoul, South Korea*
[3] *Neuroscience Graduate Program, University of Michigan Medical School, Ann Arbor, MI, USA*

Edited by:
Anthony G. Hudetz, Medical College of Wisconsin, USA

Reviewed by:
Bruce MacIver, Stanford University, USA
Jamie Sleigh, University of Auckland, New Zealand

Correspondence:
George A. Mashour, Department of Anesthesiology, Center for Consciousness Science, University of Michigan Medical School, 1H247 UH/SPC-5048, 1500 East Medical Center Drive, Ann Arbor, MI 48109-5048, USA
e-mail: gmashour@med.umich.edu

Recent studies of propofol-induced unconsciousness have identified characteristic properties of electroencephalographic alpha rhythms that may be mediated by drug activity at γ-aminobutyric acid (GABA) receptors in the thalamus. However, the effect of ketamine (a primarily non-GABAergic anesthetic drug) on alpha oscillations has not been systematically evaluated. We analyzed the electroencephalogram of 28 surgical patients during consciousness and ketamine-induced unconsciousness with a focus on frontal power, frontal cross-frequency coupling, frontal-parietal functional connectivity (measured by coherence and phase lag index), and frontal-to-parietal directional connectivity (measured by directed phase lag index) in the alpha bandwidth. Unlike past studies of propofol, ketamine-induced unconsciousness was not associated with increases in the power of frontal alpha rhythms, characteristic cross-frequency coupling patterns of frontal alpha power and slow-oscillation phase, or decreases in coherence in the alpha bandwidth. Like past studies of propofol using undirected and directed phase lag index, ketamine reduced frontal-parietal (functional) and frontal-to-parietal (directional) connectivity in the alpha bandwidth. These results suggest that directional connectivity changes in the alpha bandwidth may be state-related markers of unconsciousness induced by both GABAergic and non-GABAergic anesthetics.

Keywords: ketamine, consciousness, general anesthesia, anesthetic-induced unconsciousness, anesthetic mechanisms

INTRODUCTION

Ketamine is an anesthetic drug that was introduced into clinical practice in the 1960s (Corssen and Domino, 1966) and is currently used for the induction of unconsciousness and, at subanesthetic doses, the prevention of acute pain or the treatment of depression. Ketamine is unique in the class of general anesthetics for a number of reasons. At the molecular level, the γ-aminobutyric acid $(GABA)_A$ receptor is not the primary target for ketamine, unlike many drugs used for the induction and maintenance of general anesthesia. Rather, ketamine is thought to act by antagonizing glutamatergic N-methyl-D-aspartate (NMDA) receptors (like the related anesthetics nitrous oxide and xenon) and/or hyperpolarization-activated cyclic-nucleotide gated (HCN)1 channels (Yamamura et al., 1990; Chen et al., 2009; Zhou et al., 2013). At the neurochemical level, ketamine is unique because it increases cortical acetylcholine levels and appears to depend on noradrenergic signaling for its effects, in contrast to a number of GABAergic anesthetics (Kikuchi et al., 1997; Kushikata et al., 2011). At the systems neuroscience level, ketamine is also distinct because it does not metabolically activate the ventrolateral preoptic nucleus, a sleep-promoting nucleus in the hypothalamus that is activated by commonly-used anesthetics such as propofol and isoflurane; instead, it activates the wake-promoting locus coeruleus (Lu et al., 2008). Furthermore, in contrast to virtually all other anesthetic and sedative drugs, ketamine does not appear to metabolically depress the thalamus (Långsjö et al., 2005). Finally, at the neurophysiologic level, ketamine tends to increase the power of high-frequency electroencephalographic activity, whereas most anesthetics depress this bandwidth (Maksimow et al., 2006). Ketamine therefore fails to conform to virtually all mechanistic frameworks of anesthetic-induced unconsciousness.

Despite the many unique characteristics of ketamine, we recently demonstrated that anesthetic doses of ketamine selectively inhibit frontal-to-parietal directed connectivity, as measured by symbolic transfer entropy in electroencephalographic signals (Lee et al., 2013b). This finding was notable because selective inhibition of effective and directional connectivity from frontal to parietal regions has been demonstrated for two commonly-used anesthetics that act (at least in part) through GABA receptors: propofol [demonstrated with symbolic transfer entropy, evolution map approach, dynamic causal modeling, directed phase lag index (dPLI)] and sevoflurane (demonstrated with symbolic transfer entropy, evolution map approach) (Lee et al., 2009, 2013a; Ku et al., 2011; Boly et al., 2012). Given the proposed role of top-down reentrant processing and frontal-parietal

networks in the conscious perception of environmental stimuli (Dehaene and Changeux, 2011; Demertzi et al., 2013), this finding suggests the exciting possibility of a common neurobiology underlying anesthetic-induced unconsciousness.

In the current study, we further characterized the effects of ketamine on the electroencephalogram, with a focus on alpha rhythms (8–14 Hz). Alpha oscillations have been an active area of research into anesthetic-induced unconsciousness because of a characteristic process referred to as *anteriorization*. In the resting/eyes-closed state in humans, the electroencephalographic power of alpha is dominant over the occipital cortex. However, at the point of propofol-induced unconsciousness, the power of alpha is dominant over the frontal cortex (Feshchenko et al., 2004; Purdon et al., 2013). Computational models that account for the observed posterior-to-anterior shift of alpha rhythms are based on propofol's agonism of $GABA_A$ receptors in the thalamus (Ching et al., 2010; Vijayan et al., 2013; Ching and Brown, 2014). The anteriorization of alpha at the point of propofol-induced unconsciousness also appears to relate to a characteristic cross-frequency coupling pattern between the amplitude of alpha and the phase of slow oscillations. During transitions into and out of propofol-induced unconsciousness, there is a trough-max relationship, i.e., the maximal alpha amplitude is coupled to the trough of the slow oscillation. During deeper levels of propofol-induced unconsciousness, however, this coupling shifts to a peak-max relationship (Purdon et al., 2013; Mukamel et al., 2014). These coupling patterns have not been investigated during unconsciousness induced by ketamine or other non-GABAergic anesthetics.

The propofol-induced shift to hypersynchronous alpha in the frontal cortex has been posited to impair flexible corticocortical communication (Supp et al., 2011), a process thought to be critical for consciousness. This hypothesis is supported by our recent work demonstrating that propofol-induced unconsciousness is characterized by a depression of anterior-to-posterior corticocortical connectivity (as measured by dPLI) that is found only in the alpha bandwidth (Lee et al., 2013a). dPLI is a measure of directional connectivity that appears to be closely related to alpha, since neural mass models of the human brain demonstrate an anterior-to-posterior flow of dPLI in the alpha bandwidth (Stam and van Straaten, 2012). This finding has been confirmed empirically by our previous study of dPLI in the resting state of conscious human volunteers (Lee et al., 2013a).

The potential dependence of anteriorized alpha rhythms on $GABA_A$ effects in the thalamus leads to the prediction that a non-GABAergic drug like ketamine would differ significantly from propofol and not increase the power of frontal alpha rhythms in association with the induction of unconsciousness. Similarly, we would not predict any characteristic cross-frequency coupling patterns around the time of unconsciousness, since these relationships appear to depend on increases in the frontal power of alpha. However, if the unconscious states induced by ketamine and propofol nonetheless share an underlying neurobiology, we would predict that the directional connectivity measure of dPLI would be inhibited by ketamine (as is observed with propofol), both in terms of the specificity of the alpha bandwidth and the anterior-to-posterior directionality. We tested these predictions regarding the effects of ketamine on alpha oscillations by re-analyzing electroencephalographic data acquired during consciousness and ketamine-induced unconsciousness in human surgical patients.

METHODS

PARTICIPANTS

We collected electroencephalographic data from 30 patients undergoing elective stomach, colorectal, thyroid or breast surgery (15 males; American Society Anesthesiologists Physical Status 1 or 2; 22–64 years old) at the Asan Medical Center (Seoul, South Korea). This study was approved by the Institutional Review Board of Asan Medical Center; written consent was provided by all participants after a careful discussion of risks and benefits. Patients were excluded from the study if they had a history of cardiovascular disease (including hypertension), brain surgery, drug/alcohol dependence, neurological or psychiatric disorder, or if they were currently using psychotropic medication. The data collected were previously analyzed and published (Lee et al., 2013b); the current study uses distinct analytic methods to test distinct hypotheses. For this secondary analysis, two participants were excluded due to insufficient artifact-free data in the baseline recording period; accordingly, data from 28 participants were analyzed at the University of Michigan Medical School (Ann Arbor, MI) for the current study.

ANESTHETIC PROTOCOL

Unconsciousness was induced using an infusion of ketamine (2 mg/kg diluted in 10 mL of 0.9% normal saline) over a 2 min period (Baxter infusion pumpAS40A, Baxter Healthcare Corporation, Deerfield, IL). Consciousness was monitored by assessing the participant's response to an auditory command ("squeeze your right hand twice"), which was repeated every 10 s. Prior to loss of consciousness, no sedatives or other medications were administered to the participant. Standard intraoperative monitors (non-invasive blood pressure measurement, electrocardiography, pulse oximetry and end-tidal carbon dioxide concentration and non-invasive) were used throughout the experiment; if systolic blood pressure increased to over 30% of baseline values, 5–10 mg of labetalol were administered.

ELECTROENCEPHALOGRAM DATA ACQUISITION

The electroencephalogram was acquired at 8 electrodes located at Fp1, Fp2, F3, F4, T3, T4, P3, and P4 (International 10–20 system); all channels were referenced to A2. Electrode impedances were reduced to below 5 KΩ prior to data collection and electroencephalographic signals were collected used a Laxtha WEEG-32 amplifier (LXE3232-RF, Laxtha Inc., Daejeon, Korea) with a sampling frequency of 256 Hz. Data recording began 5 min prior to induction; during this period, participants were instructed to rest with their eyes closed. Data collection continued through anesthetic induction and was terminated five minutes following loss of consciousness.

ELECTROENCEPHALOGRAM ANALYSIS

Preprocessing: Electroencephalogram data were bandpass filtered between 0.1 and 50 Hz. The filtered data were visually

inspected and non-physiological artifacts were removed. For the spectral and cross-frequency coupling analysis, two 5-min epochs of data were extracted from every participant: (1) Baseline rest, prior to ketamine induction, and (2) Induction and unconsciousness, beginning at the start of ketamine infusion. This second epoch was chosen specifically so that the transition from consciousness to unconsciousness could be studied, as some spectrographic and phase-amplitude coupling patterns appear during this period (Purdon et al., 2013). On average, participants lost consciousness 89 ± 14 s after the start of ketamine infusion; thus, this epoch contains electroencephalographic data from both conscious and unconscious states. However, coherence, phase lag index (PLI) and dPLI measures were calculated only with the data after ketamine-induced consciousness. **Spectral Analysis:** Spectrograms were computed in Chronux (www.chronux.org), using the multitaper method, with window lengths of $T = 2$ s, step size of 0.1 s, time-bandwidth product $NW = 2$, number of tapers $K = 3$. Group spectrograms were calculated by aggregating data from frontal channels F3 and F4 across all participants. **Phase-Amplitude Coupling Analysis:** Phase-amplitude coupling was conducted using the Phase-Amplitude Coupling Toolbox (PACT) in EEGlab (Delorme and Makeig, 2004; Miyakoshi et al., 2013). Finite impulse response filters were used to extract low-frequency (0.1–1 Hz) and alpha (8–14 Hz) oscillations from channels F3 and F4 for each participant. Instantaneous phase and amplitude were extracted using a Hilbert transform. Phase-amplitude modulograms were calculated by assigning each temporal sample to one of $N = 18$ equally spaced phase bins based on the instantaneous value of the low-frequency phase and then averaging the corresponding instantaneous amplitude of alpha within a 1 min epoch. Additionally, Canolty's phase-amplitude coupling modulation index was calculated for each minute of data and averaged across all participants (Canolty et al., 2006). **Functional Connectivity Analysis with Coherence:** The magnitude squared coherence estimate was calculated between each set of channel combinations using Welch's averaged modified periodogram method (Welch, 1967). **Functional Connectivity Analysis with Phase Lag Index (PLI):** To mitigate the effects of choice of reference and volume conduction, we calculated functional connectivity using the metric PLI (Stam et al., 2007). We used a Hilbert transform to extract the instantaneous phase of the electroencephalogram from each channel and calculated the phase difference $\Delta\phi_t$ between channels, where $\Delta\phi_t = \phi_{i,t} - \phi_{j,t}$, $t = 1, 2, \ldots,$ n n is the number of samples within one epoch, and i and j were set to include all possible channel combinations. PLI was then calculated using Equation (1):

$$\mathrm{PLI}_{ij} = \left|\langle \mathrm{sign}\,(\Delta\phi_t)\rangle\right|, \quad 0 \leq \mathrm{PLI}_{ij} \leq 1. \tag{1}$$

Here, the sign() function yields: 1 if $\Delta\phi_t > 0$; 0 if $\Delta\phi_t = 0$; and -1 if $\Delta\phi_t < 0$. If the instantaneous phase of one signal is consistently ahead of the other signal, the phases are considered locked, and PLI$\approx$ 1. However, if the signals randomly alternate between a phase lead and a phase lag relationship, there is no phase locking and PLI ≈ 0. **Directed Connectivity Analysis with Directed Phase Lag Index (dPLI):** To determine the direction of the phase-lead/phase-lag relationship between channels, we calculated dPLI between signals i and j using Equation (2) (Stam and van Straaten, 2012):

$$\mathrm{dPLI}_{ij} = \langle H(\Delta\pi_t)\rangle \tag{2}$$

Here, H (x) represents the Heaviside step function, where H (x) = $1 if\ x > 0$, H (x) = $0.5\ if\ x = 0$, $and\ H$ (x) = 0 otherwise. If, on average, signal i leads signal j, $0.5 < \mathrm{dPLI}_{ij} = 1$; if signal j leads signal i, $0 = \mathrm{dPLI}_{ij} < 0.5$; and if there is no phase-lead/phase-lag relationship between signals, dPLI = 0.5. **Surrogate Data Analysis:** To quantify the effects of spurious phase relationships and power spectrum changes on functional and directed connectivity metrics, we generated surrogate data sets as follows. We calculated the instantaneous phase of each combination of channel pairs i and j for each epoch (baseline; ketamine-induced unconsciousness) using a Hilbert transform. The phase time series of channel i was maintained, whereas in channel j, the phase time series from 0 to n/2 was interchanged with the phase time series from n/2 to n, where n is the number of samples within one epoch. In this manner, existing phase relationships were eliminated while maintaining the spectral properties of each condition. PLI and dPLI were calculated for all channel combinations in the surrogate dataset. **Brain Network Visualization:** The brain networks were visualized with the BrainNet Viewer (Xia et al., 2013) (http://www.nitrc.org/projects/bnv/). Montreal Neurological Institute (MNI) coordinates of each scalp electrode were used to generate nodes that were projected onto an axial view of the brain. Coherence, PLI, and dPLI measures were indicated by varying the color and size of edges between these nodes.

STATISTICAL ANALYSIS

Phase Amplitude Coupling: To test the null hypothesis that the phase and amplitude of the frontal electroencephalogram are decoupled, we employed the surrogate data method proposed in Canolty et al. (2006). Data were divided into 1-min epochs; within each epoch, a surrogate time series was generated by shifting the amplitude by a random time Δt ($0 \leq \Delta t \leq 60$ s) while keeping the phase series fixed. The modulation index was calculated for the surrogate series. This procedure was repeated 2000 times to produce distributions of modulation index values in which the null hypothesis was true. The modulation index for the experimental data was considered significant if it exceeded 95% of the surrogate values ($p < 0.05$). **Coherence, PLI, and dPLI:** Coherence, PLI, and dPLI values were compared between (1) baseline and unconscious epochs, (2) baseline and surrogate baseline epochs, and (3) unconscious and surrogate unconscious epochs using a student's t-test. Differences were considered significant at $\alpha < 0.05$.

RESULTS

KETAMINE-INDUCED UNCONSCIOUSNESS IS NOT CHARACTERIZED BY INCREASES IN FRONTAL ALPHA POWER OR BY PHASE-AMPLITUDE COUPLING PATTERNS

The group-level spectrogram of the electroencephalogram recorded from frontal channels demonstrates a decrease in alpha power upon ketamine-induced unconsciousness (**Figure 1**). This

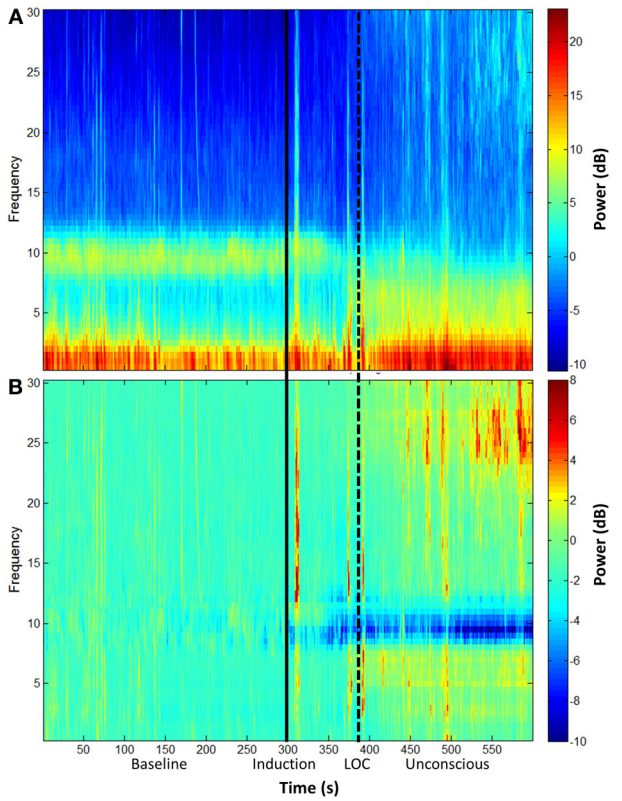

FIGURE 1 | Group spectral analysis. (A) Spectrogram and **(B)** baseline-normalized spectrogram of frontal channels (F3 and F4) demonstrate a decrease in alpha power during and after ketamine-induced unconsciousness. LOC, loss of consciousness.

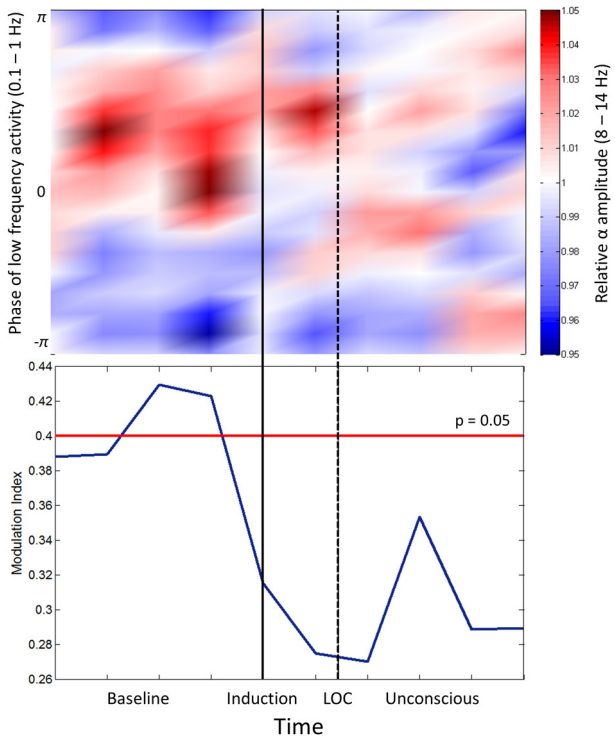

FIGURE 2 | Phase-amplitude coupling analysis. Top panel: Frontal phase-amplitude coupling across baseline and induction/unconscious epochs. **Bottom panel**: Modulation indices (blue line) of each minute of data in baseline and induction/unconscious epochs; values are significant at $p = 0.05$ above the red line. LOC, loss of consciousness.

is the opposite pattern to that observed in propofol-induced unconsciousness, which is associated with an increase in alpha power (Purdon et al., 2013).

Cross-frequency coupling patterns were calculated between slow oscillation phase and alpha amplitude in the frontal channels. Group modulograms and the group-averaged modulation index demonstrate that a significant trough-max coupling pattern existed for 40% of the baseline resting state, but no significant coupling was observed upon induction or after loss of consciousness (**Figure 2**). These patterns are in contrast to those observed with propofol, where loss of consciousness is associated with a trough-max coupling pattern (Mukamel et al., 2014). It is worthwhile noting that when the test for phase-amplitude coupling significance (Canolty et al., 2006) is applied to datasets with minimal to no cross-frequency coupling patterns, epochs with even moderate coupling patterns will exceed the modulation index associated with significance. This may explain the significant phase-amplitude coupling observed during the resting state of our study, which has not been observed in previous studies.

KETAMINE-INDUCED UNCONSCIOUSNESS IS ASSOCIATED WITH DECREASES IN PLI, BUT NOT IN COHERENCE

We examined two measures of functional connectivity in the alpha bandwidth between frontal and parietal channels: coherence and PLI. We observed no significant change in frontoparietal coherence ($p = 0.29$) between baseline resting and ketamine-induced unconsciousness (**Figure 3**).

In contrast, PLI decreased upon ketamine-induced unconsciousness. The largest decrease in PLI was observed in the alpha bandwidth, where PLI values during unconsciousness were significantly lower than PLI values calculated during baseline consciousness ($p < 0.001$) (**Figures 4A,B**). PLI values measured from surrogate data in both epochs were ∼0, indicating that the values calculated from experimental data are not the result of spurious phase relationships. While there was an overall decrease in PLI across all channel combinations, the largest decrease occurred across frontoparietal channel pairs (**Figure 4C**).

KETAMINE-INDUCED UNCONSCIOUSNESS IS ASSOCIATED WITH DECREASED FRONTOPARIETAL dPLI

We examined differences in dPLI between baseline resting and unconscious states. The greatest differences in dPLI occurred in the alpha bandwidth (**Figure 5A**) and a significant decrease in dPLI from frontal to parietal brain regions ($p < 0.001$) was observed between states (**Figure 5B**). There was no significant difference between dPLI values of the surrogate data generated from either state, indicating that the observed changes in dPLI for the experimental data cannot be attributed to changes in spectral power between conditions. Baseline dPLI indicated

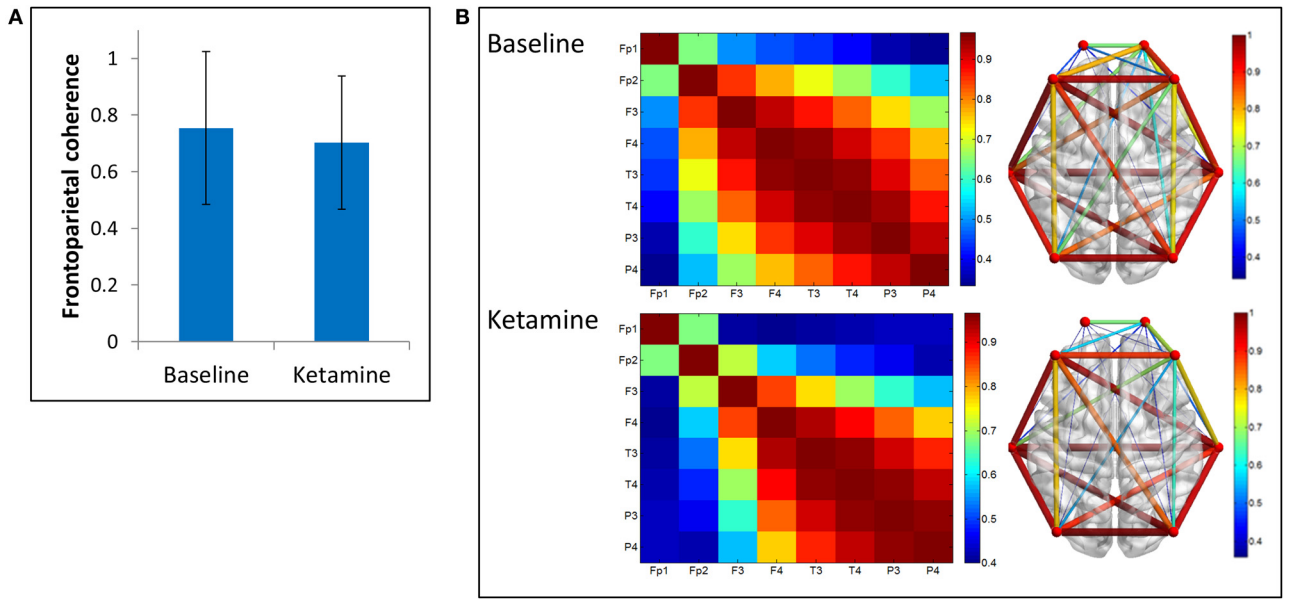

FIGURE 3 | Coherence analysis. (A) Average frontoparietal coherence across 28 participants in baseline resting and ketamine-induced unconscious states (error bars indicate standard deviation). No significant differences are observed in coherence between conditions. **(B)** Average coherence across all channel combinations in baseline rest and ketamine-induced unconscious states, represented on a channel grid (left) and on an axial view of the brain (right). On the brain network, both color and size of the edges represent strength of coherence.

that the dominant direction of connectivity is from frontal to parietal regions when participants are conscious; upon ketamine-induced unconsciousness there is a balance of frontoparietal and parietofrontal directional connectivity (**Figure 5C**).

DISCUSSION

This study of ketamine and alpha oscillations revealed both drug-related and state-related effects in association with the induction of unconsciousness. Unlike propofol, ketamine does not increase frontal alpha power or induce characteristic cross-frequency coupling patterns between the power of alpha and the phase of slow-wave oscillations. Functional connectivity in the alpha bandwidth was preserved between states when measured by coherence, but decreased upon unconsciousness when measured by PLI. The discrepancy between these two functional connectivity metrics indicates that while the correlation between electroencephalogram signals in frontal and parietal regions remains unchanged in aggregate, their specific phase-relationship is disrupted upon loss of consciousness. Directional connectivity in the alpha bandwidth (as measured by dPLI) was inhibited across the frontoparietal network by ketamine, a finding consistent with our past study of propofol-induced unconsciousness (Lee et al., 2013a). The identification of shared neural features between the unconscious states induced by GABAergic and non-GABAergic anesthetics has been a longstanding problem in the study of both anesthetic mechanisms and anesthetic monitoring. The current findings support the hypothesis that anesthetic-induced unconsciousness has a common neurobiology related to disrupted functional relationships across cortical or thalamocortical networks.

Activity and connectivity of lateral frontal and posterior parietal cortices have been hypothesized to be critical for consciousness of environmental stimuli (Boly et al., 2007; Demertzi et al., 2013). As such, the finding that a variety of general anesthetic drugs suppresses both activity and connectivity in these regions appears relevant to the proximate cause of anesthetic-induced unconsciousness. Prior preclinical studies of anterior-posterior connectivity in rat brain identified a selective inhibition of frontal-to-posterior transfer entropy in the gamma bandwidth in association with isoflurane-induced unconsciousness (Imas et al., 2005). Our laboratory first demonstrated anesthetic inhibition of frontal-to-parietal connectivity in human volunteers (Lee et al., 2009) and surgical patients (Ku et al., 2011); inhibition of functional, directional, and effective connectivity in frontal-parietal networks in association with propofol-induced unconsciousness has been identified by studies from multiple research groups using multiple analytic methods (Boveroux et al., 2010; Schrouff et al., 2011; Boly et al., 2012; Jordan et al., 2013). Of note, the recent study of Jordan et al used combined electroencephalography and functional magnetic resonance imaging with no *a priori* assumptions regarding connectivity and found that the selective loss of frontal-to-parietal connectivity (as measured by symbolic transfer entropy) was the best discriminator between consciousness and propofol-induced unconsciousness (Jordan et al., 2013). However, most studies of directional/effective connectivity in frontal-parietal networks have focused on propofol, a prototypical $GABA_A$ agonist. Recently, our laboratory demonstrated a similar and selective inhibition of frontal-to-parietal connectivity during unconsciousness induced by the diverse anesthetics ketamine, propofol, and sevoflurane (Lee et al., 2013b). This study was the first to identify a common network-level disruption induced by both GABAergic and non-GABAergic anesthetics. The

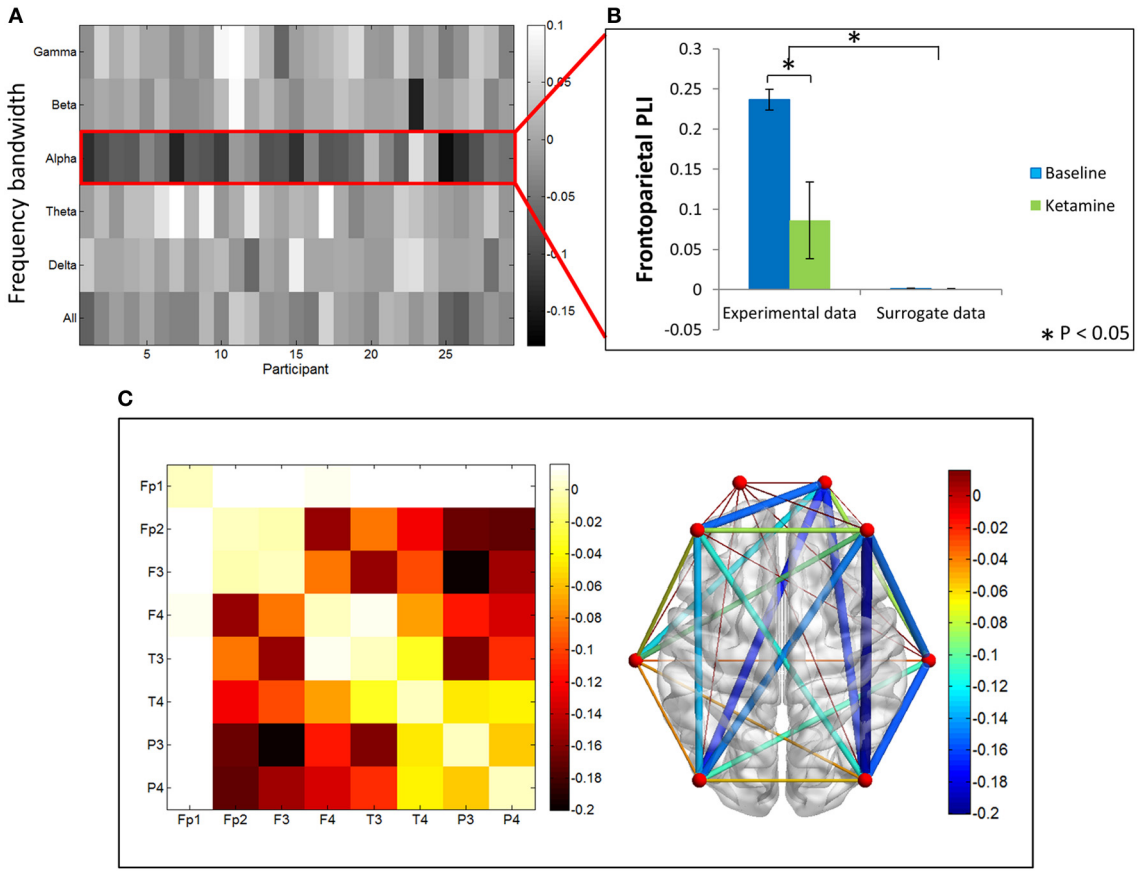

FIGURE 4 | Phase lag index analysis. (A) Difference in PLI between baseline and ketamine-induced unconscious states represented for all bandwidths, across all participants. The largest decreases in PLI are observed in the alpha bandwidth. **(B)** Average frontoparietal PLI values for experimental data and surrogate data (error bars indicate standard deviation). Frontoparietal PLI significantly decreases (as indicated by *) between states in the experimental data; no phase-locking is observed in the surrogate dataset. **(C)** Average difference in PLI between baseline and unconscious states across all channel combinations, represented on a channel grid (left), and on the axial view of the brain (right). Color and size of edges in the brain network represent the difference in PLI between baseline and unconscious states. Large decreases in PLI are observed between frontoparietal channel combinations.

current study builds on this work by using alternative connectivity measures to support the hypothesis that anesthetic-induced unconsciousness is characterized by interrupted directed connectivity from frontal to parietal regions. Impaired connectivity is of relevance to the mechanism of anesthetic-induced unconsciousness because it reduces the likelihood of achieving the neural information synthesis thought to be necessary for conscious perception (Tononi, 2011). Furthermore, by comparing ketamine's effects on the alpha bandwidth to past studies of propofol, we are now able to distinguish between drug-related and state-related effects on the electroencephalogram. Despite the divergent spectral effects on alpha oscillations induced by ketamine in this study and those reported in past studies of propofol, disruption of functional (PLI) and directional (dPLI) connectivity in the alpha bandwidth appears common to the state of unconsciousness induced by both drugs. It should be noted that changes in dPLI were reversed upon recovery from propofol; given the current study design we were not able to assess recovery of directional connectivity for ketamine.

This study has numerous limitations. First, we reanalyzed electroencephalographic data from a prior study of ketamine-induced unconsciousness (Lee et al., 2013b). It might be argued that the current findings could have been predicted from our past methodology using symbolic transfer entropy. However, this is not necessarily the case, since analysis of the same electroencephalographic dataset (Murphy et al., 2011) with dynamic causal modeling (Boly et al., 2012) and Granger causality (Barrett et al., 2012) yielded discrepant results regarding directionality across frontal and parietal cortices. Second, we used low-resolution electroencephalography given the clinical nature of the original study; thus, source-localized signals could not be analyzed. Third, there was no recording from occipital electrodes, which precluded topographic analysis that would allow comparison of alpha power in posterior and anterior structures. Fourth, it could be argued that the state of ketamine-induced unconsciousness is substantially distinct from the state of propofol-induced unconsciousness, which renders any comparisons questionable. Although it is true that ketamine-based anesthetics can

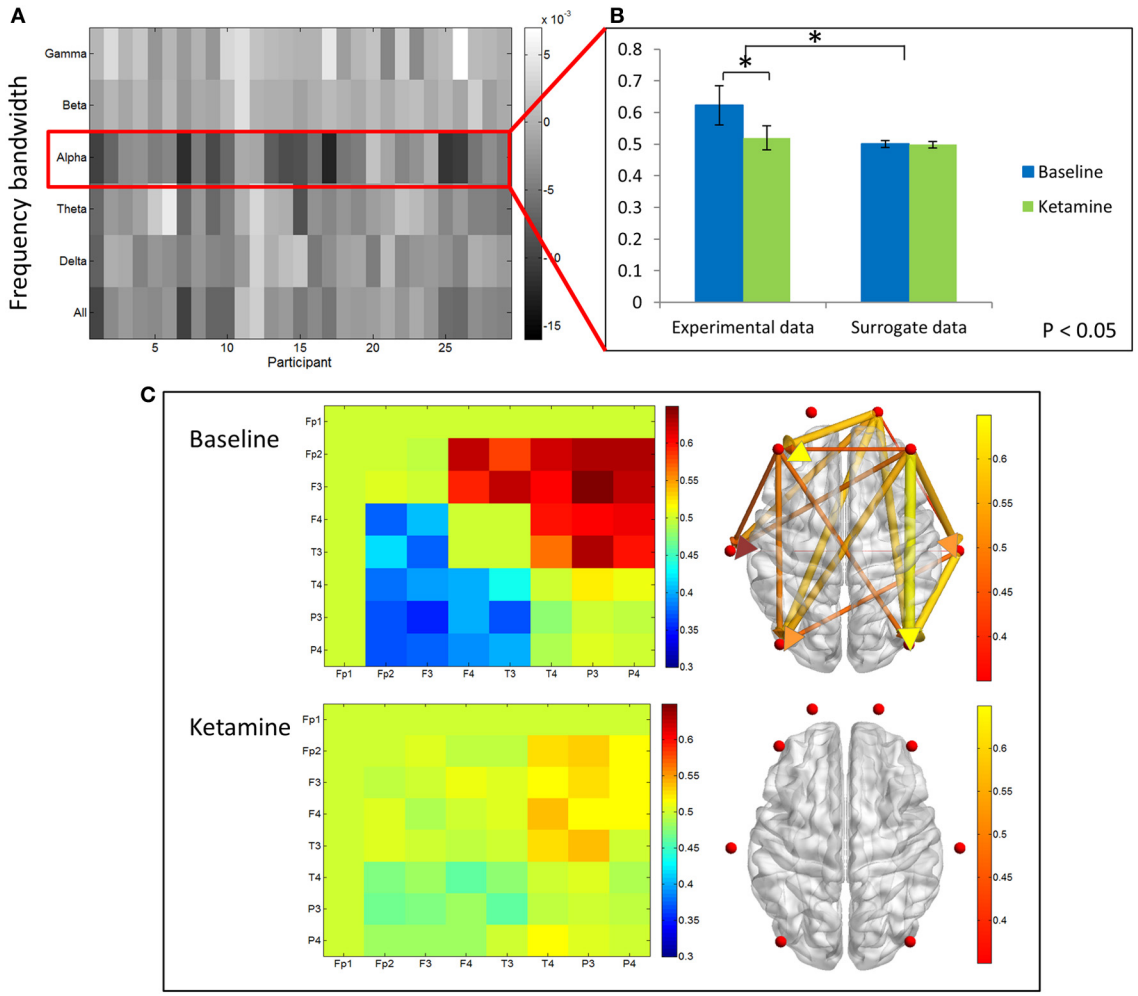

FIGURE 5 | Directed phase lag index analysis. (A) Difference in frontoparietal dPLI between baseline rest and ketamine-induced unconscious states, represented across six frequency bandwidths and all participants. The largest decreases in dPLI occur in the alpha bandwidth. Note that a dPLI value of 0.5 indicates neither phase lag nor phase lead relationship. **(B)** Average frontoparietal dPLI values for each state in experimental and surrogate data (error bars indicate standard deviation). Frontoparietal dPLI significantly decreases during ketamine-induced unconsciousness (as indicated by *). Surrogate data demonstrate no phase-lead/phase-lag relationship in either state. **(C)** Average dPLI values across all channel combinations in baseline and unconscious states. Only dPLI values greater than 0.55 are represented on the axial brain network. In this network, color, and size of the edges indicate the dPLI value between two nodes; arrows indicate the direction of phase lead and lag.

be associated with conscious states such as dreaming or hallucinations (Grace, 2003), the same could be argued—albeit to a lesser degree—for propofol (Leslie et al., 2007). Furthermore, from the functional perspective, both ketamine and propofol can be used to induce unconsciousness in clinical settings; this functional similarity motivates the search for common mechanisms. Fifth, it one could argue that the reduction in PLI and dPLI we observed in the alpha bandwidth during induction/unconsciousness can be attributed to the dramatic decrease in power upon loss of consciousness. However, we have demonstrated that PLI and dPLI values calculated for surrogate datasets that have the same spectral characteristics are not significantly different. Furthermore, the fact that coherence values are not significantly different between states demonstrates that the change in PLI and dPLI values cannot be attributed to reduced power in the alpha bandwidth. Finally, we used loss of responsiveness as a surrogate for loss of consciousness; it is well known that consciousness and responsiveness are dissociable. However, this is a limitation common to all studies of anesthetic-induced unconsciousness. Although, as noted, loss of responsiveness induced by ketamine may still be associated with conscious states such as dreams, it is the connection to the environment that is likely of primary clinical relevance (Sanders et al., 2012).

Despite these limitations, this analysis of ketamine's effects on spectral changes, cross-frequency coupling, and connectivity in the alpha bandwidth provides insight into the neurobiology of ketamine-induced unconsciousness. In comparison with past studies of propofol, the distinct effects of ketamine suggest that the ability to induce anteriorized alpha and cross-frequency coupling varies across anesthetic drugs. By contrast, disrupted

directional connectivity in the frontal-parietal network may be a common state-related feature—and, potentially, a common mechanism—of anesthetic-induced unconsciousness.

FUNDING

Supported by departmental and institutional funds.

REFERENCES

Barrett, A. B., Murphy, M., Bruno, M.-A., Noirhomme, Q., Boly, M., Laureys, S., et al. (2012). Granger causality analysis of steady-state electroencephalographic signals during propofol-induced anaesthesia. *PLoS ONE* 7:e29072. doi: 10.1371/journal.pone.0029072

Boly, M., Balteau, E., Schnakers, C., Degueldre, C., Moonen, G., Luxen, A., et al. (2007). Baseline brain activity fluctuations predict somatosensory perception in humans. *Proc. Natl. Acad. Sci. U.S.A.* 104, 12187–12192. doi: 10.1073/pnas.0611404104

Boly, M., Moran, R., Murphy, M., Boveroux, P., Bruno, M.-A., Noirhomme, Q., et al. (2012). Connectivity changes underlying spectral EEG changes during propofol-induced loss of consciousness. *J. Neurosci.* 32, 7082–7090. doi: 10.1523/JNEUROSCI.3769-11.2012

Boveroux, P., Vanhaudenhuyse, A., Bruno, M.-A., Noirhomme, Q., Lauwick, S., Luxen, A., et al. (2010). Breakdown of within- and between-network resting state functional magnetic resonance imaging connectivity during propofol-induced loss of consciousness. *Anesthesiology* 113, 1038–1053. doi: 10.1097/ALN.0b013e3181f697f5

Canolty, R. T., Edwards, E., Dalal, S. S., Soltani, M., Nagarajan, S. S., Kirsch, H. E., et al. (2006). High gamma power is phase-locked to theta oscillations in human neocortex. *Science* 313, 1626–1628. doi: 10.1126/science.1128115

Chen, X., Shu, S., and Bayliss, D. A. (2009). HCN1 channel subunits are a molecular substrate for hypnotic actions of ketamine. *J. Neurosci.* 29, 600–609. doi: 10.1523/JNEUROSCI.3481-08.2009

Ching, S., and Brown, E. N. (2014). Modeling the dynamical effects of anesthesia on brain circuits. *Curr. Opin. Neurobiol.* 25, 116–122. doi: 10.1016/j.conb.2013.12.011

Ching, S., Cimenser, A., Purdon, P. L., Brown, E. N., and Kopell, N. J. (2010). Thalamocortical model for a propofol-induced α-rhythm associated with loss of consciousness. *Proc. Natl. Acad. Sci. U.S.A.* 107, 22665–22670. doi: 10.1073/pnas.1017069108

Corssen, G., and Domino, E. F. (1966). Dissociative anesthesia: further pharmacologic studies and first clinical experience with the phencyclidine derivative CI-581. *Anesth. Analg.* 45, 29–40.

Dehaene, S., and Changeux, J.-P. (2011). Experimental and theoretical approaches to conscious processing. *Neuron* 70, 200–227. doi: 10.1016/j.neuron.2011.03.018

Delorme, A., and Makeig, S. (2004). EEGLAB: an open source toolbox for analysis of single-trial EEG dynamics including independent component analysis. *J. Neurosci. Methods* 134, 9–21. doi: 10.1016/j.jneumeth.2003.10.009

Demertzi, A., Soddu, A., and Laureys, S. (2013). Consciousness supporting networks. *Curr. Opin. Neurobiol.* 23, 239–211. doi: 10.1016/j.conb.2012.12.003

Feshchenko, V. A., Veselis, R. A., and Reinsel, R. A. (2004). Propofol-induced alpha rhythm. *Neuropsychobiology* 50, 257–266. doi: 10.1159/000079981

Grace, R. F. (2003). The effect of variable-dose diazepam on dreaming and emergence phenomena in 400 cases of ketamine-fentanyl anaesthesia. *Anaesthesia* 58, 904–910. doi: 10.1046/j.1365-2044.2003.03341.x

Imas, O. A., Ropella, K. M., Ward, B. D., Wood, J. D., and Hudetz, A. G. (2005). Volatile anesthetics disrupt frontal-posterior recurrent information transfer at gamma frequencies in rat. *Neurosci. Lett.* 387, 145–150. doi: 10.1016/j.neulet.2005.06.018

Jordan, D., Ilg, R., Riedl, V., Schorer, A., Grimberg, S., Neufang, S., et al. (2013). Simultaneous electroencephalographic and functional magnetic resonance imaging indicate impaired cortical top–down processing in association with anesthetic-induced unconsciousness. *Anesthesiology* 119, 1031–1042. doi: 10.1097/ALN.0b013e3182a7ca92

Kikuchi, T., Wang, Y., Shinbori, H., Sato, K., and Okumura, F. (1997). Effects of ketamine and pentobarbitone on acetylcholine release from the rat frontal cortex *in vivo*. *Br. J. Anaesth.* 79, 128–130.

Ku, S.-W., Lee, U., Noh, G.-J., Jun, I.-G., and Mashour, G. A. (2011). Preferential inhibition of frontal-to-parietal feedback connectivity is a neurophysiologic correlate of general anesthesia in surgical patients. *PLoS ONE* 6:e25155. doi: 10.1371/journal.pone.0025155

Kushikata, T., Yoshida, H., Kudo, M., Kudo, T., Kudo, T., and Hirota, K. (2011). Role of coerulean noradrenergic neurones in general anaesthesia in rats. *Br. J. Anaesth.* 107, 924–929. doi: 10.1093/bja/aer303

Långsjö, J. W., Maksimow, A., Salmi, E., Kaisti, K., Aalto, S., Oikonen, V., et al. (2005). S-ketamine anesthesia increases cerebral blood flow in excess of the metabolic needs in humans. *Anesthesiology* 103, 258–268. doi: 10.1097/00000542-200508000-00008

Lee, H., Mashour, G. A., Noh, G.-J., Kim, S., and Lee, U. (2013a). Reconfiguration of network hub structure after propofol-induced unconsciousness. *Anesthesiology* 119, 1347–1359. doi: 10.1097/ALN.0b013e3182a8ec8c

Lee, U., Kim, S., Noh, G.-J., Choi, B.-M., Hwang, E., and Mashour, G. A. (2009). The directionality and functional organization of frontoparietal connectivity during consciousness and anesthesia in humans. *Conscious. Cogn.* 18, 1069–1078. doi: 10.1016/j.concog.2009.04.004

Lee, U., Ku, S., Noh, G., Baek, S., Choi, B., and Mashour, G. A. (2013b). Disruption of frontal-parietal communication by ketamine, propofol, and sevoflurane. *Anesthesiology* 118, 1264–1275. doi: 10.1097/ALN.0b013e31829103f5

Leslie, K., Skrzypek, H., Paech, M., Kurowski, I., and Whybrow, T. (2007). Dreaming during anesthesia and anesthetic depth in elective surgery patients: a prospective cohort study. *Anesthesiology* 106, 33–42. doi: 10.1097/00000542-200701000-00010

Lu, J., Nelson, L. E., Franks, N., Maze, M., Chamberlin, N. L., and Saper, C. B. (2008). Role of endogenous sleep-wake and analgesic systems in anesthesia. *J. Comp. Neurol.* 508, 648–662. doi: 10.1002/cne.21685

Maksimow, A., Särkelä, M., Långsjö, J. W., Salmi, E., Kaisti, K. K., Yli-Hankala, A., et al. (2006). Increase in high frequency EEG activity explains the poor performance of EEG spectral entropy monitor during S-ketamine anesthesia. *Clin. Neurophysiol.* 117, 1660–1668. doi: 10.1016/j.clinph.2006.05.011

Miyakoshi, M., Delorme, A., Mullen, T., Kojima, K., Makeig, S., and Asano, E. (2013). Automated detection of cross-frequency coupling in the electrocorticogram for clinical inspection. *Conf. Proc. IEEE Eng. Med. Biol. Soc.* 2013, 3282–3285. doi: 10.1109/EMBC.2013.6610242

Mukamel, E. A., Pirondini, E., Babadi, B., Wong, K. F. K., Pierce, E. T., Harrell, P. G., et al. (2014). A transition in brain state during propofol-induced unconsciousness. *J. Neurosci.* 34, 839–845. doi: 10.1523/JNEUROSCI.5813-12.2014

Murphy, M., Bruno, M.-A., Riedner, B. A., Boveroux, P., Noirhomme, Q., Landsness, E. C., et al. (2011). Propofol anesthesia and sleep: a high-density EEG study. *Sleep* 34, 283–291.

Purdon, P. L., Pierce, E. T., Mukamel, E. A., Prerau, M. J., Walsh, J. L., Wong, K. F. K., et al. (2013). Electroencephalogram signatures of loss and recovery of consciousness from propofol. *Proc. Natl. Acad. Sci. U.S.A.* 110, E1142–E1151. doi: 10.1073/pnas.1221180110

Sanders, R. D., Tononi, G., Laureys, S., and Sleigh, J. W. (2012). Unresponsiveness ≠ unconsciousness. *Anesthesiology* 116, 946–959. doi: 10.1097/ALN.0b013e318249d0a7

Schrouff, J., Perlbarg, V., Boly, M., Marrelec, G., Boveroux, P., Vanhaudenhuyse, A., et al. (2011). Brain functional integration decreases during propofol-induced loss of consciousness. *Neuroimage* 57, 198–205. doi: 10.1016/j.neuroimage.2011.04.020

Stam, C. J., Nolte, G., and Daffertshofer, A. (2007). Phase lag index: assessment of functional connectivity from multi channel EEG and MEG with diminished bias from common sources. *Hum. Brain Mapp.* 28, 1178–1193. doi: 10.1002/hbm.20346

Stam, C. J., and van Straaten, E. C. W. (2012). Go with the flow: use of a directed phase lag index (dPLI) to characterize patterns of phase relations in a large-scale model of brain dynamics. *Neuroimage* 62, 1415–1428. doi: 10.1016/j.neuroimage.2012.05.050

Supp, G. G., Siegel, M., Hipp, J. F., and Engel, A. K. (2011). Cortical hypersynchrony predicts breakdown of sensory processing during loss of consciousness. *Curr. Biol.* 21, 1988–1993. doi: 10.1016/j.cub.2011.10.017

Tononi, G. (2011). The integrated information theory of consciousness: an updated account. *Arch. Ital. Biol.* 150, 56–90. doi: 10.4449/aib.v149i5.1388

Vijayan, S., Ching, S., Purdon, P. L., Brown, E. N., and Kopell, N. J. (2013). Thalamocortical mechanisms for the anteriorization of alpha rhythms during propofol-induced unconsciousness. *J. Neurosci.* 33, 11070–11075. doi: 10.1523/JNEUROSCI.5670-12.2013

Welch, P. D. (1967). The use of fast Fourier transform for the estimation of power spectra: a method based on time averaging over short, modified periodograms. *IEEE Trans. Audio Electroacoustics* 15, 70–73. doi: 10.1109/TAU.1967.1161901

Xia, M., Wang, J., and He, Y. (2013). BrainNet Viewer: a network visualization tool for human brain connectomics. *PLoS ONE* 8:e68910. doi: 10.1371/journal.pone.0068910

Yamamura, T., Harada, K., Okamura, A., and Kemmotsu, O. (1990). Is the site of action of ketamine anesthesia the N-methyl-D-aspartate receptor? *Anesthesiology* 72, 704–710.

Zhou, C., Douglas, J. E., Kumar, N. N., Shu, S., Bayliss, D. A., and Chen, X. (2013). Forebrain HCN1 channels contribute to hypnotic actions of ketamine. *Anesthesiology* 118, 785–795. doi: 10.1097/ALN.0b013e318287b7c8

Conflict of Interest Statement: Dr. George A. Mashour and Dr. UnCheol Lee have a patent pending (through the University of Michigan, Ann Arbor) on the measurement of directional connectivity for monitoring consciousness. The authors declare that the research was conducted in the absence of any commercial or financial relationships that could be construed as a potential conflict of interest.

Received: 22 April 2014; accepted: 27 May 2014; published online: 01 July 2014.
*Citation: Blain-Moraes S, Lee U, Ku S, Noh G and Mashour GA (2014) Electroencephalographic effects of ketamine on power, cross-frequency coupling, and connectivity in the alpha bandwidth. Front. Syst. Neurosci. **8**:114. doi: 10.3389/fnsys.2014.00114*
This article was submitted to the journal Frontiers in Systems Neuroscience.

frontiers in
SYSTEMS NEUROSCIENCE

ORIGINAL RESEARCH ARTICLE
published: 18 December 2014
doi: 10.3389/fnsys.2014.00237

Propofol and sevoflurane induce distinct burst suppression patterns in rats

Jonathan D. Kenny[1], M. Brandon Westover[2,3], ShiNung Ching[4], Emery N. Brown[1,5,6,7] and Ken Solt[1,5]*

[1] Department of Anesthesia, Critical Care and Pain Medicine, Massachusetts General Hospital, Boston, MA, USA
[2] Department of Neurology, Harvard Medical School, Boston, MA, USA
[3] Department of Neurology, Massachusetts General Hospital, Boston, MA, USA
[4] Department of Electrical and Systems Engineering, Washington University in St. Louis, St. Louis, Missouri, USA
[5] Department of Anaesthesia, Harvard Medical School, Boston, MA, USA
[6] Institute for Medical Engineering and Science, Massachusetts Institute of Technology, Cambridge, MA, USA
[7] Department of Brain and Cognitive Sciences, Massachusetts Institute of Technology, Cambridge, MA, USA

Edited by:
Anthony G. Hudetz, Medical College of Wisconsin, USA

Reviewed by:
Bruce MacIver, Stanford University School of Medicine, USA
Ville Jäntti, Tampere University of Technology, Finland

****Correspondence:***
Ken Solt, Department of Anesthesia, Critical Care and Pain Medicine, Massachusetts General Hospital, 55 Fruit Street, GRB-444, Boston, MA 02114, USA
e-mail: ksolt@mgh.harvard.edu

Burst suppression is an EEG pattern characterized by alternating periods of high-amplitude activity (bursts) and relatively low amplitude activity (suppressions). Burst suppression can arise from several different pathological conditions, as well as from general anesthesia. Here we review current algorithms that are used to quantify burst suppression, its various etiologies, and possible underlying mechanisms. We then review clinical applications of anesthetic-induced burst suppression. Finally, we report the results of our new study showing clear electrophysiological differences in burst suppression patterns induced by two common general anesthetics, sevoflurane and propofol. Our data suggest that the circuit mechanisms that generate burst suppression activity may differ among general anesthetics.

Keywords: burst suppression, propofol, sevoflurane, anesthesia, rodent

INTRODUCTION

Burst suppression is an EEG pattern characterized by quasiperiodic high amplitude activity (bursts) and relativity low amplitude activity (suppressions; Amzica, 2009; Brown et al., 2010). The phenomenon was first observed while recording EEG from the motor cortex of cats under tribromoethanol and pentobarbital-induced general anesthesia (Derbyshire et al., 1936). Investigations into the effects of ether and pentobarbital anesthesia on the EEG of canines led to the creation of the term "burst suppression" (Swank and Watson, 1949). Although early work on burst suppression focused on general anesthesia, burst suppression can be induced by several different etiologies (Martin et al., 1959).

In the first part of this article, algorithms employed to quantify burst suppression, different causes of burst suppression, and theories about the mechanisms underlying burst suppression are reviewed. We also describe clinical applications of burst suppression induced by general anesthetics. In the second part of this article, we present original research findings from our laboratory that demonstrate the distinct electrophysiological characteristics of burst suppression induced by the inhaled anesthetic sevoflurane and the intravenous anesthetic propofol.

QUANTIFICATION OF BURST SUPPRESSION

A widely used method for quantifying burst suppression is the burst suppression ratio (BSR; Rampil et al., 1988). **Figure 1** shows several seconds of EEG burst suppression from a rodent anesthetized with isoflurane. The BSR is calculated by segmenting the EEG into bursts and suppressions using a voltage-based threshold. Suppression is commonly defined as a voltage less than 5 μV for greater than 0.5 s. This threshold is commonly set manually (Chemali et al., 2011) though automated methods such as a time-domain based voltage envelope threshold or frequency-domain based logistic regression of the EEG spectrogram have also been reported. (Prerau and Purdon, 2013; Westover et al., 2013). For the BSR algorithm, suppressions are given a value of 1 and bursts are given a value of 0 to create a binary time-series. This binary time-series is then smoothed with a windowing function to calculate the BSR over time. The value of the BSR ranges from 0 and 1, with 0 indicating no suppression and 1 indicating a suppressed EEG. Although the BSR can be derived with relative ease, the temporal resolution/smoothness of the result depends on the size of the time windows, which must be chosen manually, and the inability to obtain a measure of confidence around BSR estimates makes it difficult to perform statistical comparisons between BSR values at different points in time. Currently available EEG-based anesthetic depth monitors usually detect and quantify the BSR.

The burst suppression probability (BSP) is an alternate approach to model the level of burst suppression (Chemali et al., 2013). The BSP is based on a state-space model of the brain state of burst suppression, and represents the instantaneous probability

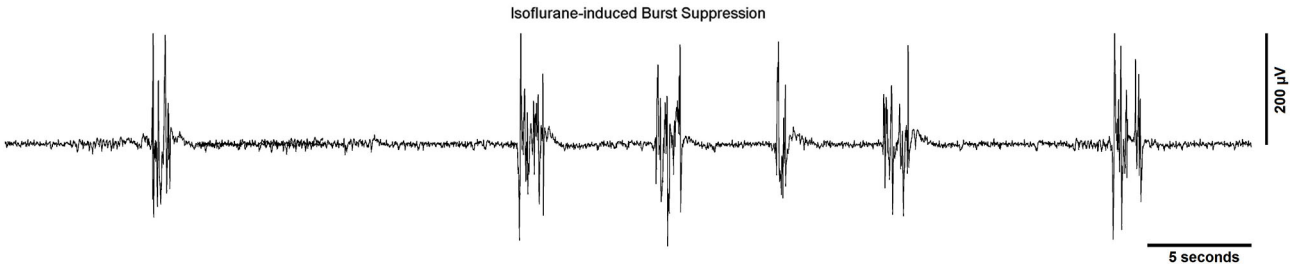

FIGURE 1 | A typical EEG recording showing a burst suppression pattern from a rodent undergoing general anesthesia from isoflurane. The sampling rate of the signal was 512 Hz and a line filter was used to eliminate 60 Hz noise.

of the brain being in a suppressed state. In contrast to the BSR, principled automated methods have been developed for setting the BSP algorithm parameters and the resulting temporal resolution/smoothness of the estimated BSP, and they also allow for statistical comparisons of the level of suppression across different points in time. Entropy measures such as approximate entropy (Bruhn et al., 2000, 2001) and machine learning methods such as artificial neural networks or support vector machines (Löfhede et al., 2007) have also been used to quantify burst suppression.

PATHOLOGICAL CAUSES OF BURST SUPPRESSION

There are several known pathological conditions that cause EEG burst suppression. Early work with animals demonstrated that local freezing of cortical sections from cats with carbon dioxide led to profoundly decreased electrical activity, both in frozen and unfrozen areas of the brain, and that rewarming led to partial recovery of electrical activity (Nims et al., 1941). In humans, lowering of the core body temperature has been shown to linearly decrease the overall spectral power of the EEG (Levy, 1984), and burst suppression is often observed in humans with temperatures below 24.4°C (Stecker et al., 2001). Hypothermia reduces the cerebral metabolic rate, and is often used to provide neuroprotection in patients with circulatory arrest (Michenfelder and Milde, 1991; Arrica and Bissonnette, 2007).

Hypoxia is a common pathological cause of burst suppression. In animal experiments, hypoxia has been shown to induce burst suppression as well as a suppressed EEG at extremely low arterial oxygen concentrations in dogs (Spoerel, 1961). G-force induced hypoxia in rodents has also induced burst suppression (Lukatch et al., 1997). In humans, fetal hypoxia during labor and delivery can lead to hypoxic-ischemic encephalopathy in the neonate and induce burst suppression patterns in the EEG (Toet et al., 1999; van Rooij et al., 2005). While recovery from burst suppression can occur within the first 48 h after birth, the appearance of burst suppression usually portends a poor prognosis for the neonate (Grigg-Damberger et al., 1989; Hellström-Westas et al., 1995).

Patients suffering from coma may exhibit EEG burst suppression due to several different underlying etiologies (Young, 2000). Post-anoxic coma (Zaret, 1985) can induce a rare burst suppression pattern where the burst patterns are identical (Hofmeijer et al., 2014). In addition, burst suppression has been described in a survivor of post-anoxic coma during behaviorally defined sleep (i.e., eyes closed with no movement) (Kheder et al., 2014). Burst suppression may also be observed when patients are in coma due to hepatic failure (Bickford and Butt, 1955), sepsis (Young et al., 1992) and hypoglycemia (Auer et al., 1984). Coma due to porphyria, a disorder of heme synthesis (Thadani et al., 2000), can also elicit a burst suppression pattern (Dow, 1961).

Ohtahara syndrome, an early infantile epilepsy syndrome, is characterized by a burst suppression pattern that persists through behaviorally defined wake and sleep states (Ohtahara and Yamatogi, 2006). Typically Ohtahara syndrome manifests itself within 3 months of birth, and is thought to be caused by structural brain lesions. Patients with Ohtahara syndrome have been reported to have lesions of the thalamus, hippocampus, and brainstem tegmentum (Itoh et al., 2001; Ohtahara and Yamatogi, 2003). Early myoclonic encephalopathy is another infantile epilepsy syndrome that results in a persistent burst suppression pattern, usually manifesting itself during the neonatal period (Aicardi and Ohtahara, 2005). Unlike Ohtahara syndrome, early myoclonic encephalopathy is hypothesized to be due to an underlying metabolic disorder (Panayiotopoulos, 2010).

Another disorder that causes burst suppression is Aicardi syndrome, a congenital disorder in which the corpus callosum fails to develop in female infants (Fariello et al., 1977; Aicardi, 2005).In patients with a damaged corpus callosum that undergo general anesthesia, burst suppression patterns have been reported to be asymmetric and asynchronous across cerebral hemispheres (Lambrakis et al., 1999; Lazar et al., 1999).

Finally, various medications and intoxicants that are not used for general anesthesia may induce burst suppression at high doses, including ethanol (Whishaw, 1976), the muscle relaxant baclofen (Weissenborn et al., 1991; Ostermann et al., 2000), and the anticonvulsant carbamazepine (De Rubeis and Young, 2001). A recent report described burst suppression in a patient suffering from an overdose of bupropion (Mundi et al., 2012), which is used to treat depression and nicotine addiction.

BURST SUPPRESSION INDUCED BY GENERAL ANESTHETICS

General anesthetics are administered by inhalation or intravenous injection. The main molecular targets for general anesthetics are thought to be gamma-aminobutyric acid type A ($GABA_A$)

receptors and N-methyl D-aspartate (NMDA) receptors (Solt et al., 2006; Brown et al., 2011), although many other targets have been identified that likely play a role in general anesthesia as well. The halogenated ethers enflurane (Lebowitz et al., 1972), isoflurane (Hartikainen et al., 1995b), sevoflurane (Scheller et al., 1990) and desflurane (Rampil et al., 1991) all induce burst suppression at sufficiently high doses. However, the haloalkane general anesthetics chloroform (Pearcy et al., 1957) and halothane (Murrell et al., 2008) have not been reported to induce burst suppression, even at high concentrations that produced suppression.

Barbiturates are intravenous anesthetics that primarily act by potentiating the function of $GABA_A$ receptors. Pentobarbital (Van Ness, 1990), methohexital (Wennberg et al., 1997), and sodium thiopental (Kassell et al., 1980) are all barbiturates that have been shown to induce burst suppression. Propofol (Huotari et al., 2004) and etomidate (Modica and Tempelhoff, 1992) are not barbiturates, but they also act primarily by enhancing $GABA_A$ receptor function, and also induce burst suppression. 13–15 Hz spindle activity, similar to that seen during NREM sleep, has been seen during both the burst and suppression phase of propofol-induced burst suppression (Särkelä et al., 2002; Huotari et al., 2004; Ferenets et al., 2006). Sharp waves resembling the vertex waves seen during NREM sleep have also been observed during the bursts and suppressions phases from propofol-induced burst suppression. These spindles and sharp waves are theorized to have been produced by the sensorimotor cortex (Sonkajärvi et al., 2008).

Gaseous anesthetics such as xenon or nitrous oxide that are NMDA receptor antagonists have not been shown to induce burst suppression, even at high doses in a hyperbaric chamber (Morris et al., 1955; Pittinger et al., 1955). Similarly, the intravenously administered NMDA receptor antagonist ketamine has not been shown to elicit burst suppression (Barash et al., 2012). However, the gaseous anesthetic cyclopropane, which is also an NMDA receptor antagonist (Solt et al., 2006), has been shown to induce burst suppression (Possati et al., 1953).

In summary, most general anesthetics that act primarily by enhancing $GABA_A$ receptors induce burst suppression, whereas NMDA antagonists typically do not. However, there are exceptions to both rules, suggesting that molecular mechanisms alone cannot account for general anesthetic-induced burst suppression.

MECHANISMS OF BURST SUPPRESSION INDUCED BY GENERAL ANESTHESIA

Intracellular recordings of cortical and subcortical neurons laid the early groundwork for investigations into the mechanisms of burst suppression. While the majority of cortical cells exhibit a pattern of alternating depolarized and hyperpolarized states that account for the burst suppression pattern observed in the electrocorticogram, thalamic cells are either silent or fire at 1–4 Hz under general anesthesia (Steriade et al., 1994).

During moderate to deep levels of isoflurane anesthesia that induce burst suppression, external mechanical, visual, and auditory stimuli have been shown to trigger bursts (Yli-Hankala et al., 1993a; Hartikainen et al., 1995b; Hudetz and Imas, 2007; Amzica, 2009). Therefore, burst suppression has been considered a state of cortical hypersensitivity (Kroeger and Amzica, 2007), although external stimuli fail to induce bursting at isoflurane levels less than 2%, or greater than 3.5% (when the EEG is completely suppressed; Kroeger and Amzica, 2007). These findings suggest that the brain is still receptive to external stimuli during anesthetic-induced burst suppression. The recording of heart rate during externally triggered bursts did not show any overt changes, suggesting the effect is not derived from the autonomic nervous system (Kroeger and Amzica, 2007).

The state of cortical hypersensitivity during burst suppression is thought to be due to changing calcium levels and the lowering of cortical inhibition by isoflurane (Kroeger and Amzica, 2007; Ferron et al., 2009). Increasing the dose of isoflurane steadily lowered the amount of extracellular calcium until a state of burst suppression was reached. During burst suppression the levels of extracellular calcium decreased during bursts, and began to increase throughout the suppression period. Triggered bursts were more easily induced by external stimuli when sufficient time had elapsed after the previous stimulus, suggesting that a refractory period exists during which the extracellular calcium must reach a threshold level before a subsequent burst can be induced (Kroeger and Amzica, 2007). Administration of the NMDA antagonist MK801 significantly diminished both the amplitude and duration of bursts, but did not alter the probability of inducing a triggered burst by an external stimulus. The gap junction blocker carbenoxolone completely eliminated any triggered response, suggesting that in addition to extracellular calcium, NMDA receptors and gap junctions may also regulate the response (Kroeger and Amzica, 2007).

Phenomenological modeling of burst suppression has been performed using non-linear dynamic systems and dynamic mean field models. Modeling using chaos theory and non-linear systems for human coma patients showed that burst frequency decreased logarithmically as burst durations increased (Rae-Grant and Kim, 1994). Mesoscopic modeling using a dynamic mean field model suggested that multiple origins of burst suppression exist through several different slow modulating circuits (Liley and Walsh, 2013).

An alternative to the phenomenological models is a neurometabolic model, which accounts for the different etiologies that lead to burst suppression activity (Ching et al., 2012). The underlying process of burst suppression is viewed as a reduction in brain metabolism, as it is known that hypothermia, hypoxia, Ohtahara syndrome, and general anesthetics that act as $GABA_A$ agonists all decrease the cerebral metabolic rate of oxygen (CMRO). The reduction of the CMRO further lowers the production rate of adenosine triphosphate, and increases cell membrane conductance. In response to lowered ATP production and increased conductance, an ATP-gated potassium channel expressed in cortical and subcortical neurons hyperpolarizes to prevent cell firing and preserve a lower energy state. This inhibition of bursting activity directly leads to the suppression period observed during burst suppression. As the suppression persists, ATP levels begin to recover and membrane conductance is lowered until another burst can occur. If the cerebral metabolic rate continues to decrease, the suppression periods will be prolonged until all

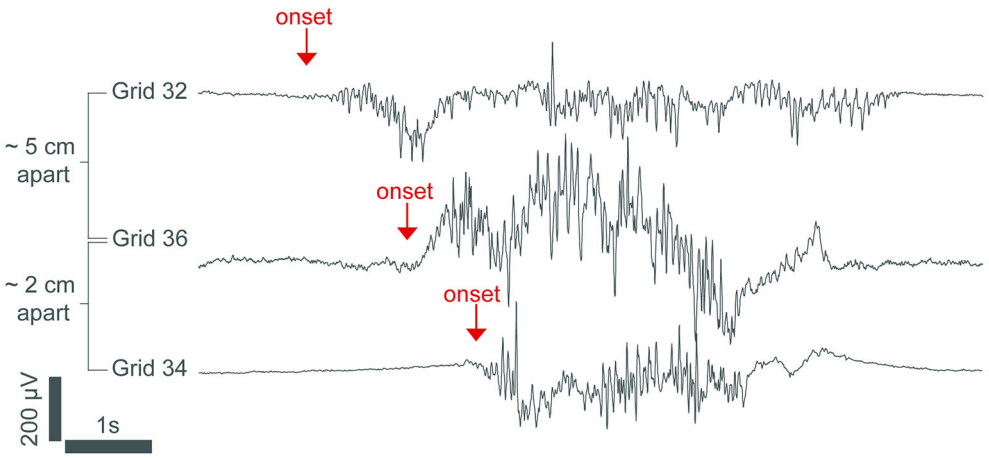

FIGURE 2 | An intracranial recording from the cortex of an epileptic patient under propofol general anesthesia. The burst in channel 32 starts hundreds of milliseconds before the bursts in channels 36 and 34, demonstrating that burst onset is heterogeneous across the cortex. The signal was low-passed filtered at 100 Hz and resampled to 250 Hz. From (Lewis et al., 2013).

bursting has ceased. This can be seen with increasing doses of general anesthetics—as the anesthetic continues to depress the cerebral metabolic rate, the EEG eventually becomes suppressed. Lowered ATP production could also lead to an impairment of calcium pumps and lead to a decrease in extracellular calcium.

This neuro-metabolic model predicts that the spectral content within bursts for a human patient undergoing propofol anesthesia will be limited to a frequency of around 10 Hz (alpha rhythm), and that this alpha rhythm can drift from having a peak power at 10 Hz at the beginning of a burst to having a peak power at 8 Hz at the end of a burst. In addition, it is thought that the spectral content of bursts reflects the neurophysiological state that was present immediately preceding burst suppression (Ching et al., 2012).

Data from human patients undergoing propofol anesthesia support this neuro-metabolic model (Lewis et al., 2013). High-density cortical recordings also revealed that burst suppression activity is not a cortex-wide phenomenon as once thought. While some regions of the cortex may be in burst suppression, other regions may not be. The occurrence of bursts can also be limited locally to discrete cortical regions. **Figure 2** shows how bursts can also be spatially asynchronous across the cortex, with adjacent cortical areas having similar burst timings compared to anatomically distant areas (Lewis et al., 2013). This phenomenon was also noted in earlier human experiments (Henry and Scoville, 1952).

CLINICAL APPLICATIONS OF ANESTHETIC-INDUCED BURST SUPPRESSION

Status epilepticus is a state of persistent seizure activity that can last for several hours or even days (Lowenstein et al., 1999), with a mortality rate of up to 35% (Prasad et al., 2001). When status epilepticus is refractory to other therapies, seizure activity is often terminated by inducing burst suppression with intravenous general anesthetics such as propofol (Stecker et al., 1998; Prasad et al., 2001) or pentobarbital (Van Ness, 1990; Claassen et al., 2002). When treating status epilepticus, burst suppression is typically maintained by manually titrating an intravenous infusion of general anesthetic to a target BSR value. Automated closed-loop anesthesia delivery (CLAD) systems have been proposed to deliver propofol (Vijn and Sneyd, 1998) and etomidate (Cotten et al., 2011) using the BSR as the control signal. Recently, CLAD systems using the BSP as the control signal have been developed to deliver intravenous propofol in rats (Ching et al., 2013; Shanechi et al., 2013a,b), and these have been shown to achieve precise control of the level of burst suppression, obviating the need for manual titration of drug delivery. **Figure 3A** shows the closed-loop design of one of these CLAD systems. **Figure 3B** shows the process for online segmentation of the EEG for calculating the BSP, and **Figure 3C** shows the compartment model used to control the propofol infusion rate. Anesthetic-induced burst suppression is also used to treat patients suffering from traumatic brain injury with elevated intracranial pressures (Doyle and Matta, 1999), as well as patients suffering from severe depression (Engelhardt et al., 1993).

A STUDY TO COMPARE THE BURST SUPPRESSION CHARACTERISTICS OF TWO GENERAL ANESTHETICS

Burst suppression is typically regarded as a neurophysiological phenomenon that may be caused by a range of etiologies. However, earlier experiments showed that volatile and intravenous anesthetics may have distinct electrophysiological characteristics during burst suppression. A study in rats comparing the EEG characteristics of isoflurane and propofol found significant differences between burst duration and peak-to-peak voltage at an equivalent BSR of 0.8 (Akrawi et al., 1996). However, the duration of the suppression and burst epochs that were compared were only 2–6 s. A study in rabbits comparing 1 min each of EEG burst suppression during propofol

and isoflurane anesthesia reported higher amplitude bursts during isoflurane anesthesia (Hartikainen et al., 1995a). Another comparison between the burst suppression patterns of isoflurane and enflurane found that suppressions were shorter in duration for enflurane (Lipping et al., 1995). Burst suppression caused by hypoxic-ischemic encephalopathy has also been reported to have a higher variability in individual suppression durations compared to pentobarbital-induced burst suppression (Beydoun et al., 1991).

Although these reports suggest that different general anesthetics and pathological states may induce distinct burst suppression patterns, a systematic study comparing a large number of bursts and suppressions induced by two different anesthetics across all levels of burst suppression has not been performed previously. In this study, we induced different levels of burst suppression in rats with the inhaled anesthetic sevoflurane and the intravenous anesthetic propofol, and quantified the level of burst suppression using BSP. A large number of bursts and suppressions ($n > 2000$) were compared to analyze the electrophysiological characteristics of burst suppression induced by sevoflurane and propofol. We found that the durations, peak-to-peak amplitudes, and spectral power of the bursts and suppressions differed substantially between the two anesthetics at equivalent BSP levels, suggesting that at least some aspects of the mechanisms underlying burst suppression induced by sevoflurane and propofol may be distinct.

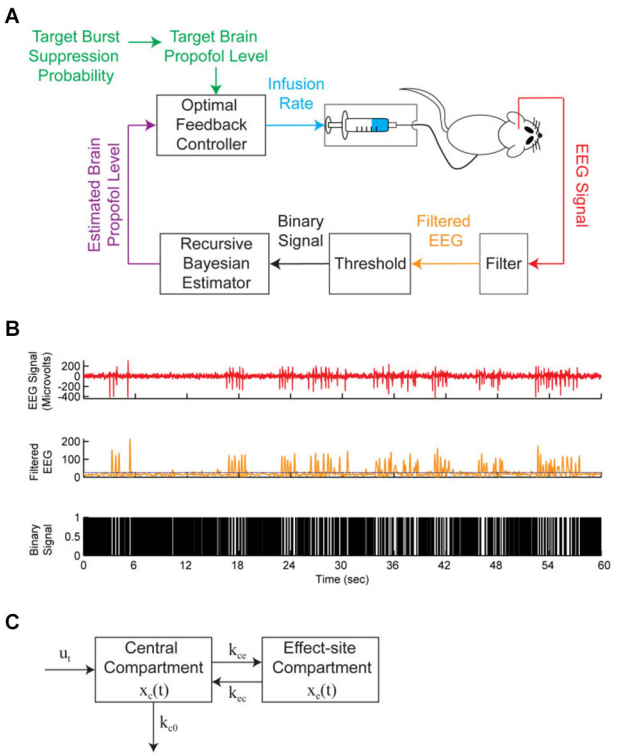

FIGURE 3 | A brain machine interface (BMI) system to control propofol-induced burst suppression. (A) The BMI records the EEG, segments the signal into a binary time-series by filtering and thresholding, estimates the BSP or equivalently the effect-site concentration level based on the binary-time series, and then uses this estimate as feedback to control the propofol infusion rate. **(B)** A sample EEG trace showing burst suppression. The top panel shows the EEG signal, the middle panel shows the corresponding filtered EEG magnitude signal (orange) and threshold (blue) used to detect the burst suppression events, and the bottom panel shows the corresponding binary time-series with black indicating suppression events and white indicating burst events. **(C)** The two-compartmental model used by the BMI to characterize the effect of propofol on the EEG. The EEG was sampled at 500 Hz and the binary sequence was created by low-pass filtering the EEG at 5 Hz and thresholding. From (Shanechi et al., 2013b).

METHODS

ANIMAL CARE AND USE

All animal studies were approved by the Institutional Animal Care and Use Committee (IACUC) at Massachusetts General Hospital, Boston, Massachusetts. Four male Sprague-Dawley rats (Charles River Laboratories, Wilmington, MA) weighing between 550–670 g were used for these studies. Animals were provided at least 3 days of rest between experiments. Animals were kept on a standard day-night cycle (lights on at 7:00 AM, and off at 7:00 PM), and all experiments were performed during the day.

SURGICAL PLACEMENT OF ELECTROENCEPHALOGRAPHY (EEG) EXTRADURAL ELECTRODES AND RECORDING

Rats were surgically implanted with extradural electrodes at least 7 days before experiments using previously described methods (Solt et al., 2011; Chemali et al., 2012; Ching et al., 2013). Electroencephalography was performed with a sampling frequency of 500 Hz using a QP511 Quad AC Amplifier System (Grass Instruments, West Warwick, RI), and a USB-6009 14-bit data acquisition board (National Instruments, Austin, TX). The electrical potential between stereotactic coordinates (relative to lambda) A0L0 and A6L-3 (left somatosensory cortex) was recorded. A line filter with cutoff frequencies of 0.3–50 Hz was used, and the signal was downsampled to 50 Hz.

PREPARATION AND DELIVERY OF DRUGS

Sevoflurane was obtained from Sigma-Aldrich (St. Louis, MO), and propofol (containing intralipid) was obtained from APP Pharmaceuticals (Schaumburg, IL). For the delivery of the intravenous anesthetic propofol, rats ($n = 4$) were anesthetized in an induction chamber with 2.0–3.0% isoflurane in oxygen. A 24-gauge intravenous catheter was placed in the lateral tail vein. Isoflurane was then discontinued, and the rat was removed from the chamber. After the rat fully recovered from isoflurane anesthesia, propofol was delivered using a Physio 22 syringe pump (Harvard Apparatus, Holliston, MA) until loss of righting occurred, at which time the EEG leads were attached and a rectal temperature probe was inserted. A heating pad was placed underneath the animal and used to maintain the core body temperature between 36.5° and 37.5°C.

For delivery of the volatile anesthetic sevoflurane, rats were initially anesthetized in an induction chamber with 5.0–6.0% sevoflurane in oxygen. After loss of righting occurred, EEG leads were attached and a rectal temperature probe was inserted. The rat was then placed inside a custom built anesthetizing chamber with

ports for anesthetic gas delivery, scavenging, and gas sampling. A heating pad was placed underneath the chamber and used to maintain a core body temperature between 36.5° and 37.5°C. Sevoflurane concentrations were sampled and monitored from the distal end of the chamber using an Ohmeda 5250 anesthetic agent analyzer (GE Healthcare, Waukesha, WI).

EEG RECORDING OF PROPOFOL-INDUCED BURST SUPPRESSION

EEG data for propofol-induced burst suppression was taken from a previous study by our group that used a CLAD system to establish and maintain targeted BSP values using propofol (Ching et al., 2013). For this experiment, the BSP levels of 0.4, 0.65, and 0.9 were targeted in each rat (n = 4). Each BSP level was maintained with propofol for at least 15 min, with 10-minute ramps to transition to new BSP levels. The system used custom software initialized with MATLAB (Mathworks, Natick, MA) and issued commands to a Physio 22 syringe pump (Harvard Apparatus, Holliston, MA) using an RS-232 serial connector. The typical duration of each experiment was between 80 and 90 min. For this study, we selected 1000 s of artifact-free EEG data from each rat to provide direct comparisons with sevoflurane-induced burst suppression at equivalent BSP values in the same animals.

EEG RECORDING OF SEVOFLURANE-INDUCED BURST SUPPRESSION

For sevoflurane-induced burst suppression recordings, the same rats (n = 4) from the propofol CLAD study were used. Once the animal was in the anesthetizing chamber, the dose of sevoflurane was initially set at 3.6% in oxygen with a fresh gas flow rate of two liters per minute. The sevoflurane concentration was increased by 0.2% every 30 min until a final concentration of 4.2% was reached. This maximal dose was maintained for an additional 30 min. The typical experiment duration was 120 min, and 1000 s of artifact-free EEG data was selected from each rat for analysis.

IDENTIFICATION OF EEG BURSTS AND SUPPRESSIONS

Bursts and suppressions from the recorded EEG were segmented using a threshold based on visual inspection. Each EEG recording (n = 8, 1000 s each) was detrended and smoothed by convolution with a Gaussian function, and the energy was calculated using the nonlinear energy operator (Kaiser, 1990). The nonlinear energy operator provides a method for clearly separating the larger energy bursts from the lower energy suppressions, and a visually-based threshold was set in the energy domain to segment the data. The EEG values that were above the threshold were classified as bursts, whereas the values that fell below the threshold were classified as suppressions. All segmentations were confirmed by one of the authors who is an experienced clinical electroencephalographer (MBW).

CALCULATION OF BSP

EEG segments were converted to a binary time series. Segments that were classified as bursts were given a value of one, and those that were classified as suppressions were given a value of zero. The BSP algorithm used this binary time-vector to find the instantaneous probability of burst suppression, and corresponding confidence intervals (Chemali et al., 2011; Ching et al., 2013). Like the BSR, a burst suppression probability value of 1 indicates a state of complete EEG suppression, while a value of 0 indicates no suppression. Individual bursts and suppressions from the propofol and sevoflurane EEG datasets were sorted by their BSP into bins of 0.3–0.4, 0.4–0.5, 0.5–0.6, 0.6–0.7, and 0.7–0.8 BSP. Bursts or suppressions that were shorter than 0.15 s were discarded, as they are too short to constitute a clear burst or suppression. **Table 1** gives the number of individual propofol or sevoflurane-induced bursts and suppressions within each bin.

Table 1 | The number of sorted individual bursts or suppressions in each BSP bin per general anesthetic.

	Propofol		Sevoflurane	
BSP	**Bursts**	**Suppressions**	**Bursts**	**Suppressions**
0.3–0.4	124	106	109	105
0.4–0.5	225	199	107	99
0.5–0.6	671	583	77	76
0.6–0.7	646	595	129	126
0.7–0.8	192	171	178	171
Total	1858	1654	600	577

The total number of bursts was 2,458 and the total number of suppressions was 2,231.

CALCULATION OF BURST AND SUPPRESSION DURATION, PEAK-TO-PEAK AMPLITUDE, AND POWER

Several features of each sorted individual burst (n = 2,458) and suppression (n = 2,231) were calculated to characterize them. Using custom scripts written in MATLAB R2013b, the duration, peak-to-peak amplitude, and power of each individual burst or suppression was calculated. Duration (sec) was the absolute length of the individual burst or suppression. Peak-to-peak voltage (μV) was the absolute difference between the maximum and minimum amplitude value within each individual burst or suppression. Power (dB $\mu V^2/s$) was the squared amplitude of the individual burst or suppression divided by its own duration.

STATISTICAL ANALYSIS OF BURST AND SUPPRESSION DURATIONS, PEAK-TO-PEAK AMPLITUDE, AND POWER

The median and accompanying 95% upper and lower confidence intervals for the distribution of burst and suppression durations, peak-to-peak amplitudes, and power for propofol and sevoflurane were constructed using the percentile bootstrap procedure (Efron and Tibshirani, 1993). Unlike hypothesis testing using p-values alone, the usage of confidence intervals gives a measure of uncertainty around the median of each feature, and testing at a 95% level is equivalent to hypothesis testing with a significance alpha of 0.05.

To make significance comparisons between the sevoflurane and propofol burst suppression features, the 95% confidence interval around the difference between sevoflurane and propofol median values was used. If the 95% confidence intervals around the differences are both positive then sevoflurane is considered to be significantly higher than propofol. If both confidence intervals are negative then propofol is considered to be significantly higher

than sevoflurane. If one confidence interval is negative, and the other is positive then no statistical significance can be determined.

Spectral analysis of burst suppression

Spectrograms of propofol and sevoflurane-induced burst suppression were computed from EEG data using multitaper methods from the Chronux toolbox in MATLAB R2013b (Thomson, 1982; Mitra and Bokil, 2008; Babadi and Brown, 2014). Spectrograms were constructed using three tapers and a two-second window stepped through 50 ms. The half-bandwidth of the spectrogram was 1 Hz.

RESULTS

SEVOFLURANE AND PROPOFOL INDUCE DISTINCT BURST SUPPRESSION PATTERNS

Figure 4A shows 1 min of EEG data from a rat during sevoflurane-induced burst suppression at a BSP of approximately 0.7, and **Figure 4B** shows the non-linear energy calculated from the EEG trace in **Figure 4A**. **Figure 4C** shows 1 min of EEG data from the same rodent during propofol-induced burst suppression at a BSP of approximately 0.7, and **Figure 4D** shows the non-linear energy calculated from the EEG trace in **Figure 4C**. The visually-based threshold that was set in the energy domain to segment data into bursts and suppressions is shown as a dotted line in **Figures 4B,D**.

Figures 5A (sevoflurane) and 5B (propofol) show the time-frequency spectrograms for five continuous minutes of burst suppression at a BSP of 0.7 in the same rat. Warm colors (e.g., red) show areas of high power, and cool colors (e.g., blue) show areas of low power. In comparison to the burst suppression pattern induced by sevoflurane, the pattern induced by propofol was characterized by lower power across all frequency bands during both bursts and suppressions, despite equivalent BSP.

DURATION IS SIGNIFICANTLY LONGER FOR SEVOFLURANE-INDUCED BURSTS AND SUPPRESSIONS THAN FOR PROPOFOL-INDUCED BURSTS AND SUPPRESSIONS ACROSS ALL BSP LEVELS

Figure 6A shows the median durations for propofol and sevoflurane-induced bursts and suppressions separated by BSP. For all BSP values (0.3–0.8) the median duration of sevoflurane-induced bursts and suppressions was greater than the median duration of propofol-induced bursts and suppressions. **Table 2** shows the median burst and suppression durations at all BSP levels (0.3–0.8) with corresponding 95% confidence intervals. The maximum median difference between propofol and sevoflurane bursts was 1.79 s at a BSP of 0.3–0.4, and the maximum median difference between propofol and sevoflurane suppressions was 3.46 s at a BSP of 0.7–0.8. The minimum median difference between propofol and sevoflurane bursts was 1.26 s at a BSP of 0.7–0.8, and the minimum median difference between propofol and sevoflurane suppressions was 0.76 s at a BSP of 0.3–0.4. All of the confidence intervals around the difference of medians were greater than 0, indicating that sevoflurane bursts and suppressions were significantly longer in duration across different BSP levels when compared to propofol.

PEAK-TO-PEAK AMPLITUDE IS SIGNIFICANTLY HIGHER FOR SEVOFLURANE-INDUCED BURSTS AND SUPPRESSIONS THAN PROPOFOL-INDUCED BURSTS AND SUPPRESSIONS ACROSS ALL BSP LEVELS

Figure 6B shows the median peak-to-peak amplitudes for propofol and sevoflurane-induced bursts and suppressions separated by BSP. For all BSP values (0.3–0.8) the median peak-to-peak amplitudes of sevoflurane-induced bursts and suppressions was greater than the median peak-to-peak amplitudes of propofol-induced bursts and suppressions. The median burst and suppression peak-to-peak amplitudes at all BSP values (0.3–0.8) with corresponding 95% confidence intervals are given in **Table 2**. The maximum median difference between propofol and sevoflurane burst peak-to-peak amplitudes was 587.73 μV at a BSP of 0.6–0.7, and the maximum median difference between propofol and sevoflurane suppression peak-to-peak amplitudes was 97.86 μV at a BSP of 0.6–0.7. The minimum median difference between propofol and sevoflurane burst peak-to-peak amplitudes was 305.02 μV at a BSP of 0.7–0.8, and the minimum median difference between propofol and sevoflurane suppression peak-to-peak amplitudes was 84.20 μV at a BSP of

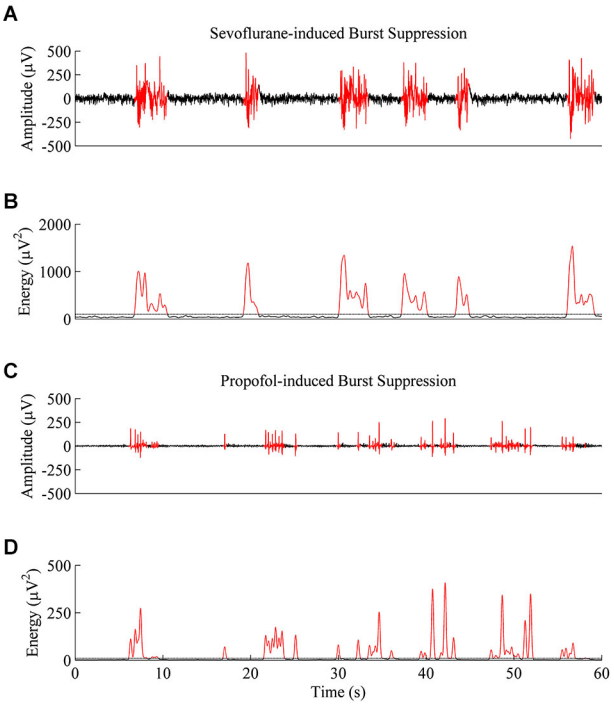

FIGURE 4 | Representative EEG traces and energy values from the same rat at a BSP of 0.7. (A) A 60-second EEG recording taken during sevoflurane-induced burst suppression. Black indicates an area threshold as suppression, and red indicates an area threshold as a burst. **(B)** Energy of the EEG trace from **(A)** that was used to segment bursts and suppressions. **(C)** 60-second EEG recording taken from the same animal during propofol-induced burst suppression. **(D)** Energy of the EEG trace from **(C)** shows that propofol-induced bursts and suppressions are shorter and lower in power then sevoflurane-induced bursts and suppressions, despite an equivalent BSP.

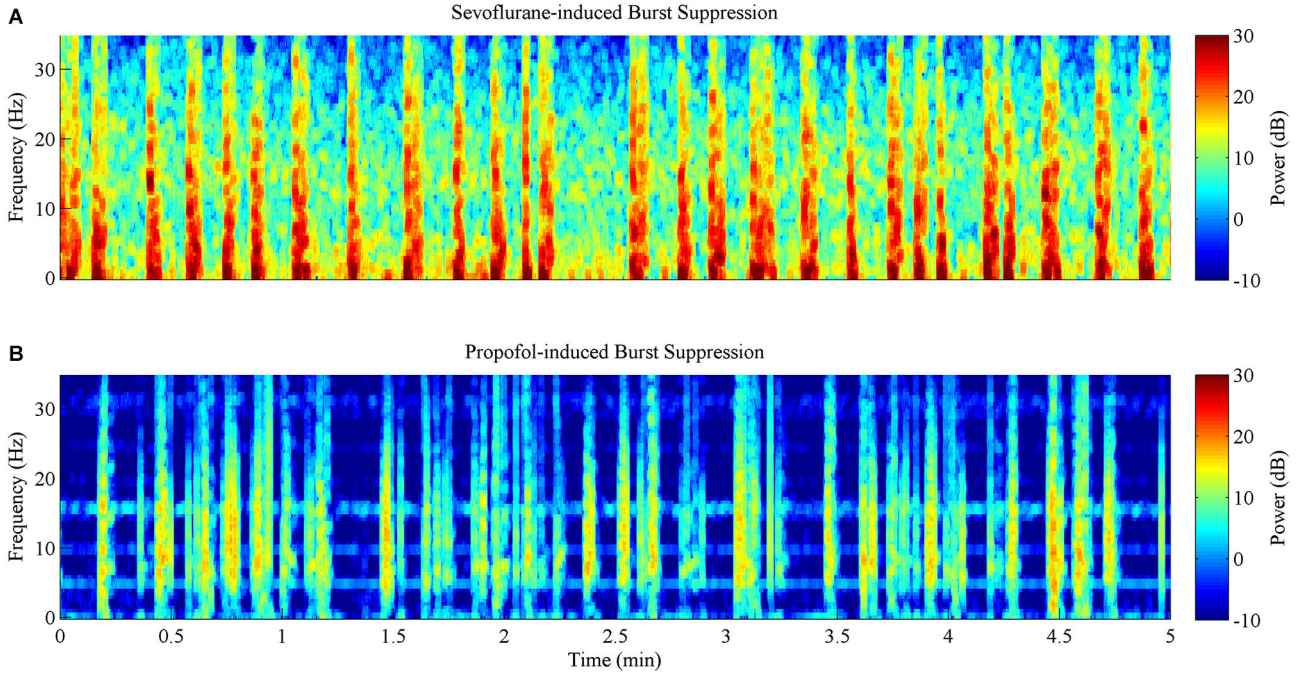

FIGURE 5 | Spectrograms computed from the same rat during 5 min of burst suppression at a BSP of 0.7. Warm colors indicate frequency components with high power, while cool colors indicate frequency components with low power. **(A)** Sevoflurane-induced burst suppression has high power between 1–10 Hz during bursts. **(B)** Propofol-induced burst suppression has lower power during bursts and suppressions across all frequencies when compared to sevoflurane.

0.5–0.6. All of the confidence intervals around the difference of medians were greater than 0, indicating that sevoflurane bursts and suppressions were significantly greater in amplitude across different BSP levels when compared with propofol.

POWER IS SIGNIFICANTLY HIGHER FOR SEVOFLURANE-INDUCED BURSTS AND SUPPRESSIONS THAN PROPOFOL-INDUCED BURSTS AND SUPPRESSIONS ACROSS ALL BSP LEVELS

Figure 6C shows the median power for propofol and sevoflurane-induced bursts and suppressions separated by BSP. For all BSP values (0.3–0.8) the median power of sevoflurane-induced bursts and suppressions was greater than the median power of propofol-induced bursts and suppressions. **Table 2** shows the median burst and suppression powers at all BSP values (0.3–0.8) with corresponding 95% confidence intervals. The maximum median difference between propofol and sevoflurane burst powers was 68.46 dB $\mu V^2/s$ at a BSP of 0.6–0.7, and the maximum median difference between propofol and sevoflurane suppression powers was 56.14 dB $\mu V^2/s$ at a BSP of 0.3–0.4. The minimum median difference between propofol and sevoflurane burst powers was 64.07 dB $\mu V^2/s$ at a BSP of 0.7–0.8, and the minimum median difference between propofol and sevoflurane suppression powers was 53.65 dB $\mu V^2/s$ at a BSP of 0.7–0.8. All of the confidence intervals around the difference of medians were greater than 0, indicating that sevoflurane bursts and suppressions were significantly larger in power across different BSP levels, when compared with propofol.

DISCUSSION

Previous studies on burst suppression induced by general anesthetics have found differences between burst and suppression durations and peak-to-peak amplitudes between propofol, etomidate, thiopental, and isoflurane in rodents, and between propofol and isoflurane in rabbits. The inhaled anesthetic isoflurane was found to produce greater amplitudes and durations than the other intravenous agents. However, these studies only compared a small number of individual bursts and suppressions, and did not systematically examine them at different depths of general anesthesia.

In this study, we gathered large amounts of EEG data during sevoflurane and propofol anesthesia from the same animals, and used the BSP to quantify anesthetic depth. We found that the durations of suppressions and bursts induced by propofol were significantly shorter than those induced by sevoflurane at all measured levels of BSP. Additionally, the peak-to-peak amplitudes of propofol-induced suppressions and bursts were significantly lower than those induced by sevoflurane at all measured levels of BSP. Sevoflurane suppressions were not completely suppressed, as the peak-to-peak amplitudes of sevoflurane suppressions were similar in size to the peak-to-peak amplitudes of propofol bursts. However, it should be noted that for these experiments, we analyzed EEG data at BSP levels ranging from 0.3–0.8. We did not compare burst suppression patterns at BSP levels below 0.3, due to the difficulty of visually segmenting propofol-induced bursts and suppressions at low BSP levels.

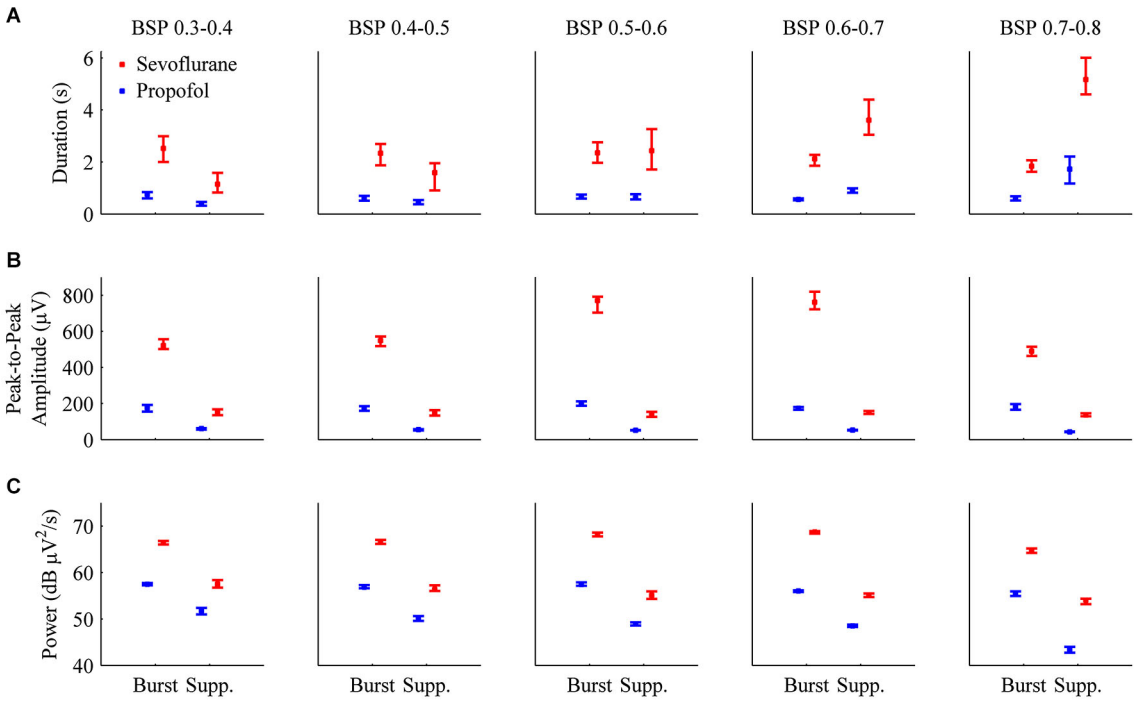

FIGURE 6 | Bar graphs with 95% confidence intervals for the median duration, peak-to-peak amplitude, and power for individual bursts and suppressions induced by propofol (blue) or sevoflurane (red) in all animals. In order to perform direct comparisons between the two drugs at similar depths of general anesthesia, the data was grouped by BSP level. **(A)** The median durations of bursts and suppressions were significantly longer during sevoflurane anesthesia than during propofol anesthesia. **(B)** Median peak-to-peak amplitudes (μV) were significantly greater during sevoflurane general anesthesia for both bursts and suppressions. **(C)** Median power (dB μV^2/s) for individual bursts and suppressions was significantly higher during sevoflurane general anesthesia.

Table 2 | The median differences between propofol and sevoflurane-induced bursts and suppressions for duration, peak-to-peak amplitude and power across BSP values of 0.3–0.8.

BSP	Duration		Peak-to-peak Amplitude		Power	
	Burst	Suppressions	Burst	Suppressions	Burst	Suppressions
0.3–0.4	1.79 s (95% CI: 1.33–2.27 s)	0.76 s (95% CI: 0.41–1.29 s)	349.77 μV (95% CI: 322.16–386.61 μV)	90.09 μV (95% CI: 74.04–107.76 μV)	65.82 dB μV2/s (95% CI: 65.37–66.30 dB μV2/s)	56.14 dB μV2/s (95% CI: 55.00–57.24 dB μV2/s)
0.4–0.5	1.76 s (95% CI: 1.27–2.11 s)	1.14 s (95% CI: 0.41–1.46 ss)	378.46 μV (95% CI: 347.70–407.31 μV)	94.20 μV (95% CI: 80.06–109.29 μV)	66.09 dB μV2/s (95% CI: 65.59–66.57 dB μV2/s)	55.24 dB μV2/s (95% CI: 54.63–56.33 dB μV2/s)
0.5–0.6	1.68 s (95% CI: 1.29–2.8 s)	1.79 s (95% CI: 1.06–2.66 s)	571.07 μV (95% CI: 506.36–601.20 μV)	84.20 μV (95% CI: 72.80–102.86 μV)	67.88 dB μV2/s (95% CI: 67.34–68.23 dB μV2/s)	53.89 dB μV2/s (95% CI: 52.97–54.89 dB μV2/s)
0.6–0.7	1.55 s (95% CI: 1.28–1.76 s)	2.73 s (95% CI: 2.16–3.53 s)	587.73 μV (95% CI: 553.49–646.48 μV)	97.86 μV (95% CI: 89.80–105.98 μV)	68.46 dB μV2/s (95% CI: 68.07–68.65 dB μV2/s)	53.99 dB μV2/s (95% CI: 53.50–54.45 dB μV2/s)
0.7–0.8	1.26 s (95% CI: 1.02–1.47 s)	3.46 s (95% CI: 2.69–4.36 s)	305.02 μV (95% CI: 274.58–334.39 μV)	93.75 μV (95% CI: 85.85–102.54 μV)	64.07 dB μV2/s (95% CI: 63.63–64.72 dB μV2/s)	53.65 dB μV2/s (95% CI: 52.71–54.02 dB μV2/s)

95% confidence intervals around the differences indicate if there is a significant increase, decrease, or no change between the two anesthetics. Sevoflurane-induced bursts and suppressions are significantly greater in magnitude than propofol-induced bursts and suppressions across all BSP values for duration, peak-to-peak amplitude, and power.

Experiments using the NMDA receptor antagonist MK801 during isoflurane-induced burst suppression showed that peak-to-peak amplitudes and durations of bursts were diminished compared to bursts induced by isoflurane alone, although the rate of bursting remained the same (Kroeger and Amzica, 2007). Nitrous oxide is an NMDA antagonist (Jevtović-Todorović et al., 1998) that decreases both suppression durations and burst amplitudes when used as an adjunct to isoflurane general anesthesia (Yli-Hankala et al., 1993b; Porkkala et al., 1997). These studies suggest that NMDA receptors play an important role in limiting the maximum amplitude of bursts and suppressions. However, in the present study we found

that sevoflurane induced greater durations and amplitudes for both bursts and suppressions when compared to propofol, even though sevoflurane inhibits NMDA receptors, and propofol is thought to act primarily via $GABA_A$ receptors (Solt and Forman, 2007). Our results demonstrate that NMDA receptor pharmacology alone does not account for the different burst suppression patterns observed with sevoflurane and propofol.

Extracellular calcium or ATP reuptake may also modulate the durations of bursts and suppressions. An increase in the rate of ATP reuptake under propofol (when compared to sevoflurane) could increase the rate of switching between bursts and suppressions. Cerebral blood flow could also be an important factor that determines the duration of bursts and suppressions (Kroeger and Amzica, 2007; Ching et al., 2012). It has also been suggested that during the state of burst suppression the cortex is more sensitive to external stimuli, since such stimuli have been shown to trigger bursts under isoflurane anesthesia (Hudetz and Imas, 2007). The cortex may be more sensitive to external stimuli during propofol-induced burst suppression compared to sevoflurane-induced burst suppression, allowing bursts to occur with greater frequency (Ferron et al., 2009). Despite equivalent global reduction in the CMRO, regional variations in CMRO reduction could account for the differences in burst suppression patterns observed between two different general anesthetics (Akrawi et al., 1996; Ching et al., 2012). *In vitro* studies of thiopental, propofol, and isoflurane show that these anesthetics potentiate $GABA_A$ receptors. The activation of these receptors leads to a burst suppression pattern, and further increasing the anesthetic concentration depresses glutamatergic transmission. This decrease in glutamatergic transmission will eventually lead to complete suppression of the EEG. (Lukatch and Maciver, 1996; Lukatch et al., 2005).

Traditionally, the period of suppression is thought to be one of electrical silence. In the present study at 0.5 BSP, the median peak-to-peak amplitude of sevoflurane suppressions was 136 μV (95% CI: 125–155 μV), whereas the median peak-to-peak amplitude of propofol suppressions was only 52 μV (95% CI: 51–53 μV). In fact, the median peak-to-peak amplitude of propofol *bursts* (196 μV, 95% CI: 187–213 μV) was similar in magnitude to the median peak-to-peak amplitude of sevoflurane *suppressions*. This illustrates why visual thresholding was necessary for this study.

The high suppression amplitudes that we observed for sevoflurane have also been described for another halogenated ether anesthetic, isoflurane (Akrawi et al., 1996). This suggests that a greater level of neuronal activity occurs during suppressions induced by sevoflurane and isoflurane when compared to intravenous anesthetics such as propofol and barbiturates. It is known that during urethane and xylazine anesthesia, thalamic neurons fire at a steady delta rhythm (1–4 Hz) during suppression (Steriade et al., 1994). Future studies are needed to test whether thalamic firing activity is greater during EEG suppression periods induced by inhaled ether anesthetics.

Burst suppression is generally viewed as a single phenomenon that can be induced by various pathological processes as well as general anesthetics. However, the present results demonstrate that even after controlling for the depth of general anesthesia, different general anesthetics induce very different patterns of burst suppression. Automated algorithms used to segment burst suppression need to be tuned to match specific general anesthetics by taking into account the large differences in amplitudes and durations. More studies are needed to elucidate the underlying physiology that governs the burst suppression features induced by different general anesthetics.

DISCLOSURE OF FUNDING

This research was supported by grants TR01-GM104948 and K08-GM094394 from the National Institutes of Health, Bethesda, Maryland.

REFERENCES

Aicardi, J. (2005). Aicardi syndrome. *Brain Dev.* 27, 164–171. doi: 10.1016/j.braindev.2003.11.011

Aicardi, J., and Ohtahara, S. (2005). "Severe neonatal epilepsies with suppression-burst pattern," in *Epileptic Syndromes in Infancy, Childhood and Adolescence* 4th Edn., eds J. Roger, M. Bureau, C. Dravet and P. Genton (London: John Libbey), 39–52.

Akrawi, W. P., Drummond, J. C., Kalkman, C. J., and Patel, P. M. (1996). A comparison of the electrophysiologic characteristics of EEG burst-suppression as produced by isoflurane, thiopental, etomidate and propofol. *J. Neurosurg. Anesthesiol.* 8, 40–46. doi: 10.1097/00008506-199601000-00010

Amzica, F. (2009). Basic physiology of burst-suppression. *Epilepsia* 50(Suppl. 12), 38–39. doi: 10.1111/j.1528-1167.2009.02345.x

Arrica, M., and Bissonnette, B. (2007). Therapeutic hypothermia. *Semin. Cardiothorac. Vasc. Anesth.* 11, 6–15. doi: 10.1177/1089253206297409

Auer, R. N., Olsson, Y., and Siesjö, B. K. (1984). Hypoglycemic brain injury in the rat. Correlation of density of brain damage with the EEG isoelectric time: a quantitative study. *Diabetes* 33, 1090–1098. doi: 10.2337/diab.33.11.1090

Babadi, B., and Brown, E. N. (2014). A review of multi-taper analysis. *IEEE Trans. Biomed. Eng.* 61, 1555–1564. doi: 10.1109/TBME.2014.2311996

Barash, P. G., Cullen, B. F., Stoelting, R. K., Cahalan, M., and Stock, M. C. (2012). *Clinical Anesthesia.* Philadelphia, PA: Lippincott Williams and Wilkins.

Beydoun, A., Yen, C. E., and Drury, I. (1991). Variance of interburst intervals in burst suppression. *Electroencephalogr. Clin. Neurophysiol.* 79, 435–439. doi: 10.1016/0013-4694(91)90162-w

Bickford, R. G., and Butt, H. R. (1955). Hepatic coma: the electroencephalographic pattern. *J. Clin. Invest.* 34, 790–799. doi: 10.1172/jci103134

Brown, E. N., Lydic, R., and Schiff, N. D. (2010). General anesthesia, sleep and coma. *N. Engl. J. Med.* 363, 2638–2650. doi: 10.1056/NEJMra0808281

Brown, E. N., Purdon, P. L., and Van Dort, C. J. (2011). General anesthesia and altered states of arousal: a systems neuroscience analysis. *Annu. Rev. Neurosci.* 34, 601–628. doi: 10.1146/annurev-neuro-060909-153200

Bruhn, J., Bouillon, T. W., and Shafer, S. L. (2001). Onset of propofol-induced burst suppression may be correctly detected as deepening of anaesthesia by approximate entropy but not by bispectral index. *Br. J. Anaesth.* 87, 505–507. doi: 10.1093/bja/87.3.505

Bruhn, J., Ropcke, H., Rehberg, B., Bouillon, T., and Hoeft, A. (2000). Electroencephalogram approximate entropy correctly classifies the occurrence of burst suppression pattern as increasing anesthetic drug effect. *Anesthesiology* 93, 981–985. doi: 10.1097/00000542-200010000-00018

Chemali, J., Ching, S., Purdon, P. L., Solt, K., and Brown, E. N. (2013). Burst suppression probability algorithms: state-space methods for tracking EEG burst suppression. *J. Neural Eng.* 10:056017. doi: 10.1088/1741-2560/10/5/056017

Chemali, J. J., Van Dort, C. J., Brown, E. N., and Solt, K. (2012). Active emergence from propofol general anesthesia is induced by methylphenidate. *Anesthesiology* 116, 998–1005. doi: 10.1097/ALN.0b013e3182518bfc

Chemali, J. J., Wong, K. F., Solt, K., and Brown, E. N. (2011). A state-space model of the burst suppression ratio. *Conf. Proc. IEEE Eng. Med. Biol. Soc.* 2011, 1431–1434. doi: 10.1109/IEMBS.2011.6090354

Ching, S., Liberman, M. Y., Chemali, J. J., Westover, M. B., Kenny, J. D., Solt, K., et al. (2013). Real-time closed-loop control in a rodent model of medically induced coma using burst suppression. *Anesthesiology* 119, 848–860. doi: 10.1097/ALN.0b013e31829d4ab4

Ching, S., Purdon, P. L., Vijayan, S., Kopell, N. J., and Brown, E. N. (2012). A neurophysiological-metabolic model for burst suppression. *Proc. Natl. Acad. Sci. U S A* 109, 3095–3100. doi: 10.1073/pnas.1121461109

Claassen, J., Hirsch, L. J., Emerson, R. G., and Mayer, S. A. (2002). Treatment of refractory status epilepticus with pentobarbital, propofol, or midazolam: a systematic review. *Epilepsia* 43, 146–153. doi: 10.1046/j.1528-1157.2002.28501.x

Cotten, J. F., Le Ge, R., Banacos, N., Pejo, E., Husain, S. S., Williams, J. H., et al. (2011). Closed-loop continuous infusions of etomidate and etomidate analogs in rats: a comparative study of dosing and the impact on adrenocortical function. *Anesthesiology* 115, 764–773. doi: 10.1097/ALN.0b013e31821950de

Derbyshire, A. J., Rempel, B., Forbes, A., and Lambert, E. (1936). The effects of anesthetics on action potentials in the cerebral cortex of the cat. *Am. J. Physiol. Leg. Content* 116, 577–596.

De Rubeis, D. A., and Young, G. B. (2001). Continuous EEG monitoring in a patient with massive carbamazepine overdose. *J. Clin. Neurophysiol.* 18, 166–168. doi: 10.1097/00004691-200103000-00008

Dow, R. S. (1961). The electroencephalographic findings in acute intermittent porphyria. *Electroencephalogr. Clin. Neurophysiol.* 13, 425–437. doi: 10.1016/0013-4694(61)90011-6

Doyle, P. W., and Matta, B. F. (1999). Burst suppression or isoelectric encephalogram for cerebral protection: evidence from metabolic suppression studies. *Br. J. Anaesth.* 83, 580–584. doi: 10.1093/bja/83.4.580

Efron, B., and Tibshirani, R. (1993). *An Introduction to the Bootstrap.* Boca Raton, FL: CRC press.

Engelhardt, W., Carl, G., and Hartung, E. (1993). Intra-individual open comparison of burst-suppression-isoflurane-anaesthesia versus electroconvulsive therapy in the treatment of severe depression. *Eur. J. Anaesthesiol.* 10, 113–118.

Fariello, R. G., Chun, R. W., Doro, J. M., Buncic, J. R., and Prichard, J. S. (1977). EEG recognition of Aicardi's syndrome. *Arch. Neurol.* 34, 563–566. doi: 10.1001/archneur.1977.00500210065012

Ferenets, R., Lipping, T., Suominen, P., Turunen, J., Puumala, P., Jantti, V., et al. (2006). "Comparison of the properties of EEG spindles in sleep and propofol anesthesia," in *Engineering in Medicine and Biology Society, 2006. EMBS'06. 28th Annual International Conference of the IEEE.* (New York, NY: IEEE), 6356–6359.

Ferron, J. F., Kroeger, D., Chever, O., and Amzica, F. (2009). Cortical inhibition during burst suppression induced with isoflurane anesthesia. *J. Neurosci.* 29, 9850–9860. doi: 10.1523/JNEUROSCI.5176-08.2009

Grigg-Damberger, M. M., Coker, S. B., Halsey, C. L., and Anderson, C. L. (1989). Neonatal burst suppression: its developmental significance. *Pediatr. Neurol.* 5, 84–92. doi: 10.1016/0887-8994(89)90032-5

Hartikainen, K., Rorarius, M., Mäkelä, K., Yli-Hankala, A., and Jäntti, V. (1995a). Propofol and isoflurane induced EEG burst suppression patterns in rabbits. *Acta Anaesthesiol. Scand.* 39, 814–818. doi: 10.1111/j.1399-6576.1995.tb04176.x

Hartikainen, K. M., Rorarius, M., Peräkylä, J. J., Laippala, P. J., and Jäntti, V. (1995b). Cortical reactivity during isoflurane burst-suppression anesthesia. *Anesth. Analg.* 81, 1223–1228. doi: 10.1097/00000539-199512000-00018

Hellström-Westas, L., Rosén, I., and Svenningsen, N. W. (1995). Predictive value of early continuous amplitude integrated EEG recordings on outcome after severe birth asphyxia in full term infants. *Arch. Dis. Child. Fetal Neonatal. Ed.* 72, F34–F38. doi: 10.1136/fn.72.1.f34

Henry, C. E., and Scoville, W. B. (1952). Suppression-burst activity from isolated cerebral cortex in man. *Electroencephalogr. Clin. Neurophysiol.* 4, 1–22. doi: 10.1016/0013-4694(52)90027-8

Hofmeijer, J., Tjepkema-Cloostermans, M. C., and van Putten, M. J. (2014). Burst-suppression with identical bursts: a distinct EEG pattern with poor outcome in postanoxic coma. *Clin. Neurophysiol.* 125, 947–954. doi: 10.1016/j.clinph.2013.10.017

Hudetz, A. G., and Imas, O. A. (2007). Burst activation of the cerebral cortex by flash stimuli during isoflurane anesthesia in rats. *Anesthesiology* 107, 983–991. doi: 10.1097/01.anes.0000291471.80659.55

Huotari, A. M., Koskinen, M., Suominen, K., Alahuhta, S., Remes, R., Hartikainen, K. M., et al. (2004). Evoked EEG patterns during burst suppression with propofol. *Br. J. Anaesth.* 92, 18–24. doi: 10.1093/bja/aeh022

Itoh, M., Hanaoka, S., Sasaki, M., Ohama, E., and Takashima, S. (2001). Neuropathology of early-infantile epileptic encephalopathy with suppression-bursts; comparison with those of early myoclonic encephalopathy and west syndrome. *Brain Dev.* 23, 721–726. doi: 10.1016/s0387-7604(01)00270-4

Jevtović-Todorović, V., Todorovć, S., Mennerick, S., Powell, S., Dikranian, K., Benshoff, N., et al. (1998). Nitrous oxide (laughing gas) is an NMDA antagonist, neuroprotectant and neurotoxin. *Nat. Med.* 4, 460–463. doi: 10.1038/nm0498-460

Kaiser, J. F. (1990). "On a simple algorithm to calculate theenergy'of a signal," in *Acoustics, Speech and Signal Processing, 1990. ICASSP-90., 1990 International Conference on.* (Albuquerque, NM: IEEE), 381–384.

Kassell, N. F., Hitchon, P. W., Gerk, M. K., Sokoll, M. D., and Hill, T. R. (1980). Alterations in cerebral blood flow, oxygen metabolism and electrical activity produced by high dose sodium thiopental. *Neurosurgery* 7, 598–603. doi: 10.1097/00006123-198012000-00011

Kheder, A., Bianchi, M. T., and Westover, M. B. (2014). Burst suppression in sleep in a routine outpatient EEG. *Epilepsy Behav. Case Rep.* 2, 71–74. doi: 10.1016/j.ebcr.2014.01.003

Kroeger, D., and Amzica, F. (2007). Hypersensitivity of the anesthesia-induced comatose brain. *J. Neurosci.* 27, 10597–10607. doi: 10.1523/jneurosci.3440-07.2007

Lambrakis, C. C., Lancman, M. E., and Romano, C. (1999). Asynchronous and asymmetric burst-suppression in a patient with a corpus callosum lesion. *Clin. Neurophysiol.* 110, 103–105. doi: 10.1016/s0013-4694(98)00102-3

Lazar, L. M., Milrod, L. M., Solomon, G. E., and Labar, D. R. (1999). Asynchronous pentobarbital-induced burst suppression with corpus callosum hemorrhage. *Clin. Neurophysiol.* 110, 1036–1040. doi: 10.1016/s1388-2457(99)00046-2

Lebowitz, M. H., Blitt, C. D., and Dillon, J. B. (1972). Enflurane-induced central nervous system excitation and its relation to carbon dioxide tension. *Anesth. Analg.* 51, 355–363. doi: 10.1213/00000539-197205000-00007

Levy, W. J. (1984). Quantitative analysis of EEG changes during hypothermia. *Anesthesiology* 60, 291–297. doi: 10.1097/00000542-198404000-00004

Lewis, L. D., Ching, S., Weiner, V. S., Peterfreund, R. A., Eskandar, E. N., Cash, S. S., et al. (2013). Local cortical dynamics of burst suppression in the anaesthetized brain. *Brain* 136, 2727–2737. doi: 10.1093/brain/awt174

Liley, D. T., and Walsh, M. (2013). The Mesoscopic modeling of burst suppression during anesthesia. *Front. Comput. Neurosci.* 7:46. doi: 10.3389/fncom.2013.00046

Lipping, T., Jäntti, V., Yli-Hankala, A., and Hartikainen, K. (1995). Adaptive segmentation of burst-suppression pattern in isoflurane and enflurane anesthesia. *Int. J. Clin. Monit. Comput.* 12, 161–167. doi: 10.1007/bf02332690

Löfhede, J., Löfgren, N., Thordstein, M., Flisberg, A., Kjellmer, I., and Lindecrantz, K. (2007). Comparison of three methods for classifying burst and suppression in the EEG of post asphyctic newborns. *Conf. Proc. IEEE Eng. Med. Biol. Soc.* 2007, 5136–5139. doi: 10.1109/iembs.2007.4353496

Lowenstein, D. H., Bleck, T., and Macdonald, R. L. (1999). It's time to revise the definition of status epilepticus. *Epilepsia* 40, 120–122. doi: 10.1111/j.1528-1157.1999.tb02000.x

Lukatch, H. S., Echon, R. M., Maciver, M. B., and Werchan, P. M. (1997). G-force induced alterations in rat EEG activity: a quantitative analysis. *Electroencephalogr. Clin. Neurophysiol.* 103, 563–573. doi: 10.1016/s0013-4694(97)00063-1

Lukatch, H. S., Kiddoo, C. E., and Maciver, M. B. (2005). Anesthetic-induced burst suppression EEG activity requires glutamate-mediated excitatory synaptic transmission. *Cereb. Cortex* 15, 1322–1331. doi: 10.1093/cercor/bhi015

Lukatch, H. S., and Maciver, M. B. (1996). Synaptic mechanisms of thiopental-induced alterations in synchronized cortical activity. *Anesthesiology* 84, 1425–1434. doi: 10.1097/00000542-199606000-00019

Martin, J. T., Faulconer, A. Jr., and Bickford, R. G. (1959). Electroencephalography in anesthesiology. *Anesthesiology* 20, 359–376. doi: 10.1097/00000542-195905000-00017

Michenfelder, J. D., and Milde, J. H. (1991). The relationship among canine brain temperature, metabolism and function during hypothermia. *Anesthesiology* 75, 130–136. doi: 10.1097/00000542-199107000-00021

Mitra, P., and Bokil, H. (2008). *Observed Brain Dynamics.* Oxford; New York: Oxford University Press.

Modica, P. A., and Tempelhoff, R. (1992). Intracranial pressure during induction of anaesthesia and tracheal intubation with etomidate-induced EEG burst suppression. *Can. J. Anaesth.* 39, 236–241. doi: 10.1007/bf03008783

Morris, L. E., Knott, J. R., and Pittinger, C. B. (1955). Electro-encephalographic and blood gas observations in human surgical patients during xenon anesthesia. *Anesthesiology* 16, 312–319. doi: 10.1097/00000542-195505000-00003

Mundi, J. P., Betancourt, J., Ezziddin, O., Tremayne, B., Majic, T., and Mosenifar, Z. (2012). Dilated and unreactive pupils and burst-suppression on electroencephalography due to buproprion overdose. *J. Intensive Care Med.* 27, 384–388. doi: 10.1177/0885066611429661

Murrell, J. C., Waters, D., and Johnson, C. B. (2008). Comparative effects of halothane, isoflurane, sevoflurane and desflurane on the electroencephalogram of the rat. *Lab. Anim.* 42, 161–170. doi: 10.1258/la.2007.06019e

Nims, L. F., Marshall, C., and Nielsen, A. (1941). Effect of local freezing on the electrical activity of the cerebral cortex. *Yale J. Biol. Med.* 13, 477–484.

Ohtahara, S., and Yamatogi, Y. (2003). Epileptic encephalopathies in early infancy with suppression-burst. *J. Clin. Neurophysiol.* 20, 398–407. doi: 10.1097/00004691-200311000-00003

Ohtahara, S., and Yamatogi, Y. (2006). Ohtahara syndrome: with special reference to its developmental aspects for differentiating from early myoclonic encephalopathy. *Epilepsy Res.* 70(Suppl. 1), S58–S67. doi: 10.1016/j.eplepsyres.2005.11.021

Ostermann, M. E., Young, B., Sibbald, W. J., and Nicolle, M. W. (2000). Coma mimicking brain death following baclofen overdose. *Intensive Care Med.* 26, 1144–1146. doi: 10.1007/s001340051330

Panayiotopoulos, C. P. (2010). *Atlas of Epilepsies*. London: Springer, 847–850. doi: 10.1007/978-1-84882-128-6_120

Pearcy, W. C., Knott, J. E., Pittinger, C. B., and Keasling, H. H. (1957). Electroencephalographic and circulatory effects of chloroform anesthesia in dogs. *Anesthesiology* 18, 88–96. doi: 10.1097/00000542-195701000-00009

Pittinger, C. B., Faulconer, A. Jr., Knott, J. R., Pender, J. W., Morris, L. E., and Bickford, R. G. (1955). Electro-encephalographic and other observations in monkeys during xenon anesthesia at elevated pressures. *Anesthesiology* 16, 551–563. doi: 10.1097/00000542-195507000-00011

Porkkala, T., Jänit, V., Kaukinen, S., and Häkkinen, V. (1997). Nitrous oxide has different effects on the EEG and somatosensory evoked potentials during isoflurane anaesthesia in patients. *Acta Anaesthesiol. Scand.* 41, 497–501. doi: 10.1111/j.1399-6576.1997.tb04730.x

Possati, S., Faulconer, A. Jr., Bickford, R. G., and Hunter, R. C. (1953). Electroencephalographic patterns during anesthesia with cyclopropane: correlation with concentration of cyclopropane in arterial blood. *Curr. Res. Anesth. Analg.* 32, 130–135. doi: 10.1213/00000539-195301000-00022

Prasad, A., Worrall, B. B., Bertram, E. H., and Bleck, T. P. (2001). Propofol and midazolam in the treatment of refractory status epilepticus. *Epilepsia* 42, 380–386. doi: 10.1046/j.1528-1157.2001.27500.x

Prerau, M. J., and Purdon, P. L. (2013). "A probabilistic framework for time-frequency detection of burst suppression," in *Neural Engineering (NER), 2013 6th International IEEE/EMBS Conference on.* (San Diego, CA: IEEE), 609–612.

Rae-Grant, A. D., and Kim, Y. W. (1994). Type III intermittency: a nonlinear dynamic model of EEG burst suppression. *Electroencephalogr. Clin. Neurophysiol.* 90, 17–23. doi: 10.1016/0013-4694(94)90109-0

Rampil, I. J., Lockhart, S. H., Eger, E. I. 2nd, Yasuda, N., Weiskopf, R. B., and Cahalan, M. K. (1991). The electroencephalographic effects of desflurane in humans. *Anesthesiology* 74, 434–439. doi: 10.1097/00000542-199103000-00008

Rampil, I. J., Weiskopf, R. B., Brown, J. G., Eger, E. I. 2nd, Johnson, B. H., Holmes, M. A., et al. (1988). I653 and isoflurane produce similar dose-related changes in the electroencephalogram of pigs. *Anesthesiology* 69, 298–302. doi: 10.1097/00000542-198809000-00002

Särkelä, M., Mustola, S., Seppänen, T., Koskinen, M., Lepola, P., Suominen, K., et al. (2002). Automatic analysis and monitoring of burst suppression in anesthesia. *J. Clin. Monit. Comput.* 17, 125–134. doi: 10.1023/A:1016393904439

Scheller, M. S., Nakakimura, K., Fleischer, J. E., and Zornow, M. H. (1990). Cerebral effects of sevoflurane in the dog: comparison with isoflurane and enflurane. *Br. J. Anaesth.* 65, 388–392. doi: 10.1093/bja/65.3.388

Shanechi, M. M., Chemali, J. J., Liberman, M., Solt, K., and Brown, E. N. (2013a). A brain-machine interface for control of burst suppression in medical coma. *Conf. Proc. IEEE Eng. Med. Biol. Soc.* 2013, 1575–1578. doi: 10.1109/EMBC.2013.6609815

Shanechi, M. M., Chemali, J. J., Liberman, M., Solt, K., and Brown, E. N. (2013b). A brain-machine interface for control of medically-induced coma. *PLoS Comput. Biol.* 9:e1003284. doi: 10.1371/journal.pcbi.1003284

Solt, K., Cotten, J. F., Cimenser, A., Wong, K. F., Chemali, J. J., and Brown, E. N. (2011). Methylphenidate actively induces emergence from general anesthesia. *Anesthesiology* 115, 791–803. doi: 10.1097/ALN.0b013e31822e92e5

Solt, K., Eger, E. I., and Raines, D. E. (2006). Differential modulation of human N-methyl-D-aspartate receptors by structurally diverse general anesthetics. *Anesth. Analg.* 102, 1407–1411. doi: 10.1213/01.ane.0000204252.07406.9f

Solt, K., and Forman, S. A. (2007). Correlating the clinical actions and molecular mechanisms of general anesthetics. *Curr. Opin. Anaesthesiol.* 20, 300–306. doi: 10.1097/aco.0b013e32816678a5

Sonkajärvi, E., Puumala, P., Erola, T., Baer, G., Karvonen, E., Suominen, K., et al. (2008). Burst suppression during propofol anaesthesia recorded from scalp and subthalamic electrodes: report of three cases. *Acta Anaesthesiol. Scand.* 52, 274–279. doi: 10.1111/j.1399-6576.2007.01501.x

Spoerel, W. E. (1961). The electroencephalogram as indicator of hypoxia. *Anesth. Analg.* 40, 94–104. doi: 10.1213/00000539-196101000-00013

Stecker, M. M., Cheung, A. T., Pochettino, A., Kent, G. P., Patterson, T., Weiss, S. J., et al. (2001). Deep hypothermic circulatory arrest: I. Effects of cooling on electroencephalogram and evoked potentials. *Ann. Thorac. Surg.* 71, 14–21. doi: 10.1016/s0003-4975(00)01592-7

Stecker, M. M., Kramer, T. H., Raps, E. C., O'Meeghan, R., Dulaney, E., and Skaar, D. J. (1998). Treatment of refractory status epilepticus with propofol: clinical and pharmacokinetic findings. *Epilepsia* 39, 18–26. doi: 10.1111/j.1528-1157.1998.tb01269.x

Steriade, M., Amzica, F., and Contreras, D. (1994). Cortical and thalamic cellular correlates of electroencephalographic burst-suppression. *Electroencephalogr. Clin. Neurophysiol.* 90, 1–16. doi: 10.1016/0013-4694(94)90108-2

Swank, R. L., and Watson, C. W. (1949). Effects of barbiturates and ether on spontaneous electrical activity of dog brain. *J. Neurophysiol.* 12, 137–160.

Thadani, H., Deacon, A., and Peters, T. (2000). Diagnosis and management of porphyria. *BMJ* 320, 1647–1651. doi: 10.1136/bmj.320.7250.1647

Thomson, D. J. (1982). Spectrum estimation and harmonic-analysis. *Proc. IEEE* 70, 1055–1096. doi: 10.1109/proc.1982.12433

Toet, M. C., Hellstrom-Westas, L., Groenendaal, F., Eken, P., and de Vries, L. S. (1999). Amplitude integrated EEG 3 and 6 hours after birth in full term neonates with hypoxic-ischaemic encephalopathy. *Arch. Dis. Child. Fetal Neonatal. Ed.* 81, F19–F23. doi: 10.1136/fn.81.1.f19

Van Ness, P. C. (1990). Pentobarbital and EEG burst suppression in treatment of status epilepticus refractory to benzodiazepines and phenytoin. *Epilepsia* 31, 61–67. doi: 10.1111/j.1528-1157.1990.tb05361.x

van Rooij, L. G., Toet, M. C., Osredkar, D., van Huffelen, A. C., Groenendaal, F., and de Vries, L. S. (2005). Recovery of amplitude integrated electroencephalographic background patterns within 24 hours of perinatal asphyxia. *Arch. Dis. Child. Fetal Neonatal. Ed.* 90, F245–F251. doi: 10.1136/adc.2004.064964

Vijn, P. C., and Sneyd, J. R. (1998). I.v. anaesthesia and EEG burst suppression in rats: bolus injections and closed-loop infusions. *Br. J. Anaesth.* 81, 415–421. doi: 10.1093/bja/81.3.415

Weissenborn, K., Wilkens, H., Hausmann, E., and Degen, P. H. (1991). Burst suppression EEG with baclofen overdose. *Clin. Neurol. Neurosurg.* 93, 77–80. doi: 10.1016/0303-8467(91)90015-h

Wennberg, R., Quesney, F., Olivier, A., and Dubeau, F. (1997). Induction of burst-suppression and activation of epileptiform activity after methohexital and selective amygdalo-hippocampectomy. *Electroencephalogr. Clin. Neurophysiol.* 102, 443–451. doi: 10.1016/s0921-884x(97)96052-5

Westover, M. B., Shafi, M. M., Ching, S., Chemali, J. J., Purdon, P. L., Cash, S. S., et al. (2013). Real-time segmentation of burst suppression patterns in critical care EEG monitoring. *J. Neurosci. Methods* 219, 131–141. doi: 10.1016/j.jneumeth.2013.07.003

Whishaw, I. Q. (1976). The effects of alcohol and atropine on EEG and behavior in the rabbit. *Psychopharmacology (Berl)* 48, 83–90. doi: 10.1007/bf00423311

Yli-Hankala, A., Jäntti, V., Pyykko, I., and Lindgren, L. (1993a). Vibration stimulus induced EEG bursts in isoflurane anaesthesia. *Electroencephalogr. Clin. Neurophysiol.* 87, 215–220. doi: 10.1016/0013-4694(93)90021-m

Yli-Hankala, A., Lindgren, L., Porkkala, T., and Jäntti, V. (1993b). Nitrous oxide-mediated activation of the EEG during isoflurane anaesthesia in patients. *Br. J. Anaesth.* 70, 54–57. doi: 10.1093/bja/70.1.54

Young, G. B. (2000). The EEG in coma. *J. Clin. Neurophysiol.* 17, 473–485. doi: 10.1097/00004691-200009000-00006

Young, G. B., Bolton, C. F., Archibald, Y. M., Austin, T. W., and Wells, G. A. (1992). The electroencephalogram in sepsis-associated encephalopathy. *J. Clin. Neurophysiol.* 9, 145–152. doi: 10.1097/00004691-199201000-00016

Zaret, B. S. (1985). Prognostic and neurophysiological implications of concurrent burst suppression and alpha patterns in the EEG of post-anoxic coma. *Electroencephalogr. Clin. Neurophysiol.* 61, 199–209. doi: 10.1016/0013-4694(85)91085-5

Conflict of Interest Statement: The authors declare that the research was conducted in the absence of any commercial or financial relationships that could be construed as a potential conflict of interest.

Received: 15 August 2014; accepted: 27 November 2014; published online: 18 December 2014.

Citation: Kenny JD, Westover MB, Ching S, Brown EN and Solt K (2014) Propofol and sevoflurane induce distinct burst suppression patterns in rats. Front. Syst. Neurosci. ***8****:237. doi: 10.3389/fnsys.2014.00237*

This article was submitted to the journal Frontiers in Systems Neuroscience.

frontiers in
SYSTEMS NEUROSCIENCE

ORIGINAL RESEARCH ARTICLE
published: 16 October 2014
doi: 10.3389/fnsys.2014.00203

Chaos analysis of EEG during isoflurane-induced loss of righting in rats

M. B. MacIver[1]* and Brian H. Bland[2]

[1] *Neuropharmacology Laboratory, Stanford University School of Medicine, Stanford, CA, USA*
[2] *Department of Psychology and Hotchkiss Brain Institute, University of Calgary, Calgary, AB, Canada*

Edited by:
Anthony G. Hudetz, Medical College of Wisconsin, USA

Reviewed by:
Axel Hutt, Institut National de Recherche en Informatique et en Automatique, France
Misha Perouansky, University of Wisconsin, USA

****Correspondence:***
M. B. MacIver, SUMC S 288 MC 5117, Stanford University, Anesthesia, Neuropharmacology Laboratory, Stanford CA 94350, USA
e-mail: maciver@stanford.edu

It has long been known that electroencephalogram (EEG) signals generate chaotic strange attractors and the shape of these attractors correlate with depth of anesthesia. We applied chaos analysis to frontal cortical and hippocampal micro-EEG signals from implanted microelectrodes (layer 4 and CA1, respectively). Rats were taken to and from loss of righting reflex (LORR) with isoflurane and behavioral measures were compared to attractor shape. Resting EEG signals at LORR differed markedly from awake signals, more similar to slow wave sleep signals, and easily discerned in raw recordings (high amplitude slow waves), and in fast Fourier transform analysis (FFT; increased delta power), in good agreement with previous studies. EEG activation stimulated by turning rats on their side, to test righting, produced signals quite similar to awake resting state EEG signals. That is, the high amplitude slow wave activity changed to low amplitude fast activity that lasted for several seconds, before returning to slow wave activity. This occurred regardless of whether the rat was able to right itself, or not. Testing paw pinch and tail clamp responses produced similar EEG activations, even from deep anesthesia when burst suppression dominated the spontaneous EEG. Chaotic attractor shape was far better at discerning between these awake-like signals, at loss of responses, than was FFT analysis. Comparisons are provided between FFT and chaos analysis of EEG during awake walking, slow wave sleep, and isoflurane-induced effects at several depths of anesthesia. Attractors readily discriminated between natural sleep and isoflurane-induced "delta" activity. Chaotic attractor shapes changed gradually through the transition from awake to LORR, indicating that this was not an on/off like transition, but rather a point along a continuum of brain states.

Keywords: anesthesia, delta activity, sleep, burst suppression, theta, behavior, cortex, consciousness

INTRODUCTION

Analysis of electroencephalogram (EEG) recordings have been used to characterize anesthetic effects at various concentration-related depths, from sedation through loss of recall, loss of consciousness, and full surgical immobility. Volatile anesthetics, barbiturates, and propofol produce a stereotypic pattern of EEG changes, with high amplitude slow wave (delta; 1–3 Hz) activity seen during sedation and loss of consciousness, and transitioning to burst suppression patterns at surgical levels of anesthesia (Clark et al., 1973; MacIver et al., 1996; Pilge et al., 2014). Previous studies have used various quantitative measures based on time-series analysis to characterize these EEG signals (Rampil, 2001). Measures based on Fourier, entropy, coherence, and/or bispectral transforms have proven useful in the design of commercially available anesthetic depth monitors. Unfortunately, these monitors have been shown to achieve accuracies/congruencies of only ∼ 85–95%, far below a level that is needed to prevent intraoperative awareness (Niedhart et al., 2006; Hrelec et al., 2010).

It has long been known that EEG signals can generate chaotic strange attractors and that the shape of these attractors correlate with depth of anesthesia (Watt and Hameroff, 1988; Walling and Hicks, 2006). One of these studies compared frequency domain measures [FFT: (Walling and Hicks, 2006)], with chaos analysis of anesthetic-induced changes in EEG signals, but the attractor density was too sparse for detailed analysis. The present study used high quality frontal and hippocampal micro-EEG recordings and high density 3D attractor plots to compare signals associated with isoflurane-induced loss of righting reflex in rats. Loss of righting reflex is a commonly used surrogate endpoint measure in rodents for loss of consciousness in humans (Frank and Jhamandas, 1970).

It is possible that anesthetic-induced changes in EEG signals represent altered states of brain processing produced by an anesthetic. In the present study we have tested the hypothesis that chaos analysis can provide a sensitive measure for isoflurane-induced changes in brain state, especially at the point of loss

of consciousness. We hope this can contribute to a better understanding anesthesia and theories of consciousness.

MATERIALS AND METHODS

ANIMALS

Animal protocols were approved by the University of Calgary Life Sciences Environmental Animal Care Committee in accordance with guidelines from the Canadian Council on Animal Care. All procedures complied with the National Institute of Health (US) and Society for Neuroscience guidelines for the care and use of research animals, and efforts were made to minimize stress, and discomfort at all stages of handling. Thirteen male Sprague-Dawley rats weighing between 300 and 450 gm were used. Rats were obtained from the Animal Care Facility at the University of Calgary.

SURGERY

Rats were deeply anesthetized with ketamine-xylazine 4:1 1.0 ml/kg and placed in a stereotaxic apparatus and prepared for electrode implantation by leveling to horizontal the plane between bregma and lambda as previously described (Bland et al., 2007). Rats spontaneously breathed and body temperature was maintained using a heating pad. An indifferent electrode consisting of small screw was placed in the skull over the cerebellar cortex to act as a ground. Bipolar twisted pair tungsten microelectrodes (Plastics One, Roanoke VA) with vertical tip separations of ∼ 1.0 mm were stereotaxically placed in layer 4 of frontal cortex (3.0 mm AB, 3.0 mm L, and 1.5 mm V) and in the CA1 region of dorsal hippocampus (4.0 mm PB, 2.0 mm L, and 2.4 mm V) to record micro-EEG signals. Animals were allowed to recover for at least a week before being placed in a small recording/anesthesia chamber (24 × 10 × 10 inches) that was continuously flushed with room air in control conditions or oxygen that was used as a carrier gas for the isoflurane vaporizer.

RECORDING

For experiments, animals were placed in the recording chamber and attached via Plastic One screw type connectors to fine shielded leads and through a commutator to allow free movement. EEG signals were recorded wideband (0.1 Hz–20 kHz) using Grass Instrument Co. P 511 EEG preamplifiers, and were conditioned (x10 gain and zero DC offset) using a BrownLee model 410 instrumentation amplifier, before being digitized at 20 kHz using a National Instruments USB 6009 A/D connected

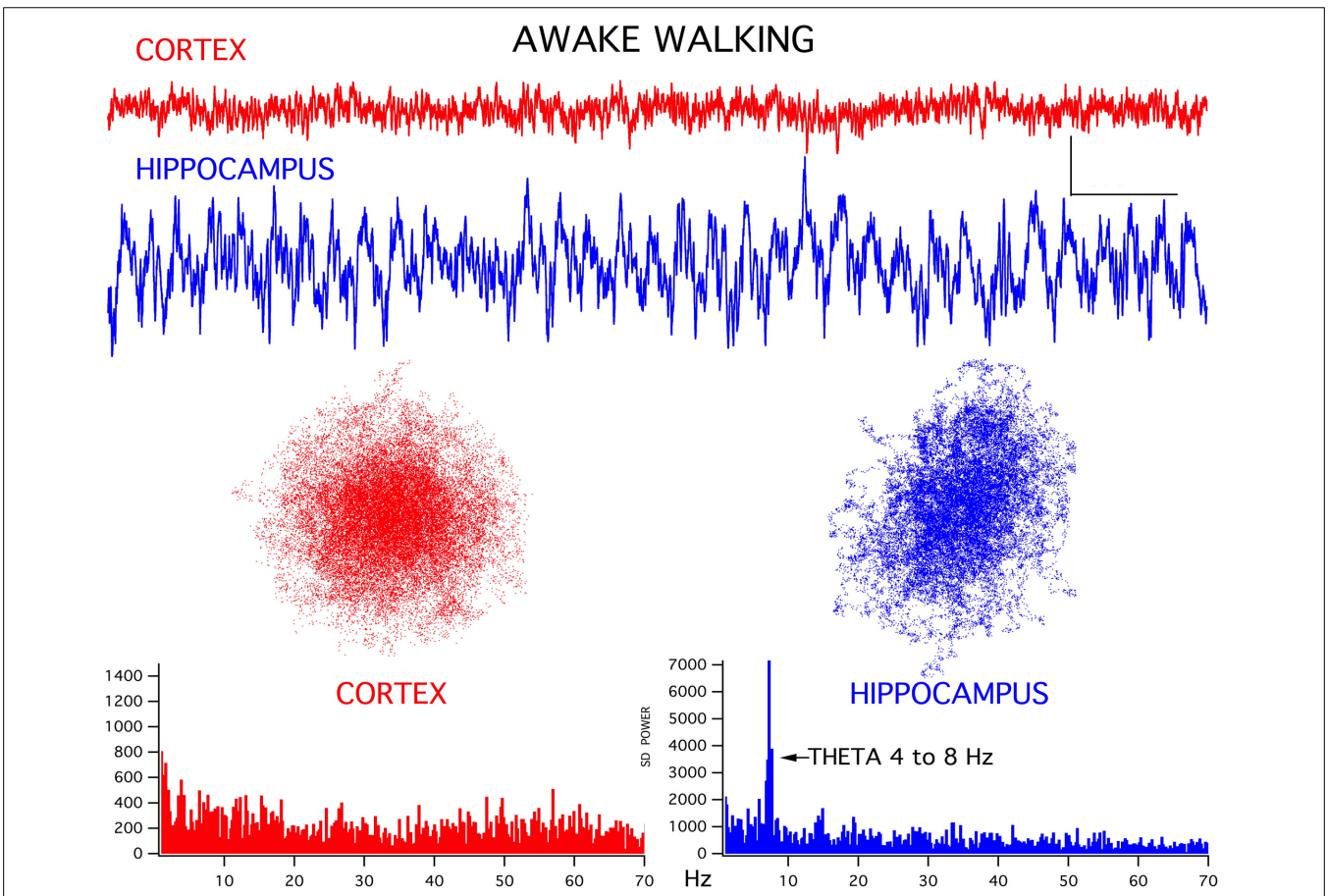

FIGURE 1 | Representative EEG recordings of frontal cortex (CORTEX) and hippocampal CA1 (HIPPOCAMPUS) signals for simultaneously recorded activity. During walking/exploring behavior, low amplitude fast activity is seen in cortex and a theta rhythm is generated in hippocampus. Chaotic attractor plots and FFT magnitude graphs, for these two records are shown below the recordings. Calibration bars = 200 μV and 500 ms. Note that the gain of the hippocampal signal was reduced by 1/3 for the analyses, to maintain scaling with respect to cortex.

to a MacBook computer running OS10.7/UNIX and Wavemetrics IgorPro acquisition software. Signals were continuously analyzed by FFT and displayed online, and were stored to disk using IgorPro. At least 20 min of control EEG signals were acquired from each rat, consisting of periods of awake immobility, exploring/walking, and sleep immobility, assessed from behavioral, and FFT observation by one of the authors. Once stable baseline recordings were complete, rats were exposed to various concentrations of isoflurane via an Isotec 3 commercial vaporizer. Isoflurane concentrations in the recording chamber were continuously measured and displayed using a Riken FI-21 agent monitor. For loss of righting experiments, isoflurane was applied for at least 20 min to achieve steady-state at each tested concentration and the righting reflex was assessed every 5 min by gently tilting the recording chamber to roll a rat on it's side. At deeper levels of isoflurane anesthesia, rats were placed on a heating pad to maintain body temperature.

DATA ANALYSIS

Behavioral observations were time-stamped to recorded EEG signals for off-line analysis/correlation. EEG signals were further processed and displayed as real component magnitude graphs using IgorPro. For chaos analysis, algorithms provided by Walling and Hicks (2006) were utilized and the results were visualized as point plots using 3D graphics in IgorPro. We used an embedding delay of 0.01 s, as this was found to be the minimal delay needed to produce a spherical attractor for the awake frontal EEG signal, sampled at 20 kHz. We found this delay worked well for EEG samples as short as 2 s, but in the examples shown we used the entire EEG trace shown with each attractor (i.e., 6.0–8.0 s).

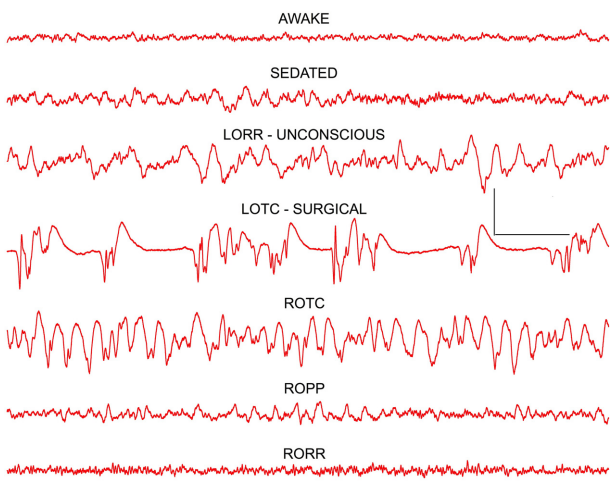

FIGURE 2 | Frontal cortex EEG recordings showing changes seen at the three anesthetic endpoints (depths) tested: LORR–loss of righting reflex, LOPP—loss of paw pinch, and LOTC—loss of tail clamp. The dominant effect at loss of consciousness (LORR) was a slowing of the EEG resulting in a high power delta signal that resembled slow wave sleep patterns. At surgical levels of anesthesia (LOTC) burst suppression activity was seen. Note a reverse pattern of changes was seen on recovery as isoflurane concentrations decreased and responses returned (ROTC, ROPP, and RORR). Calibration = 500 μV and 1.0 s.

Chaotic attractors were "flattened" by isoflurane in 2 dimensions and this was best seen in 3D rotations. For this reason, we used 3D plots to show the attractors. Quicktime movies of these 3D rotations are provided as supplemental materials. For the graphs shown in this paper, we used a projection that best showed the maximal flattening for each attractor.

RESULTS

EEG SIGNALS CORRELATED WITH BEHAVIOR

For both the frontal cortex and hippocampal EEG signals there was a good correlation between ongoing behavior and signal appearance, in agreement with previous studies (Bland and Oddie, 2001). For example, during awake exploring, the frontal cortex generated low amplitude fast activity while the hippocampus produced a theta rhythm (**Figure 1**). Interestingly, in all thirteen rats, the chaotic attractor associated with this frontal fast activity was spherical, in good agreement with attractors seen in frontal cortical signals recorded from alert humans (Walling and Hicks, 2006). The hippocampal EEG attractor during both theta activity (**Figure 1**) and large amplitude irregular activity (LIA, not shown) was somewhat flattened compared to cortex.

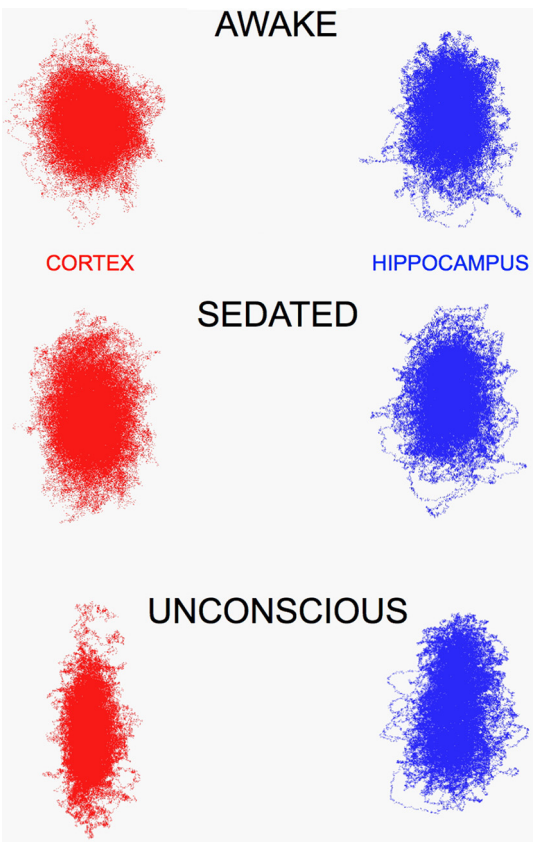

FIGURE 3 | Chaotic attractors for frontal cortex (CORTEX) flatten in the presence of increasing concentrations of isoflurane (0.5 and 0.72 vol %), however hippocampal attractors remain largely unchanged. This was evident in recordings too, LIA was the dominant pattern seen in hippocampus, until high concentrations that produced synchronized burst suppression occurred in both brain regions.

The FFT magnitude graphs associated with these signals showed the typical wideband activity in frontal cortex and a prominent theta peak (4–8 Hz) in the hippocampus (bottom graphs in **Figure 1**).

ISOFLURANE PRODUCED A STEREOTYPIC CHANGE IN EEG SIGNALS

In agreement with earlier studies in both humans (Buhrer et al., 1992) and rats (MacIver et al., 1996), undergoing thiopental anesthesia, a characteristic pattern of concentration-dependent EEG changes was produced by isoflurane (**Figure 2**). A very similar pattern was seen in all rats. Low amplitude fast activity seen in awake frontal cortex was replaced by higher amplitude slow wave activity at low concentrations of isoflurane that produced mild sedation. At concentrations of isoflurane that produced loss of righting reflex (LORR; 0.7–0.8 vol %) a further increase in amplitude and slowing of the frontal EEG signal was seen. Loss of tail clamp (LOTC; 1.3–1.5 vol %) response was used as a surrogate endpoint for a surgical plane of anesthesia (White et al., 1974). A characteristic burst suppression EEG pattern was evident in the frontal cortex at LOTC in all rats (**Figure 2**), although this pattern could change to large amplitude slow wave activity during the course of tail clamp stimulation, and even to an awake-like pattern of low amplitude fast activity in some rats, even though no behavioral response was evident. This type of cortical activation was also seen at lower concentrations of isoflurane during LORR stimulation (see below). Frontal EEG signals rapidly returned to burst suppression patterns within 20 s of removing tail clamp stimulation.

A mirror image of these EEG patterns was seen upon removal of isoflurane from the recording chamber (**Figure 2**). At return of the tail clamp response (ROTC), high amplitude slow wave activity was evident in cortex. A pattern of activity similar to that seen during mild sedation was evident when rats were able to withdraw their hind leg in response to mild paw pressure (ROPP) and, paradoxically, an awake pattern of low amplitude fast activity was seen for several seconds before rats recovered their righting reflex (RORR in **Figure 2**).

While the frontal cortex EEG signals were clearly altered by isoflurane, the hippocampal signals remained largely unchanged, and this was also true for the chaotic attractors (**Figure 3**), cortical attractors were markedly flattened by isoflurane, but hippocampal attractors remained unchanged.

ISOFLURANE-INDUCED SLOW WAVE ACTIVITY WAS DIFFERENT FROM SLOW WAVE SLEEP PATTERNS

The isoflurane-induced slow wave "delta" activity was quite different from delta activity seen during slow wave sleep in the same rats (**Figure 4**). Although both EEG signals exhibited similar high amplitudes and a 1–3 Hz dominant frequency, the isoflurane-induced delta activity was notably devoid of higher frequencies seen during sleep. This was clearly evident in the chaotic attractors associated with these two forms of delta activity. Both attractors were flattened compared to the awake condition (**Figure 1**), but the isoflurane-induced attractor was considerably more flattened and disorganized compared to the sleep attractor (**Figure 4**).

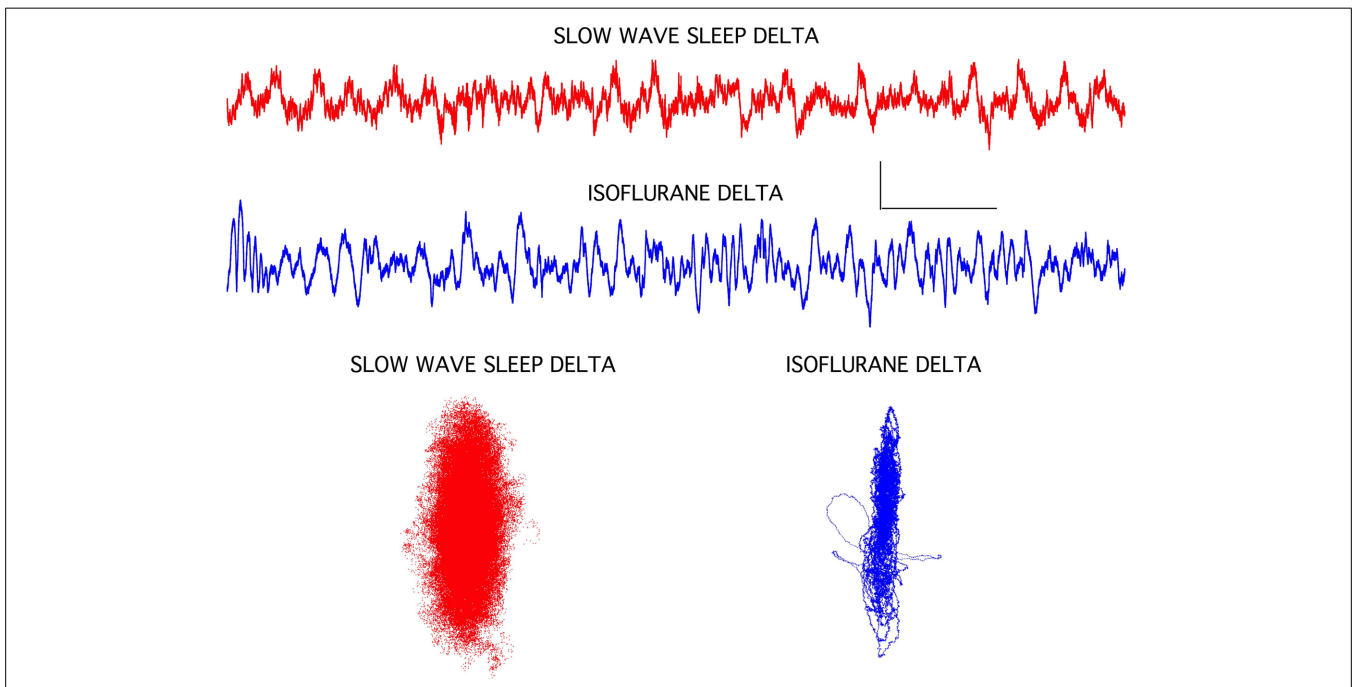

FIGURE 4 | Slow wave sleep delta EEG activity seen in frontal cortex was associated with a classic sleep posture and with isoflurane-induced loss of righting in rats. The isoflurane-induced recordings were clearly lacking some high frequency components, but overall amplitude increases and background frequencies were similar. Chaotic attractors were markedly different for these two signals, however, indicating that circuit level differences were associated with these two brain states. Each attractor plots the data for the accompanying EEG recording. Calibration = 300 μV and 1.0 s.

ISOFLURANE-INDUCED LORR

As mentioned above, testing the righting reflex in rats produced frontal cortical activation, both before and after the reflex was lost. **Figure 5** demonstrates this effect. Before testing the reflex the frontal cortex was clearly producing high amplitude slow wave delta activity with sleep spindles seen riding on 2 Hz slow waves, characteristic of isoflurane effects at a concentration of ∼ 0.7 vol %. LIA was seen in the hippocampus. When the recording chamber was tilted to test for righting, the frontal signal immediately activated into an awake-like pattern of low amplitude fast activity, and theta appeared in the hippocampus, as the rat righted itself. Five minutes later, at this same concentration of isoflurane, the rat was no longer able to right itself, yet tilting the chamber still resulted in cortical activation, but theta was no longer

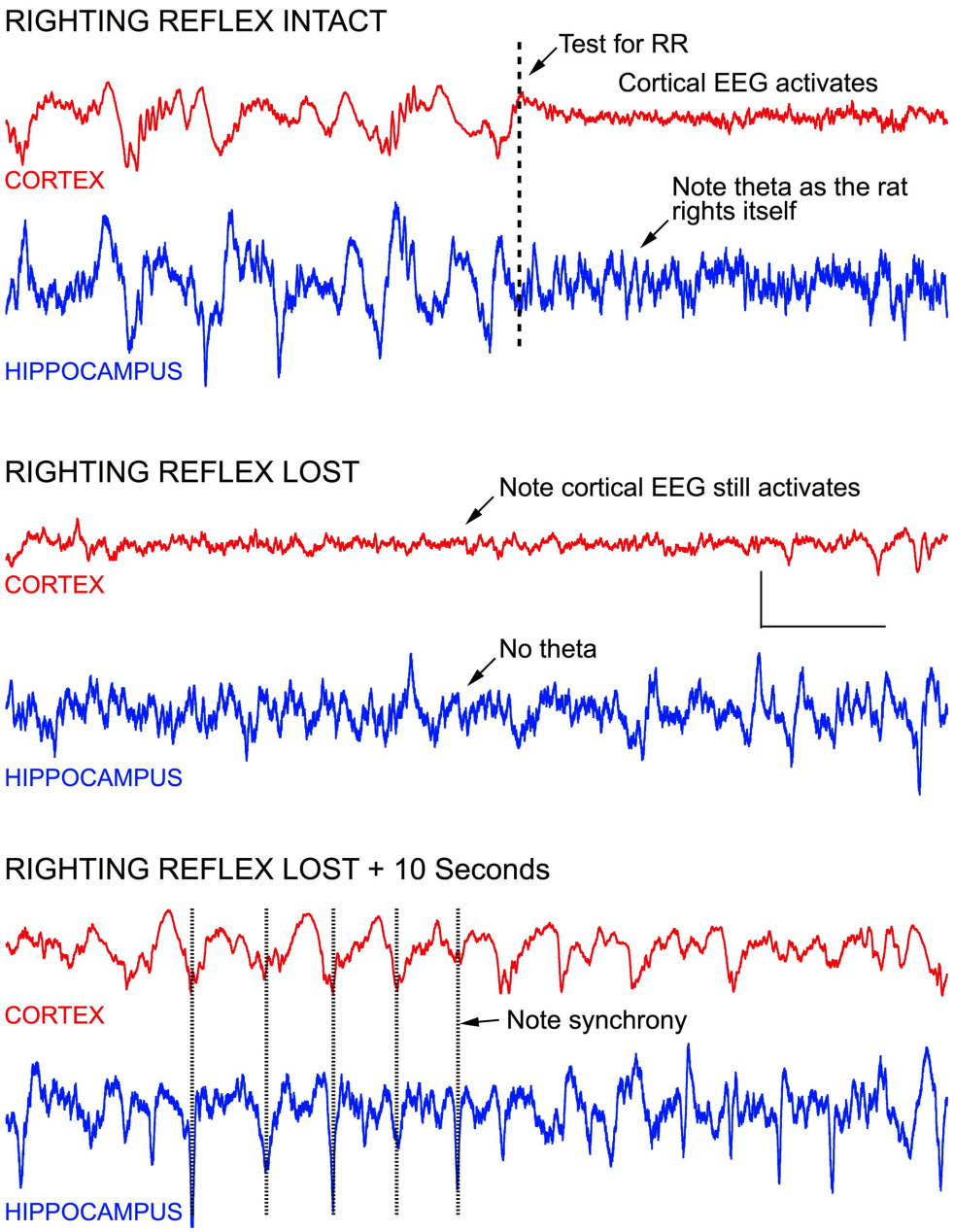

FIGURE 5 | Stimulating anesthetized rats results in cortical and hippocampal activation. For example, testing the rats righting reflex (arrow in top record) stimulates vestibular, proprioceptive, and other sensory inputs—resulting in an awake-like "activated" EEG signal. Activation occurred regardless of whether righting was lost or not, and rapidly retuned to a slow wave "delta" pattern seconds after the stimulus onset, regardless of whether the rat righted itself or not. In the middle recordings, the righting reflex was tested 1 s before the start of the recording, and an activated EEG pattern was seen for the entire recording shown (7.0 s), even though the rat failed to right itself. In the lower recording, the EEG is seen to return to slow wave activity within 10 s, and the slow wave activity in cortex appeared to be synchronized with LIA hippocampus. Calibration = 300 μV and 1.0 s.

seen in the hippocampus. Within 10 s the cortical signal returned to high amplitude delta activity and the hippocampus continued to generate LIA (bottom of **Figure 5**). Over the course of the next 30 min, maintaining this concentration of isoflurane, the rat failed to right on most trials, but was able to right on 2 trials, each separated by failed trails.

When stimulus-induced cortical signals were compared for trials before and after the loss of righting had occurred it was difficult to see any difference in the raw recordings (**Figure 6**), but there were clear differences seen in the associated attractors. The four recordings shown were for cortical activations before and after LORR, all at the same isoflurane concentration (0.72 vol %) and each separated by 5 min, in a rat that was right on the cusp of loss of righting. In comparison, only small differences were seen in Fourier analysis of these signals. **Figure 7** shows FFT magnitude graphs for the two middle traces of **Figure 6**, just before and just after LORR. As previously reported, there was an increase in delta, little change in gamma (40 Hz), and a slight decrease in high gamma power in the frontal EEG of unconscious rats (Hudetz et al., 2011), but these changes were small compared to changes in attractor shapes (**Figure 6**).

DISCUSSION

Isoflurane produced concentration dependent changes in the frontal cortical EEG signal that were similar to patterns seen in other animals, including humans (Li et al., 2013); most notably, a slowing of frequency with an increase in delta power was seen at loss of consciousness. This is similar to patterns produced by other anesthetics in humans and rats (MacIver et al., 1996; Leung et al., 2014; Pilge et al., 2014). Hippocampal EEG signals were largely unaffected by this anesthetic (**Figure 3**). This contrasts with effects produced by halothane, another volatile anesthetic, that produced a marked hippocampal theta rhythm that persisted even after rats had lost their righting reflex (Bland et al., 2003). The halothane-induced theta rhythm was slower than seen during movement (Perouansky et al., 2010) and likely consists mainly of type 2 (sensory) as opposed to type 1 (movement related) theta (Bland and Oddie, 2001). Halothane also differs from isoflurane in it's lack of burst suppression activity produced in frontal cortex, even at deep surgical levels (Orth et al., 2006; Murrell et al., 2008). Thus, different anesthetics clearly alter higher brain function in an agent, and brain region, specific manner in neocortex and hippocampus, lending support to a multisite agent specific mechanism of anesthetic action (Clark et al., 1973; MacIver and Roth, 1987; Bieda et al., 2009; MacIver, 2014).

This study compared traditional FFT *vs.* chaos analysis of isoflurane-induced changes in EEG signals, and our results suggest that chaos analysis may provide a more sensitive approach. Differences between stimulus-activated signals are considerably easier to discern (**Figures 6**, **7**). Chaos analysis may provide a better approach for the development of monitors for anesthetic depth, as previously suggested (Watt and Hameroff, 1988; Walling and Hicks, 2006). The shape of an EEG driven attractor showed continual flattening in the presence of isoflurane, especially for small changes at the point of loss of conscious behavior. Perhaps a statistical measure of the attractor, like the D_2 correlation dimension provided by Walling and Hicks (2006), or a simple percent of minimal width measure could provide a wide dynamic range for different levels of consciousness. A wide range is needed to discern stimulus dependent cortical activations produced by testing LORR, LOPP, and LOTC responses, as EEG "awakening" responses are so similar to awake signals (**Figure 6**). These awakening responses are also seen in patients at surgical planes of anesthesia, in response to particularly painful

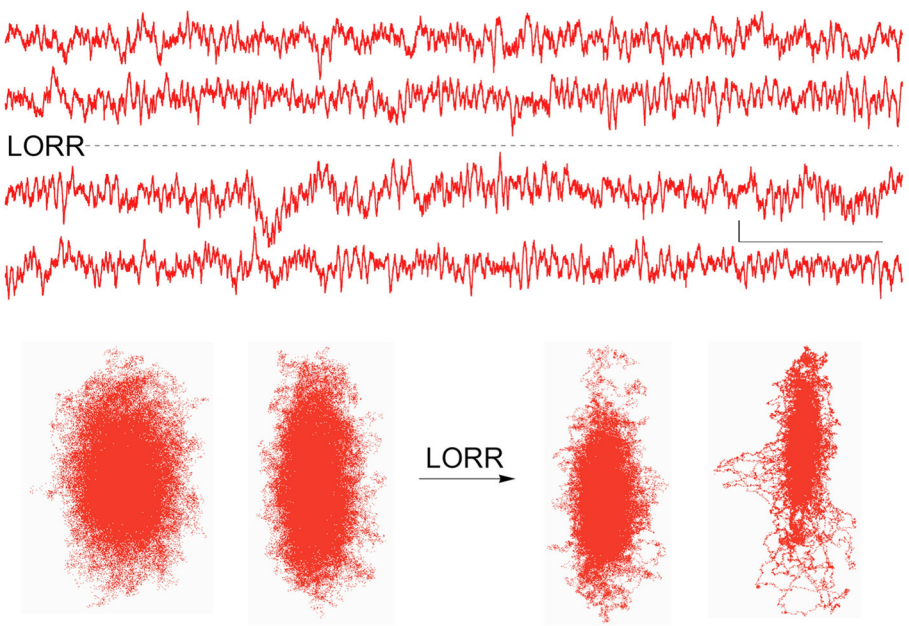

FIGURE 6 | Activated EEG records from the same rat just before and after isoflurane-induced LORR, together with each records attractor. Attractor flattening is a sensitive measure of these nearly identical frontal cortical signals. Calibration = 50 μV and 1.0 s.

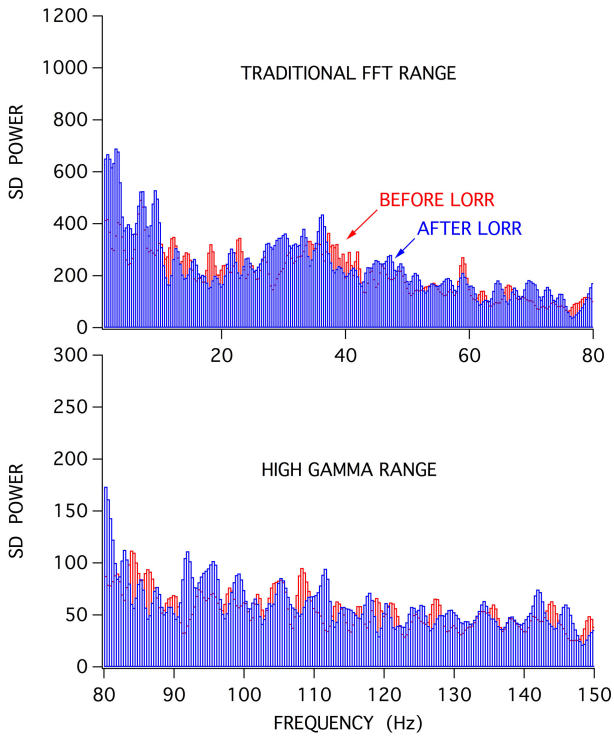

FIGURE 7 | FFT analysis of activated frontal cortical signals showed relatively little difference in the spectral content of the frontal EEG before (red) and after (blue) LORR.

stimulation, and likely contribute to "awareness" during anesthesia (Hight et al., 2014). A simple display of the frontal attractor in patients could be provided in near real-time on tablet computers and would, at least, provide a sensitive and entertaining view of anesthetic-induced changes in brain state.

Recent studies addressing the similarities between natural sleep and anesthetic-induced slow wave activity have disagreed over shared circuit-level mechanisms (Nelson et al., 2003; Murphy et al., 2011; Zecharia et al., 2012). In some cases a good deal of overlap between anesthesia and sleep was apparent, but in other cases marked differences are seen. Our results with isoflurane indicate that this anesthetic utilizes different mechanisms, or at least additional brain circuit level effects were produced, since the attractor shapes are markedly different between natural sleep and isoflurane-induced slow wave activity. It is likely that any overlap between anesthesia and sleep mechanisms is highly agent and brain region specific.

It remains unclear whether loss of consciousness occurs with an abrupt (on/off) or gradual change in brain state. Our results indicate a gradual effect on attractor shape accompanies the transition through LORR when comparing stimulated "activated" EEG signals, consistent with a gradual return of cortical discharge activities seen on RORR (Vizuete et al., 2014). Of course, spontaneous un-stimulated EEG signals were clearly different at each of the endpoint measures we used (**Figure 2**), but even the transitions from slow wave sedation through surgical burst suppression occur gradually in the un-stimulated rat as slow wave activity gradually increases in amplitude and gradually breaks up into burst patterns. In humans it appears that unique brain states can exist for different patients on emergence from anesthesia, perhaps related to the degree of painful stimulation on recovery (Hight et al., 2014). This also likely underlies the hysteresis or "neural inertia" evident for anesthetic-induced loss and regaining consciousness, seen in **Figure 2** – slow wave activity is seen when rats are not stimulated at LORR, but rats are continuously stimulated by being placed on their sides before RORR, hence the "activated" spontaneous EEG before RORR (Buhrer et al., 1992; Friedman et al., 2010). Perhaps the chaotic attractor measure will provide a wide enough dynamic range to show whether gradual, as opposed to small discrete state changes contribute to loss and regaining of consciousness in humans.

ACKNOWLEDGMENTS

Supported by NIH GM55719 to M. B. MacIver and NSERC A9935 to Brian H. Bland.

SUPPLEMENTARY MATERIAL

The Supplementary Material for this article can be found online at: http://www.frontiersin.org/journal/10.3389/fnsys.2014.00203/abstract

REFERENCES

Bieda, M. C., Su, H., and MacIver, M. B. (2009). Anesthetics discriminate between tonic and phasic gamma-aminobutyric acid receptors on hippocampal CA1 neurons. *Anesth. Analg.* 108, 484–490. doi: 10.1213/ane.0b013e3181904571

Bland, B. H., Bland, C. E., Colom, L. V., Roth, S. H., DeClerk, S., Dypvik, A., et al. (2003). Effect of halothane on type 2 immobility-related hippocampal theta field activity and theta-on/theta-off cell discharges. *Hippocampus* 13, 38–47. doi: 10.1002/hipo.10044

Bland, B. H., Declerck, S., Jackson, J., Glasgow, S., and Oddie, S. (2007). Septohippocampal properties of N-methyl-D-aspartate-induced theta-band oscillation and synchrony. *Synapse* 61, 185–197. doi: 10.1002/syn.20357

Bland, B. H., and Oddie, S. D. (2001). Theta band oscillation and synchrony in the hippocampal formation and associated structures: the case for its role in sensorimotor integration. *Behav. Brain Res.* 127, 119–136. doi: 10.1016/S0166-4328(01)00358-8

Buhrer, M., Maitre, P. O., Hung, O. R., Ebling, W. F., Shafer, S. L., and Stanski, D. R. (1992). Thiopental pharmacodynamics. I. Defining the pseudo-steady-state serum concentration-EEG effect relationship.*Anesthesiology* 77, 226–236. doi: 10.1097/00000542-199208000-00002

Clark, D. L., Hosick, E. C., Adam, N., Castro, A. D., Rosner, B. S., and Neigh, J. L. (1973). Neural effects of isoflurane (forane) in man. *Anesthesiology* 39, 261–270. doi: 10.1097/00000542-197309000-00002

Frank, G. B., and Jhamandas, K. (1970). Effects of drugs acting alone and in combination on the motor activity of intact mice. *Br. J. Pharmacol.* 39, 696–706. doi: 10.1111/j.1476-5381.1970.tb09895.x

Friedman, E. B., Sun, Y., Moore, J. T., Hung, H. T., Meng, Q. C., Perera, P., et al. (2010). A conserved behavioral state barrier impedes transitions between anesthetic-induced unconsciousness and wakefulness: evidence for neural inertia. *PLoS ONE* 5:e11903. doi: 10.1371/journal.pone.0011903

Hight, D. F., Dadok, V. M., Szeri, A. J., Garcia, P. S., Voss, L., and Sleigh, J. W. (2014). Emergence from general anesthesia and the sleep-manifold. *Front. Syst. Neurosci.* 8:146. doi: 10.3389/fnsys.2014.00146

Hrelec, C., Puente, E., Bergese, S., and Dzwonczyk, R. (2010). SNAP II versus BIS VISTA monitor comparison during general anesthesia. *J. Clin. Monit. Comput.* 24, 283–288. doi: 10.1007/s10877-010-9246-0

Hudetz, A. G., Vizuete, J. A., and Pillay, S. (2011). Differential effects of isoflurane on high-frequency and low-frequency gamma oscillations in the cerebral cortex and hippocampus in freely moving rats. *Anesthesiology* 114, 588–595. doi: 10.1097/ALN.0b013e31820ad3f9

Leung, L. S., Luo, T., Ma, J., and Herrick, I. (2014). Brain areas that influence general anesthesia. *Prog. Neurobiol.* doi: 10.1016/j.pneurobio.2014.08.001. [Epub ahead of print].

Li, D., Li, X., Hagihira, S., and Sleigh, J. W. (2013). Cross-frequency coupling during isoflurane anaesthesia as revealed by electroencephalographic harmonic wavelet bicoherence. *Br. J. Anaesth.* 110, 409–419. doi: 10.1093/bja/aes397

MacIver, M. B. (2014). Anesthetic agent-specific effects on synaptic inhibition. *Anesth. Analg.* 119, 558–569. doi: 10.1213/ANE.0000000000000321

MacIver, M. B., Mandema, J. W., Stanski, D. R., and Bland, B. H. (1996). Thiopental uncouples hippocampal and cortical synchronized electroencephalographic activity. *Anesthesiology* 84, 1411–1424. doi: 10.1097/00000542-199606000-00018

MacIver, M. B., and Roth, S. H. (1987). Anesthetics produce differential actions on the discharge activity of a single neuron. *Eur. J. Pharmacol.* 139, 43–52. doi: 10.1016/0014-2999(87)90495-X

Murphy, M., Bruno, M. A., Riedner, B. A., Boveroux, P., Noirhomme, Q., Landsness, E. C., et al. (2011). Propofol anesthesia and sleep: a high-density EEG study. *Sleep* 34, 283A–291A.

Murrell, J. C., Waters, D., and Johnson, C. B. (2008). Comparative effects of halothane, isoflurane, sevoflurane and desflurane on the electroencephalogram of the rat. *Lab. Anim.* 42, 161–170. doi: 10.1258/la.2007.06019e

Nelson, L. E., Lu, J., Guo, T., Saper, C. B., Franks, N. P., and Maze, M. (2003). The alpha2-adrenoceptor agonist dexmedetomidine converges on an endogenous sleep-promoting pathway to exert its sedative effects. *Anesthesiology* 98, 428–436. doi: 10.1097/00000542-200302000-00024

Niedhart, D. J., Kaiser, H. A., Jacobsohn, E., Hantler, C. B., Evers, A. S., and Avidan, M. S. (2006). Intrapatient reproducibility of the BISxp monitor. *Anesthesiology* 104, 242–248. doi: 10.1097/00000542-200602000-00007

Orth, M., Bravo, E., Barter, L., Carstens, E., and Antognini, J. F. (2006). The differential effects of halothane and isoflurane on electroencephalographic responses to electrical microstimulation of the reticular formation. *Anesth. Analg.* 102, 1709–1714. doi: 10.1213/01.ane.0000205752.00303.94

Perouansky, M., Rau, V., Ford, T., Oh, S. I., Perkins, M., Eger, E. I. 2nd., et al. (2010). Slowing of the hippocampal theta rhythm correlates with anesthetic-induced amnesia. *Anesthesiology* 113, 1299–1309. doi: 10.1097/ALN.0b013e3181f90ccc

Pilge, S., Jordan, D., Kreuzer, M., Kochs, E. F., and Schneider, G. (2014). Burst suppression-MAC and burst suppression-CP(5)(0) as measures of cerebral effects of anaesthetics. *Br. J. Anaesth.* 112, 1067–1074. doi: 10.1093/bja/aeu016

Rampil, I. J. (2001). Monitoring depth of anesthesia. *Curr. Opin. Anaesthesiol.* 14, 649–653. doi: 10.1097/00001503-200112000-00009

Vizuete, J. A., Pillay, S., Ropella, K. M., and Hudetz, A. G. (2014). Graded defragmentation of cortical neuronal firing during recovery of consciousness in rats. *Neuroscience* 275, 340–351. doi: 10.1016/j.neuroscience.2014.06.018

Walling, P. T., and Hicks, K. N. (2006). Nonlinear changes in brain dynamics during emergence from sevoflurane anesthesia: preliminary exploration using new software. *Anesthesiology* 105, 927–935. doi: 10.1097/00000542-200611000-00013

Watt, R. C., and Hameroff, S. R. (1988). Phase space electroencephalography (EEG): a new mode of intraoperative EEG analysis. *Int. J. Clin. Monit. Comput.* 5, 3–13. doi: 10.1007/BF01739226

White, P. F., Johnston, R. R., and Eger, E. I. 2nd. (1974). Determination of anesthetic requirement in rats. *Anesthesiology* 40, 52–57. doi: 10.1097/00000542-197401000-00012

Zecharia, A. Y., Yu, X., Gotz, T., Ye, Z., Carr, D. R., Wulff, P., et al. (2012). GABAergic inhibition of histaminergic neurons regulates active waking but not the sleep-wake switch or propofol-induced loss of consciousness. *J. Neurosci.* 32, 13062–13075. doi: 10.1523/JNEUROSCI.2931-12.2012

Conflict of Interest Statement: The authors declare that the research was conducted in the absence of any commercial or financial relationships that could be construed as a potential conflict of interest.

Received: 05 September 2014; accepted: 29 September 2014; published online: 16 October 2014.

Citation: MacIver MB and Bland BH (2014) Chaos analysis of EEG during isoflurane-induced loss of righting in rats. Front. Syst. Neurosci. ***8****:203. doi: 10.3389/fnsys.2014.00203*

This article was submitted to the journal Frontiers in Systems Neuroscience.

frontiers in
SYSTEMS NEUROSCIENCE

ORIGINAL RESEARCH ARTICLE
published: 13 August 2014
doi: 10.3389/fnsys.2014.00146

Emergence from general anesthesia and the sleep-manifold

Darren F. Hight[1], Vera M. Dadok[2], Andrew J. Szeri[2], Paul S. García[3], Logan Voss[1] and Jamie W. Sleigh[1]*

[1] *Department of Anaesthesiology, Waikato Clinical School, University of Auckland, Hamilton, New Zealand*
[2] *Department of Mechanical Engineering and Center for Neural Engineering and Prostheses, University of California, Berkeley, CA, USA*
[3] *Department of Anesthesiology, Atlanta VA Medical Center/Emory University, Atlanta, GA, USA*

Edited by:
Axel Hutt, INRIA CR Nancy, France

Reviewed by:
Axel Hutt, INRIA CR Nancy, France
Max Kelz, University of Pennsylvania, USA

****Correspondence:***
Jamie W. Sleigh, Peter Rothwell Academic Centre, Waikato Hospital, Pembroke Street, Private Bag 3200, Hamilton 3240, New Zealand
e-mail: jamie.sleigh@waikatodhb.health.nz

The electroencephalogram (EEG) during the re-establishment of consciousness after general anesthesia and surgery varies starkly between patients. Can the EEG during this emergence period provide a means of estimating the underlying biological processes underpinning the return of consciousness? Can we use a model to infer these biological processes from the EEG patterns? A frontal EEG was recorded from 84 patients. Ten patients were chosen for state-space analysis. Five showed archetypal emergences; which consisted of a progressive decrease in alpha power and increase peak alpha frequency before return of responsiveness. The five non-archetypal emergences showed almost no spectral EEG changes (even as the volatile general anesthetic decreased) and then an abrupt return of responsiveness. We used Bayesian methods to estimate the likelihood of an EEG pattern corresponding to the position of the patient on a 2-dimensional manifold in a state space of excitatory connection strength vs. change in intrinsic resting neuronal membrane conductivity. We could thus visualize the trajectory of each patient in the state-space during their emergence period. The patients who followed an archetypal emergence displayed a very consistent pattern; consisting of progressive increase in conductivity, and a temporary period of increased connection strength before return of responsiveness. The non-archetypal emergence trajectories remained fixed in a region of phase space characterized by a relatively high conductivity and low connection strength throughout emergence. This unexpected progressive increase in conductivity during archetypal emergence may be due to an abating of the surgical stimulus during this period. Periods of high connection strength could represent forays into dissociated consciousness, but the model suggests all patients reposition near the fold in the state space to take advantage of bi-stable cortical dynamics before transitioning to consciousness.

Keywords: general anesthesia, emergence, sleep-manifold, connection strength, resting membrane conductivity

INTRODUCTION

Over the last decade there has seen an increasing interest in the wake-up period following withdrawal of a general anesthetic, and in the neurobiological processes leading to the return of consciousness. We term this the emergence period; and it is defined as the time from the cessation of anesthetic delivery until the patient can make a non-reflex response to verbal command. Characterization of the changes that occur during emergence has attracted attention both from researchers searching for the neural correlates of consciousness (Mashour and Alkire, 2013) and from more clinically oriented studies, whose focus is on the quality of recovery of patients following surgery (e.g., Law et al., 2011). Much of this interest has come from the realization that the induction process (the entrance to the anesthetized state) and emergence process (the exit from the anesthetized state) are not simply the mirror image of each other, but rather that emergence is an active process characterized by a distinct neurobiology (Kelz et al., 2008; Lee et al., 2011; Kushikata and Hirota, 2014). For example, the time required for the return to consciousness shows a much greater variability than the time required for the loss of consciousness. These distinct processes occur at different drug concentrations—a classic hysteresis effect (Friedman et al., 2010). This effect, traditionally considered a pharmacokinetic "artifact" arising from a delayed and variable rate of removal of the an anesthetic agent from brain sites, may in fact be due to a biological tendency of the central nervous system to resist transitions between conscious and unconscious states. The emergence period is also of critical importance from a clinical perspective. For example, during emergence patients may infrequently face life-threatening complications (Kushikata and Hirota, 2014), but more often can wake up experiencing high levels of pain and nausea (Law et al., 2011), despite pre-emptive analgesia. Patients can also experience periods of confusion and disorientation, or even delirium following wakeup, indicating a possible incomplete

return of full consciousness. The incidence of emergence delirium in children has been reported as high as 50% in preschool children (Banchs and Lerman, 2014), but the mechanisms of this phenomenon are not well understood. Clinicians often note the huge variability in wakeup length and quality, but find the prediction of quality of recovery from the intraoperative period a major challenge.

EEG AND BEHAVIORAL CHANGES DURING EMERGENCE

The most practical non-invasive method for observing state changes in brain function during anesthesia is the electroencephalogram (EEG). Changes in the EEG have been observed in anesthetized patients since 1937 (Gibbs et al., 1937). At the deepest levels of anesthesia EEG activity is suppressed (isoelectric) for short periods before returning to bursts of activity. This pattern, labeled burst suppression, is not seen in natural sleep. At levels of anesthesia required for surgery the amplitude of the EEG is often large in the delta (1–4 Hz) and alpha (8–14 Hz) ranges, showing a similar but distinct waveform to that of slow-wave natural sleep (see Brown et al., 2010 for a review). For a more detailed treatment of the EEG during anesthesia see (Bennett et al., 2009). Following the end of surgery, when the anesthetic is turned off, it is commonly believed that the delta and/or alpha dominated waveform disappears, being replaced with a beta (15–30 Hz) waveform just prior to waking. For some patients showing alpha dominated waveforms, the alpha activity increases in frequency by about 2–3 Hz during emergence, as observed by Purdon et al. (2013). The topography of the EEG also changes during emergence, with the frontally dominant (coherent) alpha activity during anesthesia shifting to occipital areas before the patient awakes (Gugino et al., 2001). Clinically, a progression can often be seen in the patient's responses that loosely correlate with these changes in EEG pattern. These observations include a return in spontaneous respiration, followed by brainstem responses such as salivation and tearing and gagging on the endotracheal tube, if still in place. This is then followed by non-purposive or defensive movements (with eyes remaining closed), before the patient can finally respond to a command (Brown et al., 2010; Langsjo et al., 2012).

Despite a burgeoning number of anesthesia-related EEG studies in recent years, we know of only two recent research groups who have looked at the EEG in detail during the emergence period, as shown in the articles from Purdon et al. (2013) and Lee et al. (2011). Research from the group based in Massachusetts General Hospital (Purdon et al., 2013) has focused on the characteristics of the EEG during propofol anesthesia while measuring responsiveness with an auditory stimulus consisting of a tone or the patient's name being delivered to the subject every 4 s. These researchers used a 64 electrode multichannel EEG system during a slow propofol induction and subsequent emergence. When they analyzed the EEG from a temporal-spectral perspective, one of the key characteristics they noted was an increase in median frequency of the alpha band of the EEG during the return to consciousness. The authors named this increase in frequency the "traveling peak" to emphasize the continuous nature of the change in the frequency domain, an observation which is obscured if analyzing the power of the EEG in traditional separate frequency bands. From a phase-amplitude perspective, they also observed coupling between the phase of slow-wave oscillations (0.1–1 Hz) and the amplitude of the alpha (8–14 Hz) band; noting that in deep anesthesia the alpha amplitudes were highest when the slow oscillation was also highest, calling this "peak-max." During the transition to consciousness this phase relationship reversed so that the largest amplitude alpha activity occurred at the lower values of the slow oscillation, or "trough-max." Purdon and colleagues (Purdon et al., 2013) also looked at spatial coherence and reported that, at the return to consciousness, coherent spatial activity shifts from frontal to occipital regions. These researchers have been looking for a few spectral features that can reliably track anesthetic depth and the return of consciousness, and they concluded that the emergence from a propofol anesthetic was marked by a gradual transition to consciousness, the level of which is dependent on stimulus saliency—emotional or neutral auditory input.

In contrast, Lee et al. (2011) examined the network properties of the anesthetic state during emergence, using cross-correlations of the EEG in multiple channels to estimate cortical connectivity, and a novel method to account for genuine versus spurious levels of connectivity. Two different patterns of changes in connectivity strength and topography on awakening were noted, the first where the increase in connection strength was abrupt on wakeup, and the second where connection strength showed a gradual change on awakening. Subjects were then categorized into these categories for further analysis. They concluded that there were likely multiple pathways of return to consciousness, which one single theory of anesthesia would not be able to explain.

In both of the aforementioned studies, *none* of the subjects were undergoing surgery and all were healthy volunteers. However general anesthesia is administered in order to allow surgery to take place. Do EEG's recorded in the clinical context show the same patterns during emergence as those recorded from healthy volunteers, without any surgical noxious stimuli? Is there one common pathway to responsiveness or are there multiple pathways?

LINKING MOLECULAR LEVEL ACTIONS TO EEG AND BEHAVIOR IN ANESTHESIA

One of the drawbacks of the EEG is that, at best, it provides a somewhat opaque window into the underlying mechanisms governing anesthesia state changes in the brain. Thus, despite a well-advanced understanding of the molecular level mechanisms of most anesthetics (see Brown et al., 2011 or Alkire et al., 2008 for reviews), there is a gap in understanding as to how these molecular mechanisms link with the EEG patterns and associated changes in consciousness. One accepted method for attempting to bridge this gap is the use of EEG modeling of anesthesia. Here the goal is to replicate features of the clinically observed EEG with the output signal from a model which has a biologically realistic set of parameter constraints. What follows is a very short overview of types of anesthesia modeling, linking proposed molecular and neural mechanisms of anesthetic action to the structure of the EEG in anesthesia.

The previously mentioned research group (Purdon et al., 2013) have recently published a thalamocortical model as an

explanation for the EEG alpha rhythm that is seen in propofol anesthesia (Ching et al., 2010). This model exemplifies the neural-biophysical approach (Ching and Brown, 2014), and builds on an earlier cortical networks model developed by McCarthy et al. (2008). In this model a network of cortical pyramidal neurons with associated interneurons are coupled to the thalamus. The action of propofol is modeled as an increase in the conductance and decay time of the $GABA_A$ inhibitory current, which, based on earlier work proposing mechanisms for thalamic alpha activity (Contreras et al., 1997), leads to an entrainment of oscillations between the thalamus and cortex. These alpha oscillations then become visible in the frontal cortex, and in the model as the summed activity of the pyramidal neurons—a surrogate for the EEG. A spectrogram is then used to compare features of the model output to the known effect of propofol on the EEG.

Another form of modeling, the mean-field method, describes the mesoscale population activity resulting from short and long range interactions between sets of inhibitory and excitatory neurons. The advantages of this approach are that it is possible to use physiologically plausible parameter values, and that the output of the model can be related to the local field potentials and hence can be directly compared with the experimentally-obtained EEG or ECoG electrode output. Because of the averaging involved in the mean-field models, they are much less computer resource intensive than neuron-by-neuron simulations, and thus are more tractable for phenomena that involve cortical activity at larger length scales. They also have the advantage that they are often simple enough to allow the application of classical mathematical analytic methods, rather than being mere simulations. However such models do not include much specific neuroanatomy, and hence are mainly used to model widespread global central nervous system disturbances such as sleep, and seizures. The application of these methods to anesthesia modeling was first described by Steyn-Ross and Liley (Steyn-Ross et al., 1999). At its heart, this model describes the time evolution of the mean soma potential in populations of interacting inhibitory and excitatory cortical neurons. The authors modeled the propofol effect as an increase in the area under the curve of the inhibitory post synaptic potential; and found that increasing anesthetic concentration could lead to multiple stable dynamical states, and that the sudden phase transition between these states mimicked that observed in the EEG and level of consciousness during induction of anesthesia. Subsequently there has been a steady stream of papers that have looked at a variety of questions relating to various mechanisms of sleep, anesthesia, and seizures (e.g., Bojak and Liley, 2005; Sleigh et al., 2009; Hutt and Longtin, 2010; Ching et al., 2012; Liley and Walsh, 2013).We refer the reader to an excellent recent review of general anesthesia models by Foster et al. (2008). However the comparison between the "pseudo-EEG" output from the model, and the real EEG obtained from experiments, has always been semi-quantitative at best. Therefore, using the Steyn-Ross model as a basis, following Lopour et al. (2011), Dadok et al. (2014) developed Bayesian methods to solve the inverse problem of mapping experimentally derived EEG features data back onto the state-space of the model. In this way the association of specific values of model parameters corresponding to each epoch of real EEG might give insight into the underlying neurobiology. It is in some ways similar to the dynamic causal modeling approach (Marreiros et al., 2010), but is subject to more realistic neurobiological constraints. Working from sleep EEG data, they explored the statistical usefulness of combinations of various EEG "features" through which an association could be made to a specific set of parameter values in the model, and hence probabilistically estimate how the neurobiological parameters might change with time, mimicking what is happening within a patient's brain. Typically this is displayed as a progression, tracking a path on a 2-dimensional parameter manifold. In this way they successfully showed that progressive cycles of natural sleep could be displayed as a continuous trajectory on a sleep manifold (Dadok et al., 2014). This probabilistic method has never been applied to anesthesia or to the emergence period. In this study we aim to apply the method of Dadok et al. (2014) to EEG recorded during anesthesia, and over the emergence period. Specifically we wanted to answer the questions: do patients show homogenous emergence EEG patterns? Do these EEG patterns suggest different underlying biological processes? Can we use the model to infer these biological processes from the EEG patterns?

METHODS

EMERGENCE PERIOD RECORDINGS

Eight-four patients (40 females) aged between 21 and 88 (average age, 61 years) with an American Society of Anesthesiologists (ASA) physical status between I and IV having surgery at the Waikato District Health Board Hospital, Hamilton, New Zealand, were recruited for this study. Two cases were rejected due to faulty or absent EEG recordings. All participants gave informed consent and the study was approved by the New Zealand Health and Disability Ethics Committee (Ref. 12/CEN/56). EEG waveforms were recorded from the forehead (location Fpz on the 10/20 montage) via single-use electrode strips using either the Bispectral Index® (BIS®; Aspect Medical Systems, Newton, MA, USA) or Entropy (GE Healthcare, Helsinki, Finland) depth of anesthesia monitoring systems. Other routine monitoring data [such as heart rate, blood pressure, and end-tidal volatile gas anesthetic (VGA) concentrations] were recorded from the S/5 Anesthesia Monitor (GE Healthcare, Helsinki, Finland) using the S/5 Collect program provided by the same company. Delivery and dose of opioid analgesics were also recorded during and following the operation. No restrictions were placed on anesthetic conduct during the surgery. Following the operation, the time of cessation of anesthetic delivery was noted, this time point being the start of the emergence period. A standard low-stimulus emergence protocol was followed. After oropharyngeal suction the patient was not stimulated until MAC <0.1, then they were given a series of verbal commands at 30 s intervals. The end of the emergence period was counted as the moment the patient spontaneously opened their eyes for more than 5 s, clearly engaging with the environment, or could respond to the command "Open your eyes!" (ROR). In the Post-Anesthetic Care Unit (PACU) patients were asked to give a verbal pain-score ranging from 0 (no pain) to 10 (worst pain imaginable) on awakening, and at 15 and 30 min after awakening.

Ramsay Sedation scores, observed distress and instances of nausea and vomiting were also recorded.

EEG DATA COLLECTION AND PROCESSING

The raw EEG signal and monitoring data were analyzed with custom Matlab software (The MathWorks, *Inc.*, Natick, MA, USA). EEG waveforms were down-sampled to 100 Hz and were low-pass filtered using a Butterworth, non-aliasing low-pass (48.5 Hz, 3rd order) filter, to remove the 50 Hz artifact. Monitoring data were interpolated from every 5 or 10 s to one sample per second. From end-tidal VGA concentrations, brain effect-site concentrations (C_eMAC) were derived from age-adjusted MAC values (Nickalls and Mapelson, 2003) assuming a T1/2Keo of 150 s. After the patient was moved to PACU, the C_eMAC were extrapolated out until end of emergence using a decaying exponential. Opioid effect-site concentrations were converted to Fentanyl-equivalent estimates (C_eFentanyl) using a Fentanyl to Morphine efficacy ratio of 20:1. Opioid effect site concentrations were estimated using pharmacokinetic modeling based on population derived parameters. Thus the actual drug concentrations for each individual patient might be expected to lie within approximately a two-fold range.

The power spectrum (in dB) of the EEG was calculated using the multi-taper Chronux method (www.chronux.org, Mitra and Bokil, 2008) with a time-bandwidth product $TW = 4$, and $K = 7$ tapers. We used a moving window of 4 s with an overlap of 3 s in the creation of the spectrograms. Spectrograms were taken of the observation period, which included a 15 min window prior to the emergence period; the emergence period itself began at the time of shutting off the VGA and increasing the fresh gas flows in order to flush out anesthetic agent (plotted as a vertical green line) and ended with ROR (plotted as a vertical red line). For each window the local regression fitting and likelihood method of smoothing from Loader (1997), (Locfit, included in the Chronux package for Matlab) was fitted to the power spectrum (bandwidth parameter, $h = 1.5$ Hz). We particularly noted the alpha (8–16 Hz) power and frequency, the delta power (1–4 Hz), and the presence of obvious oscillation in other frequencies [beta (16–32 Hz) and theta (4–7 Hz)]. We quantitatively obtained the maximum alpha frequency (allowable range for alpha peak was between 7 and 17 Hz), and the magnitude of both the oscillatory alpha-power above the underlying broadband noise (Leslie et al., 2009, see our **Figure 1**) and the delta power. It must be noted that patients who wake after surgery often are somewhat disoriented, and thus the large amounts of electromyographic (EMG) activity make it difficult to quantitatively interpret the EEG signal after return of responsiveness to verbal command (ROR).

SLEEP-MANIFOLD MODELLING

The primary aim of this study was to examine the different biological mechanisms underlying the observed EEG changes. Because the wide variability observed between different patients during emergence will obscure the EEG changes that may be seen within each patient, we explicitly chose not to average all the results, but instead to investigate the emergence trajectories of 10 representative patients in detail. From our data-set, we chose five EEG recordings that were typical examples of gradual transitions in waveform spectral power over emergence, similar to those seen in Purdon et al. (2013). Based on previous literature, we have termed this the "archetypal" emergence trajectory. As counter-examples, we also chose another five recordings which showed no notable transition in EEG spectral power prior to abruptly awakening (i.e., our non-archetypal wakeups). We anticipate that the methodology developed in this paper might be used in subsequently studies with large enough numbers of patients to enable accurate statistical estimation methods. Thus 10 EEG recordings for the observation period were used as input into the sleep manifold model of Dadok et al. (2014). More detailed method descriptions are available in that paper, but in short, the model consists of a set of partial differential equations that describe the time evolution of the mean soma potentials of a two-dimensional homogeneous system of coupled inhibitory and excitatory neurons, representing a macrocolumn (about 100,000 neurons) of undifferentiated association cortex. This corresponds to the size of typical excitatory neuronal dendritic arborization. Each macrocolumn also receives excitatory input from surrounding cortex and nonspecific white noise input from subcortical structures. We only consider fast chemical synaptic inputs [mediated via gamma-amino-butyric acid (GABA) and α-amino-3-hydroxy-5-methyl-4-isoxazolepropionic acid (AMPA) channels]. The model parameters are chosen based on experimentally measured biological values; and include the magnitude and duration of excitatory and inhibitory synaptic potentials, the effects of reversal potentials, the form of the sigmoid relationship between probability of firing and soma potential, and the effect of leak currents on the resting membrane potential. We have chosen to

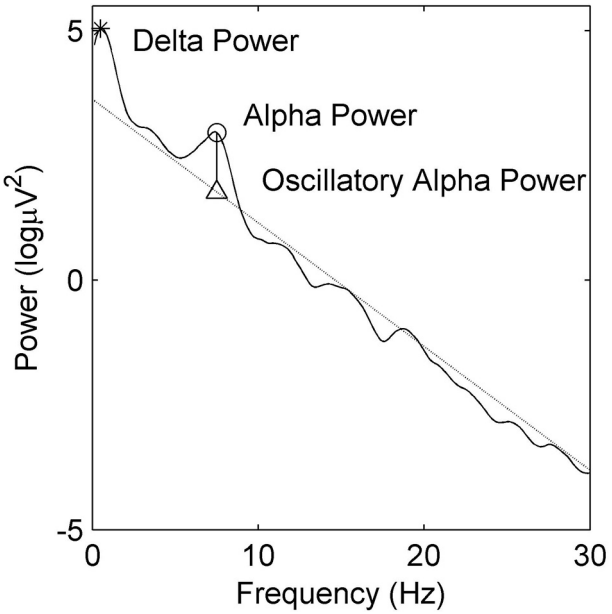

FIGURE 1 | Example power spectral density estimate showing absolute delta (∗) and alpha (○) power. Oscillatory alpha power is the difference between maximal alpha power (○) and the alpha power at the linear regression estimate (△).

describe the model output and the experimental results based on a 2-dimensional state space using the change in resting membrane impedance (Δh_e^{rest}) and the cortical excitatory synaptic strength (L) as the axes. These were chosen because:

(i) The Δh_e^{rest} is a measure of the neuronal membrane impedance. This is the inverse of conductivity, and is largely controlled by the intrinsic neuronal currents (particularly the potassium currents). These currents, in turn, are inhibited by subcortically driven aminergic and cholinergic arousal neuromodulators. Thus the conductivity may be seen as an indication of the balance between suppression and arousal—as mediated by brain stem modulation of the cortex, similar to that found in natural sleep-wake states.

(ii) The excitatory strength is an indicator of synaptic connectivity between cortical pyramidal neurons. This might be seen as a direct index of how the anesthesia directly disrupts a cortical functionality that can be directly linked to known EEG indices of regional connectivity.

Thus we attempted to somewhat separate these two known components of VGA action. As described in Dadok et al. (2014) we then solve the equations to produce a sheet manifold of steady states. The manifold is shown in **Figure 2**. It can be seen that, at low values of L and Δh_e^{rest} the resting steady state is relatively hyperpolarized (the blue area in the left lower region); as L and Δh_e^{rest} increases the steady states become more depolarized (red). However there is a region in which there are three steady states (two stable and one unstable)—the fold in the manifold. This area is within the bold black inverted "Y" region in subsequent figures. Around this area there is the possibility for the model brain to jump discontinuously between low firing and high firing modes. At each point on the manifold there are fluctuations in soma potential that produces a "pseudoEEG" for that point in state space.

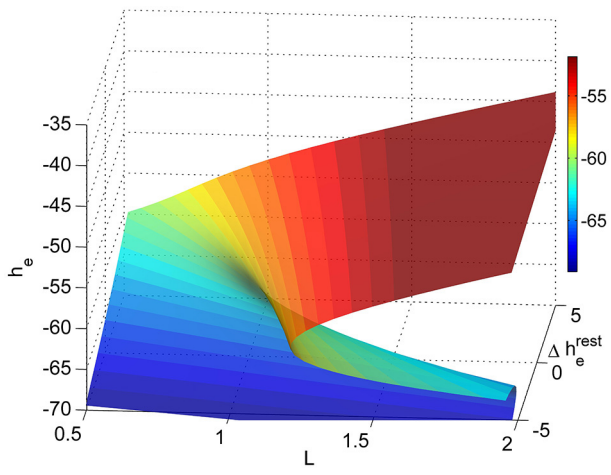

FIGURE 2 | Sleep-manifold showing the folding state-space surface (folded area is bi-stable) over a two dimensional parameter space (adapted from Dadok et al., 2014).

In brief the method of probabilistically mapping experimental data to the model manifold is as follows:

(i) "Features" are extracted from sequential 30 s segments of the raw EEG.

These features are derived indices that are felt to contain the important dynamic information contained in the raw EEG. The process of choosing features is complex and inherently heuristic. We used the same features as had been found most useful for natural sleep; namely the slope of the power spectral density, the spindle index, combination delta wave steepness (the mean delta gradient), and the equiprobable mutual information (Dadok et al., 2014).

(ii) The magnitude of each feature is mapped onto the state-space manifold of the model.

We used the same state-space manifold as used to describe natural sleep. The choice of these parameters is arbitrary to some degree, but they were chosen to reflect information about two relevant facets of neuronal function—namely synaptic efficiency and intrinsic neuronal currents.

(iii) For each real EEG segment, the probability (log-likelihood) of its associated 4-dimensional feature vector is mapped onto the state-space manifold, using a naïve Bayesian algorithm.

This procedure allows the unbiased determination of what regions of state-space are likely to be associated with any particular EEG pattern. Again this has been optimized for natural sleep, as we are able to compare the model results with established sleep scoring methods.

(iv) The temporal evolution on the state-space manifold through the course of emergence is shown by the trajectory of the probability centroid for each segment.

The trajectory thus acts as a link to indicate how changes in the scalp EEG might reflect the cortical neuronal function as the patient emerges from anesthesia. At present it is not known if this methodology is robust to EEG noise and to the choice of different model parameters.

RESULTS

VARIANCE IN ALPHA ACTIVITY PRIOR TO EMERGENCE

Patients emerge from general anesthesia differently. As an example we show the alpha frequency and power for all 82 patients for the 15 min prior to the start of emergence in **Figure 3**. The green diamonds are the centroid and the red ellipsoids the area of 80 percent of the closest points from the centroid. This figure demonstrates that there is a wide variation in alpha-power and frequency both between and within patients. Four of the ten patients of interest are displayed in blue (WH19 and WH42, gradual "archetypal" transitions in EEG waveform over the emergence

period) and black (WH9 and WH57, "non-archetypal" transitions in EEG during emergence period). All of these four patients emerged from a sevoflurane anesthesia, except for patient WH9 who had a desflurane anesthesia. We now describe, in more detail, the changes in EEG, drug concentrations, and putative modeled changes in biological parameters during emergence period for these four examples—two archetypal and two non-archetypal.

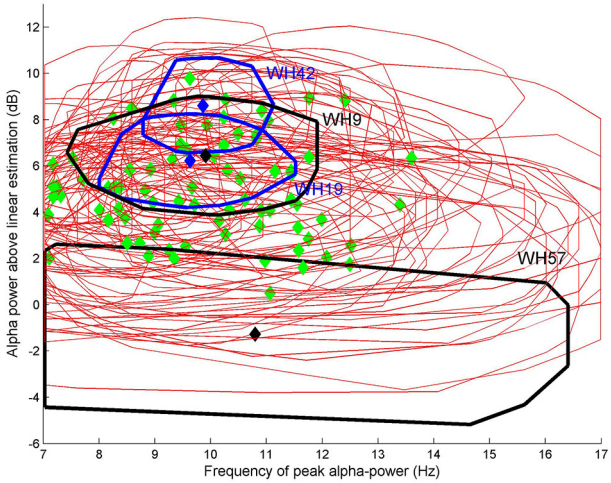

FIGURE 3 | Oscillatory alpha power against alpha frequency for each of 82 patients for the 15 min prior to the start of emergence. Green diamonds are the centroid and red ellipsoids the area of 80% of the closest points from the centroid. Four patients are displayed in either blue (WH19 and WH42, "archetypal" transitions) or black (WH9 and WH57, "non-archetypal" transition).

PATIENT WH19: ARCHETYPAL EMERGENCE (ALPHA FREQUENCY INCREASE, ALPHA LOSS, DELTA LOSS)

In **Figure 4** the spectrogram of the observation period (**Figure 4A**) for patient WH19 is shown from 15 min prior to start of emergence (vertical green line at 900 s) until after patient response (ROR, vertical red line). Prior to start of emergence it shows clear bands of alpha (centered at 10 Hz as seen in **Figure 4B**) and delta activity. Over this period (until 900 seconds) anesthetic concentration had decreased slightly from 1.2 to 0.8 C_eMAC, while opioid levels remained low (C_eFentanyl 0.2 ng/ml) over the whole observation period (**Figure 4C**). Following start of emergence the frequency of maximal alpha power is seen to increase by 2–3 Hz (**Figure 4B**) and then disappearing several min before ROR. A band of beta activity centered at 30 Hz can also be seen beginning at around 1100 s and continuing until ROR. From 1000 s onwards the alpha band in the spectrogram (**Figure 4A**) became smaller and there was an increase in spread of frequencies in **Figure 4B**, so that there was more variation in the detection of the alpha oscillatory peak. In **Figure 4D** it can be seen that the pre-emergence waveform (black circles) is tightly constrained, maintaining uniform levels of alpha and delta power. During emergence (blue circles) a clear progressive decrease in both alpha and delta power is seen, decreasing to a level of 0 dB for both bands. This absence of both alpha and delta power can also be seen clearly in the spectrogram (**Figure 4A**). After emergence, delta power increases (red circles in **Figure 4D**), as does power in all frequency bands (seen in the

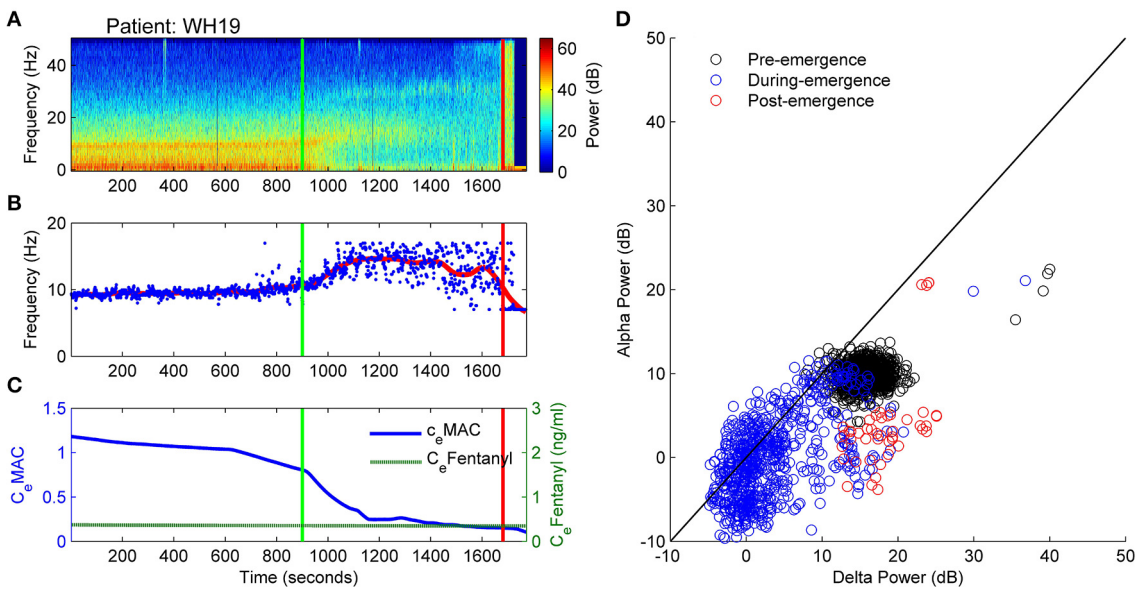

FIGURE 4 | Patient WH19: Archetypal emergence (alpha frequency increase, alpha loss, delta loss). (A) Spectrogram of the observation period. Start of emergence shown as a vertical green line at 900 s, time of patient response as a vertical red line. **(B)** Frequency of maximal oscillatory alpha power. **(C)** Concentration of anesthetic gas (C_eMAC), blue line, left vertical axis, and opioid levels as equivalent Fentanyl (C_eFentanyl, ng/ml), green line, right vertical axis. **(D)** Absolute alpha power (dB) against absolute delta power (dB) for prior to start of emergence (black circles), during emergence period (blue circles), and following recovery of response (ROR).

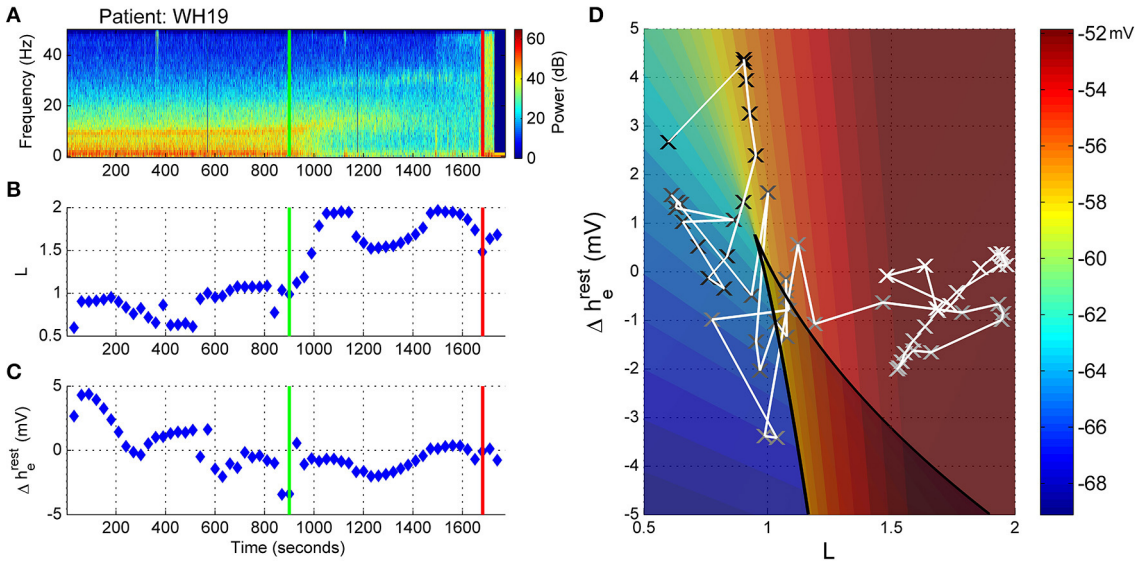

FIGURE 5 | Patient WH19, Sleep Manifold. (A) Spectrogram as in **Figure 4**. **(B)** Excitatory connection strength (L-parameter) over period of observation. **(C)** Change in resting membrane impedance (Δh_e^{rest}) over period of observation. **(D)** Resultant positioning on the sleep-manifold, with a black cross being the start of, and a white cross being the end of the observation period, with intermediate shades on the gray-scale representing the time progression between these time-points.

orange vertical band following the vertical red-line at around 1700 seconds in **Figure 4A**).

How do these EEG alterations translate into changes in the underlying model (and perhaps brain) parameters? **Figure 5D** depicts the progression in L and Δh_e^{rest} parameters on the 2D sleep-manifold over the same time-period—with a black cross being the start and a white cross being the end, and intermediate shades on the gray-scale representing the progression between these time-points. In **Figure 5** excitatory connection strength (parameter L, shown in **Figure 5B**) remained at low levels prior to emergence, and doubled after the start of emergence. The neuronal membrane impedance (Δh_e^{rest} in **Figure 5C**) progressively decreased in the period before emergence had even started. The resultant trajectory occupies two regions on the sleep-manifold. In the first phase, which corresponds to the time before the start of emergence, there was a large decrease in resting membrane impedance with little change in connection strength, resulting in a migration down the sleep-manifold. The reasons for this are not clear, but may be related to the small changes in C_eMAC or decreasing surgical stimulus. The second phase, corresponding to the emergence period, showed a sharp increase in connection strength with minimal change in resting impedance, resulting in a jump to a new parameter state-space position on the higher branch of the sleep-manifold before jumping back to the lower branch before ROR (**Figure 5D**)—apparently entering a preliminary period of high firing without successfully achieving responsiveness.

PATIENT WH42: ARCHETYPAL EMERGENCE. (ALPHA FREQUENCY INCREASE, ALPHA LOSS, PERSISTENT DELTA)

The spectrogram of Patient 42 (**Figure 6A**) is similar to that of patient WH19 above in that a clear alpha and delta band is seen prior to start of emergence, with the alpha activity increasing, before disappearing following the start of emergence (**Figure 6B**). However, patient WH42 starts with stronger alpha and delta power and does not lose the delta power at all prior to ROR. C_eFentanyl levels were also quite low [0.7–0.5 ng/ml over the observation period (**Figure 6C**)]. **Figure 6D** is also similar to that of patient WH19 in **Figure 4D** in that the absolute alpha and delta power are uniform prior to emergence (black circles), and show a decreasing alpha power over emergence (blue circles). In contrast to WH19 delta power remains high at around 15 dB even during the later phases of emergence. After emergence the broad band high power is caused by EMG activation and movement.

Similar to WH19, patient WH42 has a low connection strength value (L parameter) prior to start of emergence. As the alpha power decreases in the emergence period (**Figure 7A**), the connection strength rapidly increases to a value of nearly 2.0 from 1100 to 1300 s (**Figure 7B**). For the remaining part of the emergence period connection strength falls again to values between 0.7 and 1.1. Presumably the algorithm is being controlled by the persistent strong delta power in this phase. The change in resting impedance Δh_e^{rest} parameter in **Figure 7C** is high for most of the period prior to start of emergence, but quickly drops to −5 mV just prior to start of emergence and remains low for the emergence period. When seen on the sleep-manifold (**Figure 7D**), the patient appears to move between three distinct parameter attractors, corresponding to: (i) prior to start of emergence (ii) early and late sections of the emergence period, and (iii) a short period of high connection strength in the middle of the emergence period, similar to the previous patient. This patient mentioned they had been having very realistic dreams before awakening.

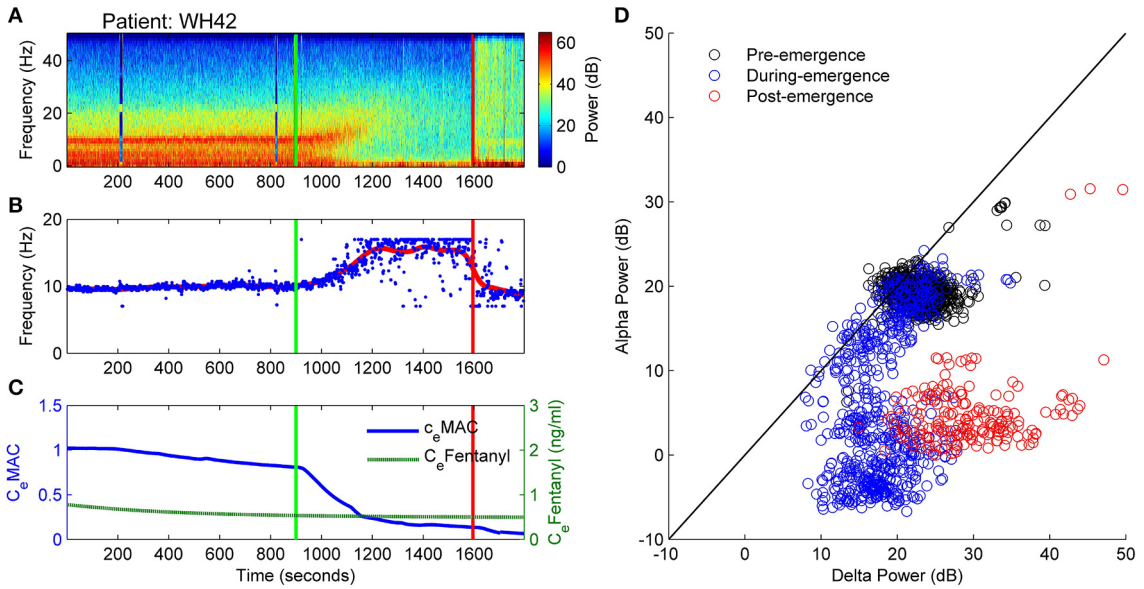

FIGURE 6 | Patient WH42. Archetypal emergence. (alpha frequency increase, alpha loss, persistent delta). **(A)** Spectrogram of the observation period. Start of emergence shown as a vertical green line at 900 s, time of patient response as a vertical red line. **(B)** Frequency of maximal oscillatory alpha power. **(C)** Concentration of anesthetic gas (C_eMAC), blue line, left vertical axis, and opioid levels as equivalent Fentanyl (C_eFentanyl, ng/ml), green line, right vertical axis. **(D)** Absolute alpha power (dB) against absolute delta power (dB) for prior to start of emergence (black circles), during emergence period (blue circles), and following recovery of response (ROR).

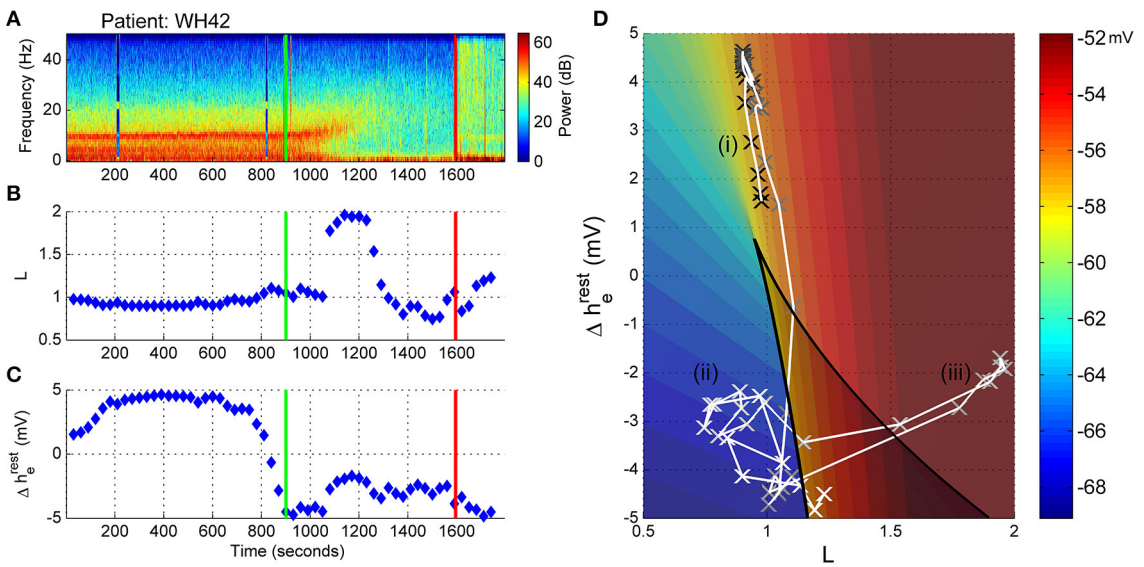

FIGURE 7 | Patient WH42, Sleep-Manifold. (A) Spectrogram as in **Figure 6**. **(B)** Excitatory connection strength (L-parameter) over period of observation. **(C)** Change in resting membrane impedance (Δh_e^{rest}) over period of observation. **(D)** Resultant positioning on the sleep-manifold, with a black cross being the start of, and a white cross being the end of the observation period, with intermediate shades on the gray-scale representing the time progression between these time-points.

PATIENT WH9: NON-ARCHETYPAL EMERGENCE: MINIMAL ALPHA LOSS, PERSISTENT THETA AND DELTA

This patient showed no warning of imminent ROR. **Figure 8A** displays the spectrogram for patient WH9. Power was concentrated in bands of waveform activity corresponding to the alpha, theta and delta bands. In contrast to the previously described archetypal patterns, there was absolutely no change in power in any of these bands until ROR—with the exception of a decrease in 10 Hz alpha from about 950 s, as seen in **Figure 8D**, and also shown in **Figure 8B** as artefactual

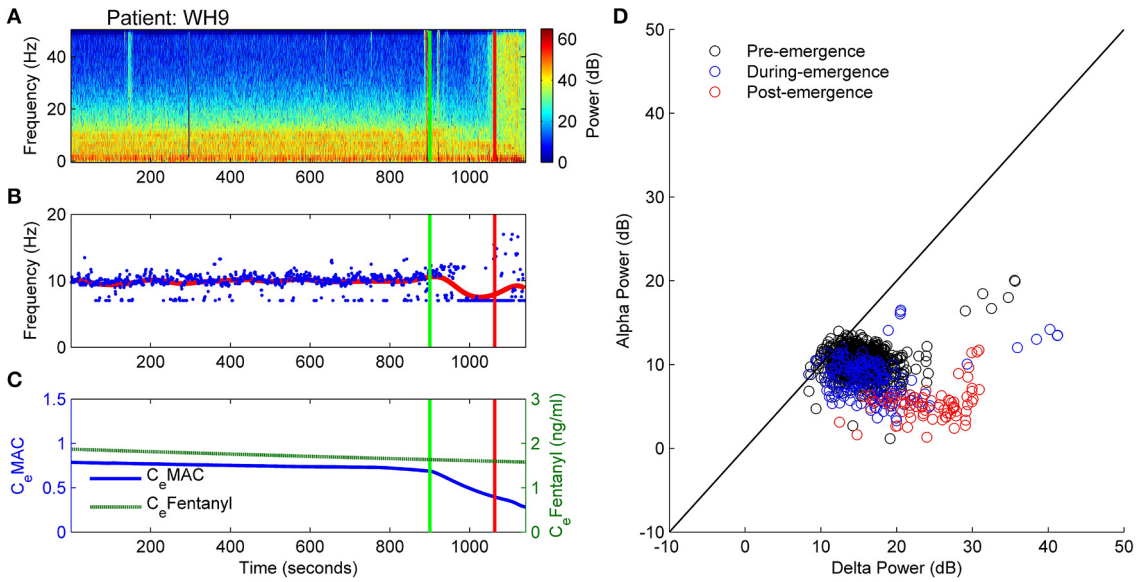

FIGURE 8 | Patient WH9: Non-archetypal emergence: minimal alpha loss, persistent theta and delta. (A) Spectrogram of the observation period. Start of emergence shown as a vertical green line at 900 s, time of patient response as a vertical red line. **(B)** Frequency of maximal oscillatory alpha power. **(C)** Concentration of anesthetic gas (C_eMAC), blue line, left vertical axis, and opioid levels as equivalent Fentanyl (C_eFentanyl, ng/ml), green line, right vertical axis. **(D)** Absolute alpha power (dB) against absolute delta power (dB) for prior to start of emergence (black circles), during emergence period (blue circles), and following recovery of response (ROR).

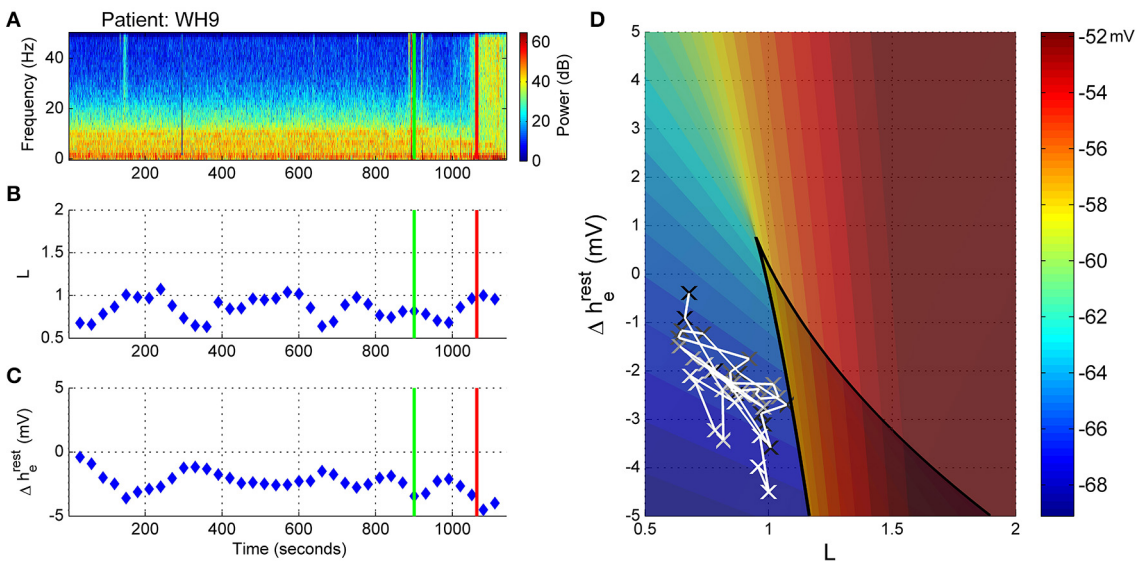

FIGURE 9 | Patient WH9, Sleep manifold. (A) Spectrogram as in **Figure 8**. **(B)** Excitatory connection strength (L-parameter) over period of observation. **(C)** Change in resting membrane impedance (Δh_e^{rest}) over period of observation. **(D)** Resultant positioning on the sleep-manifold, with a black cross being the start of, and a white cross being the end of the observation period, with intermediate shades on the gray-scale representing the time progression between these time-points.

detection of the theta band at the lower limit of 7 Hz. After emergence, high levels of power were distributed evenly over the frequency spectrum, indicating the return of muscle activity artifact. C_eFentanyl was relatively high (1.5–2 ng/ml) (**Figure 8C**).

The trajectory in the state space reflected the lack of changes seen in the spectrogram. For the whole observation period, including the emergence period itself, the level of connection strength (L-parameter in **Figure 9B**) was generally low, while the resting impedance (Δh_e^{rest} parameter in **Figure 9C**) showed

a gradual decrease. We would conclude that there were no clear shifts in the emergence trajectory of the EEG in parameter space (**Figure 9D**), but rather this patient remained situated on the lower branch of the sleep-manifold for the entire emergence period. After ROR the apparent lack of increase in the excitatory connection strength is possibly caused by the ongoing strong delta and theta power that is dominating the spectrogram (see **Figure 9A**). It is likely to be due to muscle artifact, as evidenced by the sudden increase in broad-band high frequency power seen in the spectrogram.

PATIENT WH57: NON-ARCHETYPAL EMERGENCE (NO ALPHA, PERSISTENT DELTA, PERIODS OF HIGH FREQUENCY ACTIVITY)

In **Figure 10** the EEG from an elderly patient shows a complete absence of alpha activity even during the maintenance phase of anesthesia. The frequency at maximal alpha peak in **Figure 10B** is purely artefactual, and jumping randomly between the 7 and 17Hz peak search limitation values. In the spectrogram (**Figure 10A**) episodes of high-frequency (20 to >50 Hz) activity are seen during emergence, indicated by the paler section between 1500 and 2000 s, the two dark-blue lines being recording artifact. Anesthetic concentrations were high for age adjusted MAC. C_eFentanyl levels ranged between 0.2 and 0.8 ng/ml (**Figure 10C**). The alpha and delta power levels remained at the same levels over the whole emergence process, the pre-emergence points (black circles) being obscured by the during- and post-emergence points at the same position (blue and red, **Figure 10D**).

Before the start of emergence there was a stable connection strength value of around 1.2 (**Figure 11B**). As the C_eMAC decreased during the emergence period the connection strength initially decreased, but then increased (between 1600 and 2000 s), which corresponded to the period of high-frequency activity seen in **Figure 11A**. During this period the patient was flexing their arms to their head, but was not localizing and was not responsive to auditory commands in any way. The change in resting impedance (Δh_e^{rest}) climbs from −4 to 0 mV at 300 s prior to start of emergence, followed by a progressive decrease back to low levels over the emergence period.

On the sleep-manifold (**Figure 11D**) the most distinct finding was the excursion to, and return from, the top manifold of the state-space during the short period of increased connection strength. We infer, from the increase in L parameter and clinical state, that this patient had entered some pathological state of consciousness for about 10 min before falling back to unconsciousness and then becoming responsive.

DOSE RESPONSE CURVES

The somewhat perplexing differences in spectrogram and state-space trajectory, for the different patients, require some explanation. To examine the relationship between the anesthetic drugs and the EEG and state space parameters we plotted the dose response curves for C_eMAC verses L and Δh_e^{rest}. We see that the five archetypal emergence patients (upper half of **Figure 12**) had very consistent patterns, consisting of an initial decrease in Δh_e^{rest} occurring at around 0.8 MAC (blue line, left axis). (i.e., as surgery finishes, and often even before the anesthetic decreases much, they become hyperpolarized and move to the lower left region of the manifold). This seems to be a preliminary stage before a stereotypical pattern in late emergence when, at about 0.4 MAC, the L parameter (green line, right axis) suddenly

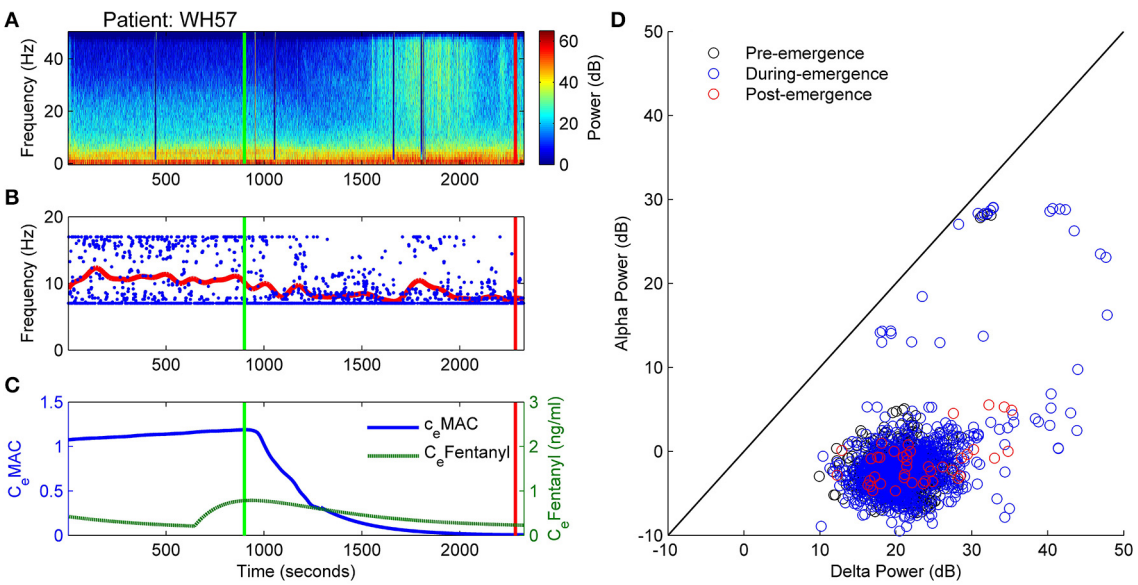

FIGURE 10 | Patient WH57: Non-archetypal emergence (no alpha, persistent delta, periods of high frequency activity). (A) Spectrogram of the observation period. Start of emergence shown as a vertical green line at 900 s, time of patient response as a vertical red line. **(B)** Frequency of maximal oscillatory alpha power. **(C)** Concentration of anesthetic gas (C_eMAC), blue line, left vertical axis, and opioid levels as equivalent Fentanyl (C_eFentanyl, ng/ml), green line, right vertical axis. (**D**) Absolute alpha power (dB) against absolute delta power (dB) for prior to start of emergence (black circles), during emergence period (blue circles), and following recovery of response (ROR).

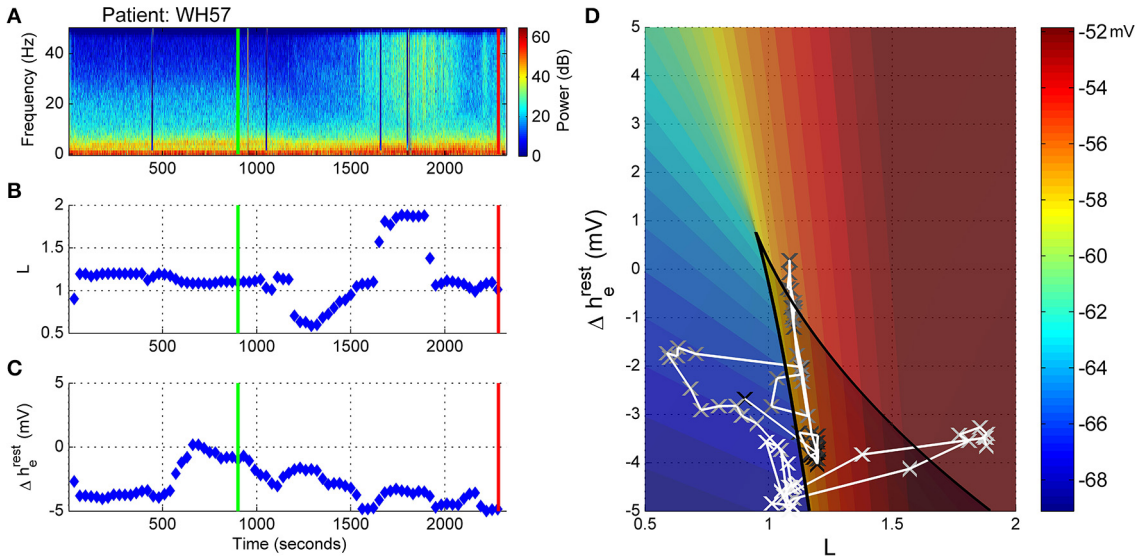

FIGURE 11 | Patient WH57, Sleep Manifold. (A) Spectrogram as in **Figure 10**. **(B)** Excitatory connection strength (L-parameter) over period of observation. **(C)** Change in resting membrane impedance (Δh_e^{rest}) over period of observation. **(D)** Resultant positioning on the sleep-manifold, with a black cross being the start of, and a white cross being the end of the observation period, with intermediate shades on the gray-scale representing the time progression between these time-points.

increased for some time until abruptly decreasing again around 0.1 MAC; followed by the patient waking up a short time later. The non-archetypal patients (see lower half of **Figure 12**) showed much smaller changes in parameters—with a modest decrease in Δh_e^{rest}, and no change in L being the most consistent features.

DISCUSSION

At this early stage in developing the methodology, we are cautious in interpreting these results—and full quantitative analysis will require statistical evaluation of hundreds of case records. However we can conclude from our preliminary data that it is feasible to map features from the frontal EEG onto a state space of underlying biological parameters during emergence from general anesthesia. We also note that the changes observed in parameter values do not have an obvious direct correlation to simple observable features in the spectrogram. For example periods of high frequency activity do not consistently result in an increase in neuronal connection strength (L), and hence it would seem that the probabilistic mapping of multiple EEG features to the model appears to be a way of using the EEG to estimate changes of factors at a more abstract level than simply the obvious changes in frequency content of the EEG waveform itself. Model parameter and EEG feature choice will probably have to be further optimized for anesthesia, but we have at shown that intra- and inter-neuronal factors can behave independently. We view these results as part of an exploratory analysis, helping to determine which factors are relevant for further analysis with larger patient groups.

Patients who follow an archetypal emergence pattern seem to start with their cortex in a relatively low conductance state, and with poor cortical connection strength. They then follow quite a long trajectory in the state space before achieving the externally directed consciousness (the so-called "connected" consciousness) as described by Sanders et al. (2012). In contrast, patients who do not follow this archetypal emergence pattern typically have a hyperpolarized cortex for the whole observation period, irrespective of the level of anesthetic, and do not exhibit periods of high connection strength before the sudden engagement with the external environment. The fact that we have found many counterexamples to the archetypal pattern suggests that this pattern will not be completely reliable as an indicator of the causal biological processes that are necessary for the return of consciousness following general anesthesia and surgery.

It could be argued that—according to this model—a state of hyperpolarization (i.e., high neuronal conductance and low connectivity) is a prerequisite for the return of engaged consciousness as, for both groups, the transition to ROR took place from a hyperpolarized state—and that no patients transitioned to ROR from a depolarized state. The apparent hyperpolarization drift (occurring as the C_eMAC *decreases* in emergence) seems to be opposite to the results of various animal studies using intraneuronal recordings, which suggest that *increased* anesthesia is associated with some degree of neuronal *hyper*polarization. The whole methodology relies on the model having a reasonable fidelity to real physiology. There are two possibilities. Firstly, the model may be correct, and the animal experiments may be wrong, because they were conducted in the absence of surgical stimulation—which has a potent cortical depolarizing effect via aminergic activation. Or the model may be incorrect, and the observed hyperpolarization may be an artifact of the model stability. In essence, around the cusp of the fold on the manifold, the real parts of the eigenvalues for the system of equations are close to zero (or even positive depending on the parameter settings); and hence the steady-states of the model show marginal

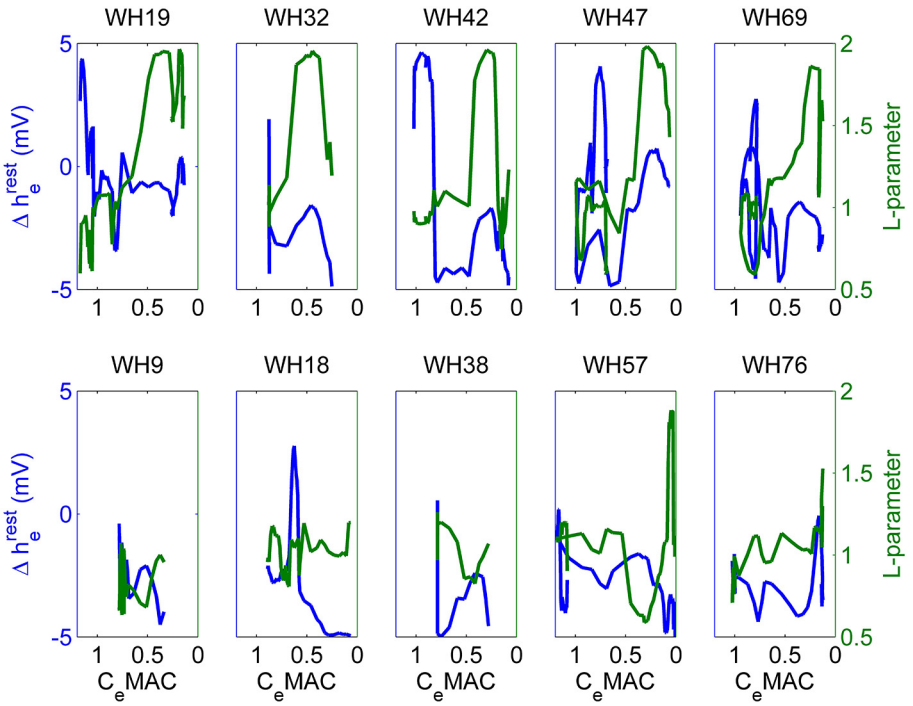

FIGURE 12 | Change in resting membrane impedance (Δh_e^{rest}, blue line, left axis), and excitatory connection strength (L-parameter, green line, right axis) plotted against decreasing anesthetic concentrations (C_eMAC) for the entire observation period for 10 patients. The five patients in the upper-half of the figure show "archetypal" emergences, those in the lower-half display "non-archetypal" emergences.

stability. This is manifest in the EEG as maximal delta and alpha oscillations in this region (see Figure 11 in Dadok et al., 2014). As the surgical stimulation subsides toward the end of the operation, and the C_eMAC starts to decrease, the mean delta gradient decreases and the state of the cortex as represented on the manifold moves downwards away from the cusp to a more stable state. In fact the idea of delta waves as a sign of a very hyperpolarized thalamo-cortical system is over-simplistic. For example in the well-described phenomenon of "delta-arousal," there is an *increase* in delta power associated with increased surgical noxious stimulation (Morimoto et al., 2005). It is possible that we are seeing the opposite phenomenon—a decrease in painful stimulation resulting in a decrease in delta power. There also are other data that suggest that large amplitude EEG is a sign of excessive noxious stimulation or inadequate analgesic medication (Liley et al., 2010) or even nitrous oxide withdrawal (Foster and Liley, 2011).

A characteristic feature of the archetypal patients is the consistent increase in the L-parameter for a period prior to ROR. It is tempting to associate these episodes with the first forays into consciousness, although this would have to be described as a dissociated consciousness, i.e., not engaged with the outside world, indicative of something like dreaming, as these patients were still unresponsive at that time. Yet given that only one group displayed these episodes of increased connection strength we would have to conclude that, assuming a well-functioning model, either connection strength is irrelevant to engaged (externally directed) consciousness, or that the mechanisms required for engaged consciousness are hidden from the model. For both groups discontinuous, abrupt changes were seen in brain dynamics. For the archetypal patients the changes in L were abrupt, not gradual progressive changes; and for the non-archetypal patients the ROR was not preceded by any indicators in the spectrogram. The model has all patients positioned in the left lower corner of manifold prior to ROR. The important feature of this region is that it is near to the 3-root area of the manifold; an area of instability where a small change in parameter value results in discontinuous transitions in state. We speculate that the reason all patients either migrated to, or were already present in this area prior to ROR is that this would make it much easier for the brain to transition to another state. In contrast, if patients showing the archetypal pattern of emergence remained at a depolarized state, a small change in parameter would not lead to a large change in state given the gradient. It is much harder for the cortex to climb than to jump. This may help to explain the "flip-flop" phenomena that have been described in the natural sleep literature (Saper et al., 2001).

The above argument only holds if one assumes the true position for the wakeful cortex is on the higher branch of the manifold; in our data this has been obscured by the presence of broadband EMG, or it may have been overlooked due to a very short lasting ROR, e.g., 5 s, prior to a return to some sedation; this would not show on the model which requires 30 s sections of EEG. These results are provisional, and there are some significant issues still to be resolved. Our EEG data were collected from a single pre-frontal channel, and hence completely lacking

in spatial information. We also note that the "sleep" model is in some respects incomplete when applied to general anesthesia, because it does not produce burst suppression patterns, various high frequency oscillations, and does not distinguish between the dissociated consciousness of REM sleep and true wakeful consciousness.

CONCLUSIONS

The archetypal EEG pattern of emergence is not the only pattern of emergence seen in surgical patients, with many patients showing no obvious progressive changes in their EEG until sudden recovery of responsiveness. When the EEG features are mapped onto a model state space of cortical connection strength and intrinsic resting neuronal conductivity, patients consistently show a low level of excitatory connectedness during anesthesia. During emergence the archetypal patients show a very consistent trajectory of progressive decrease in neuronal impedance and sudden increase in connection strength before waking. In contrast, the non-archetypal patients showed minimal changes in either parameter before waking. We therefore conclude that the archetypal EEG emergence pattern is not a necessary prelude to recovery of responsiveness; and hence is probably an epiphenomenon as regards our understanding of the mechanisms and signs of anesthetic-induced unconsciousness.

ACKNOWLEDGMENTS

This project has been funded in whole or in part with funds from the James S. McDonnell Foundation under Grant Award No. 220020346. The results were independently derived and do not reflect any endorsement on the part of the James S. McDonnell Foundation or AREF. This work was partially supported by a U.S. National Science Foundation Graduate Research Fellowship (to VMD) and in part by the National Science Foundation through the research grant CMMI 1031811 (to AJS).

REFERENCES

Alkire, M. T., Hudetz, A. G., and Tononi, G. (2008). Consciousness and anesthesia. *Science* 322, 876–880. doi: 10.1126/science.1149213

Banchs, R. J., and Lerman, J. (2014). Preoperative anxiety management, emergence delirium, and postoperative behavior. *Anesthesiol. Clin.* 32, 1–23. doi: 10.1016/j.anclin.2013.10.011

Bennett, C., Voss, L. J., Barnard, J. P. M., and Sleigh, J. W. (2009). Practical use of the raw electroencephalogram waveform during general anesthesia: the art and science. *Anesth. Analg.* 109, 539–550. doi: 10.1213/ane.0b013e3181a9fc38

Bojak, I., and Liley, D. (2005). Modeling the effects of anesthesia on the electroencephalogram. *Phys. Rev. E Stat. Nonlin. Soft Matter Phys.* 71:041902. doi: 10.1103/PhysRevE.71.041902

Brown, E. N., Lydic, R., and Schiff, N. D. (2010). General anesthesia, sleep, and coma. *N. Engl. J. Med.* 363, 2638–2650. doi: 10.1056/NEJMra0808281

Brown, E. N., Purdon, P. L., and Van Dort, C. J. (2011). General anesthesia and altered states of arousal: a systems neuroscience analysis. *Annu. Rev. Neurosci.* 34, 601–628. doi: 10.1146/annurev-neuro-060909-153200

Ching, S., and Brown, E. N. (2014). Modeling the dynamical effects of anesthesia on brain circuits. *Curr. Opin. Neurobiol.* 25, 116–122. doi: 10.1016/j.conb.2013.12.011

Ching, S., Brown, E. N., and Kramer, M. A. (2012). Distributed control in a mean-field cortical network model: implications for seizure suppression. *Phys. Rev. E Stat. Nonlin. Soft Matter Phys.* 86:021920. doi: 10.1103/PhysRevE.86.021920

Ching, S., Cimenser, A., Purdon, P. L., Brown, E. N., and Kopell, N. J. (2010). Thalamocortical model for a propofol-induced -rhythm associated with loss of consciousness. *Proc. Natl. Acad. Sci. U.S.A.* 107, 22665–22670. doi: 10.1073/pnas.1017069108

Contreras, D., Destexhe, A., Sejnowski, T. J., and Steriade, M. (1997). Spatiotemporal patterns of spindle oscillations in cortex and thalamus. *J. Neurosci.* 17, 1179–1196.

Dadok, V. M., Kirsch, H. E., Sleigh, J. W., Lopour, B. A., and Szeri, A. J. (2014). A probabilistic framework for a physiological representation of dynamically evolving sleep state. *J. Comput. Neurosci.* 37, 105–124. doi: 10.1007/s10827-013-0489-x

Foster, B. L., Bojak, I., and Liley, D. T. J. (2008). Population based models of cortical drug response: insights from anaesthesia. *Cogn. Neurodyn.* 2, 283–296. doi: 10.1007/s11571-008-9063-z

Foster, B. L., and Liley, D. T. J. (2011). Nitrous oxide paradoxically modulates slow electroencephalogram oscillations: implications for anesthesia monitoring. *Anesth. Analg.* 113, 758–765. doi: 10.1213/ANE.0b013e318227b688

Friedman, E. B., Sun, Y., Moore, J. T., Hung, H.-T., Meng, Q. C., Perera, P., et al. (2010). A conserved behavioral state barrier impedes transitions between anesthetic-induced unconsciousness and wakefulness: evidence for neural inertia. *PLoS ONE* 5:e11903. doi: 10.1371/journal.pone.0011903

Gibbs, F., Gibbs, E., and Lennox, W. (1937). Effect on the electro-encephalogram of certain drugs which influence nervous activity. *Arch. Intern. Med.* 60, 154–166. doi: 10.1001/archinte.1937.00180010159012

Gugino, L., Chabot, R., Prichep, L., John, E., Formanek, V., and Aglio, L. (2001). Quantitative EEG changes associated with loss and return of consciousness in healthy adult volunteers anaesthetized with propofol or sevoflurane. *Br. J. Anaesth.* 87, 421–428. doi: 10.1093/bja/87.3.421

Hutt, A., and Longtin, A. (2010). Effects of the anesthetic agent propofol on neural populations. *Cogn. Neurodyn.* 4, 37–59. doi: 10.1007/s11571-009-9092-2

Kelz, M. B., Sun, Y., Chen, J., Meng, Q. C., Moore, J. T., Veasey, S. C., et al. (2008). An essential role for orexins in emergence from general anesthesia. *Proc. Natl. Acad. Sci. U.S.A.* 105, 1309–1314. doi: 10.1073/pnas.0707146105

Kushikata, T., and Hirota, K. (2014). Mechanisms of anesthetic emergence: evidence for active reanimation. *Curr. Anesthesiol. Rep.* 4, 49–56. doi: 10.1007/s40140-013-0045-2

Langsjo, J. W., Alkire, M. T., Kaskinoro, K., Hayama, H., Maksimow, A., Kaisti, K. K., et al. (2012). Returning from oblivion: imaging the neural core of consciousness. *J. Neurosci.* 32, 4935–4943. doi: 10.1523/JNEUROSCI.4962-11.2012

Law, C., Sleigh, J., Barnard, J., and MacColl, J. (2011). The association between intraoperative electroencephalogram-based measures and pain severity in the post-anaesthesia care unit. *Anaesth. Intensive Care* 39, 875–880.

Lee, U., Müller, M., Noh, G.-J., Choi, B., and Mashour, G. A. (2011). Dissociable network properties of anesthetic state transitions. *Anesthesiology* 114, 872–881. doi: 10.1097/ALN.0b013e31821102c9

Leslie, K., Sleigh, J., Paech, M. J., Voss, L., Lim, C. W., and Sleigh, C. (2009). Dreaming and electroencephalographic changes during anesthesia maintained with propofol or desflurane. *Anesthesiology* 111, 547–555. doi: 10.1097/ALN.0b013e3181adf768

Liley, D. T. J., Sinclair, N. C., Lipping, T., Heyse, B., Vereecke, H. E. M., and Struys, M. M. R. F. (2010). Propofol and remifentanil differentially modulate frontal electroencephalographic activity. *Anesthesiology* 113, 292–304. doi: 10.1097/ALN.0b013e3181e3d8a6

Liley, D. T. J., and Walsh, M. (2013). The mesoscopic modeling of burst suppression during anesthesia. *Front. Comput. Neurosci.* 7:46. doi: 10.3389/fncom.2013.00046

Loader, C. (1997). LOCFIT: an introduction. *Stat. Comput. Graph. Newsl.* 8, 11–17.

Lopour, B. A., Tasoglu, S., Kirsch, H. E., Sleigh, J. W., and Szeri, A. J. (2011). A continuous mapping of sleep states through association of EEG with a mesoscale cortical model. *J. Comput. Neurosci.* 30, 471–487. doi: 10.1007/s10827-010-0272-1

Marreiros, A. C., Stephan, K. E., and Friston, K. J. (2010). Dynamic causal modeling. *Scholarpedia* 5, 9568. doi: 10.4249/scholarpedia.9568

Mashour, G. A., and Alkire, M. T. (2013). Evolution of consciousness: phylogeny, ontogeny, and emergence from general anesthesia. *Proc. Natl. Acad. Sci. U.S.A.* 110, 10357–10364. doi: 10.1073/pnas.1301188110

McCarthy, M. M., Brown, E. N., and Kopell, N. (2008). Potential network mechanisms mediating electroencephalographic beta rhythm changes during

propofol-induced paradoxical excitation. *J. Neurosci.* 28, 13488–13504. doi: 10.1523/JNEUROSCI.3536-08.2008

Mitra, P., and Bokil, H. (2008). *Observed Brain Dynamics*. New York, NY: Oxford University Press.

Morimoto, Y., Matsumoto, A., Koizumi, Y., Gohara, T., Sakabe, T., and Hagihira, S. (2005). Changes in the bispectral index during intraabdominal irrigation in patients anesthetized with nitrous oxide and sevoflurane. *Anesth. Analg.* 100, 1370–1374. doi: 10.1213/01.ANE.0000148124.02288.D1

Nickalls, R. W. D., and Mapelson, W. W. (2003). Age-related iso-MAC charts for isoflurane, sevoflurane and desflurane in man. *Br. J. Anaesth.* 91, 170–174. doi: 10.1093/bja/aeg132

Purdon, P. L., Pierce, E. T., Mukamel, E. A., Prerau, M. J., Walsh, J. L., Wong, K. F. K., et al. (2013). Electroencephalogram signatures of loss and recovery of consciousness from propofol. *Proc. Natl. Acad. Sci. U.S.A.* 110, E1142–E1151. doi: 10.1073/pnas.1221180110

Sanders, R. D., Tononi, G., Laureys, S., and Sleigh, J. (2012). Unresponsiveness not equal unconsciousness. *Anesthesiology* 116, 946. doi: 10.1097/ALN.0b013e318249d0a7

Saper, C. B., Chou, T. C., and Scammell, T. E. (2001). The sleep switch: hypothalamic control of sleep and wakefulness. *Trends Neurosci.* 24, 726–731. doi: 10.1016/S0166-2236(00)02002-6

Sleigh, J. W., Vizuete, J. A., Voss, L., Steyn-Ross, A., Steyn-Ross, M., Marcuccilli, C. J., et al. (2009). The electrocortical effects of enflurane: experiment and theory: *Anesth. Analg.* 109, 1253–1262. doi: 10.1213/ANE.0b013e3181add06b

Steyn-Ross, M. L., Steyn-Ross, D. A., Sleigh, J. W., and Liley, D. T. J. (1999). Theoretical electroencephalogram stationary spectrum for a white-noise-driven cortex: evidence for a general anesthetic-induced phase transition. *Phys. Rev. E Stat. Phys. Plasmas Fluids Relat. Interdiscip. Topics* 60, 7299. doi: 10.1103/PhysRevE.60.7299

Conflict of Interest Statement: The authors declare that the research was conducted in the absence of any commercial or financial relationships that could be construed as a potential conflict of interest.

Received: 28 May 2014; accepted: 24 July 2014; published online: 13 August 2014.
Citation: Hight DF, Dadok VM, Szeri AJ, García PS, Voss L and Sleigh JW (2014) Emergence from general anesthesia and the sleep-manifold. Front. Syst. Neurosci. ***8****:146. doi: 10.3389/fnsys.2014.00146*
This article was submitted to the journal Frontiers in Systems Neuroscience.

frontiers in
SYSTEMS NEUROSCIENCE

ORIGINAL RESEARCH ARTICLE
published: 11 December 2014
doi: 10.3389/fnsys.2014.00234

Spin-glass model predicts metastable brain states that diminish in anesthesia

Anthony G. Hudetz[1]*, Colin J. Humphries[2] and Jeffrey R. Binder[2]

[1] *Department of Anesthesiology, Medical College of Wisconsin, Milwaukee, WI, USA*
[2] *Department of Neurology, Medical College of Wisconsin, Milwaukee, WI, USA*

Edited by:
Axel Hutt, Institut National de Recherche en Informatique et en Automatique, France

Reviewed by:
Peter Beim Graben, Humboldt-Universität zu Berlin, Germany
Meysam Hashemi, Institut National de Recherche en Informatique et en Automatique, France

***Correspondence:**
Anthony G. Hudetz, Department of Anesthesiology, Medical College of Wisconsin, 8701 Watertown Plank Road, Milwaukee, WI 53226, USA
e-mail: ahudetz@mcw.edu

Patterns of resting state connectivity change dynamically and may represent modes of cognitive information processing. The diversity of connectivity patterns (global brain states) reflects the information capacity of the brain and determines the state of consciousness. In this work, computer simulation was used to explore the repertoire of global brain states as a function of cortical activation level. We implemented a modified spin glass model to describe UP/DOWN state transitions of neuronal populations at a mesoscopic scale based on resting state BOLD fMRI data. Resting state fMRI was recorded in 20 participants and mapped to 10,000 cortical regions (sites) defined on a group-aligned cortical surface map. Each site represented the population activity of a $\sim$20 mm^2 area of the cortex. Cross-correlation matrices of the mapped BOLD time courses of the set of sites were calculated and averaged across subjects. In the model, each cortical site was allowed to interact with the 16 other sites that had the highest pair-wise correlation values. All sites stochastically transitioned between UP and DOWN states under the net influence of their 16 pairs. The probability of local state transitions was controlled by a single parameter T corresponding to the level of global cortical activation. To estimate the number of distinct global states, first we ran 10,000 simulations at T = 0. Simulations were started from random configurations that converged to one of several distinct patterns. Using hierarchical clustering, at 99% similarity, close to 300 distinct states were found. At intermediate T, metastable state configurations were formed suggesting critical behavior with a sharp increase in the number of metastable states at an optimal T. Both reduced activation (anesthesia, sleep) and increased activation (hyper-activation) moved the system away from equilibrium, presumably incompatible with conscious mentation. During equilibrium, the diversity of large-scale brain states was maximum, compatible with maximum information capacity—a presumed condition of consciousness.

Keywords: anesthesia, consciousness, information, criticality, metastability, fMRI, resting state, functional connectivity

INTRODUCTION

Cognitive functioning of the conscious human brain is thought to depend on the formation of dynamic patterns of neuronal coalitions and large-scale connectivity (Werner, 2009; Bressler and Menon, 2010). Moreover, the diversity or *repertoire* of distinct functional patterns reflects the information capacity of the brain that is thought to be central to consciousness (Tononi, 2008; Deco et al., 2014). The repertoire of brain states over time can be large if there is sufficient flexibility in the system to rapidly switch to new configurations and maintain these configurations for a finite amount of time. The time necessary for maintaining a configuration should roughly coincide with the duration of a conscious perceptual frame (Bachmann, 2013). The dynamic nature of the ongoing stream of consciousness may reflect this rapid sequence of state configurations (Werner, 2007). Moreover, the disruption of the sequence of states may account for the anesthetic suppression of consciousness (Hudetz et al., 2014).

Various physical, chemical, and biological systems are able to produce *metastable states* that satisfy the requirement for a large repertoire. Metastable states typically arise in critical systems that operate at the border of order and disorder and are characterized by complex patterns of fluctuations (Werner, 2007; Beggs, 2008; Kitzbichler et al., 2009; Deco and Jirsa, 2012; Tagliazucchi et al., 2012). Self-organization is often the underlying mechanism of criticality. Recent computational and empirical studies based on electrophysiology, fMRI, and EEG lend support to the existence of this behavior in the brain (Friston, 1997; Freeman and Holmes, 2005; Werner, 2007; Kitzbichler et al., 2009; Kelso, 2012; Bhowmik and Shanahan, 2013; Tognoli and Kelso, 2014). This metastability is considered essential to the subjective mental state and consciousness (Kitzbichler et al., 2009). Its restoration may be the hallmark of recovery from unconsciousness (Hudson et al., 2014).

Self-organization can also lead to scale-free behavior, in which similar interactions are present at different temporal or spatial

scales (Tognoli and Kelso, 2014). The scaling of the magnitude of interactions is typically 1/f, where f is the frequency (Kello et al., 2008). Interestingly, the scale-free property of EEG or fMRI BOLD signals is preserved under anesthesia (Lee et al., 2010; Liu et al., 2014) but not in disorders of consciousness associated with diffuse brain damage (Liu et al., 2014). In light of this dissociation, conscious information processing may depend more closely on the dynamic repertoire and metastability of brain states than their spatio-temporal scaling laws.

Recent fMRI investigations have convincingly demonstrated that brain networks undergo dynamic reconfigurations even in the absence of novel stimuli or cognitive tasks (Britz et al., 2010; Chang and Glover, 2010; Sakoglu et al., 2010; Kang et al., 2011; Allen et al., 2012; Glerean et al., 2012; Handwerker et al., 2012; Jones et al., 2012; Cribben et al., 2013; Di and Biswal, 2013; Hutchison et al., 2013b; Keilholz et al., 2013; Liu and Duyn, 2013). Such resting state network dynamics have been ascribed to the general phenomena of spontaneous mentation, imagery, task-independent thoughts or daydreaming (Mckiernan et al., 2006).

The standard method for characterizing dynamic networks of the brain has been the sliding window analysis of functional connectivity (Hutchison et al., 2013a), sometimes combined with independent component analysis (ICA) (Kiviniemi et al., 2011), temporal ICA (Smith et al., 2012), and other source separation methods (Cribben et al., 2013). Connectivity analysis at higher temporal resolution has also been attempted with various point-process methods (Tagliazucchi et al., 2011), revealing so-called spontaneous co-activation patterns (Liu and Duyn, 2013; Liu et al., 2013). In all cases, a main limiting factor is the duration of the fMRI scan, which limits the number of connectivity patterns that can be extracted from a finite sample. On the other hand, the limited spatial resolution of EEG does not allow the imaging of spatially complex patterns. Moreover, collecting a sufficient amount of experimental data across the full range of brain states in the same subject, including multiple states of sleep, wakefulness, anesthesia, etc., is difficult.

As an alternative approach to explore the probability space of correlated brain states, we used a combination of empirical connectivity data and computer simulation. In the simulation, functional connectivity patterns were evolved by simulating the dynamic interaction of mesoscopic brain regions using a modified spin-glass model. This model is well-suited to describe the large-scale, globally distributed effect of the dynamic interaction of functionally connected brain regions. The model is relatively simple, as it does not include cell-specific or synaptic connections but it is minimally sufficient to account for an arbitrary pattern of neuronal interactions of distant, mesoscopic brain regions. Moreover, the model includes a single parameter to control the general cortical arousal level analogous in physical systems to the absolute temperature that determines the probability of spin fluctuations. The biological equivalent of spins in our model is the UP and DOWN states of neuronal activity.

As a novel feature, our model was constrained by using empirically derived resting state connectivity to set the spatial pattern of long-range interactions. The present approach is similar to the previously described Ising model (Fraiman et al., 2009; Das et al., 2014; Marinazzo et al., 2014), with the exception that our model is based on empirically derived long-range interactions. We show that with the chosen constraints set by the connectivity matrix, the model predicts critical behavior at the optimal activation level at which metastable states occur. Both reduced activation (anesthesia, sleep) and increased activation (epilepsy) moves the system away from equilibrium, presumably incompatible with conscious mentation. In equilibrium, the diversity of large-scale brain states is maximum, implying maximum information capacity—a previously postulated prerequisite of consciousness according to the Information Integration Theory (Tononi, 2008).

MATERIALS AND METHODS

fMRI EXPERIMENTS AND DATA ANALYSIS

Resting-state BOLD fMRI data were collected from 20 subjects. Subjects were instructed to lie still with eyes open and avoid falling asleep. After each run, they were requested to rate their alertness level during the previous run. All imaging procedures were conducted on a 3.0 Tesla GE Excite scanner. For each subject, an anatomical scan was acquired using an SPGR pulse sequence (130 axial slices, slice thickness = 1.0 mm, TE = 3.2 ms, TR = 8.2 s, flip angle = 12 degrees, FOV = 240 × 180 mm, matrix size = 256 × 224). Resting state functional images were obtained using gradient-EPI (41 axial slices, slice thickness = 2.5 mm, TE = 25 ms, TR = 3 s, flip angle = 84°, FOV = 240 mm, matrix size = 96 × 96). In each subject, we obtained 6 runs of 7 min each (140 time points per run) for a total of 42 min of resting data.

Preprocessing of functional images included slice-timing correction, motion correction, and co-registration with the anatomical scan. To remove the effects of signal drift and possible artifacts due to motion, a regression analysis was conducted with third-order polynomial, the parameters from the motion correction algorithm, and a global signal regressor. These steps were performed using the software Analysis of Functional Neuroimages (AFNI, NIH). Cortical surface models were created from the anatomical scan of each subject using Freesurfer software. The subjects' surface model was aligned to an average surface atlas (FS Average brain in Freesurfer) using spherical surface-based alignment (Fischl et al., 1999). The triangular mesh of the FS Average brain was subsampled to 10,000 vertices across both hemispheres (Matlab reducepatch). The BOLD time courses were mapped to the 10,000 points by averaging all voxels overlapping with the cortical surface nearest to each of the 10,000 points. Each of the 10,000 points represents the average activity within a ∼20 mm^2 diameter patch of cortex. For spatial smoothing, an estimate of the distance between each of the points along the cortical surface was calculated by the fast marching algorithm (Sethian, 1996). Finally, correlation values were calculated between all pairwise combinations of the 10,000 points. The resulting correlation matrices were averaged across subjects to create a single group connectivity matrix used for the simulation.

SPIN-GLASS MODEL

The model was based on the standard assumption that global brain states evolve due to the ongoing interaction of mesoscopic brain regions, from here on called *sites*. The size of these sites was taken as that of the cortical surface patches of 20 mm^2 from

the fMRI data, each representing a vertical slab or macro-column of cortex. According to the standard Ising or spin-glass models, at any given time, each of the sites was assumed to be in one of two local states: UP (active) or DOWN (inactive). Further detailed description of the Ising model is available in previous publications (Fraiman et al., 2009; Kitzbichler et al., 2009; Das et al., 2014; Marinazzo et al., 2014). The essential difference between the Ising and spin-glass models is that the latter includes long-range interactions and variable interaction probabilities. Following the Monte-Carlo implementation of the Metropolis algorithm (Metropolis et al., 1953; Fricke, 2006), local states were allowed to flip with probability p_i as

$$p_i \sim \exp(-\Delta E_i/T)$$

$$\Delta E_i = \frac{1}{2} S_i \sum_{k=1}^{n} A_{ik} S_k$$

$$S_i = [+1, -1], \; i = 1, .., n, \; k \neq i$$

In these equations, i and k index the cortical sites such that k is the index of sites interacting with site i, n is the total number of sites in the model, and A_{ik} is the connection matrix that defines the interacting sites. For each site i, S_i is the state variable (UP or DOWN), ΔE_i is the activation energy, and T is the global activation level—analogous to temperature in the physical literature.

To define the interacting sites, we used the fMRI functional connectivity data. For each site as a reference, the 16 other sites with the strongest correlation with the reference site were identified from the all pair-wise BOLD signal correlation matrix. Each site was then allowed to interact with their 16 pairs at a probability determined by the site's activation energy and the overall activation level.

In various runs, the activation level T was varied from zero to 4.0. Low values of T were taken as corresponding to reduced activation, such as in sleep, anesthesia or coma, and high values of T were taken as corresponding to hyper-activation, as in seizure. Each simulation started with a random distribution of UP/DOWN states as an initial condition. The system was then allowed to evolve for 10,000 time steps. Depending on the chosen value of T, the states converged or continued to change until the simulation was terminated.

RESULTS

BOLD FUNCTIONAL CONNECTIVITY

For a compact illustration of BOLD functional connectivity, the pair-wise correlation values between each site and the rest of the brain were averaged yielding a spatial map of global correlation strength. **Figure 1** shows the results for 20 subjects. There is a noticeable variation of connectivity patterns however, the connectivity of a few structures appears to be conserved in most subjects. The global connectivity pattern averaged across all subjects is illustrated in **Figure 2**. This map emphasizes regions that were most strongly connected with the rest of the brain in all subjects. The average connectivity matrix that gave rise to this figure was used as input data for the simulation. **Figure 3** shows an example of the spatial distribution of several sets of 16 interacting sites, i.e., those with the highest correlation with each reference site. Clearly, these interactions reach over large regions of the brain.

SPIN-GLASS SIMULATION

First we examined the types of global state patterns that emerged at low activation level T. As anticipated, various metastable state configurations were formed at intermediate T, and they were frozen at low T (Supplementary electronic material). Specifically, at $T \leq 2$, the patterns converged, although this sometimes took a long time. To reduce the simulation time to convergence, we performed 10,000 runs at $T = 0$. This rapidly drove the system to one of many final configurations. We then sought to estimate the diversity of distinct global states. To suppress the effect of

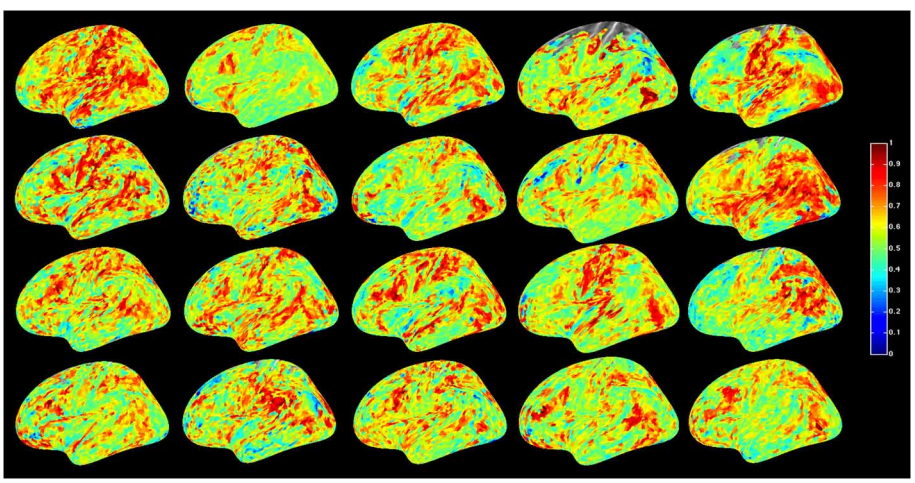

FIGURE 1 | Global resting-state cortical correlation maps in 20 subjects. Pseudo-color indicates the average cross-correlation of each voxel with the rest of the brain.

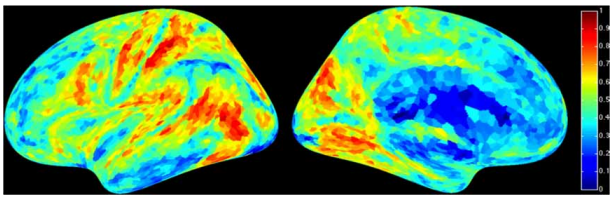

FIGURE 2 | Average global resting-state cortical correlation map from 20 subjects. Pseudo-color indicates the average cross-correlation of each voxel with the rest of the brain.

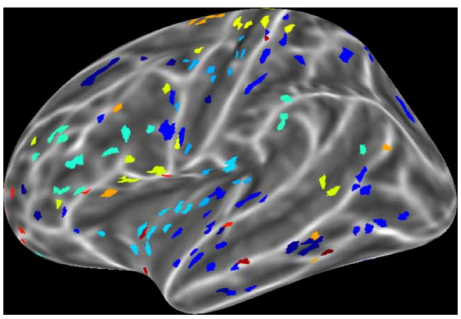

FIGURE 3 | An example of interacting cortical sites for 10 randomly selected seeds in the model. Each color indicates a set of 16 sites that interact with the same seed. Interacting sites are chosen based on the 16 highest correlation coefficients of each seed in the all pair-wise correlation matrix.

local variations, we first performed spatial averaging of each pattern within 5 or 15 mm. The averaging facilitated the comparison of global similarity without local noise. We then used hierarchical clustering of the 10,000 patterns and estimated the relative frequency of patterns. **Figure 4** shows the 40 most frequent patterns. All patterns are distinct and they generally reflect known functional regions of the brain (prefrontal, temporal, parietal, occipital, pre- and post-central, etc.).

Next, we compared the dynamics of global state patterns at intermediate activation levels. A convenient measure of the dynamics is the temporal correlation of patterns at successive time points (**Figure 5**). The correlation matrix at activation level T = 2.7 suggests patterns that are typical of systems with metastable states. At high T, the patterns become random; whereas at low T, the patterns become stereotypic, showing temporal hypersynchrony. Increasing the time lag (embedding delay) from one time step to 2, 4, 8, 16, and 32, reduced the mean and augmented the fluctuation in the correlation of states (**Figure 6**). This effect was further quantified by the homogeneity index H, defined as the reciprocal of the coefficient of variation:

$$H = < cc > /SD(cc),$$

where SD is the standard deviation and brackets <..> indicate averaging. **Figure 7A** illustrates the results for three levels of activation, T. The H-T relationship followed power law up to a lag of approximately 20 time steps. The power law was preserved at reduced T, although its exponent (the slope of linear regression slope in a log-log plot) was reduced.

To measure the temporal diversity of metastable states, we introduced the *dispersion index* D defined as:

$$D = K < (1 - cc) > /var\,(cc)$$

where cc stands for the elements of the all pair-wise correlation matrix of the simulated states, var stands for variance, and K is a normalization constant equal to the variance of the uniform random distribution of the same size as the cc matrix. As defined, D measures the temporal diversity or *repertoire* of global states over time at all time lags. It can be easily seen that the value of D is low for both random and regular systems. **Figure 7B** shows calculated values of D as a function of activation level T. The plot suggests the presence of typical second-order phase transition. D reaches maximum at T = 2.7; its value drops sharply at both smaller and larger T. Low values of T are thought to characterize suppressed states such as anesthesia or deep sleep, and high values of T are thought to correspond to hyper-activated states, e.g., seizure. At the critical T, metastable states dominate and the diversity of brain states as measured by D is maximum. The high repertoire of states at critical T is consistent with the formerly postulated condition to support conscious cognition.

DISCUSSION

The goal of this investigation was to demonstrate that long-range neuronal interactions based on empirical measurements in the human brain produce large-scale dynamic patterns of activity. To this end, we applied computer simulation with a modified spin-glass model of site interactions that were constrained by BOLD fMRI functional connectivity. As anticipated, our results predicted large-scale metastable brain states that occurred at an optimal activation level. Simultaneously, at the optimal level of activation, the diversity of state configurations was maximized—consistent with its postulated role in brain functioning in the conscious state. Moreover, the diversity of states was reduced when moving away from criticality—presumably corresponding to states of diminished consciousness.

While a few similar computational studies have been conducted in the past, the present work is novel in several ways. First, the simulation was based specifically on long-range interactions that spanned distances among remote cortical regions. This is the defining difference between the spin-glass model and the Ising model, which considers only nearest neighbor interactions. Second, we used BOLD functional connectivity to select the interacting sites. These empirically-determined connectivity constraints ensure that the model contains connectivity structure similar to that of the actual human brain. Third, we used a novel measure of dispersion to estimate the diversity of global brain states and their dependence on activation level. Therefore, it is of substantial interest that the long-range interacting system, as constrained by real probabilistic data from the brain, readily produced metastable states.

Kitzbichler et al. (2009) demonstrated power law scaling of the synchrony in resting-state fMRI and MEG data, suggesting that the presence of self-organized criticality in the brain is analogous

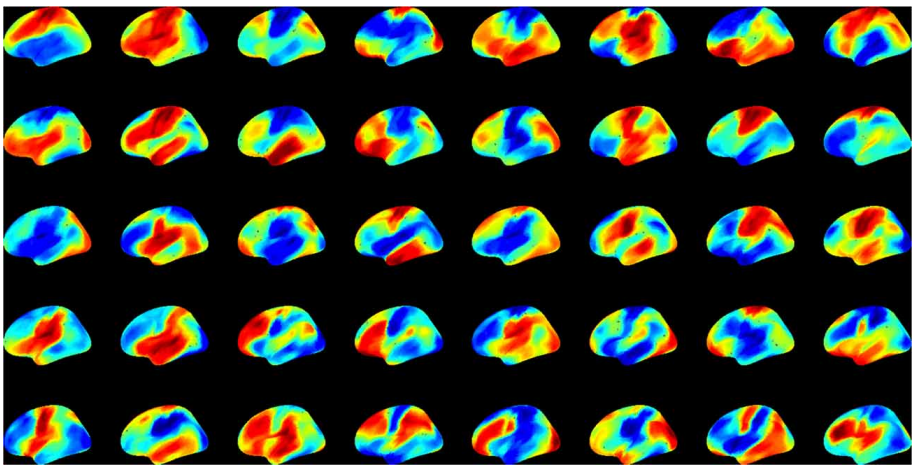

FIGURE 4 | The 40 most frequent equilibrium patterns at T = 0 activation level from the spin-glass model. Pseudo-color indicates the probability of UP (red) and DOWN (blue) states of each site (scale is arbitrary). Patterns were classified using hierarchical clustering at 99% similarity after 15 mm spatial smoothing.

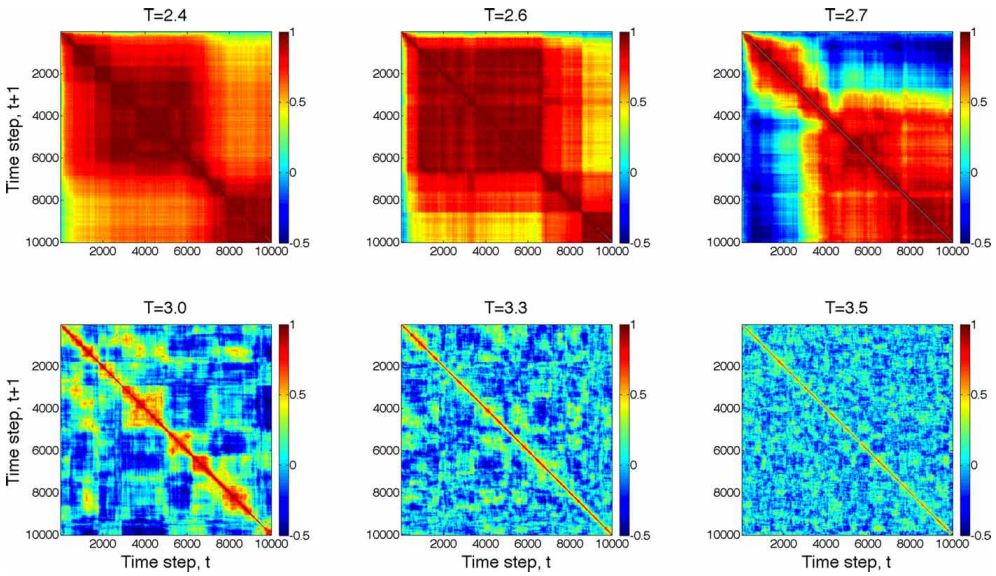

FIGURE 5 | Temporal correlation of global state patterns at successive time points and different activation levels, T. Simulation consisted of 10,000 time steps. Pseudo-color indicates the correlation coefficient, cc, of consecutive patterns. Metastable states are formed at T = 2.7 suggesting critical, "edge-of-chaos" behavior. Higher T leads to more random patterns, whereas lower T yields hyper-synchronous, stereotypic patterns.

to that obtained from computer simulations on an Ising system. Their simulation was not constrained by actual empirical data. Das et al. (2014) also used the two-dimensional Ising model to illustrate the similarity of measured and simulated fMRI BOLD signals in human subjects. Different from our study, they analyzed BOLD signal distributions above and below threshold to show that the Ising model can predict activity patterns similar to that of BOLD.

Our simulation was different from both of these studies in that ours was based on long-range interactions derived from empirical BOLD functional connectivity. The spatial distribution of interacting sites was determined by the strength of long-range correlations. As a result, the predicted global states resembled large-scale functional patterns of the human brain. Finally, we simulated global brain states at different activation levels.

Another recent simulation study applied the Ising model to fiber-tract data obtained with diffusion tensor imaging (Marinazzo et al., 2014). The outgoing and the incoming information at each network node was quantified as related to the summated input weights and to the time elapsed between consecutive flips of Ising spins. The simulation predicted critical behavior although the profile of state transition was not as rapid as in our simulation.

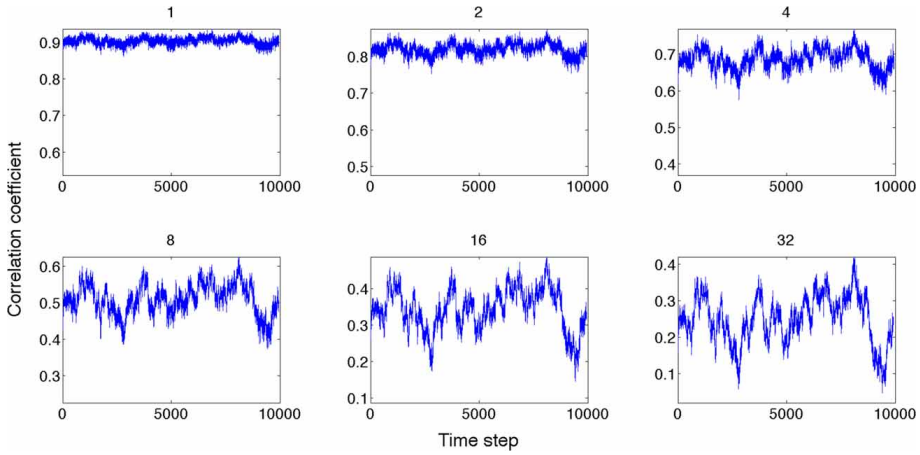

FIGURE 6 | Global state correlation as a function of time at various time lags (shown on top of each panel). Global state patterns become decorrelated at increasing time delays.

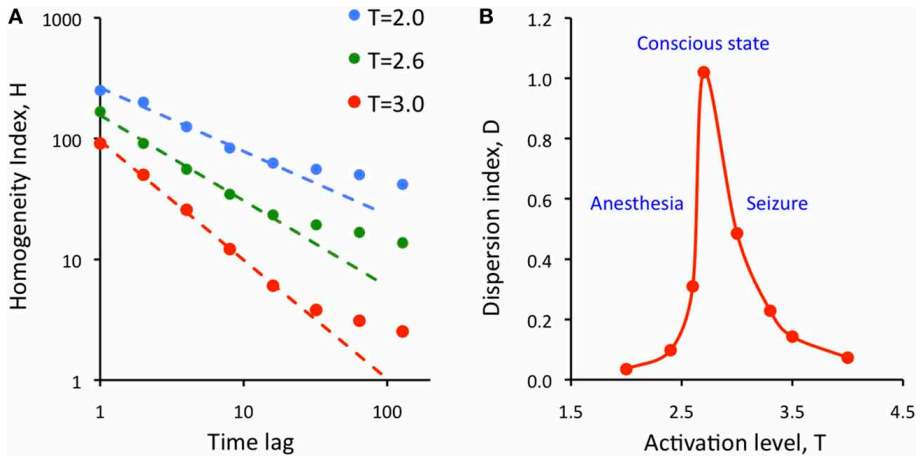

FIGURE 7 | Dependence of the state repertoire on cortical activation level and embedding time lag. (A) Homogeneity index, H decreases as a function of the time lag of according to power law up to a lag of 20. Decreasing the activation level T (anesthesia) decreases the regression slope. **(B)** Dispersion index, D shows critical behavior as a function of activation level, T. Maximum of D is thought to correspond to the conscious state. D drops at low T (anesthesia) and at high T (seizure).

It could be argued that fiber tract distribution is a more appropriate constraint for the model than functional connectivity. Functional connectivity may not always correspond to direct anatomical connection due to common input or third party interactions. However, a counter argument is that only a fraction of fiber tracts may be used for neuronal communication at any one time, and, therefore, functional connectivity provides a better approximation of the probability of functional interactions regardless of the exact underlying mechanism. Conceivably, real-time measurement of neuronal communication across the whole brain will be the ideal data used as an input to the model when such technology becomes available in the future.

The neurophysiological relevance of the spin-glass model depends on the temporal and spatial scales that it represents. Although the temporal scale of the simulation is arbitrary, it can be grounded in real neuronal events based on empirical data. Spontaneous activity of neuronal populations forms transient spatiotemporal clusters often described as neuronal avalanches (Beggs and Plenz, 2003). The time scale of these events is on the order of 10 ms. Such an alternation between activity and silence of neuronal populations is consistent with the representation of UP and DOWN states of mesoscopic sites in the spin-glass model. On a global spatial scale, EEG topographic maps alternate among microstates at a time scale of approximately 100 ms (Koenig et al., 2002). These states have been linked to fMRI signals (Lehmann, 2010; Musso et al., 2010). The temporal resolution of elementary conscious sensory perception also falls in this order (Bachmann, 2013). The lifetime of the simulated metastable states depends on the chosen level of similarity of the states, i.e., the minimum cross-correlation coefficient at which they are considered equivalent. Accepting a cross-correlation threshold of 0.95, the median lifetime of metastable states at the critical activation

level is around 440 ms that is in the timeframe of cognitive phenomena.

We found that the homogeneity index H depended on the embedding time lag according to power law, suggesting scale-free behavior up to a lag of approximately 20 time steps. Based on the preceding considerations, 20 time steps would correspond to approximately 200 ms duration, which agrees with the presumed unit of processing time for conscious computations. Nevertheless, the power law of H does not imply criticality because the power law exponent was close to −1.0 (at T = 3) or less, not −1.5 as previously proposed for critical processes (Beggs and Plenz, 2003). On the other hand, the dispersion index D suggests critical behavior at the phase transition at T = 2.7. D measures the overall diversity of global state configurations across all time points, not only the states' consecutive (or delayed) similarity as H does. At low T, D is small because global brain states are highly correlated and thus (1−cc) is low. Because the sites stochastically fluctuate between UP and DOWN states, the variance of cc does not go to zero and D does not diverge. At high T, D is small again because the variance is large due to the intense random fluctuations. Thus D is high only at intermediate T. The repertoire of global states accessed by the brain over time reaches maximum at a critical point.

During the course of clustering global brain states, a challenge was to define their similarity at a mesoscopic scale with 5000 sites per hemisphere. On one hand, cluster membership had to be defined at a chosen degree of similarity; the number of distinct brain states depended on this choice. We carried out clustering at 99.0 and 99.9% similarity; yielding a higher number of distinct states when the similarity requirement was stricter. Another factor that influenced the clustering was the degree of spatial averaging, for which we used either a 5 or 15 mm radius. This choice made a significant difference at 99.9% similarity but it made very little difference at 99.0% similarity. Guided by these preliminary assessments, we chose 15 mm spatial averaging and 99.0% similarity level for the final simulations.

In this work we sought to gain insight into the possible diversity and dynamics of UP/DOWN state patterns as a measure of complex brain states. It has been hypothesized that dynamic states of connectivity represent modes of cognitive information processing in the brain (Bressler and Menon, 2010). Moreover, the diversity or *repertoire* of brain sates has been postulated as one of the fundamental conditions for information integration in the conscious state or more specifically consciousness itself (Tononi, 2008).

In the spin-glass model, the overall probability of UP/DOWN transitions of mesoscopic sites was controlled by the global activation level T. We saw that at a critical activation level, large-scale metastable states were frequent, and the diversity of global brain states was enhanced. Although this may not be a stable state *in vivo*, approaching criticality may be facilitated by the phasic increases in ascending arousal (Buzsaki et al., 1988), which would repeatedly randomize the system (at high T), and then allow it to sink into new configurations. The latter may have an additional effect on augmenting the repertoire of brain states over time.

If information processing indeed depends on the repertoire of brain states, the question one may ask is how many distinct brain states exist. The answer to this question obviously depends on what we consider the smallest units of the system. The organizational complexity and the number of distinct functional states of the brain would plausibly increase at finer spatial and temporal scales, spanning several hierarchical levels from synapses, neurons, local circuits, to regions and networks. Although the spatiotemporal resolution of fMRI is relatively coarse, the number of combinatorially possible network patterns defined at near voxel level is enormous, and properly sampling these patterns using fMRI is limited. Computer simulation helps extend our ability to estimate the brains state repertoire within empirically set constraints.

An application of interest of the model is examining the effects of general anesthesia, which is characterized by reduced global activation due to a suppression of the ascending arousal system (Nelson et al., 2002; Alkire et al., 2007). As we saw, decreasing the activation level T retards the dynamic transition of global metastable states by reducing the probability of UP/DOWN transitions. As a result, fewer distinct brain states occur over time, which predicts reduced information capacity. As we formerly argued, a reduction in the repertoire of global brain states may underlie anesthetic loss of consciousness (Alkire et al., 2008). An alternative mechanism that may diminish information integration during anesthesia is the weakening of site interactions. This may lead to breakdown of meaningful communication within the brain's critically important functional networks. Although this has not been tested here, the overall effect of reduced connectivity on the global dynamics is expected to be similar to that of reduced cortical arousal. Both mechanisms are likely at work in the mediation of the anesthetic effect.

Although we have emphasized the application to anesthesia, the simulation results equally apply to altered states of consciousness such as deep sleep, vegetative state, coma, or, at the other end of the spectrum, seizure. We saw that both low and high activation levels reduced the diversity of global brain states, presumably pushing the brain away from optimal information processing and integration.

Current views differ on whether critical behavior in the cortex is associated with normal conscious behavior or a transition to altered states of consciousness. Previously, Steyn-Ross et al. (1999) examined first-order phase transitions using a mean-field model of excitatory and inhibitory neuronal groups with relevance to the anesthetic modulation of the state of consciousness. They hypothesized that the anesthetic acted as a randomizing agent to break down the connections between interacting neuronal populations and that this loss of neuronal cooperativity accounted for the loss of consciousness under anesthesia. Alternatively, spontaneous ongoing activity may play a role in inducing state transitions that may be important for maintaining conscious awareness. Recently, Steyn-Ross et al. (2009) suggested that patterns of cortical activation arise from spontaneous self-organization of interacting neuronal populations at a mesoscopic scale. They simulated metastable activation patterns that were altered when the somato-dendritic feedback of neurons was reduced; reflecting a decrease in excitatory neuro-modulation as seen during sleep or anesthesia. We interpret our simulations to be consistent with the ongoing formation of a large diversity of

metastable states that are essential for the stream of conscious thought (Werner, 2009). Although the patterns also change spontaneously, fluctuations in the level of cortical activation (cortical arousal) via its randomizing effect may facilitate the rapid formation and transition of consecutive activity patterns, thereby further augmenting the repertoire states accessed by the brain over time.

ACKNOWLEDGMENTS

Research reported in this publication was supported by the National Institute of General Medical Sciences of the National Institutes of Health under Award Numbers R01-GM056398 and R01-GM103894. The content is solely the responsibility of the authors and does not necessarily represent the official views of the National Institutes of Health.

SUPPLEMENTARY MATERIAL

The Supplementary Material for this article can be found online at: http://www.frontiersin.org/journal/10.3389/fnsys.2014.00234/abstract

REFERENCES

Alkire, M. T., Hudetz, A. G., and Tononi, G. (2008). Consciousness and anesthesia. *Science* 322, 876–880. doi: 10.1126/science.1149213

Alkire, M. T., Mcreynolds, J. R., Hahn, E. L., and Trivedi, A. N. (2007). Thalamic microinjection of nicotine reverses sevoflurane-induced loss of righting reflex in the rat. *Anesthesiology* 107, 264–272. doi: 10.1097/01.anes.0000270741.33766.24

Allen, E. A., Damaraju, E., Plis, S. M., Erhardt, E. B., Eichele, T., and Calhoun, V. D. (2012). Tracking whole-brain connectivity dynamics in the resting state. *Cereb. Cortex* 24, 663–676. doi: 10.1093/cercor/bhs352

Bachmann, T. (2013). On the all-or-none rule of conscious perception. *Front. Hum. Neurosci.* 7:387. doi: 10.3389/fnhum.2013.00387

Beggs, J. M. (2008). The criticality hypothesis: how local cortical networks might optimize information processing. *Philos. Trans. A Math. Phys. Eng. Sci.* 366, 329–343. doi: 10.1098/rsta.2007.2092

Beggs, J. M., and Plenz, D. (2003). Neuronal avalanches in neocortical circuits. *J. Neurosci.* 23, 11167–11177.

Bhowmik, D., and Shanahan, M. (2013). Metastability and inter-band frequency modulation in networks of oscillating spiking neuron populations. *PLoS ONE* 8:e62234. doi: 10.1371/journal.pone.0062234

Bressler, S. L., and Menon, V. (2010). Large-scale brain networks in cognition: emerging methods and principles. *Trends Cogn. Sci.* 14, 277–290. doi: 10.1016/j.tics.2010.04.004

Britz, J., Van De Ville, D., and Michel, C. M. (2010). BOLD correlates of EEG topography reveal rapid resting-state network dynamics. *Neuroimage* 52, 1162–1170. doi: 10.1016/j.neuroimage.2010.02.052

Buzsaki, G., Bickford, R. G., Ponomareff, G., Thal, L. J., Mandel, R., and Gage, F. H. (1988). Nucleus basalis and thalamic control of neocortical activity in the freely moving rat. *J. Neurosci.* 8, 4007–4026.

Chang, C., and Glover, G. H. (2010). Time-frequency dynamics of resting-state brain connectivity measured with fMRI. *Neuroimage* 50, 81–98. doi: 10.1016/j.neuroimage.2009.12.011

Cribben, I., Wager, T. D., and Lindquist, M. A. (2013). Detecting functional connectivity change points for single-subject fMRI data. *Front. Comput. Neurosci.* 7:143. doi: 10.3389/fncom.2013.00143

Das, T. K., Abeyasinghe, P. M., Crone, J. S., Sosnowski, A., Laureys, S., Owen, A. M., et al. (2014). Highlighting the structure-function relationship of the brain with the ising model and graph theory. *BioMed Res. Int.* 2014, 14. doi: 10.1155/2014/237898

Deco, G., Hagmann, P., Hudetz, A. G., and Tononi, G. (2014). Modeling resting-state functional networks when the cortex falls sleep: local and global changes. *Cereb Cortex* 12, 3180–3194. doi: 10.1093/cercor/bht176

Deco, G., and Jirsa, V. K. (2012). Ongoing cortical activity at rest: criticality, multistability, and ghost attractors. *J. Neurosci.* 32, 3366–3375. doi: 10.1523/JNEUROSCI.2523-11.2012

Di, X., and Biswal, B. B. (2013). Dynamic brain functional connectivity modulated by resting-state networks. *Brain Struct. Funct.* doi: 10.1007/s00429-013-0634-3. [Epub ahead of print].

Fischl, B., Sereno, M. I., and Dale, A. M. (1999). Cortical surface-based analysis. II: Inflation, flattening, and a surface-based coordinate system. *Neuroimage* 9, 195–207. doi: 10.1006/nimg.1998.0396

Fraiman, D., Balenzuela, P., Foss, J., and Chialvo, D. R. (2009). Ising-like dynamics in large-scale functional brain networks. *Phys. Rev. E Stat. Nonlin. Soft Matter Phys.* 79:061922. doi: 10.1103/PhysRevE.79.061922

Freeman, W. J., and Holmes, M. D. (2005). Metastability, instability, and state transition in neocortex. *Neural Netw.* 18, 497–504. doi: 10.1016/j.neunet.2005.06.014

Fricke, T. (2006). Monte Carlo investigation of the Ising model. 1–7. Available online at: http://www.physics.ohio-state.edu/~braaten/statphys/Ising_MatLab.pdf

Friston, K. J. (1997). Transients, metastability, and neuronal dynamics. *Neuroimage* 5, 164–171. doi: 10.1006/nimg.1997.0259

Glerean, E., Salmi, J., Lahnakoski, J. M., Jaaskelainen, I. P., and Sams, M. (2012). Functional magnetic resonance imaging phase synchronization as a measure of dynamic functional connectivity. *Brain Connect.* 2, 91–101. doi: 10.1089/brain.2011.0068

Handwerker, D. A., Roopchansingh, V., Gonzalez-Castillo, J., and Bandettini, P. A. (2012). Periodic changes in fMRI connectivity. *Neuroimage* 63, 1712–1719. doi: 10.1016/j.neuroimage.2012.06.078

Hudetz, A. G., Liu, X., and Pillay, S. (2014). Dynamic repertoire of intrinsic brain states is reduced in propofol-induced unconsciousness. *Brain Connect.* doi: 10.1089/brain.2014.0230. [Epub ahead of print].

Hudson, A. E., Calderon, D. P., Pfaff, D. W., and Proekt, A. (2014). Recovery of consciousness is mediated by a network of discrete metastable activity states. *Proc. Natl. Acad. Sci. U.S.A.* 111, 9283–9288. doi: 10.1073/pnas.1408296111

Hutchison, R. M., Womelsdorf, T., Allen, E. A., Bandettini, P. A., Calhoun, V. D., Corbetta, M., et al. (2013a). Dynamic functional connectivity: promise, issues, and interpretations. *Neuroimage* 80, 360–378. doi: 10.1016/j.neuroimage.2013.05.079

Hutchison, R. M., Womelsdorf, T., Gati, J. S., Everling, S., and Menon, R. S. (2013b). Resting-state networks show dynamic functional connectivity in awake humans and anesthetized macaques. *Hum. Brain Mapp.* 34, 2154–2177. doi: 10.1002/hbm.22058

Jones, D. T., Vemuri, P., Murphy, M. C., Gunter, J. L., Senjem, M. L., Machulda, M. M., et al. (2012). Non-stationarity in the "resting brain's" modular architecture. *PLoS ONE* 7:e39731. doi: 10.1371/journal.pone.0039731

Kang, J., Wang, L., Yan, C., Wang, J., Liang, X., and He, Y. (2011). Characterizing dynamic functional connectivity in the resting brain using variable parameter regression and Kalman filtering approaches. *Neuroimage* 56, 1222–1234. doi: 10.1016/j.neuroimage.2011.03.033

Keilholz, S. D., Magnuson, M. E., Pan, W. J., Willis, M., and Thompson, G. J. (2013). Dynamic properties of functional connectivity in the rodent. *Brain Connect.* 3, 31–40. doi: 10.1089/brain.2012.0115

Kello, C. T., Anderson, G. G., Holden, J. G., and Van Orden, G. C. (2008). The Pervasiveness of 1/f scaling in speech reflects the metastable basis of cognition. *Cogn. Sci.* 32, 1217–1231. doi: 10.1080/03640210801944898

Kelso, J. A. (2012). Multistability and metastability: understanding dynamic coordination in the brain. *Philos. Trans. R Soc. Lond. B Biol. Sci.* 367, 906–918. doi: 10.1098/rstb.2011.0351

Kitzbichler, M. G., Smith, M. L., Christensen, S. R., and Bullmore, E. (2009). Broadband criticality of human brain network synchronization. *PLoS Comput. Biol.* 5:e1000314. doi: 10.1371/journal.pcbi.1000314

Kiviniemi, V., Vire, T., Remes, J., Elseoud, A., Starck, T., Tervonen, O., et al. (2011). A sliding time-window ICA reveals spatial variability of the default mode network in time. *Brain Connect.* 1, 339–347. doi: 10.1089/brain.2011.0036

Koenig, T., Prichep, L., Lehmann, D., Sosa, P. V., Braeker, E., Kleinlogel, H., et al. (2002). Millisecond by millisecond, year by year: normative EEG microstates and developmental stages. *Neuroimage* 16, 41–48. doi: 10.1006/nimg.2002.1070

Lee, U., Oh, G., Kim, S., Noh, G., Choi, B., and Mashour, G. A. (2010). Brain networks maintain a scale-free organization across consciousness, anesthesia, and recovery: evidence for adaptive reconfiguration. *Anesthesiology* 113, 1081–1091. doi: 10.1097/ALN.0b013e3181f229b5

Lehmann, D. (2010). Multimodal analysis of resting state cortical activity: what does fMRI add to our knowledge of microstates in resting state

EEG activity? Commentary to the papers by Britz et al. and Musso et al. in the current issue of NeuroImage. *Neuroimage* 52, 1173–1174. doi: 10.1016/j.neuroimage.2010.05.033

Liu, X., and Duyn, J. H. (2013). Time-varying functional network information extracted from brief instances of spontaneous brain activity. *Proc. Natl. Acad. Sci. U.S.A.* 110, 4392–4397. doi: 10.1073/pnas.1216856110

Liu, X., Ward, B. D., Binder, J. R., Li, S. J., and Hudetz, A. G. (2014). Scale-free functional connectivity of the brain is maintained in anesthetized healthy participants but not in patients with unresponsive wakefulness syndrome. *PLoS ONE* 9:e92182. doi: 10.1371/journal.pone.0092182

Liu, Z., De Zwart, J. A., Chang, C., Duan, Q., Van Gelderen, P., and Duyn, J. H. (2013). Neuroelectrical decomposition of spontaneous brain activity measured with functional magnetic resonance imaging. *Cereb. Cortex* 24, 3080–3089. doi: 10.1093/cercor/bht164

Marinazzo, D., Pellicoro, M., Wu, G., Angelini, L., Cortes, J. M., and Stramaglia, S. (2014). Information transfer and criticality in the Ising model on the human connectome. *PLoS ONE* 9:e93616. doi: 10.1371/journal.pone.0093616

Mckiernan, K. A., D'angelo, B. R., Kaufman, J. N., and Binder, J. R. (2006). Interrupting the "stream of consciousness": an fMRI investigation. *Neuroimage* 29, 1185–1191. doi: 10.1016/j.neuroimage.2005.09.030

Metropolis, N., Rosenbluth, A. W., Rosenbluth, M. N., Teller, A. H., and Teller, E. (1953). Equation of state calculations by fast computing machines. *J. Chem. Phys.* 21, 1087–1092. doi: 10.1063/1.1699114

Musso, F., Brinkmeyer, J., Mobascher, A., Warbrick, T., and Winterer, G. (2010). Spontaneous brain activity and EEG microstates. A novel EEG/fMRI analysis approach to explore resting-state networks. *Neuroimage* 52, 1149–1161. doi: 10.1016/j.neuroimage.2010.01.093

Nelson, L. E., Guo, T. Z., Lu, J., Saper, C. B., Franks, N. P., and Maze, M. (2002). The sedative component of anesthesia is mediated by GABA(A) receptors in an endogenous sleep pathway. *Nat. Neurosci.* 5, 979–984. doi: 10.1038/nn913

Sakoglu, U., Pearlson, G. D., Kiehl, K. A., Wang, Y. M., Michael, A. M., and Calhoun, V. D. (2010). A method for evaluating dynamic functional network connectivity and task-modulation: application to schizophrenia. *MAGMA* 23, 351–366. doi: 10.1007/s10334-010-0197-8

Sethian, J. A. (1996). A fast marching level set method for monotonically advancing fronts. *Proc. Natl. Acad. Sci. U.S.A.* 93, 1591–1595. doi: 10.1073/pnas.93.4.1591

Smith, S. M., Miller, K. L., Moeller, S., Xu, J., Auerbach, E. J., Woolrich, M. W., et al. (2012). Temporally-independent functional modes of spontaneous brain activity. *Proc. Natl. Acad. Sci. U.S.A.* 109, 3131–3136. doi: 10.1073/pnas.1121329109

Steyn-Ross, M. L., Steyn-Ross, D. A., Sleigh, J. W., and Liley, D. T. (1999). Theoretical electroencephalogram stationary spectrum for a white-noise-driven cortex: evidence for a general anesthetic-induced phase transition. *Phys. Rev. E Stat. Phys. Plasmas Fluids Relat. Interdiscip. Topics* 60, 7299–7311. doi: 10.1103/PhysRevE.60.7299

Steyn-Ross, M. L., Steyn-Ross, D. A., Wilson, M. T., and Sleigh, J. W. (2009). Modeling brain activation patterns for the default and cognitive states. *Neuroimage* 45, 298–311. doi: 10.1016/j.neuroimage.2008.11.036

Tagliazucchi, E., Balenzuela, P., Fraiman, D., and Chialvo, D. R. (2012). Criticality in large-scale brain FMRI dynamics unveiled by a novel point process analysis. *Front. Physiol.* 3:15. doi: 10.3389/fphys.2012.00015

Tagliazucchi, E., Balenzuela, P., Fraiman, D., Montoya, P., and Chialvo, D. R. (2011). Spontaneous BOLD event triggered averages for estimating functional connectivity at resting state. *Neurosci. Lett.* 488, 158–163. doi: 10.1016/j.neulet.2010.11.020

Tognoli, E., and Kelso, J. A. (2014). The metastable brain. *Neuron* 81, 35–48. doi: 10.1016/j.neuron.2013.12.022

Tononi, G. (2008). Consciousness as integrated information: a provisional manifesto. *Biol. Bull.* 215, 216–242. doi: 10.2307/25470707

Werner, G. (2007). Metastability, criticality and phase transitions in brain and its models. *Biosystems* 90, 496–508. doi: 10.1016/j.biosystems.2006.12.001

Werner, G. (2009). Viewing brain processes as critical state transitions across levels of organization: neural events in cognition and consciousness, and general principles. *Biosystems* 96, 114–119. doi: 10.1016/j.biosystems.2008.11.011

Conflict of Interest Statement: The authors declare that the research was conducted in the absence of any commercial or financial relationships that could be construed as a potential conflict of interest.

Received: 26 September 2014; accepted: 24 November 2014; published online: 11 December 2014.

Citation: Hudetz AG, Humphries CJ and Binder JR (2014) Spin-glass model predicts metastable brain states that diminish in anesthesia. Front. Syst. Neurosci. ***8****:234. doi: 10.3389/fnsys.2014.00234*

This article was submitted to the journal Frontiers in Systems Neuroscience.

frontiers in
SYSTEMS NEUROSCIENCE

ORIGINAL RESEARCH ARTICLE
published: 29 October 2014
doi: 10.3389/fnsys.2014.00215

EEG slow-wave coherence changes in propofol-induced general anesthesia: experiment and theory

Kaier Wang[1], Moira L. Steyn-Ross[1], D. A. Steyn-Ross[1]*, Marcus T. Wilson[1] and Jamie W. Sleigh[2]

[1] *School of Engineering, The University of Waikato, Hamilton, New Zealand*
[2] *Waikato Clinical School, The University of Auckland, Waikato Hospital, Hamilton, New Zealand*

Edited by:
Axel Hutt, INRIA CR Nancy, France

Reviewed by:
Axel Hutt, INRIA CR Nancy, France
Jens Christian Claussen, Jacobs University Bremen, Germany
Helmut Schmidt, University of Exeter, UK

****Correspondence:***
D. A. Steyn-Ross, School of Engineering, The University of Waikato, Private Bag 3105, Hamilton 3240, New Zealand
e-mail: asr@waikato.ac.nz

The electroencephalogram (EEG) patterns recorded during general anesthetic-induced coma are closely similar to those seen during slow-wave sleep, the deepest stage of natural sleep; both states show patterns dominated by large amplitude slow waves. Slow oscillations are believed to be important for memory consolidation during natural sleep. Tracking the emergence of slow-wave oscillations during transition to unconsciousness may help us to identify drug-induced alterations of the underlying brain state, and provide insight into the mechanisms of general anesthesia. Although cellular-based mechanisms have been proposed, the origin of the slow oscillation has not yet been unambiguously established. A recent theoretical study by Steyn-Ross et al. (2013) proposes that the slow oscillation is a network, rather than cellular phenomenon. Modeling anesthesia as a moderate reduction in gap-junction interneuronal coupling, they predict an unconscious state signposted by emergent low-frequency oscillations with chaotic dynamics in space and time. They suggest that anesthetic slow-waves arise from a competitive interaction between symmetry-breaking instabilities in space (Turing) and time (Hopf), modulated by gap-junction coupling strength. A significant prediction of their model is that EEG phase coherence will decrease as the cortex transits from Turing–Hopf balance (wake) to Hopf-dominated chaotic slow-waves (unconsciousness). Here, we investigate changes in phase coherence during induction of general anesthesia. After examining 128-channel EEG traces recorded from five volunteers undergoing propofol anesthesia, we report a significant drop in sub-delta band (0.05–1.5 Hz) slow-wave coherence between frontal, occipital, and frontal–occipital electrode pairs, with the most pronounced wake-vs.-unconscious coherence changes occurring at the frontal cortex.

Keywords: slow-wave sleep, phase-coherence measure, mean-field cortical model, gap-junction, Turing–Hopf instabilities

1. INTRODUCTION

General anesthetic drugs act to suppress the conscious state of the cortex, leading it to a natural sleep-like mode (Lancel, 1999; Franks, 2008). There is clinical evidence showing that such sedated unconsciousness can be induced by the injection of anesthetic substances into some discrete brain areas which are critical in the coordination of sleep-wake transitions (Sukhotinsky et al., 2007). Further evidence to support the notion of strong similarity between natural deep sleep and anesthesia can be seen in the electrical activity of the cortex: both states are signposted by the abrupt onset of large, slow oscillations (0.1–1.5 Hz) in the electroencephalogram (EEG) and local field potential (Steriade et al., 1993). These rhythmic signals, which sweep through the brain during deep sleep at the rate of about 1 cycle per second (Massimini et al., 2004), have been shown to play a role in memory encoding and consolidation (Steriade and Timofeev, 2002; Walker, 2009).

Although EEG slow waves are manifest in an unconscious state, they are also superimposed on the alpha and theta waves when our brain is in a low conscious level, the so-called "idling" state where the brain is not engaged in the active processing of information (Uusberg et al., 2013). Clinical studies show a stable increase in power of the lowest frequency components of the EEG signal as anesthesia deepens, while higher frequency components (theta, alpha, gamma) are highly variable during and after loss of consciousness (Sleigh et al., 2000; Lewis et al., 2012). Thus, tracking the emergence of slow-wave oscillations during transition to unconsciousness may help us to identify drug-induced alterations of the underlying brain state, and provide insight into the mechanisms of general anesthesia.

In the last decades, there has been a growing understanding of how slow waves are generated during sleep. Steriade et al. (1989) reported slow-wave activity (SWA) from *in vitro* thalamic slices. In thalamocortical (TC) neurons, SWA depends on voltage-sensitive properties of low-threshold calcium channels [known as "T" type (David et al., 2013)] that may provide a pacemaking role, mediating the transition between tonic firing and low-threshold spiking (Suzuki and Rogawski, 1989; Astori et al., 2011). However, the "clock-like" SWA generated by TC neurons is more regular than that of slow-wave sleep (Nir et al., 2010). Further, it is known

that *in vitro* cortical slices can produce slow oscillations of local field potential in the absence of thalamic inputs (McCormick and Sanchez-Vives, 2000). So slow rhythmic thalamic activity may not be relevant to the onset of slow cortical waves.

Human EEG recordings show that the slow oscillations seem to originate from nearly any region of the scalp and behave as a traveling wave propagating in any direction (Massimini et al., 2004). Yet, recent clinical studies demonstrate that the slow waves can be locally regulated (Huber et al., 2004, 2006; Murphy et al., 2009). Therefore, questions remain about where slow waves originate and whether all cortical areas engage equally in slow-wave activity.

To help address this deficit, Steyn-Ross et al. (2013) presented a physiologically-motivated mathematical model of the cortex that demonstrates how coupling via inhibitory electrical synapses (gap-junctions) mediates the generation of propofol anesthetic slow waves. The model envisions the cortex as a *mean-field* continuum in which pools of neurons are linked via chemical and electrical synapses. GABAergic anesthetic agents, such as propofol, act at chemical synapses to hyperpolarize postsynaptic neurons by prolonging the duration of the inhibitory postsynaptic potential (IPSP) via increased influx of chloride ions (Franks and Lieb, 1994; Kitamura et al., 2003). In addition to chemical neuromodulation, there is evidence that propofol reduces the resistive gap-junction coupling between adjoining inhibitory neurons (Wentlandt et al., 2006; Huang et al., 2014) that is proposed to form a broad diffusive syncytium linking inhibitory neural populations (Fukuda et al., 2006). Accordingly, we model anesthetic effect as a moderate reduction in inhibitory diffusion, paired with an increase in inhibitory postsynaptic potential. In the vicinity of a general-anesthetic induced transition from wake to coma, the Steyn-Ross model describes a subtle rebalancing of cortical Turing (spatial) and Hopf (temporal) instabilities to an unconscious state that is characterized by Hopf-dominated slow waves whose dynamics is chaotic in time and space.

Identifying the specific dynamics of slow waves associated with loss of consciousness requires an examination of the transition into unconsciousness. In this paper, we examine the clinical EEG recordings in terms of slow-wave phase-coherence between different electrode-pairs, comparing coherence values before and after the induction of propofol anesthetic. Propofol, a widely used anesthetic drug, enhances GABAergic inhibitory input to neurons (Bai et al., 1999; Rudolph and Antkowiak, 2004), with effects in cortex, brainstem, thalamus and spinal cord (Fiset et al., 1999; Kungys et al., 2009). EEG coherence is considered to be a qualitative measure of the degree of association or coupling between two EEG channels. Coherence estimation for high-density EEG recording is able to demonstrate functional cooperation between two brain regions (Nunez and Srinivasan, 2006), revealing subtle changes in brain dynamics. We compare our findings with a testable prediction by Steyn-Ross et al. (2013) and illustrated here in **Figures 9E**, **10E**, **11** (compare "non-cognitive wake" with "anesthetic slow-wave"): namely, introduction of anesthetic to the awake brain should lead to a significant *decline* in low-frequency EEG phase-synchrony.

2. MATERIALS

The EEG dataset used in this study are archived files from Waikato Clinical School, Hamilton, New Zealand, previously used to investigate anesthetic response of EEG across different frequency bands (Johnson et al., 2003). The dataset contains pairs of 60-s EEG (sampling frequency 250 Hz) recordings for two distinct well-developed brain states: wake and propofol anesthetic coma, recorded from 5 healthy adult subjects via 129 electrodes[1] using an EGI™ dense array with Cz (vertex) being the reference electrode. The archival EEG dataset are manually selected epochs that are relatively artifact-free.

An example of EEG recorded from electrode Fp1 is represented in **Figure 1**. This demonstrates the clear contrast between wakefulness (upper EEG trace) and sedated unconsciousness (lower trace) with the appearance of spindles (12–15 Hz) and slow rhythms including delta activity (1–4 Hz) and slow oscillations (0.2–1 Hz). By focusing on the EEG in sub-delta band ($\leq$1.5 Hz), **Figure 2** shows that the power of the slow-waves in sedated unconsciousness is nearly twice as large as that in the wake state.

3. METHODS

3.1. MEASURING EEG COHERENCE

EEG coherence between two electrode sites is usually computed by one of two methods: the Fourier transform (FT) cross spectrum (Achermann and Borbely, 1998), or the Hilbert transform (HT) instantaneous phase difference (Mormann et al., 2000) between two EEG time-series.

Since EEG represents the activities of the non-linearly interacting neuronal populations, it is neither truly linear nor stationary. Thus, it may be unreliable to use FT-based methods for EEG analysis since these assume that the time-series is stationary (Lo et al., 2009; Zhang et al., 2010).

The Hilbert transform (Huang et al., 1998; Sweeney-Reed and Nasuto, 2007) circumvents the requirement for stationarity by generating an analytic signal to extract the instantaneous frequency and phase angle from the original non-stationary signal. The mean of the phase divergence between two time-series yields an index characterizing the phase synchronization between them. The advantages of the HT over the traditional FT-based approaches have been appreciated in many studies of cortical neuronal synchronization under different circumstances such as Parkinson's disease (Tass et al., 1998), abrupt seizure (Oweis and Abdulhay, 2011), sleep (Yi et al., 2009), and anesthetic coma (Koskinen et al., 2001).

3.2. HILBERT TRANSFORM

A real time-series $X(t)$ can be transformed to a complex function known as the analytic signal:

$$\hat{X}(t) = X_r(t) + iX_i(t) \quad (1)$$

where $X_r(t)$ is the original series $X(t)$ and $X_i(t)$ is the Hilbert transform of $X(t)$ (Mormann et al., 2000; Koskinen et al., 2001). The instantaneous phase of $X(t)$ is computed by:

[1]The electrodes map is available at http://psychophysiology.cpmc.columbia.edu/software/CSDtoolbox/tutorial.html

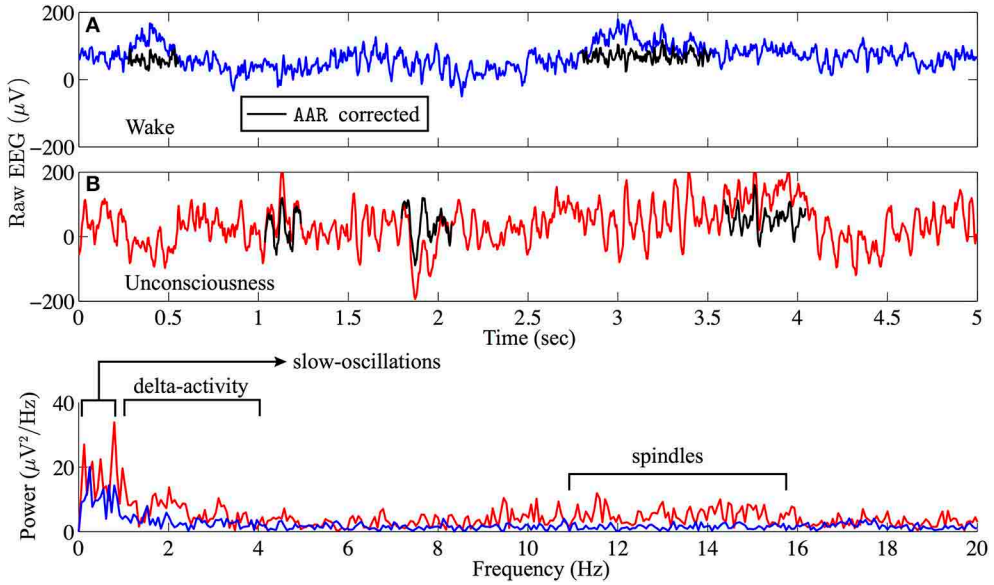

FIGURE 1 | Sample (A) wake (blue) and (B) sedated unconsciousness (red) EEG from archival Fp1 recording. Raw EEG data are filtered via AAR[2] to remove eye-blink artifacts. AAR-corrected EEG are marked in black. The power spectra show that slow-wave oscillations are dominant in the sedated unconsciousness state.

$$\phi(t) = \tan^{-1}\left(\frac{X_i(t)}{X_r(t)}\right) \tag{2}$$

To quantify the phase synchronization between two time-series $X_m(t)$ and $X_n(t)$, a coherence index based on work by Kuramoto (Kuramoto, 1984; Kuramoto and Nishikawa, 1987) is used:

$$R_{(m,n)} = |\langle e^{i[\phi_m(t)-\phi_n(t)]}\rangle| \tag{3}$$

The mean phase coherence R measures the time-averaged phasor for the angular distribution of the phase difference between the two time-series; R lies between 0 and 1, with 1 representing perfect phase coupling. This style of Kuramoto order-parameter has been widely used in the study of synchronization dynamics (e.g., Acebrón et al., 2005; Steyn-Ross et al., 2013).

A MATLAB implementation for computing the mean phase coherence between two signals reads as follows Steyn-Ross et al. (2012):

```
% Compute analytic (complex) signals for Xm and Xn
  Xmc = hilbert(Xm);  Xnc = hilbert(Xn);
% Extract instantaneous phase angles
  phi_Xm = angle(Xmc); phi_Xn = angle(Xnc);
% Measure the average phase-coherence
  R = abs(mean(exp( 1i*(phi_Xm - phi_Xn))));
```

[2]Automatic Artifact Removal toolbox, an EEGLAB plug-in available at http://www.germangh.com/eeglab_plugin_aar/index.html
AAR is based on blind source separation (BSS), and, in contrast to methods already available in the literatures (Jung et al., 2000; Faul et al., 2005), is completely automatic since the user is not required to select any critical analysis parameter. AAR uses a second-order-blind-identification (SOBI) algorithm (Belouchrani et al., 1997) to estimate the mixing matrix that separates the EEG sources and artifacts. The advantages of SOBI over other BSS algorithms are detailed in Gomez-Herrero et al. (2006).

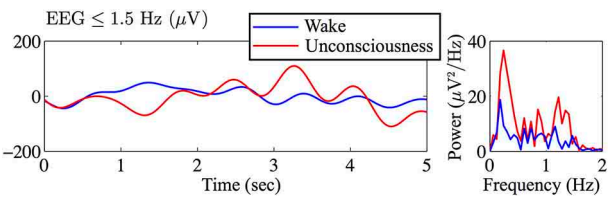

FIGURE 2 | Filtered Figure 1 EEG in sub-delta band (≤1.5 Hz) and corresponding power spectra (computed by MATLAB fft) revealing a strong slow-wave (~0.3 Hz) in the sedated unconsciousness state.

Let $X_m(t)$ and $X_n(t)$ be a pair of EEG recordings, respectively, from the electrodes m and n. A 129-channel EEG recording has, in principle, a total of 128 × 128 pairs of R-values (excluding the reference channel), but half of these are redundant since $R_{(m,n)} = R_{(n,m)}$. The coherence matrix is represented as an $m \times n = 128 \times 128$ square grid with the unit diagonal $[R_{(m,n)} = 1$ when $m = n]$, which separates the matrix into two symmetrical triangles $[R_{(m,n)} = R_{(n,m)}]$. Practically, we need only examine the upper triangle [i.e., $R_{(m,n)}$] of the R matrix. See **Figures 3**, **9E** for an illustration of the structure of the coherence matrix.

For coherence calculations, we use a 5-s moving window with 1-s overlap, and follow Mormann et al. (2000) and Steyn-Ross et al. (2012, 2013) in applying a Hann window, retaining only the middle 80% of each segment to minimize edge distortions from the Hilbert transform. The final determined coherence is the average of those obtained from the windowed signal segments. We repeated the coherence calculations using longer windows, including the full 60-s extent, and found no significant changes, so we concluded that, provided the brain dynamical state does not vary dramatically during the windowed interval,

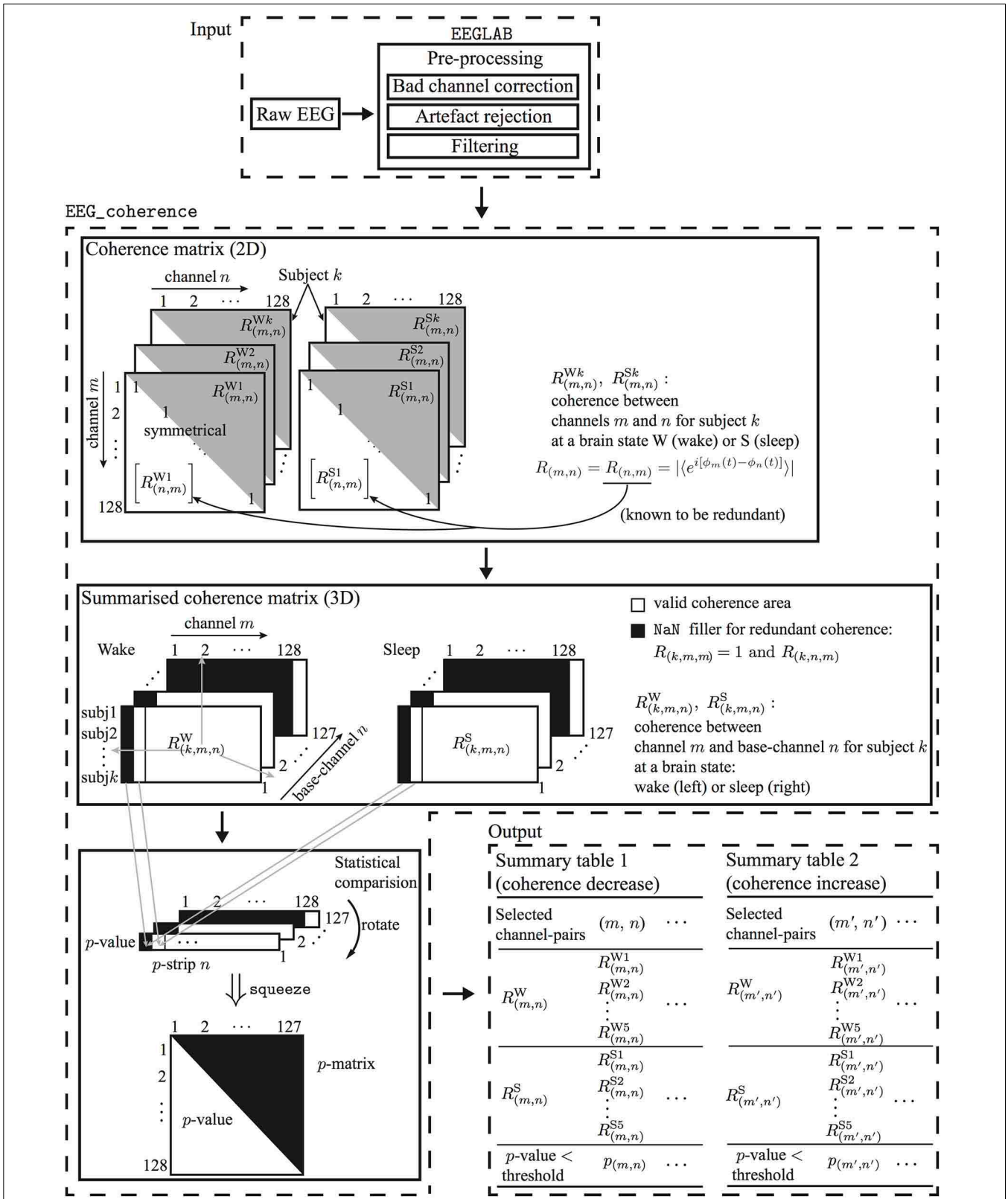

FIGURE 3 | Flowchart for processing EEG of two brain states to determine electrode-pairs with significantly altered phase-coherence. EEG data undergo preprocessing in EEGLAB before passing to EEG_coherence, a customized MATLAB algorithm that automatically identifies electrode-pairs with significantly altered phase-coherence between two brain states across multiple subjects, then stores these electrode-pair results in a summary table.

the sub-delta coherence measure is not particularly sensitive to window size.

3.3. EEG_COHERENCE: AN AUTOMATIC EEG PROCESSING ALGORITHM FOR EEG COHERENCE ANALYSIS

The raw EEG data were visually inspected and the artifacts were manually marked using EEGLAB[3] (Delorme and Makeig, 2004). The one or two bad channels were replaced by substituting with the average of the four neighboring channels. Eye-blink artifacts were removed using AAR (see **Figure 1** for definition and details), then the repaired traces were inspected for smoothness and continuity. Since the archival EEG data are relatively artifact-free, only minor corrections were needed. We filtered EEG to the sub-delta band ($\leq$1.5 Hz) using EEGLAB built-in basic FIR (linear finite impulse response) order-2 filter with the pass-band between 0.05 and 1.5 Hz. During filtering, EEGLAB uses the MATLAB routine `filtfilt()` to apply the filter forward and then backward, ensuring that phase delays introduced by the filter are nullified. The resulting sub-delta band EEG traces show characteristic slow oscillations; this is the prominent feature of EEG activity during non-rapid eye movement (non-REM) sleep in humans (see **Figure 2** for an example) (Marshall et al., 2003).

The EEGLAB pre-processed EEG data were then passed to `EEG_coherence`, a custom MATLAB algorithm that identifies electrode-pairs with significantly altered phase-coherence between the two brain states. The user specifies the folder location where the EEG data are stored and configures some basic parameters (e.g., window and overlap length for the coherence measure). `EEG_coherence` automatically generates a summary table including identified electrode-pairs and their corresponding phase-coherence indices at two distinct brain states for all subjects. *p*-values that are used to identify those electrode-pairs whose phase-coherence has significantly altered are included in the table to permit further statistical analysis.

As shown in **Figure 3**, `EEG_coherence` processes EEG data in three steps:

1. Construction of coherence matrices: The phase-coherence measure is based on the Hilbert transform, as described in Section 3.2. Each subject will have two coherence matrices, `awake` and `sleep`, for the wake and unconscious states, respectively.
2. Extraction of coherence summaries: For each brain state (wake or unconsciousness), `EEG_coherence` will construct a consolidated tableau of matrices by concatenating the coherence matrices for all five subjects. This consolidated table has three dimensions: the first dimension (row-index $k = 1 \ldots 5$) points to the subject, while the second (channel-index $m = 1 \ldots 128$), and third dimensions (base-channel index $n = 1 \ldots 127$) identify the specific pair of electrodes whose phase similarity is being assessed. Thus, coordinate (k, m, n) captures the coherence $R_{(k,m,n)}$ between EEG channels m and n for subject k. Since we only consider the upper triangle of the coherence matrix, the redundant coherence entries[4] in the summary matrix will be filled with `NaN` (not a number). The output from this step is a pair of coherence summary matrices for wake and unconscious states.
3. Statistical comparison: A one-tail Mann-Whitney *U*-test is performed to test the null hypothesis H_0 that the five pairs of wake/sleep coherence values—at a given (m, n) matrix coordinate—are drawn from populations with *equal* medians against the alternative that they are not. With reference to **Figure 3**, this means that we are comparing the median of the 5×1 column-vector for wake $[R^{W}_{(1,m,n)}, R^{W}_{(2,m,n)}, \cdots, R^{W}_{(5,m,n)}]^{T}$ against the median for the corresponding vector for sleep $[R^{S}_{(1,m,n)}, R^{S}_{(2,m,n)}, \cdots, R^{S}_{(5,m,n)}]^{T}$. This comparison is repeated across all non-redundant channel pairs.
   In fact, the Mann-Whitney calculation is run twice to allow for testing against two distinct alternative hypotheses; namely, H_1: that the median coherence is *higher* in wake than in sleep (i.e., right-tailed test), and, H_2: that the median coherence is *lower* in wake than in sleep (left-tailed).
   The statistical comparison for a base-channel n returns a three-dimensional matrix named *p*-strip; this matrix contains *p*-values for channel-pairs 1-*n*, 2-*n*,. . .,128-*n*. The *p*-strip matrices are generated via the following MATLAB implementation:

```
awake_size = size(awake);
prop_size = size(sleep);

% Check if two coherence matrices have the same
  size
if ~isempty(find((awake == sleep)==0))
    error('unequal size');
end

% Create p-strip matrix
for base_ch = 1: size(awake, 3)
    for ch_ind = 1: size(awake, 2)
        if isnan(awake(:,ch_ind, base_ch))
            p(:,ch_ind, base_ch) = NaN;
        else
            [p(:,ch_ind, base_ch), h(:,ch_ind,
              base_ch)]...
            = ranksum(awake(:,ch_ind,
              base_ch),
                sleep(:,ch_ind, base_ch),...
                'alpha', p_limit, 'tail',
                  direction);
            % direction: left: wake < sleep;
              right: wake > sleep
        end
    end
end
% Squeeze the 3D p-strip matrix, leading to a 2D
  p-matrix
p_matrix = squeeze(p);
    % e.g. E1-E2 is at row 2 (channel), col 1
     (base-channel)
```

If, across all subjects, a given electrode-pair shows a statistically significant difference in coherence between wake and unconscious state (i.e., $p <$ `p_limit`), `EEG_coherence` will store this electrode-pair in the summary table.

[3]An open source EEG processing MATLAB toolbox available at http://sccn.ucsd.edu/eeglab/

[4]The lower triangle of the coherence matrix $R_{(k,n,m)}$ and the diagonal unit coherence.

4. RESULTS

4.1. SUB-DELTA EEG COHERENCE CHANGES ACROSS FIVE SUBJECTS

We first examine the across-subject wake-vs.-sleep changes in sub-delta phase coherence using the methodology described in the previous section; then in Section 4.2 we analyze the coherence matrices for each individual subject.

Figure 4 visualizes those electrode-pairs identified by `EEG_coherence` as having significantly altered (i.e., decreased or increased) coherence between wake and unconscious states. The comparison between the upper and lower panels of **Figure 4** reveals two major features of the coherence changes with respect to propofol anesthesia:

- Decreased coherence for frontal, occipital, and frontal–occipital electrode-pairs: The electrode-pairs showing significantly reduced coherence form dense clusters for pairs lying within the frontal area of the cortex, within the occipital area, and also for pairs spanning the frontal–occipital scalp sites. These observations suggest that neuronal activities within frontal cortex and within occipital cortex, and cooperative behavior between them, are less strongly coupled when the brain is switched to the unconscious state. Scanning the top panels of **Figure 4** from left to right, we see that the front electrodes manifest the most robust decreases in phase coherence, indicating that propofol anesthesia leads to increased disorder in neuronal activity in the frontal cortex.
- Increased coherence for left- and right-temporal electrode-pairs: Electrodes at the left- and right-temporal areas detect enhanced coherence. These maps of enhanced connectivities seem to be complementary to the preceding maps showing decreased frontal–occipital connectivity: coherence trends have been reversed with the significant front–back *uncoupling* (top panel) occurring simultaneously with a left–right *coupling*. Examining the lower panels of **Figure 4**, we see evidence of strengthened left–right electrode connectivity, showing increased EEG coherence with the induction of propofol anesthesia.

If we overlap the upper and lower panels of **Figure 4**, we find some frontal electrodes have decreased coherence with the occipital electrodes, while having increased coherence with the left- and right-temporal electrodes. Similarly, some occipital electrodes have decreased coherence with the electrodes in the frontal area, while having increased coherence with those in the temporal areas. These observations suggest an underlying compensatory mechanism between a subsystem of fronto–occipital and other cortical regions at sub-delta frequencies. Cantero

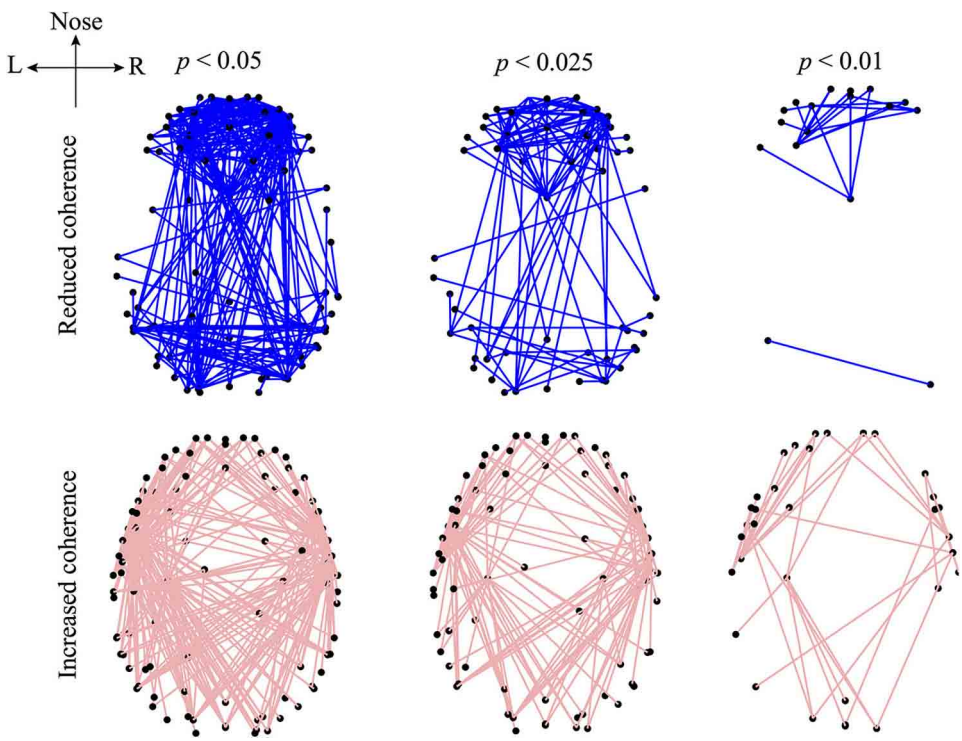

FIGURE 4 | Graphical representations of the electrode pairs with significantly *reduced* (upper panel) or *increased* (lower panel) phase-coherence of the sub-delta band (0.05–1.5 Hz) EEG induced by propofol anesthesia. EEG data (128-channel recording) were recorded from 5 subjects and processed by the `EEG_coherence` algorithm diagrammed in **Figure 3**. The electrode pairs with significant ($p < 0.05$) changes in phase coherence are connected with lines. The electrode-pair map is represented in a bird's-eye view of the 3D head model (created via the modified `EEGLAB` function `plotchans3d`). The black dots are `EEG_coherence` selected electrodes. Electrode pairs for altered phase coherence are determined with different levels of significance (significance-level p was set at 0.05, 0.025, and 0.01 in the Mann-Whitney U-test). Smaller p thresholds result in a lower density of electrode-pair cluster due to the stricter selection criterion, however, the electrode-pair distributions are generally preserved in trend.

et al. (2002) reported a similar compensatory phenomenon in coherence between the temporal and other cortical regions for the alpha (8–12 Hz) and sleep spindle (12–15 Hz) frequency ranges.

Furthermore, we examined the decreased EEG coherence patterns across nine electrodes (see the description of **Figure 5**) that Koskinen et al. utilized in their work (Koskinen et al., 2001), in which systematic phase synchronization changes were evaluated between EEG channel-pairs in various frequency bands during induction and recovery from propofol anesthesia. Koskinen et al. detected passband-specific behaviors in these changes, and identified a sub-delta EEG coherence decrease due to propofol-induced anesthesia. We set the significance level ($p < 0.05$) in `EEG_coherence` to be the same as that used by Koskinen et al. The comparison shown in **Figure 5** illustrates that `EEG_coherence` produced a similar electrode-pair distribution pattern to the Koskinen findings, reinforcing our observation of sub-delta EEG coherence reduction in the frontal cortex. However, we need to add the caveat that the choice of reference electrode (Cz for the Koskinen recordings; FCz for the Waikato data) is reversed between the two experiments; fortunately these sites are adjacent on the scalp centerline, so can be expected to result in closely similar EEG traces.

We must acknowledge the possibility that the coherence changes we have detected may simply be the result of randomness: of the ∼8000 network connections, by chance we can expect about 400 to show significant change at the uncorrected $p = 0.05$ level (1 in 20). To reduce the possibility of spurious significance (false positives), one could apply some form of p-value correction (such as Bonferroni) to compensate for multiple testing, but it is not clear how to do this straightforwardly with only five subjects. This motivates us to apply a clustering analysis to the individual coherence-change patterns as an alternative way of demonstrating robustness of our results.

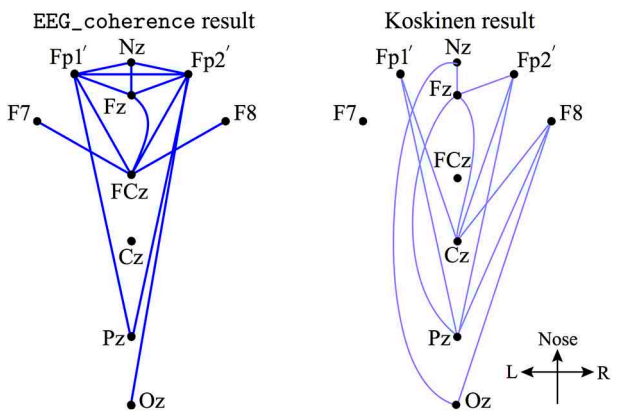

FIGURE 5 | A subset of electrode-pairs (left) showing significant ($p < 0.05$) reduction in phase coherence extracted from the upper left corner plot of Figure 4 (referenced to Cz, in dark blue lines) and Koskinen et al. reported pattern (Koskinen et al., 2001) (right, referenced to FCz, in light blue lines) for the coherence measured from 9 electrodes: Nz (nasion), Fp1′(about 1 cm down from Fp1, just above the eyebrow), Fp2′, Fz, F7, F8, Cz, Pz, and Oz.

4.2. EEG COHERENCE CHANGES FOR INDIVIDUAL SUBJECTS

The coherence changes described in the previous section represent a population response across multiple subjects. Here, we present a much simpler analysis of the coherence changes for each of the five individuals, and show that the resulting clustering patterns are highly unlikely to have arisen by chance.

The top two rows of **Figure 6** are generated by a simple ranking of the (wake minus sleep) coherence differences for each individual. The first row shows the 5% of electrode-pairs exhibiting the largest positive difference (i.e., coherence *decreased* in sleep); the second row shows the 5% of electrode-pairs with the largest negative difference (i.e., coherence *increased* in sleep). We see that the spatial distribution of electrode-pairs with significantly altered coherence is generally preserved across the five subjects. The first row reveals clusters of electrode-pairs in the frontal and occipital areas with significantly *decreased* coherence; the second row shows the dense pairing of left–right electrodes with *increased* coherence along the temporal axis.

To quantify the coherence changes in specific areas of the cortex, we counted the number of electrode-pairs in the frontal region showing significantly *decreased* coherence (N^-) and subtracted this from the number of frontal pairs with significantly *increased* coherence (N^+). The difference ($N^- - N^+$) is strongly positive (third row of figure), confirming that N^- (coherence decrease) is dominant in the frontal area. An opposite conclusion is reached for the left–right temporal electrode-pairs: ($N^- - N^+$) is strongly negative with N^+ being dominant (coherence increase), implying strengthened regional connections between hemispheres under anesthesia. We repeated these number difference calculation for ten cortical regions (see row 3). Blue (pink) shading indicates N^- (N^+) dominance in a given cortical region.

To demonstrate that the clustering patterns shown in **Figure 6** represent meaningful and consistent changes in network connectivity—and are not simply the outcome of random happenstance—we apply a permutation test to each coherence-change matrix. In this test, we shuffled the elements of the coherence matrix. The null hypothesis is that the permuted coherence matrix could result in an electrode-pair distribution similar to that seen in **Figure 6**; the alternative hypothesis is that the electrode-pair distribution generated from the permuted coherence matrix is significantly different with the originally observed pattern. A chi-squared statistic is applied in estimating the p-value. We first divided the brain into five areas: frontal, occipital, left-temporal, right-temporal, and parietal. The chi-squared distribution index is given by

$$\chi^2 = \sum_{i=1}^{5} \frac{\left(E^i_{\text{original}} - E^i_{\text{perm}}\right)^2}{E^i_{\text{original}}} \tag{4}$$

where E^i_{original} is the original number of electrodes (i.e., the dot coordinates in the first row of **Figure 7**) in section i; E^i_{perm} is the number of permuted electrodes (e.g., the dot coordinates in the second row of **Figure 7**) in the same section. The p-value is calculated by the MATLAB command `p = 1 - chi2cdf(`χ^2`,`

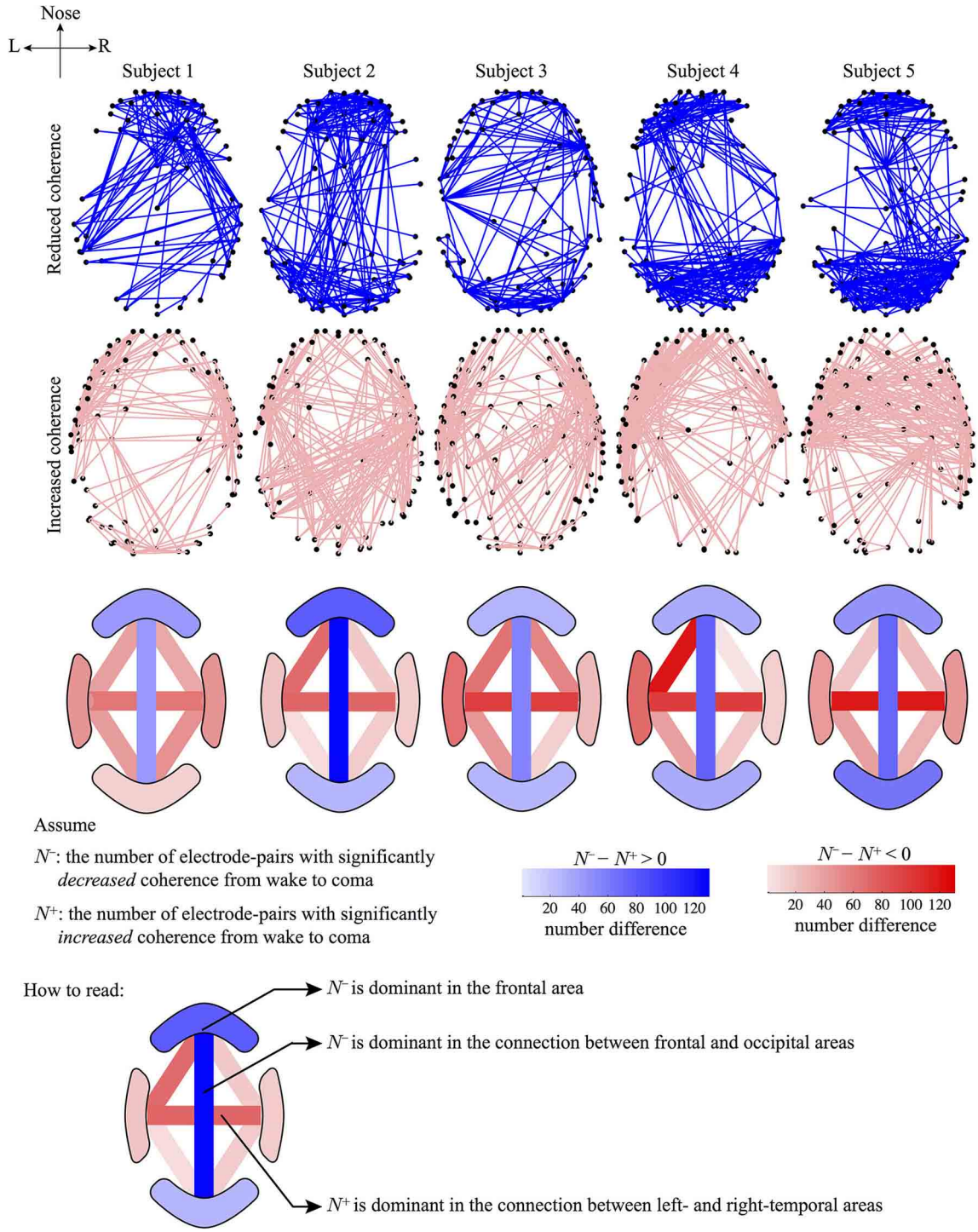

FIGURE 6 | Graphical representations of the electrode-pairs with significantly altered coherence from wake to coma for five subjects. The first and second rows represent electrode-pairs with significantly *reduced* (blue lines) or *increased* (pink lines) coherence, respectively: selected electrode-pairs correspond to the top 5% most changed (i.e., most increased or most decreased) coherence during the wake to coma transition. The third row describes the number difference of electrode-pairs between the first and second rows for four regions: frontal, occipital, left- and right-temporal; and for six pair-wise connections *between* regions: frontal–left temporal, frontal–right temporal, frontal–occipital, left temporal–occipital, right temporal–occipital, left–right temporal. The number of electrode-pairs with significantly reduced (or increased) coherence in a region is counted as N^- (N^+). The sign of ($N^- - N^+$) determines the dominance of a coherence trend: if ($N^- - N^+$) > 0, the region will be colored blue (decreased coherence); otherwise if ($N^- - N^+$) < 0, the region will be colored red (increased coherence). The ($N^- - N^+$) difference is calibrated by the color-gradient bar. (Note that the color-bar for the third row is not related to the first and second rows.)

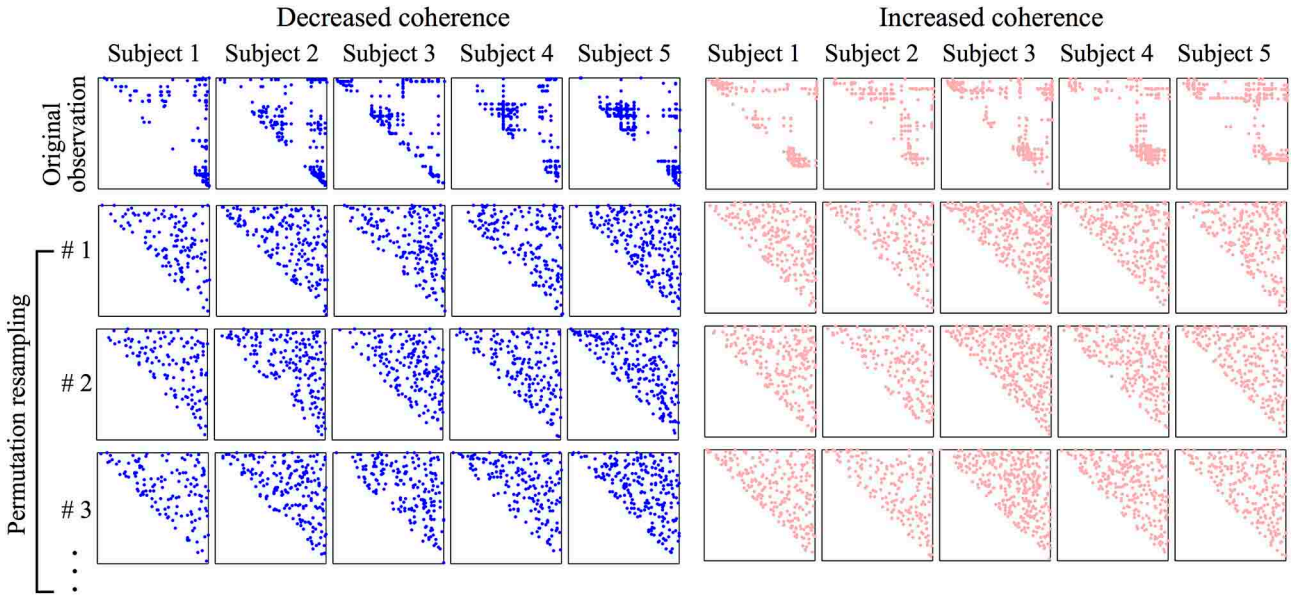

FIGURE 7 | Coherence matrices showing spatial distribution of electrode-pairs with significant wake vs. coma coherence difference. The coherence matrix is diagonally symmetric, we need only display its upper half. The first row of the left panel corresponds to the first row of **Figure 6**; the first row of the right panel corresponds to the second row of **Figure 6**. The marked (either in blue or pink) dots in the matrix are the top 5% most changed (decreased: blue; increased: pink) phase-coherence during transit from wake to coma. The row and column indices of a marked dot identify a pair of electrodes shown in **Figure 6**. To test the significance of the dot distribution in the first row, a permutation resampling is applied to each original matrix, and repeated 10,000 times. In each shuffling, the upper-triangle elements are randomly allocated, and a significance test is applied to achieve a *p*-value quantifying the structural difference between the permuted and original matrices. The first three permuted coherence matrices are shown. The averaged *p*-value over the 10,000 permutation tests for the original observations (first row) are all smaller than 10^{-5}, revealing a significant difference between the original distribution and its permutations.

`dof`), in which `dof` (degree of freedom) is set to 4 (`dof` = number of data category −1).

After 10,000 permutation tests, all permuted electrode-pair distributions are found to be significantly ($\overline{p} < 10^{-5}$) different from the original one. This statistical result supports our alternative hypothesis that the derived electrode-pair distribution pattern is meaningful and cannot be randomly generated. Actually, visual examination of the first row in **Figure 7** clearly reveals genuine dot clusters, the structure of which disappears in the permuted matrices, so it is not surprising that the original data complexity cannot be reproduced from the randomized data distribution. We applied the same statistical test to the coherence matrices corresponding to the patterns shown in **Figure 4** and obtained the same result, namely, that the original distribution is significantly different from its permutation resampling.

4.3. COMPARISON WITH THEORY: INTERACTING TURING–HOPF INDUCED CHAOTIC SLOW-WAVES

A recent theoretical prediction by Steyn-Ross et al. (2013) introduces an interacting Turing–Hopf mechanism as a source for sub-delta slow-waves that emerge during propofol anesthesia. We now give a brief overview of the cortical model; for full mathematical details refer to Steyn-Ross et al. (2013).

The cortex is represented as a set of eight coupled partial-differential equations that describe the mean-field (spatially-averaged) firing activity of populations of excitatory and inhibitory neurons that are uniformly distributed across a two-dimensional sheet of gray-matter cortical tissue. The neural populations communicate locally and at longer ranges via chemical synapses, and also through electrical synapses (gap junctions) that allow direct diffusive currents to flow between adjoining neurons. Inhibitory-to-inhibitory (*i-i*) gap-junction connections are abundant and ubiquitous throughout the central nervous system (Bennett and Zukin, 2004). Fukuda et al. (2006) characterized the dendritic gap-junction connections in cat visual cortex as forming "dense and far-ranging networks." Using the Fukuda measurements, we estimated an upper bound for the per-neuron region of gap-junction influence as an area $D_2 \lesssim 0.6\,\text{cm}^2$ (Steyn-Ross et al., 2007), with symbol D chosen to indicate a *diffusive* coupling strength. Using a dendritic relaxation time of $\tau \approx 40\,\text{ms}$ as our time-scale, the ratio D_2/τ defines a diffusion coefficient (with dimensions area/time) for voltage change in the inhibitory population. In contrast to the relative abundance of *i-i* gap junctions, evidence for excitatory-to-excitatory (*e-e*) diffusive coupling is very sparse (Bennett and Zukin, 2004), so we have set the excitatory coupling strength at an arbitrarily small fraction of the inhibitory value: $D_1 = D_2/100$. We note that inhibitory diffusive dominance is a prerequisite for the spontaneous formation of Turing structures (Turing, 1952) of spatially-patterned cortical activity.

For the model results reported here, we used the same parameter settings as listed in Table I of Steyn-Ross et al. (2013), apart

from the white-matter long-range connections which have been ignored for simplicity.

Figure 8 shows that the steady-state excitatory neuronal firing rates Q_e^o of the model forms a reversed S-shape distribution with the upper branch corresponding to an activated cortical state identified as awake (or REM sleep), and the lower branch corresponding to a suppressed cortical state identified as propofol anesthetic induced coma (or SWS) (Steyn-Ross et al., 2005, 2012). By increasing the concentration of propofol anesthesia λ_i, the model describes the anesthesia-induced transition from consciousness to unconsciousness.

Inhibitory gap-junction strength D_2 is treated as a bifurcation parameter controlling the stability and the emergent behavior of the cortical model. The effect of interneuronal gap junctions is to produce diffusion terms similar in form to those found in standard reaction-diffusion models that support Turing structures (Turing, 1952). The cortical dynamics at selected "awake" and "coma" coordinates in **Figure 8** with respect to the variation of D_2 were examined by the stability analysis, and numerical simulations are shown in **Figures 9**, **10**.

In the awake cortical simulations of **Figure 9**, when the gap-junction strength is sufficiently large ($D_2 = 0.7\,\text{cm}^2$), linear stability analysis of the up-branch steady-state at $\lambda_i = 1$ in **Figure 8** predicts whole-of-cortex Hopf oscillations; while the down-branch steady-state shows a damped-Hopf at wavenumber $q = 0$ plus a damped-Turing at $q \neq 0$. The time-series and strip-chart depict a stable Turing–Hopf mode evolution where the cortical Turing patterns oscillate in small amplitudes. Such Turing-interacted Hopf slow-oscillation have been interpreted as representing the resting state of the cortex (Steyn-Ross et al., 2012) or non-cognitive idling state (Steyn-Ross et al., 2011). These slow patterned oscillations may relate to very slow ($\leq$0.1 Hz) fluctuations in BOLD (blood-oxygen-level dependent) signals detected using fMRI (functional magnetic resonance imaging) of relaxed, non-tasked human brains (Fox et al., 2005; Fransson, 2005).

On the other hand, for the anesthetized cortex, anesthetic effect $\lambda_i = 1.018$ is just beyond the multiple steady-states region where the awake cortex stays at the up-branch of $\lambda_i = 1.0$. This subtle change in coordinates means that the cortical stability is guided only by the steady-state at the low-firing bottom branch. In **Figure 10**, at the closure of the gap-junction $D_2 = 0.1\,\text{cm}^2$, linear stability analysis [column (a)] predicts a heavily damped Hopf, which is consistent with computer simulations of the cortical equations. Most general anesthetics will enhance the strength of the inhibitory postsynaptic potential (IPSP) (Franks and Lieb, 1994; Kitamura et al., 2002), as well inhibit gap-junction communication (Wentlandt et al., 2006). Consequently further increases in D_2 (for $D_2 < 0.7\,\text{cm}^2$ of **Figure 10**) lead the cortex into a chaotic phase, arising from the competitive interference between Hopf and Turing instabilities. Such mixed instabilities may provide a mechanism for the emergence of turbulent slow-waves of inductive anesthesia, characterized by low phase-coherence. $D_2 = 0.7\,\text{cm}^2$ is the border of the anesthetic slow oscillations; larger values of D_2 (e.g., $D_2 = 0.8\,\text{cm}^2$) rebalances the Turing and Hopf instabilities in favor of spatially structured Turing pattern oscillating at a low Hopf frequency ($\sim$3 Hz). Such mixed-mode interference is very similar to the non cognitive-wake cortex at $D_2 = 0.7\,\text{cm}^2$ in **Figure 9**. Nevertheless, because the cortex is still under anesthetic coma, Steyn-Ross et al. label this coherent oscillation as "anesthetic delirium," a clinical state common during emergence from general anesthesia and associated with excitability and confusion (Olympio, 1991).

Figures 9, **10** indicate that Turing–Hopf interaction dynamics arise from variations in D_2 inhibitory strength. To further track these Turing–Hopf dynamics, Steyn-Ross et al. computed the global coherence of a given D_2 by taking the mean of the upper-triangle of the coherence matrix $R(x', x)$ defined in **Figures 9E**, **10E**. A comprehensive inspection of the global coherence relating to the inhibitory strength is presented in **Figure 11**. We see a high global coherence in the non-cognitive state, where the inhibitory

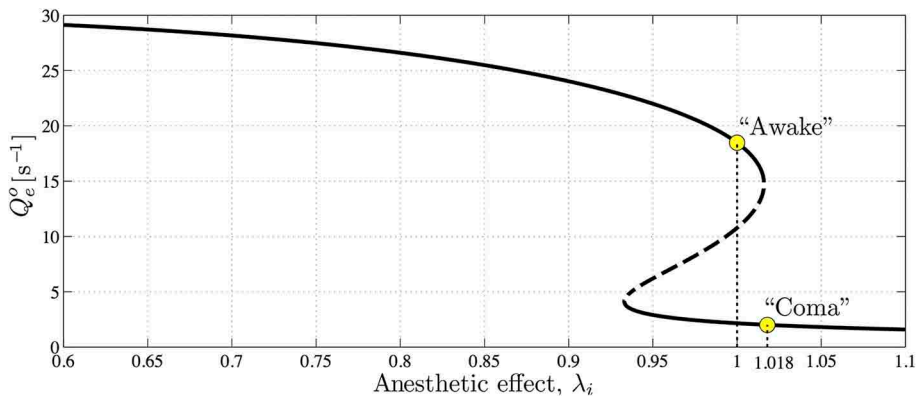

FIGURE 8 | The steady-state firing rates Q_e^o as a function of varying anesthetic inhibition λ_i at a particular cortical excitation. The upper, high-firing and lower, low-firing branches (solid curve) are considered to be "awake" and "coma" states, respectively, with the "coma" state being associated with anesthetic-induced unconsciousness. Dashed curve indicates an unstable branch from which the cortex has the potential to jump to either the upper or lower stable branches. Upper and lower marked circles indicate references at $\lambda_i = 1.0$ and 1.018 on awake and coma branches, respectively. (Figure reproduced from Steyn-Ross et al., 2013).

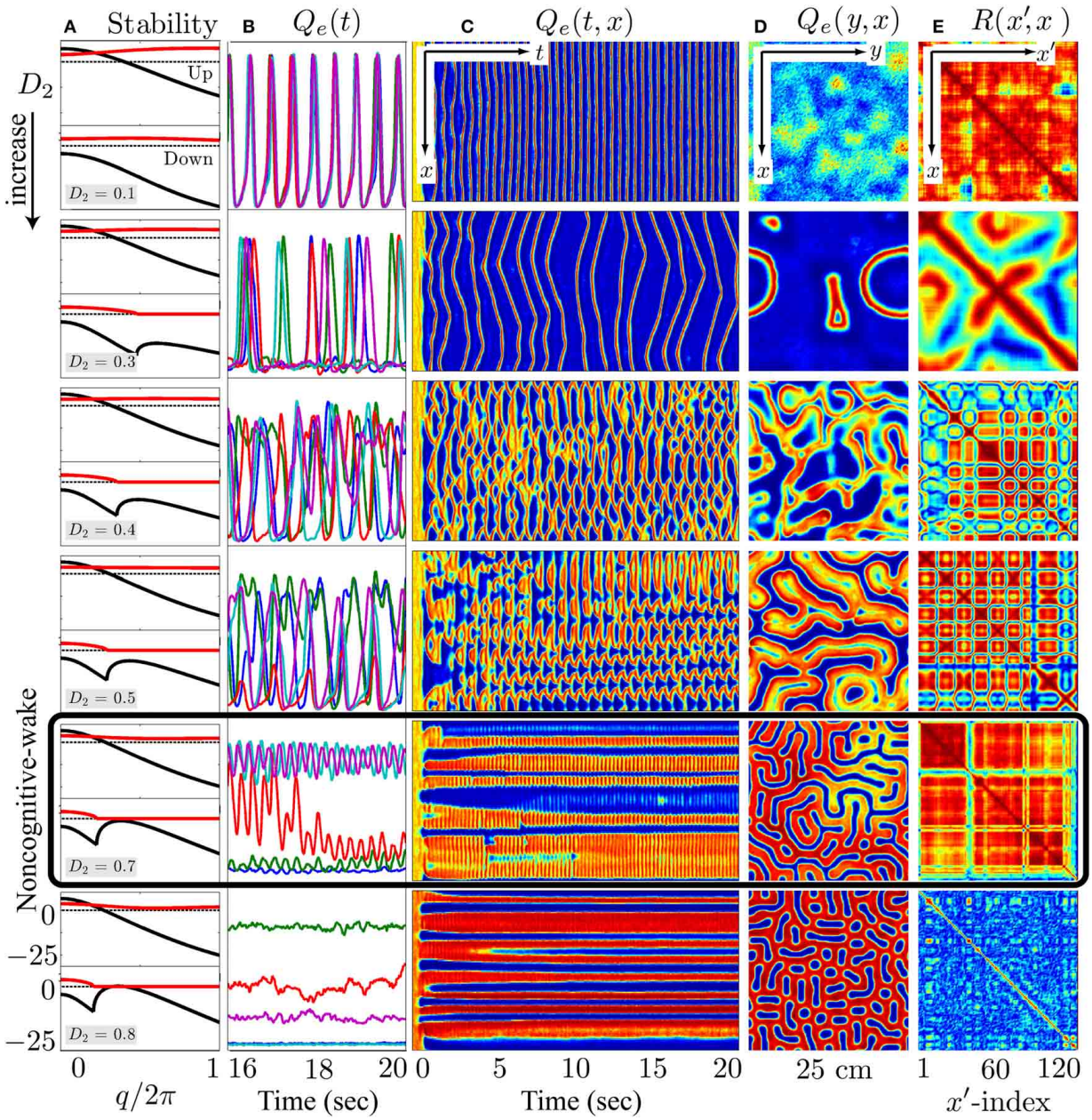

FIGURE 9 | At the $\lambda_i = 1.0$ wake state, cortical stability analysis and spatiotemporal dynamics for varying gap-junction strength D_2 from 0.1 (top row) to 0.8 cm^2 (bottom). Model cortex is initialized from the top high-firing branch of steady-state manifold marked as "Awake" in **Figure 8**. **(A)** Cortical stability analysis showing dominant eigenvalue dispersion curve of the real (black) and imaginary (red) parts as a function of scaled wavenumber for top- and bottom-branch equilibria at fixed anesthetic effect $\lambda_i = 1.0$ in **Figure 8**. Thus, each panel has two parts in it—the upper part corresponds to the top-branch, the lower part to the bottom-branch. The dotted line marks zero. **(B)** Last 4-s time-series of excitatory firing-rate $Q_e(t)$ extracted from 5 equally-spaced grid-points in **(C)** $Q_e(t, x)$ space-time chart representing the full 20-s time-evolution of cortical activity along the $y = 60$ midline strip; y-axis ranges from 0 to 30 s^{-1}. **(D)** Bird's-eye snapshot $Q_e(y, x)$ of the cortex when $t = 20$ s. **(E)** Phase coherence map $R(x', x)$ showing synchronization level of firing-rate between $Q_e(t, x)$ and $Q_e(t, x')$ for the final 5-s time evolution. The coherence level is computed via Hilbert transform Equation (3) with a transition from *red* to *blue* meaning high to low coherence. In **(C–E)**, color scale from blue to red indicates the numerical range from low to high. (Figure modified from Steyn-Ross et al., 2013).

diffusion is moderately strong $D_2 \simeq 0.7$ cm^2. For the anesthetized cortex, the anesthetic drug shifts the activated "Noncognitive-wake" coherence peak to the right, implying a possible hysteresis effect such that an anesthetized cortex requires a stronger Turing instability to reinforce an activated state. To the left of the peak for the delirium state, there is a broad intermediate zone of D_2 experiencing reduced coherence, which results from large, low frequency chaotic oscillations.

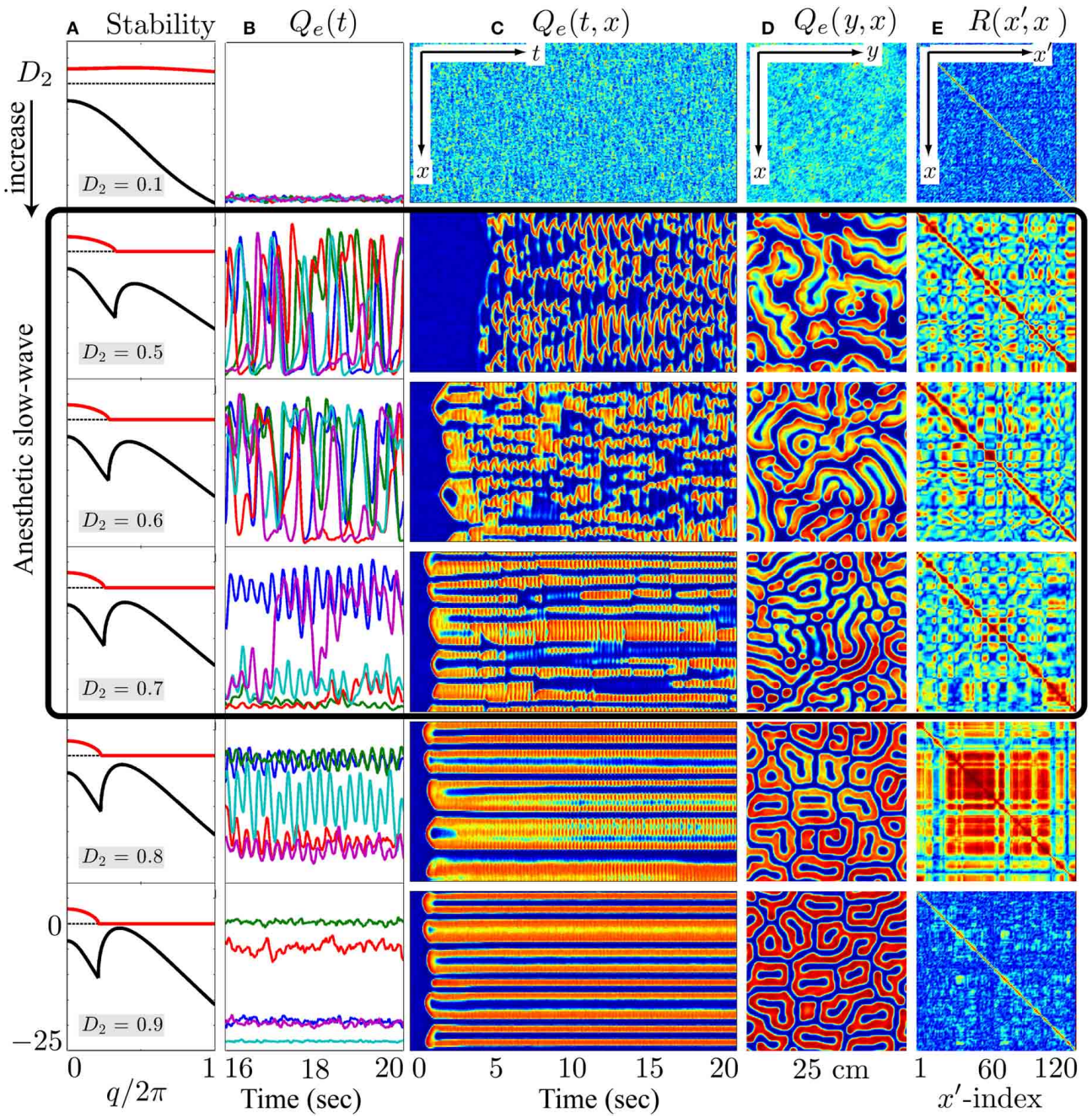

FIGURE 10 | At the $\lambda_i = 1.018$ coma state, cortical stability analysis and spatiotemporal dynamics of varying gap-junction strength D_2 from 0.1 (top row) to 0.9 cm^2 (bottom). Model cortex is initialized from the bottom low-firing branch of steady-state manifold marked as "Coma" in **Figure 8**. **(A)** Cortical stability analysis showing dominant eigenvalue dispersion curve of the real (*black*) and imaginary (*red*) parts as a function of scaled wavenumber at anesthetic effect $\lambda_i = 1.018$ in **Figure 8**. **(B)** Last 4-s time-series of excitatory firing-rate $Q_e(t)$ extracted from 5 equal-spaced grid-points in **(C)** $Q_e(t, x)$ space-time chart representing the full 20-s time-evolution of cortical activity along the $y = 60$ midline strip. **(D)** Bird's-eye snapshot $Q_e(y, x)$ of the cortex when $t = 20$ s. **(E)** Phase coherence map $R(x', x)$ showing synchronization level of firing-rate between $Q_e(t, x)$ and $Q_e(t, x')$ for the final 5-s time evolution. In **(C–E)**, color scale from blue to red indicates the numerical range from low to high. (Figure modified from Steyn-Ross et al., 2013).

These model results drawn from Steyn-Ross et al. (2013) allow a prediction that the passage from wake to anesthetic unconsciousness should manifest as a decrease in phase coherence between separated cortical electrodes.

5. DISCUSSION

Phase-coherence is a measure that quantifies the degree to which the same frequency components of two EEG channels preserve their relative phase over a certain time period. The phase stability

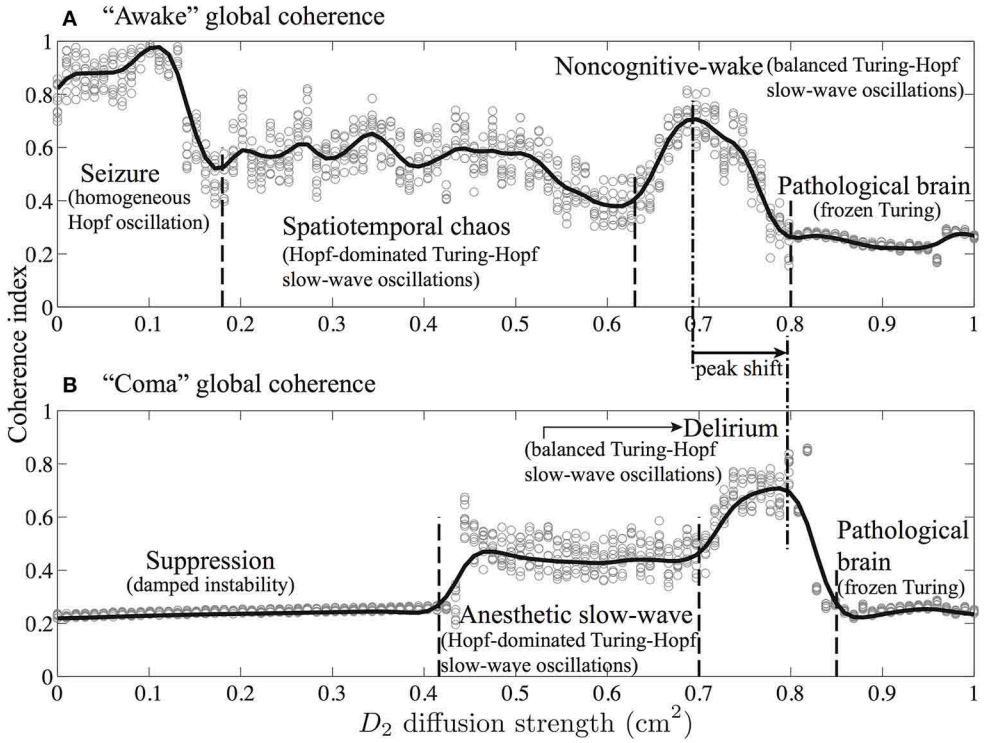

FIGURE 11 | Global phase-coherence trends with respect to inhibitory strength for the cortex at (A) awake ($\lambda_i = 1$) and (B) comatose ($\lambda_i = 1.018$) states. Inhibitory strength D_2 is evenly spaced (0.01 cm^2 interval) in the range 0.0–1.0 cm^2. At a given D_2, simulations were repeated 10 times. For each simulation, we first computed the phase-coherence matrix $R(x', x)$ for the final 5-s time evolution (see **Figures 9E**, **10E**), then extracted its upper-triangular matrix mean as an estimate of global phase-coherence, which is represented as a gray cycle in the figure. The trend curves were produced by spline function in MATLAB curve-fitting toolbox. (Figure modified from Steyn-Ross et al., 2013).

between two EEG channels indicates their phase synchronization, reflecting the functional correlations of spatially divergent cortical regions.

In this study, we investigated systematic phase-synchronization changes between pairs of EEG channels in the sub-delta band, during propofol anesthetic induction. An EEG phase-coherence processing algorithm, `EEG_coherence`, was developed in MATLAB and applied to archival EEG data from a group of subjects. `EEG_coherence` uses the Hilbert transform to extract instantaneous phase-angles from non-stationary EEG signals, and yields a phase-coupling index appraising the phase-shift consistency between pairs of EEG channels. The trends of such EEG coherence change between two brain states are statistically tested via a Mann-Whitney U-test, which is a simple non-parametric test without the requirement of a specific data distribution.

Our sub-delta band ($\lesssim$1.5 Hz) EEG study discloses a regional *decrease* in phase coherence under propofol anesthesia in both the frontal and the occipital cortical areas, and also for electrode pairs that link these two areas. Simultaneously, more strongly phase-coupled neuronal activity is found in the temporal–frontal, temporal–occipital and left–right temporal regions. Such contrasts in coherence change suggest an underlying compensatory mechanism of sub-delta band activity between a subsystem of fronto–occipital and temporal cortical regions. Our findings of reduced-coherence between particular electrode-pairs is similar to clinical reports (Morikawa et al., 1997; Koskinen et al., 2001) where the frontal cortical region exhibits a negative inter-correlation during anesthetic coma.

Such changes in large-scale neuronal coupling may be an anesthetic indicator of unconsciousness when the subject is disconnected from the environment with reduced cognition level. A leading hypothesis suggests that anesthetics cause unconsciousness by disrupting functional connectivity between cortical areas (Mashour, 2004; Alkire et al., 2008). A recent work by Lewis et al. (2012) found that the slow oscillation is a fundamental component of propofol-induced unconsciousness and it occurs asynchronously across cortex, interrupting the cortical integration of information processing. Thus, spatiotemporal slow oscillation dynamics may mediate the fragmentation of cortical networks at both the local and global scale, leading to reduced coherence in neuronal communications. Meanwhile, the presented reduced phase-coherence along the fronto-occipital axis is consistent with an animal study by Imas et al. (2006) that the anterio–posterior coherence in both 5–25 and 26–50 Hz bands was significantly reduced by isoflurane in the rat.

In contrast, Dumermuth and Lehmann (1981) reported a high interhemispheric coherence between the left and right parietal areas with deepening slow wave sleep. They postulated that the high coherence may reflect the interhemispheric transfer of

information. Later, research by Mölle et al. (2004) reinforced Dumermuth and Lehmann's findings and verified their hypothesis by comparing coherence changes for subjects during the slow-wave sleep with or without pre-learning tasks. Mölle et al. observed significantly increased coherence during the occurrence of slow oscillations (<1 Hz) for subjects after learning tasks; Figures 1, 2 in Mölle et al. (2004) show increased sub-delta band EEG coherence between the left- and right-temporal regions. This left–right strengthening is concordant with our propofol results shown in **Figure 4** (lower panel).

The apparently compensatory weakening of frontal and occipital coherence (upper panel of **Figure 4**) supports the hypothesis of Steyn-Ross et al. (2013) that propofol anesthesia should induce a decrease in EEG coherence. When there is little or no anesthetic effect, a sufficiently strong inhibitory diffusion (i.e., gap-junction strength) allows a rough balance between Turing pattern and Hopf oscillation instabilities, leading to a slow Hopf oscillations of high global coherence with sustained spatial structure (see $D_2 = 0.7\,\mathrm{cm}^2$ simulation in **Figure 9**). Such interacting low-frequency Hopf and Turing instabilities may form the substrate for the cognitive state, namely, the "default" background state for the non-cognitive brain during wake. Its slow beating dynamics ($\leq$0.1 Hz) is similar to what is observed in BOLD functional MRI recording of relaxed, non-tasked human brains (Fox et al., 2005; Fransson, 2005).

An increase in anesthetic effect λ_i suppresses cortical activity, leading to an anesthetized coma state. Here, intermediate values of D_2 are expected since propofol anesthetic will tend to block gap-junctions (Wentlandt et al., 2006) and thus weaken inhibitory diffusion. This will damp the Turing instability, allowing the Hopf instability to become dominant, leading to spontaneous emergence of large-amplitude slow chaotic oscillations (see the highlighted simulations in **Figure 10**). We note that this dynamical mechanism for the slow oscillation is quite distinct from the conventional view of cyclic alternations in extracellular ionic (Ca^{2+}) concentration (Massimini and Amzica, 2001) that may be initiated by tiny clusters of pacemaker neurons in layer-5 of cerebral cortex (Stroh et al., 2013).

The emergent slow oscillation is predicted to be chaotic in space and time, and this is the reason for the expected decrease in phase coherence with descent into anesthetic hypnosis. Therefore, the *increase* in coherence seen in the left–right electrode pairs cannot be explained by the model. A possible resolution for this discrepancy may lie in the model's neglect of a major component of cortical white-matter architecture, namely the corpus callosum that connects left and right hemispheres of the cortex. It is possible that as local independent activity is suppressed during deep anesthesia, the anatomical left–right connectivity becomes *functionally* stronger, thus invalidating the model assumption of a homogeneous cortex. In future modeling work it would be useful to investigate if an imposed left–right cortical connection symmetry might tend to enhance inter-hemispheric coherence while leaving frontal–occipital dynamics unchanged.

AUTHOR CONTRIBUTIONS

All authors contributed extensively to the work presented in this paper: Moira L. Steyn-Ross, D. A. Steyn-Ross, Marcus T. Wilson and Jamie W. Sleigh developed the cortical model and proposed the stability analysis. Moira L. Steyn-Ross, D. A. Steyn-Ross and Jamie W. Sleigh developed the Hilbert transform-based phase-coherence index. Jamie W. Sleigh provided the EEG data and clinical references relating to the paper. Kaier Wang developed `EEG_coherence` algorithm and performed EEG processing and analysis. All authors contributed to the writing of the paper.

ACKNOWLEDGMENT

We acknowledge support from the University of Waikato Strategic Investment in Biological Research.

REFERENCES

Acebrón, J., Bonilla, L., Pérez Vicente, C., Ritort, F., and Spigler, R. (2005). The Kuramoto model: a simple paradigm for synchronization phenomena. *Rev. Mod. Phys.* 77, 137–185. doi: 10.1103/RevModPhys.77.137

Achermann, P., and Borbely, A. (1998). Coherence analysis of the human sleep electroencephalogram. *Neuroscience* 85, 1195–1208. doi: 10.1016/S0306-4522(97)00692-1

Alkire, M. T., Hudetz, A. G., and Tononi, G. (2008). Consciousness and anesthesia. *Science* 322, 876. doi: 10.1126/science.1149213

Astori, S., Wimmer, R. D., Prosser, H. M., Corti, C., Corsi, M., Liaudet, N., et al. (2011). The $Ca_V3.3$ calcium channel is the major sleep spindle pacemaker in thalamus. *Proc. Natl. Acad. Sci. U.S.A.* 108, 13823–13828. doi: 10.1073/pnas.1105115108

Bai, D., Pennefather, P. S., MacDonald, J. F., and Orser, B. A. (1999). The general anesthetic propofol slows deactivation and desensitization of GABA(A) receptors. *J. Neurosci.* 19, 10635–10646.

Belouchrani, A., Abed-Meraim, K., Cardoso, J. F., and Moulines, E. (1997). A blind source separation technique using second-order statistics. *IEEE Trans. Signal Process.* 45, 434–444. doi: 10.1109/78.554307

Bennett, M. V., and Zukin, R. S. (2004). Electrical coupling and neuronal synchronization in the mammalian brain. *Neuron* 41, 495–511. doi: 10.1016/S0896-6273(04)00043-1

Cantero, J. L., Atienza, M., Salas, R. M., and Dominguez-Marin, E. (2002). Effects of prolonged waking-auditory stimulation on electroencephalogram synchronization and cortical coherence during subsequent slow-wave sleep. *J. Neurosci.* 22, 4702–4708.

David, F., Schmiedt, J. T., Taylor, H. L., Orban, G., Di Giovanni, G., Uebele, V. N., et al. (2013). Essential thalamic contribution to slow waves of natural sleep. *J. Neurosci.* 33, 19599–19610. doi: 10.1523/JNEUROSCI.3169-13.2013

Delorme, A., and Makeig, S. (2004). EEGLAB: an open source toolbox for analysis of single-trial EEG dynamics including independent component analysis. *J. Neurosci. Methods* 134, 9–21. doi: 10.1016/j.jneumeth.2003.10.009

Dumermuth, G., and Lehmann, D. (1981). EEG power and coherence during non-REM and REM phases in humans in all-night sleep analyses. *Eur. Neurol.* 20, 429–434. doi: 10.1159/000115274

Faul, S., Marnane, L., Lightbody, G., Boylan, G., and Connolly, S. (2005). "A method for the blind separation of sources for use as the first stage of a neonatal seizure detection system," in *Proceedings of the IEEE International Conference on Acoustics, Speech and Signal Processing* (Philadelphia, PA), 409–412.

Fiset, P., Paus, T., Daloze, T., Plourde, G., Meuret, P., Bonhomme, V., et al. (1999). Brain mechanisms of propofol-induced loss of consciousness in humans: a positron emission tomographic study. *J. Neurosci.* 19, 5506–5513.

Fox, M. D. M., Snyder, A. Z. A., Vincent, J. L. J., Corbetta, M. M., Van Essen, D. C. D., and Raichle, M. E. M. (2005). The human brain is intrinsically organized into dynamic, anticorrelated functional networks. *Proc. Natl. Acad. Sci. U.S.A.* 102, 9673–9678. doi: 10.1073/pnas.0504136102

Franks, N., and Lieb, W. (1994). Molecular and cellular mechanisms of general-anesthesia. *Nature* 367, 607–614. doi: 10.1038/367607a0

Franks, N. P. (2008). General anaesthesia: from molecular targets to neuronal pathways of sleep and arousal. *Nat. Rev. Neurosci.* 9, 370–386. doi: 10.1038/nrn2372

Fransson, P. (2005). Spontaneous low-frequency BOLD signal fluctuations: an fMRI investigation of the resting-state default mode of brain function hypothesis. *Hum. Brain Mapp.* 26, 15–29. doi: 10.1002/hbm.20113

Fukuda, T., Kosaka, T., Singer, W., and Galuske, R. A. W. (2006). Gap junctions among dendrites of cortical GABAergic neurons establish a dense

and widespread intercolumnar network. *J. Neurosci.* 26, 3434–3443. doi: 10.1523/JNEUROSCI.4076-05.2006

Gomez-Herrero, G., De Clercq, W., Anwar, H., Kara, O., Egiazarian, K., Van Huffel, S., et al. (2006). "Automatic removal of ocular artifacts in the EEG without an EOG reference channel," in *Proceedings of the 7th Nordic Signal Processing Symposium* (Rejkjavik), 130–133.

Huang, F., Li, S., Gan, X., Wang, R., and Chen, Z. (2014). Propofol inhibits gap junctions by attenuating sevoflurane-induced cytotoxicity against rat liver cells *in vitro*. *Eur. J. Anaesthesiol.* 31, 219–224. doi: 10.1097/01.EJA.0000435059.98170.da

Huang, N. E., Shen, Z., Long, S. R., Wu, M. C., Shih, H. H., Zheng, Q., et al. (1998). The empirical mode decomposition and the Hilbert spectrum for nonlinear and non-stationary time series analysis. *Proc. R. Soc. A* 454, 903–995. doi: 10.1098/rspa.1998.0193

Huber, R., Felice Ghilardi, M., Massimini, M., and Tononi, G. (2004). Local sleep and learning. *Nature* 430, 78–81. doi: 10.1038/nature02663

Huber, R., Ghilardi, M. F., Massimini, M., Ferrarelli, F., Riedner, B. A., Peterson, M. J., et al. (2006). Arm immobilization causes cortical plastic changes and locally decreases sleep slow wave activity. *Nat. Neurosci.* 9, 1169–1176. doi: 10.1038/nn1758

Imas, O. A., Ropella, K. M., Wood, J. D., and Hudetz, A. G. (2006). Isoflurane disrupts anterio-posterior phase synchronization of flash-induced field potentials in the rat. *Neurosci. Lett.* 402, 216–221. doi: 10.1016/j.neulet.2006.04.003

Johnson, B. W., Sleigh, J. W., Kirk, I. J., and Williams, M. L. (2003). High-density EEG mapping during general anaesthesia with xenon and propofol: a pilot study. *Anaesth. Intens. Care* 31, 155–163.

Jung, T. P., Makeig, S., Humphries, C., Lee, T. W., McKeown, M. J., Iragui, V., et al. (2000). Removing electroencephalographic artifacts by blind source separation. *Psychophysiology* 37, 163–178. doi: 10.1111/1469-8986.3720163

Kitamura, A., Marszalec, W., Yeh, J. Z., and Narahashi, T. (2002). Effects of halothane and propofol on excitatory and inhibitory synaptic transmission in rat cortical neurons. *J. Pharmacol. Exp. Ther.* 304, 162–171. doi: 10.1124/jpet.102.043273

Kitamura, A., Marszalec, W., Yeh, J. Z., and Narahashi, T. (2003). Effects of halothane and propofol on excitatory and inhibitory synaptic transmission in rat cortical neurons. *J. Pharmacol. Exp. Ther.* 304, 162–171. doi: 10.1124/jpet.102.043273

Koskinen, M., Seppänen, T., Tuukkanen, J., Yli-Hankala, A., and Jäntti, V. (2001). Propofol anesthesia induces phase synchronization changes in EEG. *Clin. Neurophysiol.* 112, 386–392. doi: 10.1016/S1388-2457(00)00538-1

Kungys, G., Kim, J., Jinks, S. L., Atherley, R. J., and Antognini, J. F. (2009). Propofol produces immobility via action in the ventral horn of the spinal cord by a GABAergic mechanism. *Anesth. Analg.* 108, 1531–1537. doi: 10.1213/ane.0b013e31819d9308

Kuramoto, Y. (1984). *Chemical Oscillations, Waves, and Turbulence*. New York, NY: Springer-Verlag. doi: 10.1007/978-3-642-69689-3

Kuramoto, Y., and Nishikawa, I. (1987). Statistical macrodynamics of large dynamical systems. Case of a phase transition in oscillator communities. *J. Stat. Phys.* 49, 569–605. doi: 10.1007/BF01009349

Lancel, M. (1999). Role of GABAA receptors in the regulation of sleep: initial sleep responses to peripherally administered modulators and agonists. *Sleep* 22, 33–42.

Lewis, L. D., Weiner, V. S., Mukamel, E. A., Donoghue, J. A., Eskandar, E. N., Madsen, J. R., et al. (2012). Rapid fragmentation of neuronal networks at the onset of propofol-induced unconsciousness. *Proc. Natl. Acad. Sci. U.S.A.* 109, E3377–E3386. doi: 10.1073/pnas.1210907109

Lo, M. T., Tsai, P. H., Lin, P. F., Lin, C., and Hsin, Y. L. (2009). The nonlinear and nonstationary properties in EEG signals: probing the complex fluctuations by Hilbert–Huang transform. *Adv. Adapt. Data Anal.* 1, 461–482. doi: 10.1142/S1793536909000199

Marshall, L., Mölle, M., and Born, J. (2003). Spindle and slow wave rhythms at slow wave sleep transitions are linked to strong shifts in the cortical direct current potential. *Neuroscience* 121, 1047–1053. doi: 10.1016/S0306-4522(03)00458-5

Mashour, G. A. (2004). Consciousness unbound: toward a paradigm of general anesthesia. *Anesthesiology* 100, 428. doi: 10.1097/00000542-200402000-00035

Massimini, M., and Amzica, F. (2001). Extracellular calcium fluctuations and intracellular potentials in the cortex during the slow sleep oscillation. *J. Neurophysiol.* 85, 1346–1350.

Massimini, M., Huber, R., Ferrarelli, F., Hill, S., and Tononi, G. (2004). The sleep slow oscillation as a traveling wave. *J. Neurosci.* 24, 6862–6870. doi: 10.1523/JNEUROSCI.1318-04.2004

McCormick, D. A., and Sanchez-Vives, M. V. (2000). Cellular and network mechanisms of rhythmic recurrent activity in neocortex. *Nat. Neurosci.* 3, 1027–1034. doi: 10.1038/79848

Mölle, M., Marshall, L., Gais, S., and Born, J. (2004). Learning increases human electroencephalographic coherence during subsequent slow sleep oscillations. *Proc. Natl. Acad. Sci. U.S.A.* 101, 13963–13968. doi: 10.1073/pnas.0402820101

Morikawa, T. T., Hayashi, M. M., and Hori, T. T. (1997). Auto power and coherence analysis of delta-theta band EEG during the waking-sleeping transition period. *Electroencephalogr. Clin. Neurophysiol.* 103, 633–641. doi: 10.1016/S0013-4694(97)00048-5

Mormann, F., Lehnertz, K., David, P., and E Elger, C. (2000). Mean phase coherence as a measure for phase synchronization and its application to the EEG of epilepsy patients. *Phys. D Nonlinear Phenom.* 144, 358–369. doi: 10.1016/S0167-2789(00)00087-7

Murphy, M., Riedner, B. A., Huber, R., Massimini, M., Ferrarelli, F., and Tononi, G. (2009). Source modeling sleep slow waves. *Proc. Natl. Acad. Sci. U.S.A.* 106, 1608–1613. doi: 10.1073/pnas.0807933106

Nir, Y., Staba, R. J., Andrillon, T., Vyazovskiy, V. V., Cirelli, C., Fried, I., et al. (2010). Regional slow waves and spindles in human Sleep. *Neuron* 70, 153–169. doi: 10.1016/j.neuron.2011.02.043

Nunez, P. L., and Srinivasan, R. (2006). *Electric Fields of The Brain. The Neurophysics of EEG*. Oxford, UK: Oxford University Press. doi: 10.1093/acprof:oso/9780195050387.001.0001

Olympio, M. A. (1991). Postanesthetic delirium: historical perspectives. *J. Clin. Anesth.* 3, 60–63. doi: 10.1016/0952-8180(91)90209-6

Oweis, R. J., and Abdulhay, E. W. (2011). Seizure classification in EEG signals utilizing Hilbert-Huang transform. *BioMed. Eng. Online* 10, 38. doi: 10.1186/1475-925X-10-38

Rudolph, U., and Antkowiak, B. (2004). Molecular and neuronal substrates for general anaesthetics. *Nat. Rev. Neurosci.* 5, 709–720. doi: 10.1038/nrn1496

Sleigh, J. W., Steyn-Ross, D. A., Steyn-Ross, M. L., Williams, M. L., and Smith, P. (2000). Comparison of changes in electroencephalographic measures during induction of general anaesthesia: influence of the gamma frequency band and electromyogram signal. *Br. J. Anaesth.* 86, 50–58. doi: 10.1093/bja/86.1.50

Steriade, M., Gloor, P., Llinás, R. R., da Silva, F. L., and Mesulam, M.-M. (1989). Basic mechanisms of cerebral rhythmic activities. *Electroencephalogr. Clin. Neurophysiol.* 76, 481–508. doi: 10.1016/0013-4694(90)90001-Z

Steriade, M., Nuñez, A., and Amzica, F. (1993). A novel slow ($<$ 1 Hz) oscillation of neocortical neurons *in vivo*: depolarizing and hyperpolarizing components. *J. Neurosci.* 13, 3252–3265.

Steriade, M., and Timofeev, I. (2002). Neuronal plasticity in thalamocortical networks during sleep and waking oscillations. *Neuron* 37, 563–576. doi: 10.1016/S0896-6273(03)00065-5

Steyn-Ross, D. A., Steyn-Ross, M. L., Sleigh, J. W., Wilson, M. T., Gillies, I. P., and Wright, J. J. (2005). The sleep cycle modelled as a cortical phase transition. *J. Biol. Phys.* 31, 547–569. doi: 10.1007/s10867-005-1285-2

Steyn-Ross, M. L., Steyn-Ross, D. A., and Sleigh, J. W. (2012). Gap junctions modulate seizures in a mean-field model of general anesthesia for the cortex. *Cogn. Neurodynam.* 6, 215–225. doi: 10.1007/s11571-012-9194-0

Steyn-Ross, M. L., Steyn-Ross, D. A., and Sleigh, J. W. (2013). Interacting Turing-Hopf instabilities drive symmetry-breaking transitions in a mean-field model of the cortex: a mechanism for the slow oscillation. *Phys. Rev. X* 3, 021005. doi: 10.1103/PhysRevX.3.021005

Steyn-Ross, M. L., Steyn-Ross, D. A., Sleigh, J. W., and Wilson, M. T. (2011). A mechanism for ultra-slow oscillations in the cortical default network. *Bull. Math. Biol.* 73, 398–416. doi: 10.1007/s11538-010-9565-9

Steyn-Ross, M. L., Steyn-Ross, D. A., Wilson, M. T., and Sleigh, J. W. (2007). Gap junctions mediate large-scale Turing structures in a mean-field cortex driven by subcortical noise. *Phys. Rev. E* 76, 011916–011916. doi: 10.1103/PhysRevE.76.011916

Stroh, A., Adelsberger, H., Groh, A., Rühlmann, C., Fischer, S., Schierloh, A., et al. (2013). Making waves: initiation and propagation of corticothalamic Ca^{2+} waves *in vivo*. *Neuron* 77, 1136–1150. doi: 10.1016/j.neuron.2013.01.031

Sukhotinsky, I., Zalkind, V., Lu, J., Hopkins, D. A., Saper, C. B., and Devor, M. (2007). Neural pathways associated with loss of consciousness caused by

intracerebral microinjection of $GABA_A$-active anesthetics. *Eur. J. Neurosci.* 25, 1417–1436. doi: 10.1111/j.1460-9568.2007.05399.x

Suzuki, S., and Rogawski, M. A. (1989). T-type calcium channels mediate the transition between tonic and phasic firing in thalamic neurons. *Proc. Natl. Acad. Sci. U.S.A.* 86, 7228–7232. doi: 10.1073/pnas.86.18.7228

Sweeney-Reed, C. M., and Nasuto, S. J. (2007). A novel approach to the detection of synchronisation in EEG based on empirical mode decomposition. *J. Comput. Neurosci.* 23, 79–111. doi: 10.1007/s10827-007-0020-3

Tass, P., Rosenblum, M. G., Weule, J., Kurths, J., Pikovsky, A., Volkmann, J., et al. (1998). Detection of n:m phase locking from noisy data: application to magnetoencephalography. *Phys. Rev. Lett.* 81, 3291–3294. doi: 10.1103/PhysRevLett.81.3291

Turing, A. M. (1952). The chemical basis of morphogenesis. *Philos. Trans. R. Soc. Lond. Ser. B* 237, 37–72. doi: 10.1098/rstb.1952.0012

Uusberg, A., Uibo, H., Kreegipuu, K., and Allik, J. (2013). EEG alpha and cortical inhibition in affective attention. *Int. J. Psychophysiol.* 89, 26–36. doi: 10.1016/j.ijpsycho.2013.04.020

Walker, M. P. (2009). The role of slow wave sleep in memory processing. *J. Clin. Sleep Med.* 5(Suppl. 2), S20–S26.

Wentlandt, K., Samoilova, M., Carlen, P. L., and El Beheiry, H. (2006). General anesthetics inhibit gap junction communication in cultured organotypic hippocampal slices. *Anesth. Analg.* 102, 1692–1698. doi: 10.1213/01.ane.0000202472.41103.78

Yi, L., Fan, Y. L., Li, G., and Tong, Q. Y. (2009). "Sleep stage classification based on EEG Hilbert-Huang transform," in *2009 4th IEEE Conference on Industrial Electronics and Applications (ICIEA)* (Xi'an), 3676–3681.

Zhang, X. Z., Yin, L., and Wang, W. X. (2010). Wavelet time-frequency analysis of electroencephalogram (EEG) processing. *Int. J. Adv. Comput. Sci. Appl.* 1, 1–5. doi: 10.14569/IJACSA.2010.010501

Conflict of Interest Statement: The authors declare that the research was conducted in the absence of any commercial or financial relationships that could be construed as a potential conflict of interest.

Received: 04 July 2014; accepted: 10 October 2014; published online: 29 October 2014.
Citation: Wang K, Steyn-Ross ML, Steyn-Ross DA, Wilson MT and Sleigh JW (2014) EEG slow-wave coherence changes in propofol-induced general anesthesia: experiment and theory. Front. Syst. Neurosci. ***8****:215. doi: 10.3389/fnsys.2014.00215*
This article was submitted to the journal Frontiers in Systems Neuroscience.

frontiers in
SYSTEMS NEUROSCIENCE

HYPOTHESIS AND THEORY ARTICLE
published: 10 December 2014
doi: 10.3389/fnsys.2014.00232

Anesthetic action on extra-synaptic receptors: effects in neural population models of EEG activity

***Meysam Hashemi*[1], *Axel Hutt*[1]* *and Jamie Sleigh*[2]**

[1] *INRIA CR Nancy - Grand Est, Team Neurosys, Villers-les-Nancy, France*
[2] *Department of Anaesthesiology, Waikato Clinical School, University of Auckland, Hamilton, New Zealand*

Edited by:
Anthony G. Hudetz, Medical College of Wisconsin, USA

Reviewed by:
Ingo Bojak, University of Reading, UK
Kingsley Paul Storer, Weill Cornell Medical College, USA

***Correspondence:**
Axel Hutt, INRIA CR Nancy - Grand, 615 Rue du Jardin Botanique, Villers-les-Nancy, France
e-mail: axel.hutt@inria.fr

The role of extra-synaptic receptors in the regulation of excitation and inhibition in the brain has attracted increasing attention. Because activity in the extra-synaptic receptors plays a role in regulating the level of excitation and inhibition in the brain, they may be important in determining the level of consciousness. This paper reviews briefly the literature on extra-synaptic GABA and NMDA receptors and their affinity to anesthetic drugs. We propose a neural population model that illustrates how the effect of the anesthetic drug propofol on GABAergic extra-synaptic receptors results in changes in neural population activity and the electroencephalogram (EEG). Our results show that increased tonic inhibition in inhibitory cortical neurons cause a dramatic increase in the power of both $\delta-$ and $\alpha-$ bands. Conversely, the effects of increased tonic inhibition in cortical excitatory neurons and thalamic relay neurons have the opposite effect and decrease the power in these bands. The increased $\delta-$activity is in accord with observed data for deepening propofol anesthesia; but is absolutely dependent on the inclusion of extrasynaptic (tonic) GABA action in the model.

Keywords: GABA receptor, neural mass, propofol, power spectrum, general anesthesia

1. INTRODUCTION

General anesthesia is used daily to enable surgery, but its underlying mechanisms of action are still largely a mystery. In recent decades there have been successful efforts to reveal the drug action on single receptors (Franks and Lieb, 1994; Alkire et al., 2008; Brickley and Mody, 2012), however their effect on neural populations, networks of neural populations, and brain areas, still remains unsolved. To explain the underlying neural mechanism during the loss of consciousness, two prominent hypotheses are the loss of integration information, developed by Tononi (Tononi, 2004; Murphy et al., 2011; Boly et al., 2012), and a sharp phase transition of the brain activity involving a drop of neural activity, put forward by Steyn-Ross et al. (Steyn-Ross et al., 2004; Friedman et al., 2010). These hypotheses are not mutually exclusive. For instance, a recent experimental study on the effects of propofol on neural activity measured at various spatial scales (Lewis et al., 2012) has revealed both decreased functional connectivity between brain areas and a dramatic drop of neuron firing rates after loss of consciousness. A large amount of experimental literature has revealed characteristic spectral signal changes in electroencephalographic data (EEG) and Local Field Potentials (LFPs) during general anesthesia (Cimenser et al., 2011; Lewis et al., 2012; Purdon et al., 2012; Sellers et al., 2013; Vizuete et al., 2014). Moreover, several previous theoretical studies have proposed neural models to explain certain EEG signal features observed during anesthesia (Steyn-Ross et al., 1999, 2013; Bojak and Liley, 2005; Wilson et al., 2006; Foster et al., 2008; McCarthy et al., 2008; Ching et al., 2010, 2012; Hutt, 2013; Liley and Walsh, 2013; Hutt et al., 2013; Hutt and Buhry, 2014). Although these studies may incorporate realistic neurobiological details of the brains' network topology and neuronal function, they have simplified dramatically the anesthetic action by considering only synaptic excitatory and inhibitory receptors. There is a growing amount of experimental research that has revealed the importance of extra-synaptic receptors (ESR) for neural interactions in general (Brickley and Mody, 2012; Hardingham and Bading, 2012), and for anesthesia especially, see Alkire et al. (2008); Hutt (2012) and references therein.

To elucidate the role of ESR in the context of anesthesia, one approach might be to do a theoretical study of a realistic neural population model which reproduces the characteristic signal features observed in EEG. To perform such a theoretical study, it is necessary to incorporate physiological properties of extrasynaptic receptors into neural population models.

Gamma-aminobutyric acid (GABA) receptors are a large and important class of inotropic receptors. These receptors are located in the neuron's membrane and respond to the neurotransmitter GABA by opening Cl^- channels and inducing an inward hyperpolarizing membrane current. This response may either be: phasic at synaptic receptors or, tonic at ESR which lie distant from synaptic terminals (Kaneda et al., 1995; Brickley et al., 1996; Semyanov et al., 2003, 2004; Yeung et al., 2003; Belelli et al., 2009). The phasic response evolves on a time scale of 10–200 ms whereas tonic response evolves on a much longer time scale (Hamann et al., 2002; Cavalier et al., 2005).

The precise biochemical origin of tonic inhibition is still heavily debated (Farrant and Nusser, 2005; Bright et al., 2011). A rather simple and intuitive model explains the tonic current

as a spillover of excess neurotransmitter from synapses. This is due to incomplete GABA uptake by nearby synaptic $GABA_A$-receptors. The remaining neurotransmitter is thus able to diffuse to more distant $GABA_A$-receptors via extracellular space (Nusser et al., 1997; Semyanov et al., 2004; Farrant and Nusser, 2005; Bright et al., 2007). This spillover may explain the longer time scale of tonic responses found experimentally. In addition, this explanation implies that even small concentrations of neurotransmitters are sufficient to generate tonic activity because of the high sensitivity of ESRs.

The effect of ESRs on the dendritic activity has not attracted much attention. This may because there are only a relatively small number of such receptors as compared to synaptic receptors (Kopanitsa, 1997; Farrant and Nusser, 2005). Moreover, only recently have experimental studies been able to classify and localize different sub-types of $GABA_A$ receptors (Semyanov et al., 2004; Farrant and Nusser, 2005). $GABA_A$ receptors are pentameric ligand-gated ion channels and it has been found that $\delta-$sub units of $GABA_A$ receptors occur exclusively at ESRs (Nusser et al., 1998; Wei et al., 2003; Farrant and Nusser, 2005; Belelli et al., 2009; Ye et al., 2013). This indicates a specific role of these receptors for the neural information processing in general with specific implications in diseases (Brickley and Mody, 2012) and consciousness (Kopanitsa, 1997).

Tonic inhibition induced by extra-synaptic $GABA_A$-receptors represents a persistent increase in the cell membrane's conductance. On the single neuron level, this diminishes the membrane time constant and, consequently, reduces the size and duration of excitatory post-synaptic potentials propagating on the dendrite. Hence tonic inhibition reduces the excitability of the membrane and increases the effective firing threshold (Farrant and Nusser, 2005). At the neural population level, ESRs affect the excitability of interneuron-pyramidal cell networks and thus modify network oscillations (Semyanov et al., 2003). Kopanitsa (1997) argues that the sustained spatially widespread tonic inhibition is energetically more effective for the system to diminish neural population activity than short-lasting local phasic inhibition, since lower neurotransmitter concentrations are sufficient. The critical factor in this mechanism is the the relatively high sensitivity of ESRs to modulations by anesthetic agents (Yeung et al., 2003; Farrant and Nusser, 2005; Orser, 2006; Houston et al., 2012). The brain areas that have been shown to be affected by anesthetic-induced tonic inhibition are the hippocampus (Bai et al., 2001), brain stem (McDougall et al., 2008), cerebellum (Houston et al., 2012), and the thalamus (Belelli et al., 2009). Since these areas are supposed to play a role in general anesthesia (Alkire et al., 2008), ESRs may mediate clinical anesthetic effects, such as hypnosis and amnesia (Kretschmannova et al., 2013). Thus, it is reasonable to argue that $GABA_A$ ESRs set the background inhibition of neural populations and the brain network and mediate slow consciousness phenomena, such as loss of consciousness, sleep or arousal (Kopanitsa, 1997).

Converse to GABAergic receptors, N-methyl-D-aspartate (NMDA) receptors respond to the neurotransmitter glutamate by excitatory inward Na^+ and Ca^{2+} currents and K^+ outward currents. The response of NMDA receptors to glutamate depends on their spatial location with respect to synaptic terminals and the presence of co-agonists. A recent experimental study has revealed that the population of NMDA receptors, which are close to synaptic terminals, are primarily activated by the co-agonist d-serine in the presence of glutamate; while extra-synaptic NMDA receptors (more distant from the synaptic terminals) respond primarily to glutamate and the co-agonist glycine (Mothet et al., 2000; Papouin et al., 2012). D-serine and glycine are endogenous amino acids found naturally in the brain (d-serine is a derivative of glycine). Similar to GABAergic ESRs, it has been shown that there exists a significant ambient glutamate concentration which induces a tonic excitatory current (Sah et al., 1989; Fleming et al., 2011). This current is evoked primarily at extra-synaptic NMDA receptors (Le Meur et al., 2007) and may be regulated by other cells, such as neighboring astrocytes (Panatier et al., 2006; Fleming et al., 2011) which control glutamate uptake and also synthesize d-serine (Wolosker et al., 1999).

Commonly-used GABAergic anesthetic drugs directly modify the corresponding receptors. However, various anesthetics are also known to affect the endogenous co-agonists of NMDA receptors (Martin et al., 1995; Daniels and Roberts, 1998; Papouin et al., 2012). Hence, the possible anesthetic effect on NMDA receptors is more complex and indirect than for GABAergic ESRs. There is a large class of NMDA receptor antagonists, that inhibit the excitatory action of NMDA receptors. These anesthetics induce so-called dissociative anesthesia (Pender, 1970) leading to amnesia and analgesia without depressing respiration, but also characterized by distorted perceptions of sight and sound and feelings of dissociation from the environment. An example of a dissociative anesthetic drug is the inhalational anesthetic xenon which—amongst other actions—binds primarily to the extra-synaptic glycine site of NMDA receptors (Dickinson et al., 2007) and attenuates long-term potentiation present in the hippocampus by reducing extrasynaptic receptor currents (Kratzer et al., 2012).

To understand how the anesthetic effect of ESR activity on the microscopic single neuron scale could lead to changes in EEG and behavior that can be observed at macroscopic scales, it is necessary to establish a bridge between the two scales. This bridge may be formulated as a dynamical theoretical model. Neural population models represent a good candidate for a dynamic description of neural activity at an intermediate mesoscopic scale (Coombes, 2006; Nunez and Srinivasan, 2006; Bressloff, 2012). These models describe properties of ensembles of neurons, such as the mean firing rate and the mean dendritic current (Hutt, 2009), whilst their output variables can be strongly linked to macroscopic experimental quantities such as Local Field Potentials (LFPs) and EEG (Wright and Kydd, 1992; Nunez and Srinivasan, 2006). An increasing number of theoretical studies have used neural population models to describe signal features in LFPs and EEG observed during anesthesia (Foster et al., 2008; Hutt et al., 2013). Most of these studies take into account anesthetic action on excitatory and/or inhibitory synapses (Steyn-Ross et al., 2004; Liley and Bojak, 2005; Hutt and Longtin, 2009; Ching et al., 2010; Hindriks and van Putten, 2012) while few consider ESRs (Talavera et al., 2009). This link between the synaptic receptor properties in an ensemble of neurons and the average population dynamics is straight-forward, since classical neural population models already

involve the average synaptic response function. The situation is different for ESRs, since their action is not incorporated into the classical models. A very recent work has filled this gap (Hutt and Buhry, 2014). This theoretical work demonstrated a method to include mathematically extra-synaptic $GABA_A$ receptor action in neural population models; which enables researchers to study how changing anesthetic ESR action modifies spectral features in the EEG, which might then be observed experimentally.

The current work uses a thalamo-cortical neural population model involving anesthetic synaptic inhibition with a well-established connection topology; and then extends this model by including the effects of extra-synaptic GABAergic receptor action in the presence of the anesthetic drug propofol. With the help of this model, we demonstrate the role of extra-synaptic GABAergic inhibition, and the importance of tonic inhibition in the cortical inhibitory neuronal population, in explaining experimental EEG power spectra.

2. MATERIALS AND METHODS

2.1. EEG DATA

We re-analyzed previously-obtained experimental data from subjects that had been given a short propofol anesthetic. The details of the methods can be found in Johnson et al. (2003). In brief, after obtaining regional ethical committee approval and written informed consent, five healthy subjects (mean age 27.7 yrs, four males) were studied. They were on no psychoactive drugs and had been starved for at least 6 h prior to the study. They were monitored and managed as per clinical anesthesia, according to the Australia and New Zealand College of Anesthetists best practice guidelines. The induction consisted of an intravenous infusion of propofol at 1500 mg/hr until the subject no longer responded to verbal command. Typically this occurred about 5 min into the infusion. The estimated effect-site concentrations of propofol were calculated using standard population-based pharmacokinetics models.

The EEG was acquired using the Electrical Geodesics 128 channel Ag/AgCl electrode system (Eugene, CO, USA) referenced to Cz. Electrode impedances were below 30 KOhm (100 MOhm input impedance amplifier). The sampling frequency was 250 Hz, with a 0.1–100 Hz analog band pass filter, and A–D conversion was at 12 bits precision. The EEG data were re-referenced to a grand mean, and band-pass filtered using 3-rd order Butterworth filters 0.2–45 Hz to eliminate line-noise. An additional Whittaker filter was applied to reduce movement and blink artifacts. The power in each frequency was obtained applying a short-time Fourier transform with a moving window of 60 s and 54 s overlap. The power spectra have been computed 1 min before infusion start ($t = 1$ min) and 4 min after infusion ($t = 5$ min). For visualization reasons, these power spectra at different time instances have been smoothed by a running average over frequencies with a 1 Hz window and a 0.017 Hz frequency step.

2.2. THALAMO-CORTICAL MODEL

The body of the model (Robinson et al., 2001; Rennie et al., 2002) is based on a population-level description of a single thalamo-cortical module comprising four populations of neurons, namely excitatory (E) and inhibitory (I) cortical population, a population built of thalamo-cortical relay neurons (S) and of thalamic reticular neurons (R), as shown in **Figure 1**. The details of the model and the nominal parameter values are taken from a previous work (Robinson et al., 2001, 2002). This model is based on the original idea of Lopes da Silva et al., stating that the α-rhythm represents the noisy thalamic input signal band-pass filtered by feedback-connected cortical and thalamic neural populations (Lopes da Silva et al., 1974). Here we just briefly describe the key concepts of the model. The average soma membrane potential denoted by V_a, for $a = E, I, S, R$ is modeled by

$$V_a(t) = \sum_{b=E,I,R,S} h_b(t) \otimes \nu_{ab}\phi_b(t - \tau_{ab}), \tag{1}$$

where $\otimes$ represents the temporal convolution, $h_b(t) = H_b\bar{h}_b(t)$ where $\bar{h}_b(t)$ denotes the mean synaptic response function defined by

$$\bar{h}_b(t) = \frac{\alpha\beta_b}{\alpha - \beta_b}\left(e^{-\beta_b t} - e^{-\alpha t}\right), \tag{2}$$

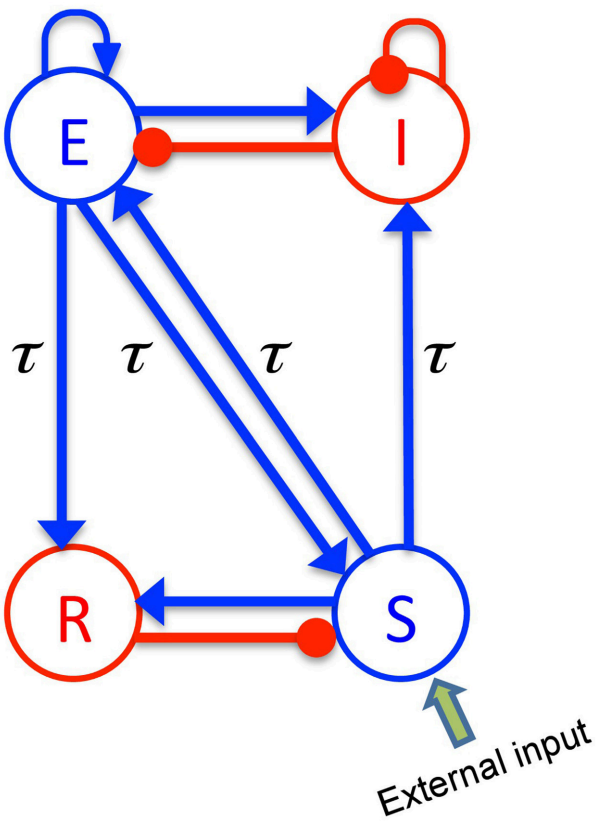

FIGURE 1 | The schematic of a thalamo-cortical module. The blue arrows indicate excitatory connections while the red connections with filled circle ends denote inhibitory connections. The symbols *E*, *I*, *S*, and *R* denote the excitatory and inhibitory cortical neurons, thalamo-cortical relay, and thalamic reticular neurons, respectively. In addition thalamocortical and corticothalamic connections exhibit the same nonzero time delay τ.

and α and β_b (with units Hz) are the synaptic rise and decay rates of the synaptic response, respectively. The synaptic decay rates and synaptic response functions depend on the source neurons of type b only and are independent of the target neurons. The constant pre-factor H_b defines the response function amplitude subject to the anesthetic concentration. Here, we assume identical excitatory synaptic receptors with constant rise and decay rate. Inhibitory synaptic receptors are also assumed to exhibit identical constant rise and decay rates while their decay rates depend on the anesthetic concentration. This strong approximation is taken from a previous study (Hindriks and van Putten, 2012) to be able to compare our results, while preliminary studies with more realistic parameters show similar results (not shown).

The constants ν_{ab} are the strengths of the connections from population of type b to population of type a (in mVs), and ϕ_b is the average firing rate of the population b (in Hz). The connections between cortex and thalamus are associated with a same nonzero time delay, $\tau_{ab} = \tau$, while the delay term is assumed to be zero within the cortex and within the thalamus (Victor et al., 2011).

By virtue of long-range axonal projections of excitatory cortical neurons and by assuming the spatially-homogeneous dynamics on the cortex, the average firing rate ϕ_E obeys the damped oscillator equation

$$D\phi_E = S(V_E), \tag{3}$$

where the operator D is defined as

$$D = \left(\frac{1}{\gamma}\frac{\partial}{\partial t} + 1\right)^2, \tag{4}$$

and γ is the cortical damping rate. It is assumed that the spatial spread of activity is very fast in other populations and the activity variable can be approximated by a sigmoidal function as $\phi_b = S(V_b)$, for $b = I, S, R$. Conversely to the original model (Robinson et al., 2001, 2002; Victor et al., 2011) we use a more realistic transfer function derived from properties of type I-neurons given by Hutt and Buhry (2014)

$$S(V_a) = Sig(V_a, 0) - Sig(V_a, \rho), \tag{5}$$

with

$$Sig(V_a, \rho) = \frac{S_a^{max}}{2}\left(1 + \mathrm{erf}\left(\frac{V_a - \theta_a - \rho\sigma^2}{\sqrt{2}\sigma}\right)\right) e^{-\rho(V_a-\theta_a)+\rho^2\sigma^2/2}, \tag{6}$$

with $\sigma = 10\,\mathrm{mV}$ and $\rho = 0.08\,\mathrm{mV}^{-1}$, where σ is related to the standard deviation of firing thresholds, the parameter $\rho < \infty$ reflects the properties of type I-neurons, S^{max} is the maximum population firing rate, and θ_a is the mean firing threshold of neurons in population a. In contrast to the standard transfer function given in Robinson et al. (2001), the transfer function in Equation (6) is not anti-symmetric to its inflection point anymore (Hutt, 2012) and exhibits a larger non-linear gain (slope) for large potentials $V_a > \theta_a$ compared to small potentials $V_a < \theta_a$. This asymmetry results from the firing properties of type-I neurons, see Hutt (2012); Hutt and Buhry (2014) for more details. For $\rho \to \infty$, the sigmoid function becomes the conventional antisymmetric transfer function.

The external input to the system is considered as a non-specific input to thalamo-cortical relay neurons as

$$\phi_N = \langle\phi_N\rangle + \sqrt{2\kappa}\xi(t), \tag{7}$$

where $\langle\phi_N\rangle$ indicates its mean value and $\xi(t)$ is a zero average Gaussian white noise and κ is the noise intensity.

The power spectrum characterizes small fluctuations about the resting state of the system defined by $dV_a(t)/dt = 0$. Following Robinson et al. (2001); Nunez and Srinivasan (2006), it is assumed that the activity of excitatory cortical neurons generates the EEG, and due to the specific choice of external input to thalamo-cortical relay neurons, the power spectrum of the EEG is related to the Greens function of linear deviations about the resting state by Hutt (2013)

$$P_E(\omega) = 2\kappa\sqrt{2\pi}\left|\tilde{G}_{1,3}(\omega)\right|^2, \tag{8}$$

in which $P_E(\omega)$ depends just on one matrix component of the matrix Greens function $\tilde{G}(\omega)$, see the Supplementary Material for its definition. We point out that the subsequent power spectrum analysis is based on Equation (8) and changing a system parameter, such as the factor p, changes the resting state, the corresponding non-linear gains and consequently the power spectrum. In addition, the power spectrum analysis is valid only if the resting state is stable and hence the fluctuations do not diverge. We have taken care of this additional condition and all given parameters guarantee the existence and stability of the resting state.

2.3. EFFECT OF PROPOFOL ON NEURAL POPULATIONS

In order to mimic anesthetic action, we consider the general anesthetic propofol which affects synaptic and extra-synaptic GABAergic receptors. We assume that the decay rate of inhibitory synapses is identical in all neural populations under study, and decreases with increasing propofol concentration in accordance with experimental findings (Kitamura et al., 2002; Hutt and Longtin, 2009). Mathematically, such a dependence on the anesthetic concentration can be taken into account by a concentration factor $p \geq 1$ and $\beta_b = \beta_0/p$ while increasing p reflects an increase of the on-site concentration of propofol (Foster et al., 2008; Hindriks and van Putten, 2012; Hutt et al., 2013). Since propofol has been shown to retain the amplitude of inhibitory synaptic response functions (Kitamura et al., 2002), one can define $H_b = \Gamma(\alpha, \beta_0)/\Gamma(\alpha, \beta_b)$ for $b = I, R$, where

$$\Gamma(\alpha, \beta) = \frac{\alpha\beta}{\alpha - \beta}\left[(\alpha/\beta)^{\frac{-\beta}{\alpha-\beta}} - (\alpha/\beta)^{\frac{-\alpha}{\alpha-\beta}}\right],$$

i.e., $\Gamma(\alpha, \beta_b) = \bar{h}_b(t_0)$ is the peak amplitude of $\bar{h}_b(t)$ at time $t_0 = \ln(\alpha/\beta_b)/(\alpha - \beta_b)$. Thereby the maximum height of $h_b(t)$ is $h_{max} = \Gamma(\alpha, \beta_0)$ which is independent of the action of propofol (Hindriks and van Putten, 2012). Moreover, since it is assumed

that propofol does not act on excitatory synaptic transmission, $H_b = 1$ and $h_b(t) = \bar{h}_b(t)$ for $b = E, S$. The GABAergic ESR tonic inhibition can be represented in the model as a constant shift of the firing threshold in neural population models (Hutt and Buhry, 2014). For simplicity, we assume a linear relationship between the anesthetic concentration parameter p and the extra-synaptic threshold shift

$$\theta_a = \theta_0 + (p-1)k_a \tag{9}$$

with the unique firing threshold $\theta_0 = 15\,\text{mV}$ identical for all populations in the absence of propofol and the extra-synaptic anesthetic sensitivity $k_a > 0$. Here, $(p-1)k_a$ is the tonic inhibition induced by extra-synaptic action which depends linearly on the propofol concentration. Future experimental studies may motivate a more realistic relationship of threshold shift and the anesthetic concentration parameter. Summarizing, synaptic and extra-synaptic inhibition, and hence anesthetic action, is present in the cortical populations E and I and in the thalamic population of relay neurons S.

2.4. POWER SPECTRUM

The present study examines the effect of tonic inhibition in various populations E, I, S on the power spectrum of neural activity in cortical excitatory neurons, i.e., population E. We will focus on the power in the $\delta-$ and $\alpha-$ frequency ranges in the interval [0.5 Hz−4Hz] and [8 Hz−12 Hz], respectively.

The subsequent analysis reveals power peaks in these frequency ranges, whose magnitude changes with the level of tonic inhibition. These power peaks exhibit a maximum of power, expressed mathematically as a local maximum of the function $P_E(f)$ where P_E is taken from Equation (8). The local maximum at frequency f_0 is defined as $dP_E/df = 0$, $d^2P_E/df^2 < 0$ computed at f_0. If there is a local maximum of power in the $\delta-$ frequency range, then $\delta-$activity is present, whereas a missing local maximum in the $\delta-$frequency range indicates missing $\delta-$activity. Since the magnitude and frequency of power peaks change with the propofol concentration and extra-synaptic threshold, the concentration factor p and the extra-synaptic anesthetic sensitivity k_a are the parameters of the power spectrum, i.e., $P_E = P_E(p, k_a, f)$.

To illustrate the usefulness of this parametrization, let us assume a factor k_{a0} for which no $\delta-$power peak exists in the power spectrum $P_E(p, k_{a0}, f)$, and k_{a1}, $k_{a1} > k_{a0}$ is the extra-synaptic anesthetic sensitivity leading to a spectral $\delta-$power peak in $P_E(p, k_{a1}, f)$ with $dP_E(p, k_{a1}, f_{max})/df_{max} = 0$ where f_{max} is a frequency in the $\delta-$frequency range. Mathematically, then the continuity of all model functions and variables guarantee that there is a threshold for the emergence of $\delta-$activity at a certain extra-synaptic anesthetic sensitivity $k_{a,thr}$ with $k_{a0} \leq k_{a,thr} \leq k_{a1}$. Consequently, if a threshold extra-synaptic anesthetic sensitivity for $\delta-$activity exists, then the variation of model variables about this critical point guarantees the emergence of $\delta-$activity. This mathematical reasoning allows us to investigate conditions under which $\delta-$activity may emerge.

3. RESULTS

Figure 2 illustrates how the EEG power spectrum depends on the concentration of propofol for a single subject. After starting the infusion at $t = 0$ min, the estimated propofol effect-site concentration increases gradually with time (**Figure 2A**); resulting in increased power in the $\delta-$ and $\alpha-$frequency ranges (**Figure 2B**). Over the period of the spectrogram the subject has become progressively more sedated; until a $t = 5$ min the subject no longer responds to verbal command but would still be responsive to nociceptive stimuli. **Figure 2C** shows the power spectra in the awake and sedation conditions. We observe a power enhancement primarily in the $\delta-$ and $\alpha-$frequency ranges.

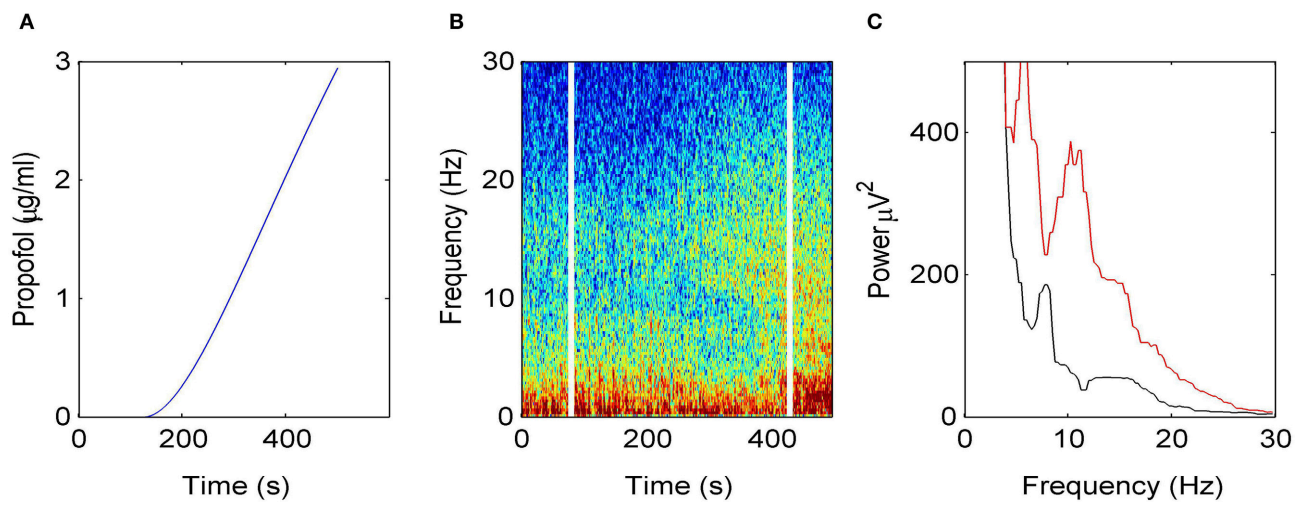

FIGURE 2 | Electroencephalographic data observed under anesthesia sedation in a single subject while increasing the propofol concentration. (A) Blood plasma concentration of propofol with respect to administration time. **(B)** Spectrogram of frontal EEG power. The vertical lines denote time windows well before the administration (left line) and at about 5 min after the start of propofol infusion (right side); **(C)** Power spectra computed before the infusion of propofol (black) and 5 min after the start of infusion (red).

To understand how propofol might enhance $\delta-$ and $\alpha-$power, we study the power spectrum of our theoretical model for different anesthetic concentration levels and examine the impact of adding tonic inhibition via extra-synaptic $GABA_A$ receptors. **Figure 3A** shows the interaction between propofol and tonic inhibition in the cortical inhibitory neuronal population. If we set the tonic inhibition to zero ($k_I = 0\,\text{mV}$), we observe a decrease in spectral power as propofol concentrations increase (i.e., the power moves from the black line to the blue line in the figure). If we set the tonic inhibition to $(p-1)\cdot 15\,\text{mV}$ we see the opposite effect—there is an increase of $\delta-$ and $\alpha-$power (black line to red line), with increasing propofol concentration.

Previous studies have indicated that extra-synaptic inhibition in thalamic relay neurons may control the level of inhibition in the brain (Brickley and Mody, 2012). However, **Figure 3B** reveals that adding a nonzero tonic inhibition in the thalamic relay neurons causes a decrease in the spectral power, similar to the previous case of absent tonic inhibition in the inhibitory cortical neurons.

It is well-known that GABAergic anesthetics change the EEG from high frequency-low amplitude signals to low frequency-high amplitude signals (Gugino et al., 2001; Feshchenko et al., 2004). **Figures 3C,D** show simulated time series in the absence and presence of tonic inhibition in cortical inhibitory cells reproducing this experimental finding.

Our results elucidates that tonic inhibition in cortical interneurons and thalamic relay neurons affect the cortical power spectrum differently. This finding is similar to results of a previous computational neural population study of a cortico-thalamic feedback single-neuron model (Talavera et al., 2009). **Figure 4** shows how the resting membrane potential (**Figure 4A**) and the non-linear gain (**Figure 4B**) in the cortical excitatory population change with differing extra-synaptic anesthetic sensitivity in cortical inhibitory neurons (k_I) and in the thalamic relay neurons (k_S). We observe that both the resting potential and the non-linear gain of cortical excitatory neurons increase when the cortical inhibitory extra-synaptic anesthetic sensitivity k_I increases,

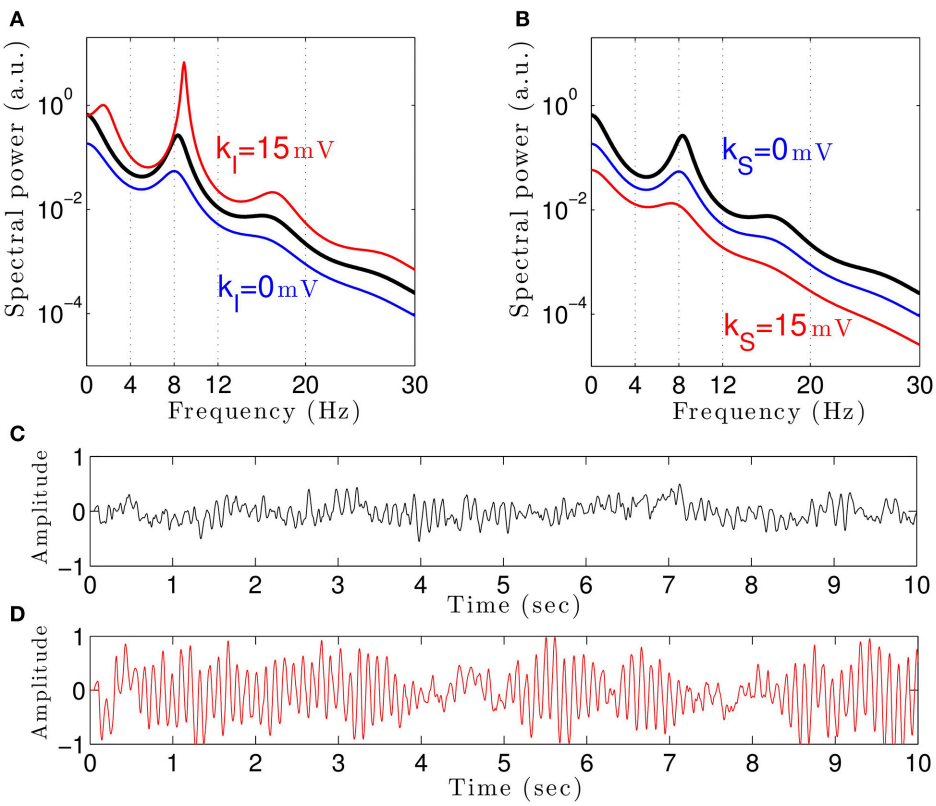

FIGURE 3 | The theoretical EEG power spectrum in the baseline and in the sedation condition with and without tonic inhibition in the cortical inhibitory neurons *I* in (A) and the thalamic relay neurons *S* in (B) and corresponding simulated EEG time-seris. In **(A)** the administration of propofol without tonic inhibition (blue line) attenuates the power spectrum compared to the baseline condition (black line) while the tonic inhibition (red line) increases the global power and generates oscillatory activity in the $\delta-$frequency range. In **(B)** increasing the anesthetic concentration yields a global power decrease in the sedation condition without tonic inhibition (blue line) and a further power decrease in the presence of tonic inhibition (red line). In **(A)** and **(B)**, the black lines indicate the EEG-spectral power in the baseline condition ($p = 1$), and the blue and red lines show the power spectrum in anesthesia condition ($p = 1.125$) in the absence ($k_a = 0$) and in the presence ($k_a = 15\,\text{mV}$) of tonic inhibition, respectively. **(C)** The simulated EEG time-series ($\phi_E(t)$ defined in Equation (3)) in the absence of extra-synaptic effects, i.e., $k_E = k_I = k_S = 0\,\text{mV}$. **(D)** The EEG time-series in the presence of extra-synaptic action in cortical inhibitory neurons with $k_I = 15\,\text{mV}$, $k_E = k_S = 0\,\text{mV}$. The tonic inhibition changes the EEGs from low-amplitude, high-frequency pattern to high-amplitude, low-frequency pattern. In addition, the strength of cortical self-inhibition is $\nu_{ii} = -1.8\,\text{mVs}$.

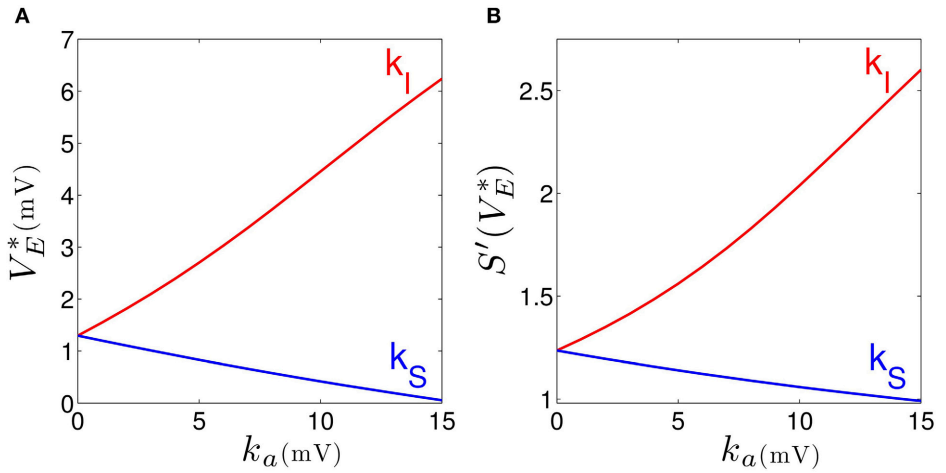

FIGURE 4 | Increasing the tonic inhibition (factor k_a for $a = I$ and S) affects the resting state of excitatory cortical neurons V_E^* (A) and the corresponding non-linear cortical gain function (B). Here the anesthetic concentration factor is identical in the populations $a = E, I$ and S to $p = 1.125$. In addition, the strength of cortical self-inhibition is $\nu_{ii} = -1.8$ mVs.

whereas resting potential and non-linear gain of cortical excitatory neurons decrease when the extra-synaptic anesthetic sensitivity in thalamic relay neuron k_S increases. Since the non-linear gain is proportional to the systems responsiveness to external stimuli, the power enhancement in population I may be explained by the augmented responsiveness of the cortical excitatory neurons. This responsiveness depends on the sub-circuit in which the neurons are involved. Since relay neurons are part of the thalamo-cortical feedback loop, while cortical inhibitory neurons contribute to the cortical loop, the cell types respond differently to the thalamic input. Essentially assuming tonic inhibition in the population of cortical excitatory neurons E, the study reveals a similar propofol concentration dependence of the power spectrum, the resting state potential and the non-linear gain as for the thalamic tonic inhibition S. This shows the unique tonic inhibition effect in the cortical inhibitory neurons.

Figure 3A shows the power spectrum for single values of the extra-synaptic sensitivity k_I, for single values of the concentration factor p and fixed strength of cortical self-inhibition ν_{ii}, while **Figure 4** gives more details on the role of extra-synaptic sensitivity for fixed values of the concentration factor p and fixed cortical self-inhibition. To understand better the interplay between tonic inhibition, synaptic inhibition and the strength of cortical self-inhibition, **Figure 5** shows the parameter pairs of synaptic inhibition p and the threshold of extra-synaptic sensitivity $k_{I,thr}$ at different self-inhibition levels, for which a peak in the $\delta-$frequency range emerges. Recall that the $k_{I,\,thr}$ is the critical (smallest) value of extra-synaptic sensitivity in cortical inhibitory neurons k_I, that lead to $dP_E/df = 0$, $d^2P_E/df^2 < 0$ computed at $f_{max} \in \delta-$range, cf. the subsection on the power spectrum in Section 2. Parameter values beyond the respective curves lead to $\delta-$activity power peaks. We observe that $\delta-$activity always emerges for sufficiently strong tonic inhibition (large extra-synaptic sensitivity k_I) and sufficiently strong self-inhibition ν_{ii}, while the weaker the self-inhibition is the larger is

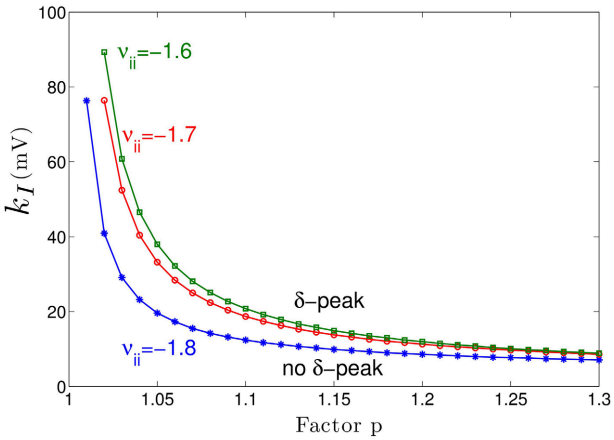

FIGURE 5 | Parameter space for $\delta-$power peak. The lines give the smallest (threshold) value of the extra-synaptic sensitivity $k_{I,\,thr}$ that induces $\delta-$ oscillations in the sedation condition with respect to the concentration factor p for different values of self-inhibitory connections ν_{ii}. The weaker the cortical self-inhibition (the smaller $|\nu_{ii}|$), the higher the necessary level of propofol concentration (larger p) and the tonic inhibition [larger $(p-1)\cdot k_I$] to induce $\delta-$activity.

the necessary extra-synaptic sensitivity or the synaptic inhibition to generate $\delta-$activity. Even for vanishing cortical self-inhibition ($\nu_{ii} = 0$), mathematical analysis (not shown) reveals that there is still a $\delta-$peak in the power spectrum for large enough synaptic or tonic inhibition (for p or k_I large enough).

Moreover, **Figure 5** reveals a minimum tonic inhibition level (minimum value of k_I) beneath which no $\delta-$power peak emerges, irrespective of the level of synaptic inhibition (p). This result indicates a major role of tonic inhibition in the generation of $\delta-$activity, since it may support $\delta-$activity even if the synaptic inhibition level is not sufficient to support it.

4. DISCUSSION

In the sedation phase, for modest concentrations of propofol, the EEG power spectrum exhibits an increase in the $\delta-$ and $\alpha-$frequency ranges (**Figure 2**) as found experimentally in the induction phase of propofol anesthesia (San-Juan et al., 2010). One possible explanation for these phenomena is by postulating stronger GABAergic potentiation within cortical inhibitory neurons than within cortical pyramidal neurons (Hindriks and van Putten, 2012). We hypothesize, that cortical GABAergic self-inhibition plays a decisive role. **Figure 3** reveals that the power surge in these frequency ranges might also result from extra-synaptic tonic inhibition active in cortical inhibitory neurons. Tonic inhibition increases the firing threshold and hence diminishes the output of inhibitory neurons to excitatory cortical neurons, which then allows increased excitation in the excitatory population and a power surge in the EEG. Conversely tonic inhibition in the thalamic relay cells does not induce power surge in EEG since augmented inhibition in the thalamic relay cells yields diminished excitation in cortical excitatory neurons, leading to a decrease in EEG power. This interpretation is corroborated by **Figure 4** which demonstrates augmented and diminished nonlinear gain in cortical excitatory neurons assuming tonic inhibition in inhibitory and thalamic relay population, respectively. This reflects enhanced and weakened response to the noisy thalamic external input, see previous theoretical studies (Hindriks and van Putten, 2012; Hutt, 2013) for a similar line of argument.

Figure 3 clearly reveals the emergence of $\delta-$activity caused by extra-synaptic tonic inhibition which is affirmed by the existence of a minimum level of extra-synaptic inhibition shown in **Figure 5**. Conversely, $\alpha-$activity appears to be much less sensitive to tonic inhibition since it is present for all tonic inhibition levels. One interpretation may be the generation of $\alpha-$activity by the cortico-thalamic feedback as hypothesized theoretically (Robinson et al., 2004) while $\delta-$activity results from the cortical interaction of excitatory and inhibitory neurons. The exact origins of propofol-induced $\alpha-$ and $\delta-$activity are not known for certain. We find that the $\alpha-$oscillations arise from thalamocortical resonances. These oscillations are commonly synchronous across widespread cortical regions and are not easily generated in isolated cortical tissue (Contreras et al., 1996; Destexhe et al., 1999). This affirms the original model of Lopes da Silva et al. (1974). However, our model results are equivalent to results of other models describing $\alpha-$activity by purely cortical interactions. We are not aware of a methodology ruling out one or the other model and this is not the aim of the present work. Our work just reveals the additional possibility that the thalamus serves as a possible (indirect) source of $\alpha-$activity. Similarly, the origin of $\delta-$activity is not clear, but slow activity does increase at higher concentrations of propofol—which may be associated with decreasing $\alpha-$waves as observed during desflurane general anesthesia (Mulholland et al., 2014). This is in keeping with $\delta-$waves becoming more pronounced as the cortico-thalamic systems becomes increasingly hyperpolarized. However, there is a lot of variability between patients as regards the relative power of $\alpha-$ and $\delta-$activity during general anesthesia; which would suggest that the true explanation is more complex, and requires recognition of other factors such as the one presented in this paper—the influence of the propofol on extra-synaptic inhibition.

Although anesthetic action on synaptic and extra-synaptic GABAergic receptors is different, both actions diminish neural activity and hence increase inhibition. **Figure 5** elucidates that strong enough extra-synaptic or synaptic inhibition induce $\delta-$activity. Hence, one may argue that the level of inhibition plays an important role while its origin, i.e., synaptic or extra-synaptic, plays a secondary role. This interpretation corroborates the idea of the balance of excitation and inhibition as the major mechanism in general anesthesia. This interpretation is in good accordance to previous experimental findings on the important role of the balance of excitation and inhibition in brain network under anesthesia (Okun and Lampl, 2008; Taub et al., 2013). Such global concepts as excitation-inhibition balance are attractive to describe complex processes in general anesthesia. For instance, anesthetics alter arousal in several pathways, such as the cholinergic pathway (Brown et al., 2010) and the orexinergic pathway which has been identified to activate a complex functional network controlling, inter alia, the emergence from unconsciousness (Kelz et al., 2008).

Our theoretical study considers the anesthetic propofol and its corresponding action at synaptic and extra-synaptic GABAergic receptors only, whereas it is known that propofol induces inhibition at various other receptors as well (Alkire et al., 2008; Nguyen et al., 2009) including minor effects on NMDA-receptors and voltage-gated potassium channels (Alkire et al., 2008). Propofol also potentiates glycine receptors which are are found all over the central nervous system and have a major role in regulating inhibition, e.g., in the brain stem (Lynch, 2004).

Similar to extra-synaptic inhibition resulting from ambient GABA concentrations, the presence of ambient concentrations of glycine close to NMDA-receptors entails tonic depolarization. This tonic excitation diminishes the firing threshold of neurons and hence may counteract inhibition. The present work considers tonic inhibition only and neglects tonic excitation effect. Although it would be important to study tonic excitation effects, this additional study would exceed the major aim of the manuscript, namely demonstrating the fundamental effect of tonic anesthetic action.

In addition, by virtue of the focus on extra-synaptic action, the model proposed neglects known anesthetic effects on different receptors and ion channels, although they have been shown experimentally, e.g., Grasshoff et al. (2006); Alkire et al. (2008) and references therein, and theoretically (Bojak et al., 2013) to affect EEG activity. Specifically, the latter work of Bojak et al. (2013) considers anesthetic effects on hyperpolarization-activated cyclic nucleotide-gated potassium channel 1 (HCN1) subunits which, effectively, increase the mean firing threshold in neural populations and strongly resembles the tonic inhibition induced by extra-synaptic GABA-receptors.

The model network topology includes a single module of a closed thalamo-cortical feedback loop (Granger and Hearn, 2007) comprising two thalamic nuclei and cortical excitatory and inhibitory neurons. This model represents a first approximation of brain networks since it neglects brain stem activity including the reticular activating system (RAS) (Magoun, 1952) which

has significant modulating effects on attention, arousal and consciousness. Future work will include structures of the brain stem, propofol action on glycine receptors, and will take into account the RAS—since its neural structures involved exhibit strong extra-synaptic inhibition (Fiset et al., 1999; Franks, 2008; Vanini and Baghdoyan, 2013). The model also neglects the cholinergic pathway originating from the basal forebrain (Laalou et al., 2008) which is known to co-regulate the level of consciousness (Brown et al., 2010).

Essentially, our theoretical model assumes population coding implying rate-coding response activity of neuron populations subjected to external thalamic noise. The model does not consider specific single neuron dynamics found experimentally under anesthetic conditions. For instance, it has been hypothesized that, at certain levels of anesthetic concentration, thalamic neurons switch their activity from tonic firing to bursting and induce loss of consciousness (Alkire et al., 2000).

In spite of these limitations, our model reproduces qualitatively the action of propofol on EEG and reveals the possible impact of extra-synaptic GABAergic receptors on the EEG power. To our knowledge, the present work is the first to link extra-synaptic GABAergic action and experimental EEG. Future work will refine the model involving additional receptor action, e.g., tonic excitation caused by ambient glycine concentrations, and sub-cortical brain structures.

AUTHOR CONTRIBUTIONS

Meysam Hashemi has chosen the model and performed the model analysis, Axel Hutt has conceived the study and Jamie Sleigh has acquired and analyzed the experimental data. The authors have written the manuscript to equal parts and have approved the final version.

FUNDING

The research resulting to the presented work has received funding from the European Research Council under the European Unions Seventh Framework Programme (FP7/2007-2013) / ERC grant agreement no. 257253.

SUPPLEMENTARY MATERIAL

The Supplementary Material for this article can be found online at: http://www.frontiersin.org/journal/10.3389/fnsys.2014.00232/abstract

REFERENCES

Alkire, M., Haier, R. J., and Fallon, J. H. (2000). Toward a unified theory of narcosis: brain imaging evidence for a thalamocortical switch as the neurophysiologic basis of anesthetic-induced unconsciousness. *Conscious. Cogn.* 9, 370–386. doi: 10.1006/ccog.1999.0423

Alkire, M., Hudetz, A., and Tononi, G. (2008). Consciousness and anesthesia. *Science* 322, 876–880. doi: 10.1126/science.1149213

Bai, D., Zhu, G., Pennefather, P., Jackson, M. F., MacDonald, J. F., and Orser, B. (2001). Distinct functional and pharmacological properties of tonic and quantal inhibitory postsynaptic currents mediated by γ−aminobutyric acid a receptors in hippocampal neurons. *Mol. Pharmacol.* 59, 814–824. doi: 10.1124/mol.59.4.814

Belelli, D., Harrison, N. L., Maguire, J., MacDonald, R. L., Walker, M. C., and Cope, D. W. (2009). Extra-synaptic GABAA receptors: form, pharmacology, and function. *J. Neurosci.* 29, 12757–12763. doi: 10.1523/JNEUROSCI.3340-09.2009

Bojak, I., Day, H., and Liley, D. (2013). Ketamine, propofol, and the eeg: a neural field analysis of hcn1-mediated interactions. *Front. Comput. Neurosci.* 7:22. doi: 10.3389/fncom.2013.00022

Bojak, I. and Liley, D. (2005). Modeling the effects of anesthesia on the electroencephalogram. *Phys. Rev. E Stat. Nonlin. Soft. Matter Phys.* 71:041902. doi: 10.1103/PhysRevE.71.041902

Boly, M., Moran, R., Murphy, M., Boveroux, P., Bruno, M. A., Noirhomme, Q., et al. (2012). Connectivity changes underlying spectral EEG changes during propofol-induced loss of consciousness. *J. Neurosci.* 32, 7082–7090. doi: 10.1523/JNEUROSCI.3769-11.2012

Bressloff, P. (2012). Spatiotemporal dynamics of continuum neural fields. *J. Phys. A Math. Theor.* 45:033001. doi: 10.1088/1751-8113/45/3/033001

Brickley, S. G., Cull-Candy, S. G., and Farrant, M. (1996). Development of a tonic form of synaptic inhibition in rat cerebellar granule cells resulting from persistent activation of GABAA receptors. *J. Physiol.* 497, 753–759.

Brickley, S. G. and Mody, S. (2012). Extrasynaptic $GABA_A$ receptors: their function in the cns and implications for disease. *Neuron* 73, 23–34. doi: 10.1016/j.neuron.2011.12.012

Bright, D. P., Aller, M., and Brickley, S. (2007). Synaptic relase generates a tonic $GABA_A$ receptor-mediated conductance that modulates burst precision in thalamic relay neurons. *J. Neurosci.* 27, 2560–2569. doi: 10.1523/JNEUROSCI.5100-06.2007

Bright, D. P., Renzi, M., Bartram, J., McGee, T. P., MacKenzie, G., Hosie, A. M., et al. (2011). Profound desensitization by ambient GABA limits activation of delta-containing GABAA receptors during spillover. *J. Neurosci.* 31, 753–763. doi: 10.1523/JNEUROSCI.2996-10.2011

Brown, E., Lydic, R., and Schiff, N. (2010). General anesthesia, sleep, and coma. *N. Engl. J. Med.* 363, 2638–2650. doi: 10.1056/NEJMra0808281

Cavalier, P., Hamann, M., Rossi, D., Mobbs, P., and Attwell, D. (2005). Tonic excitation and inhibition of neurons: ambient transmitter sources and computational consequences. *Prog. Biophys. Mol. Biol.* 87, 3–16. doi: 10.1016/j.pbiomolbio.2004.06.001

Ching, S., Cimenser, A., Purdon, P. L., Brown, E. N., and Kopell, N. J. (2010). Thalamocortical model for a propofol-induced-rhythm associated with loss of consciousness. *Proc. Natl. Acad. Sci. U.S.A.* 107, 22665–22670. doi: 10.1073/pnas.1017069108

Ching, S., Purdon, P. L., Vijayand, S., Kopell, N. J., and Brown, E. N. (2012). A neurophysiologicalmetabolic model for burst suppression. *Proc. Natl. Acad. Sci. U.S.A.* 109, 3095–3100. doi: 10.1073/pnas.1121461109

Cimenser, A., Purdon, P. L., Pierce, E. T., Walsh, J. L., Salazar-Gomez, A. F., Harrell, P. G., et al. (2011). Tracking brain states under general anesthesia by using global coherence analysis. *Proc. Natl. Acad. Sci. U.S.A.* 108, 8832–8837. doi: 10.1073/pnas.1017041108

Contreras, D., Destexhe, A., Sejnowski, T., and Steriade, M. (1996). Control of spatiotemporal coherence of a thalamic oscillation by corticothalamic feedback. *Science* 274, 771–774. doi: 10.1126/science.274.5288.771

Coombes, S. (2006). Neural Fields. *Scholarpedia* 1:1373. doi: 10.4249/scholarpedia.1373

Daniels, S. and Roberts, R. (1998). Post-synaptic inhibitory mechanisms of anaesthesia: glycine receptors. *Toxicol. Lett.* 100-101, 71–76. doi: 10.1016/S0378-4274(98)00167-2

Destexhe, A., Contreras, D., and Steriade, M. (1999). Mechanisms underlying the synchronizing action of corticothalamic feedback through inhibition of thalamic relay cells. *J. Neurophysiol.* 79, 999–1016.

Dickinson, R., Peterson, B., Banks, P., Simillis, C., Martin, J., Valenzuela, C., et al. (2007). Competitive inhibition at the glycine site of the n-methyl-d-aspartate receptor by the anesthetics xenon and isoflurane: evidence from molecular modeling and electrophysiology. *Anesthesiology* 107, 756–767. doi: 10.1097/01.anes.0000287061.77674.71

Farrant, M. and Nusser, Z. (2005). Variations on an inhibitory theme: phasic and tonic activation of GABAA receptors. *Nat. Rev. Neurosci.* 6, 215–229. doi: 10.1038/nrn1625

Feshchenko, V. A., Veselis, R. A., and Reinsel, R. A. (2004). Propofol-induced alpha rhythm. *Neuropsychobiology* 50, 257–266. doi: 10.1159/000079981

Fiset, P., Paus, T., Daloze, T., Plourde, G., Meuret, P., Bonhomme, V., et al. (1999). Brain mechanisms of propofol-induced loss of consciousness in humans: a positron emission tomographic study. *J. Neurosci.* 19, 5506–5513.

Fleming, T., Scott, V., Naskar, K., Joe, N., Brown, C., and Stern, J. (2011). State-dependent changes in astrocyte regulation of extrasynaptic nmda

receptor signalling in neurosecretory neurons. *J. Physiol.* 589, 3929–3941. doi: 10.1113/jphysiol.2011.207340

Foster, B., Bojak, I., and Liley, D. J. (2008). Population based models of cortical drug response: insights from anaesthesia. *Cogn. Neurodyn.* 2, 283–296. doi: 10.1007/s11571-008-9063-z

Franks, N. (2008). General anesthesia: from molecular targets to neuronal pathways of sleep and arousal. *Nat. Rev. Neurosci.* 9, 370–386. doi: 10.1038/nrn2372

Franks, N. and Lieb, W. (1994). Molecular and cellular mechanisms of general anesthesia. *Nature* 367, 607–614. doi: 10.1038/367607a0

Friedman, E. B., Sun, Y., Moore, J. T., Hung, H.-T., Meng, Q. C., Perera, P., et al. (2010). A conserved behavioral state barrier impedes transitions between anesthetic-induced unconsciousness and wakefulness: evidence for neural inertia. *PLoS ONE* 5:e11903. doi: 10.1371/journal.pone.0011903

Granger, R. and Hearn, R. (2007). Models of thalamocortical system. *Scholarpedia* 2:1796. doi: 10.4249/scholarpedia.1796

Grasshoff, C., Drexler, B., Rudolph, U., and Antkowiak, B. (2006). Anaesthetic drugs: linking molecular actions to clinical effects. *Curr. Pharm. Des.* 12, 3665–3679. doi: 10.2174/138161206778522038

Gugino, L. D., Chabot, R. J., Prichep, L. S., John, E. R., Formanek, V., and Aglio, L. S. (2001). Quantitative EEG changes associated with loss and return of consciousness in healthy adult volunteers anaesthetized with propofol or sevoflurane. *Br. J. Anaesth.* 87, 421–428. doi: 10.1093/bja/87.3.421

Hamann, M., Rossi, D., and Attwell, D. (2002). Tonic and spillover inhibition of grnule cells control information flow through cerebellar cortex. *Neuron* 33, 625–633. doi: 10.1016/S0896-6273(02)00593-7

Hardingham, G. E. and Bading, H. (2012). Synaptic versus extrasynaptic nmda receptor signalling: implications for neurodegenerative disorders. *Nat. Rev. Neurosci.* 11, 682–696. doi: 10.1038/nrn2911

Hindriks, R. and van Putten, M. J. A. M. (2012). Meanfield modeling of propofol-induced changes in spontaneous EEG rhythms. *Neuroimage* 60, 2323–2344. doi: 10.1016/j.neuroimage.2012.02.042

Houston, C., McGee, T., MacKenzie, G., Troyano-Cuturi, K., Mateos Rodriguez, P., Kutsarova, E., et al. (2012). Are extrasynaptic $gaba_a$ receptors important targets for sedative/hypnotic drugs? *J. Neurosci.* 32, 3887–3897. doi: 10.1523/JNEUROSCI.5406-11.2012

Hutt, A. (2009). Oscillatory activity in excitable neural systems. *Contemp. Phys.* 51, 3–16. doi: 10.1080/00107510903293710

Hutt, A. (2012). The population firing rate in the presence of GABAergic tonic inhibition in single neurons and application to general anaesthesia. *Cogn. Neurodyn.* 6, 227–237. doi: 10.1007/s11571-011-9182-9

Hutt, A. (2013). The anaesthetic propofol shifts the frequency of maximum spectral power in EEG during general anaesthesia: analytical insights from a linear model. *Front. Comput. Neurosci.* 7:2. doi: 10.3389/fncom.2013.00002

Hutt, A. and Buhry, L. (2014). Study of GABAergic extra-synaptic tonic inhibition in single neurons and neural populations by traversing neural scales: application to propofol-induced anaesthesia. *J. Comput. Neurosci.* 37, 417–437. doi: 10.1007/s10827-014-0512-x

Hutt, A. and Longtin, A. (2009). Effects of the anesthetic agent propofol on neural populations. *Cogn. Neurodyn.* 4, 37–59. doi: 10.1007/s11571-009-9092-2

Hutt, A., Sleigh, J., Steyn-Ross, A., and Steyn-Ross, M. L. (2013). General anaesthesia. *Scholarpedia* 8:30485. doi: 10.4249/scholarpedia.30485

Johnson, B., Sleigh, J., Kirk, I., and Williams, M. (2003). High-density EEG mapping during general anaesthesia with xenon and propofol: a pilot study. *Anaesth. Intensive Care.* 31, 155–163. Available online at: http://www.aaic.net.au/Document/D=2002375

Kaneda, M., Farrant, M., and Cull-Candy, S. G. (1995). Whole-cell and single-channel currents activated by GABA and glycine in granule cells of the rat cerebellum. *J. Physiol.* 485, 419–435.

Kelz, M., Sun, Y., Chen, J., Cheng Meng, Q., Moore, J., Veasey, S., et al. (2008). An essential role for orexins in emergence from general anesthesia. *Proc. Natl. Acad. Sci. U.S.A.* 105, 1309–1314. doi: 10.1073/pnas.0707146105

Kitamura, A., Marszalec, W., Yeh, J., and Narahashi, T. (2002). Effects of halothane and propofol on excitatory and inhibitory synaptic transmission in rat cortical neurons. *J. Pharmacol.* 304, 162–171. doi: 10.1124/jpet.102.043273

Kopanitsa, M. V. (1997). Extrasynaptic receptors of neurotransmitters: distribution, mechanisms of activation, and physiological role. *Neurophysiology* 29, 448–458. doi: 10.1007/BF02463356

Kratzer, S., Mattusch, C., Kochs, E., Eder, M., Haseneder, R., and Rammes, G. (2012). Xenon attenuates hippocampal long-term potentiation by diminishing synaptic and extrasynaptic n-methyl-d- aspartate receptor currents. *Anesthesiology* 116, 673–682. doi: 10.1097/ALN.0b013e3182475d66

Kretschmannova, K., Hines, R. M., Revilla-Sanchez, R., Terunuma, M., Tretter, V., Jurd, R., et al. (2013). Enhanced tonic inhibition influences the hypnotic and amnestic actions of the intravenous anesthetics etomidate and propofol. *J. Neurosci.* 33, 7264–7273. doi: 10.1523/JNEUROSCI.5475-12.2013

Laalou, F., de Vasconcelos, A., Oberling, P., Jeltsch, H., Cassel, J., and Pain, L. (2008). Involvement of the basal cholinergic forebrain in the mediation of general (propofol) anesthesia. *Anesthesiology* 108, 888–896. doi: 10.1097/ALN.0b013e31816d919b

Le Meur, K., Galante, M., Angulo, M.-C., and Audinat, E. (2007). Tonic activation of nmda receptors by ambient glutamate of non-synaptic origin in the rat hippocampus. *J. Physiol.* 580, 373–383. doi: 10.1113/jphysiol.2006.123570

Lewis, L., Weiner, V., Mukamel, E., Donoghue, J., Eskandar, E., Madsen, J., et al. (2012). Rapid fragmentation of neuronal networks at the onset of propofol-induced unconsciousness. *Proc. Natl. Acad. Sci. U.S.A.* 109, E3377–E3386. doi: 10.1073/pnas.1210907109

Liley, D. and Bojak, I. (2005). Understanding the transition to seizure by modeling the epileptiform activity of general anaesthetic agents. *J. Clin. Neurophysiol.* 22, 300–313. Available online at: http://journals.lww.com/clinicalneurophys/Abstract/2005/10000/Understanding_the_Transition_to_Seizure_by.3.aspx

Liley, D. and Walsh, M. (2013). The mesoscopic modeling of burst suppression during anesthesia. *Front. Comput. Neurosci.* 7:46. doi: 10.3389/fncom.2013.00046

Lopes da Silva, F., Hoeks, A., Smits, H., and Zetterberg, L. (1974). Model of brain rhythmic activity. *Kybernetik* 15, 27–37. doi: 10.1007/BF00270757

Lynch, J. (2004). Molecular structure and function of the glycine receptor chloride channel. *Physiol. Rev.* 84, 1051–1095. doi: 10.1152/physrev.00042.2003

Magoun, H. (1952). An ascending reticular activating system in the brain stem. *AMA Arch. Neurol. Psychiatry* 67, 145–154. doi: 10.1001/archneurpsyc.1952.02320140013002

Martin, D., Plagenhoef, M., Abraham, J., Dennison, R., and Aronstam, R. (1995). Volatile anesthetics and glutamate activation of n-methyl-d-aspartate receptors. *Biochem. Pharmacol.* 49, 809–817. doi: 10.1016/0006-2952(94)00519-R

McCarthy, M. M., Brown, E. N., and Kopell, N. (2008). Potential network mechanisms mediating electroencephalographic beta rhythm changes during propofol-induced paradoxical excitation. *J. Neurosci.* 28, 13488–13504. doi: 10.1523/JNEUROSCI.3536-08.2008

McDougall, S. J., Bailey, T. W., Mendelowitz, D., and Andresen, M. C. (2008). Propofol enhances both tonic and phasic inhibitory currents in second-order neurons of the solitary tract nucleus (nts). *Neuropharmacology* 54, 552–563. doi: 10.1016/j.neuropharm.2007.11.001

Mothet, J., Parent, A., Wolosker, H., Brady, Jr., R., Linden, D., Ferris, C., et al. (2000). d-serine is an endogenous ligand for the glycine site of the n-methyl-d-aspartate receptor. *Proc. Natl. Acad. Sci. U.S.A.* 97, 4926–4931. doi: 10.1073/pnas.97.9.4926

Mulholland, C., Somogyi, A., Barratt, D., Coller, J., Hutchinson, M., Jacobson, G., et al. (2014). Association of innate immune single-nucleotide polymorphisms with the electroencephalogram during desflurane general anaesthesia. *J. Mol. Neurosci.* 52, 497–506. doi: 10.1007/s12031-013-0201-7

Murphy, M., Bruno, M.-A., Riedner, B. A., Boveroux, P., Noirhomme, Q., Landsness, E. C., et al. (2011). Propofol anesthesia and sleep: a high-density EEG study. *Sleep* 34, 283–291. Available online at: http://www.journalsleep.org/ViewAbstract.aspx?pid=28064

Nguyen, H., Li, K., da Graca, R., Delphin, E., Xiong, M., and Ye, J. (2009). Behavior and cellular evidence for propofol-induced hypnosis involving brain glycine receptors. *Anesthesiology* 110, 326–332. doi: 10.1097/ALN.0b013e3181942b5b

Nunez, P. and Srinivasan, R. (2006). *Electric Fields of the Brain: The Neurophysics of EEG*. Oxford, NY: Oxford University Press. doi: 10.1093/acprof:oso/9780195050387.001.0001

Nusser, Z., Cull-Candy, S., and Farrant, M. (1997). Differences in synaptic GABAA receptor number underlie variation in GABA mini amplitude. *Neuron* 19, 697–709. doi: 10.1016/S0896-6273(00)80382-7

Nusser, Z., Sieghart, W., and Somogyi, P. (1998). Segregation of different GABAA receptors to synaptic and extrasynaptic membranes of cerebellar granule cells. *J. Neurosci.* 18, 1693–1703.

Okun, M. and Lampl, I. (2008). Instantaneous correlation of excitation and inhibition during ongoing and sensory-evoked activities. *Nat. Neurosci.* 11, 535–537. doi: 10.1038/nn.2105

Orser, B. (2006). Extrasynaptic GABAA receptors are critical targets for sedative-hypnotic drugs. *J. Clin. Sleep Med.* 2, S12–S18. Available online at: http://www.aasmnet.org/jcsm/ViewAbstract.aspx?pid=26526

Panatier, A., Theodosis, D., Mothet, J.-P., Touquet, B., Pollegioni, L., Poulain, D., et al. (2006). Glia-derived d-serine controls nmda receptor activity and synaptic memory. *Cell* 125, 775–784. doi: 10.1016/j.cell.2006.02.051

Papouin, T., Ladépêche, L., Ruel, J., Sacchi, S., Labasque, M., Hanini, M., et al. (2012). Synaptic and extrasynaptic nmda receptors are gated by different endogeneous coagonists. *Cell* 150, 633–646. doi: 10.1016/j.cell.2012.06.029

Pender, J. (1970). Dissociative anesthesia. *Calif. Med.* 113, 73.

Purdon, P. L., Pierce, E. T., Mukamel, E. A., Prerau, M. J., Walsh, J. L., Wong, K. F., et al. (2012). Electroencephalogram signatures of loss and recovery of consciousness from propofol. *Proc. Natl. Acad. Sci. U.S.A* 110, E1142–E1150. doi: 10.1073/pnas.1221180110

Rennie, C., Robinson, P., and Wright, J. (2002). Unified neurophysical model of EEG spectra and evoked potentials. *Biol. Cybern.* 86, 457–471. doi: 10.1007/s00422-002-0310-9

Robinson, P., Rennie, C. J., Rowe, D. L., and O'Connor, S. C. (2004). Estimation of multiscale neurophysiologic parameters by electroencephalographic means. *Hum. Brain Mapp.* 23, 53–72. doi: 10.1002/hbm.20032

Robinson, P., Loxley, P., O'Connor, S., and Rennie, C. (2001). Modal analysis of corticothalamic dynamics, electroencephalographic spectra and evoked potentials. *Phys. Rev. E Stat. Nonlin. Soft. Matter Phys.* 63:041909. doi: 10.1103/PhysRevE.63.041909

Robinson, P., Rennie, C., and Rowe, D. (2002). Dynamics of large-scale brain activity in normal arousal states and epileptic seizures. *Phys. Rev. E Stat. Nonlin. Soft. Matter Phys.* 65:041924. doi: 10.1103/PhysRevE.65.041924

Sah, P., Hestrin, S., and Nicoli, R. (1989). Tonic activation of nmda receptors by ambient glutamate enhances excitability on neurons. *Science* 246, 815–818. doi: 10.1126/science.2573153

San-Juan, D., Chiappa, K., and Cole, A. (2010). Propofol and the electroencephalogram. *Clin. Neurophysiol.* 121, 998–1006. doi: 10.1016/j.clinph.2009.12.016

Sellers, K. K., Bennett, D. V., Hutt, A., and Frohlich, F. (2013). Anesthesia differentially modulates spontaneous network dynamics by cortical area and layer. *J. Neurophysiol.* 110, 2739–2751. doi: 10.1152/jn.00404.2013

Semyanov, A., Walker, M. C., and Kullmann, D. M. (2003). Gaba uptake regulates cortical excitability via cell-type specific tonic inhibition. *Nat. Neurosci.* 6, 484–490.

Semyanov, A., Walker, M. C., Kullmann, D. M., and Silver, R. A. (2004). Tonically active GABAA receptors: modulating gain and maintaining the tone. *Trends Neurosci.* 27, 262–269. doi: 10.1016/j.tins.2004.03.005

Steyn-Ross, M., Steyn-Ross, D., and Sleigh, J. (2004). Modelling general anaesthesia as a first-order phase transition in the cortex. *Prog. Biophys. Mol. Biol.* 85, 369–385. doi: 10.1016/j.pbiomolbio.2004.02.001

Steyn-Ross, M., Steyn-Ross, D., and Sleigh, J. (2013). Interacting turing-hopf instabilities drive symmetry-breaking transitions in a mean-field model of the cortex: a mechanism for the slow oscillation. *Phys. Rev. X* 3:021005. doi: 10.1103/PhysRevX.3.021005

Steyn-Ross, M., Steyn-Ross, D., Sleigh, J. W., and Liley, D. T. J. (1999). Theoretical electroencephalogram stationary spectrum for a white-noise-driven cortex: evidence for a general anesthetic-induced phase transition. *Phys. Rev. E Stat. Phys. Plasmas Fluids Relat. Interdiscip. Topics* 60, 7299–7311. doi: 10.1103/PhysRevE.60.7299

Talavera, J., Esser, S., Amzica, F., and Antognini, J. (2009). Modeling the GABAergic action of etomidate on the thalamocortical system. *Anesth Analg.* 108, 160–167. doi: 10.1213/ane.0b013e31818d40aa

Taub, A., Katz, Y., and Lampl, I. (2013). Cortical balance of excitation and inhibition is regulated by the rate of synaptic activity. *J. Neurosci.* 33, 14359–14368. doi: 10.1523/JNEUROSCI.1748-13.2013

Tononi, G. (2004). An information integration theory of consciousness. *BMC Neurosci.* 5:42. doi: 10.1186/1471-2202-5-42

Vanini, G. and Baghdoyan, H. (2013). Extrasynaptic GABAA receptors in rat pontine reticular formation increase wakefulness. *Sleep* 36, 337–343. doi: 10.5665/sleep.2444

Victor, J., Drover, J., Conte, M., and Schiff, N. (2011). Mean-field modeling of thalamocortical dynamics and a model-driven approach to EEG analysis. *Proc. Natl. Acad. Sci. U.S.A.* 118, 15631–15638. doi: 10.1073/pnas.1012168108

Vizuete, J., Pillay, S., Ropella, K., and Hudetz, A. (2014). Graded defragmentation of cortical neuronal firing during recovery of consciousness in rats. *Neuroscience* 275, 340–351. doi: 10.1016/j.neuroscience.2014.06.018

Wei, W., Zhang, N., Peng, Z., Houser, C. R., and Mody, I. (2003). Perisynaptic localization of subunit-containing GABAA receptors and their activation by GABA spillover in the mouse dentate gyrus. *J. Neurosci.* 23, 10650–10661. Available online at: http://www.jneurosci.org/content/23/33/10650.short

Wilson, M., Sleigh, J., Steyn-Ross, A., and Steyn-Ross, M. (2006). General anesthetic-induced seizures can be explained by a mean-field model of cortical dynamics. *Anesthesiology* 104, 588–593. doi: 10.1097/00000542-200603000-00026

Wolosker, H., Blackshaw, S., and Snyder, S. (1999). Serine racemase: a glial enzyme synthesizing d-serine to regulate glutamate-n-methyl-d-aspartate neurotransmission. *Proc. Natl. Acad. Sci. U.S.A.* 96, 13409–13414. doi: 10.1073/pnas.96.23.13409

Wright, J. and Kydd, R. (1992). The electroencephaloggram and cortical neural networks. *Network* 3, 341–362. doi: 10.1088/0954-898X/3/3/006

Ye, Z., McGee, T., Houston, C., and Brickley, S. (2013). The contribution of δ subunit-containing $gaba_a$ receptors to phasic and tonic conductance changes in cerebellum, thalamus and neocortex. *Front. Neural Circuit.* 7,1–8. doi: 10.3389/fncir.2013.00203

Yeung, J. Y. T., Canning, K. J., Zhu, G., Pennefather, P., MacDonald, J. F., and Orser, B. A. (2003). Tonically activated GABAA receptors in hippocampal neurons are high-affinity, low-conductance sensors for extracellular gaba. *Mol. Pharmacol.* 63, 2–8. doi: 10.1124/mol.63.1.2

Conflict of Interest Statement: The authors declare that the research was conducted in the absence of any commercial or financial relationships that could be construed as a potential conflict of interest.

Received: 12 September 2014; accepted: 19 November 2014; published online: 10 December 2014.

*Citation: Hashemi M, Hutt A and Sleigh J (2014) Anesthetic action on extra-synaptic receptors: effects in neural population models of EEG activity. Front. Syst. Neurosci. **8**:232. doi: 10.3389/fnsys.2014.00232*

This article was submitted to the journal Frontiers in Systems Neuroscience.

frontiers in
SYSTEMS NEUROSCIENCE

ORIGINAL RESEARCH ARTICLE
published: 26 February 2015
doi: 10.3389/fnsys.2015.00018

Emergence of spatially heterogeneous burst suppression in a neural field model of electrocortical activity

Ingo Bojak[1], Zhivko V. Stoyanov[1] and David T. J. Liley[2]*

[1] *Systems Neuroscience Research Group, School of Systems Engineering, University of Reading, Reading, UK*
[2] *Brain and Psychological Sciences Research Centre, School of Health Sciences, Swinburne University of Technology, Hawthorn, VIC, Australia*

Edited by:
Axel Hutt, INRIA CR Nancy - Grand Est, France

Reviewed by:
Meysam Hashemi, INRIA CR Nancy - Grand Est, France
Sid Visser, University of Nottingham, UK

***Correspondence:**
David T. J. Liley, Brain and Psychological Scieces Research Centre, School of Health Sciences, Swinburne University of Technology, John Street, Hawthorn, VIC 3122, Australia
e-mail: dliley@swin.edu.au

Burst suppression in the electroencephalogram (EEG) is a well-described phenomenon that occurs during deep anesthesia, as well as in a variety of congenital and acquired brain insults. Classically it is thought of as spatially synchronous, quasi-periodic bursts of high amplitude EEG separated by low amplitude activity. However, its characterization as a "global brain state" has been challenged by recent results obtained with intracranial electrocortigraphy. Not only does it appear that burst suppression activity is highly asynchronous across cortex, but also that it may occur in isolated regions of circumscribed spatial extent. Here we outline a realistic neural field model for burst suppression by adding a slow process of synaptic resource depletion and recovery, which is able to reproduce qualitatively the empirically observed features during general anesthesia at the whole cortex level. Simulations reveal heterogeneous bursting over the model cortex and complex spatiotemporal dynamics during simulated anesthetic action, and provide forward predictions of neuroimaging signals for subsequent empirical comparisons and more detailed characterization. Because burst suppression corresponds to a dynamical end-point of brain activity, theoretically accounting for its spatiotemporal emergence will vitally contribute to efforts aimed at clarifying whether a common physiological trajectory is induced by the actions of general anesthetic agents. We have taken a first step in this direction by showing that a neural field model can qualitatively match recent experimental data that indicate spatial differentiation of burst suppression activity across cortex.

Keywords: burst suppression, anesthesia, EEG, neural field model, neuronal hyperexcitability

1. INTRODUCTION

Over the many years since its discovery in humans (Berger, 1929, 1930; Adrian and Matthews, 1934), the electroencephalogram (EEG) has been shown to be a sensitive, and often specific, indicator of brain state and function (Schomer and Lopes da Silva, 2010). In the case of the deeply inactivated brain, whether through trauma or medical intervention, a burst suppression pattern is typically observed (Niedermeyer, 2009; Ching et al., 2012). Consisting of quasi-periodic alternations of high amplitude periods of spiking activity with low amplitude periods that are near isoelectric, the burst suppression pattern is associated with a range of central insults or interventions that include cortical deafferentation (Henry and Scoville, 1952; Kellaway et al., 1966; Lukatch and MacIver, 1996), cerebral ischaemia (Bauer et al., 2013), deep coma (Young, 2000), various infantile encephalopathies (Grigg-Damberger et al., 1989), the final stages of deteriorated status epilepticus (Treiman et al., 1990), hypothermia (Stecker et al., 2001), and high levels of many anesthetic and sedative drugs (Schwartz et al., 1989; Akrawi et al., 1996).

The burst suppression pattern can show a significant degree of variation depending on its aetiology. For example, in the case of infantile hypoxic-ischemic encephalopathy the burst suppression pattern can be quite complex; and due to significant variability in the amplitude of individual bursts a clear transition to suppression may not readily be apparent (Lamblin et al., 2013). In contrast, in deep anesthesia bursts are typically separated by clear isoelectric periods, the duration (relative and absolute) of which increases systematically with increasing anesthetic level. This systematic dependence on anesthetic level can be utilized in the treatment of status epilepticus (Kalviainen et al., 2005) and the management of brain trauma in the intensive care setting (Doyle and Matta, 1999) by defining an endpoint in which more than 50% of an EEG recording consists of suppressions.

In what follows we will provide an overview of the phenomenon of burst suppression and summarize the current understanding regarding its physiological genesis. This will then be followed by a detailed outline of a neural field model developed to describe the emergence of burst suppression during anesthesia, which notably, and for the first time, incorporates the empirically realistic modeling of a general anesthetic agent (isoflurane) and the spatio-temporal propagation of cortical activity.

1.1. PHYSIOLOGICAL BASIS OF BURST SUPPRESSION

Despite its clear aetiological associations and clinical utility, little is known about the physiological mechanisms responsible for the genesis of burst suppression (Liley and Walsh, 2013). On

the basis of brain slice and *in vivo* animal studies, a number of hypotheses have been advanced with sometimes contradictory conclusions. For example both increases (Steriade et al., 1994) and decreases (Ferron et al., 2009) in GABAergic inhibitory activity have been speculated to have causal roles in the onset of burst suppression. Supporting reductions in inhibition are *in vivo* whole-brain animal studies suggesting that enhanced network excitability (Detsch et al., 2002; Hudetz and Imas, 2007; Kroeger and Amzica, 2007; Land et al., 2012), possibly mediated through alterations in extracellular calcium (Kroeger and Amzica, 2007), is responsible for driving transitions between low amplitude quiescence and high amplitude bursting. The study of Land et al. (2012) is particularly relevant in this regard. Not only do they report that auditory and visual stimuli readily evoke burst activity in visual cortex (V1) and subiculum during deep anesthesia in rats, but (i) such excitability does not occur in the absence of burst suppression, (ii) V1 and subiculum bursting, in response to the cortically remote auditory stimulus, emerges abruptly with increasing anesthetic (isoflurane) concentration, and (iii) hysteresis occurs in both stimulus-induced and spontaneous bursting during isoflurane wash-in and wash-out. Thus, the phenomenon of burst suppression might be explicable in terms of the emergence of propagating excitability through a dynamical bifurcation parametrically regulated by isoflurane concentration.

Clinically it is well-established that bursting responses during burst suppression in deep anesthesia can be readily evoked by noxious and sensory stimulation, thus further implicating a role for alterations in cortical excitability in the genesis of burst suppression. For example, in probably the first systematic study on evoked bursts, Yli-Hankala et al. (1993) observed that a vibratory stimulus applied to the palm of the hand was readily able to evoke electroencephalographic bursts in patients during moderately deep isoflurane anesthesia. Subsequently it has been found that a range of visual, auditory, tactile and noxious stimuli are able to evoke electroencephalographic bursts during deep anesthesia in which burst suppression has been variously induced with isoflurane (Hartikainen et al., 1995), sevoflurane (Jantti et al., 1998) or propofol (Huotari et al., 2004).

Complementing this empirical and clinical research are recent modeling studies (Ching et al., 2012; Liley and Walsh, 2013), which suggest that the onset or unmasking of slow and activity-dependent modulations of network excitability might account for burst suppression patterns. Because it is observed that the spectral characteristics of the EEG just prior to the onset of the anesthesia-induced burst suppression are conserved in the bursts[1], such theoretical approaches typically modulate the oscillatory system that accounts for the dynamical emergence of the resting and anesthetic EEG. In order to simulate burst suppression during deep propofol anesthesia, Ching et al. (2012) utilize a thalamo-cortical model based on individual neurons previously developed to account for the propofol-induced emergence of frontal alpha-spindle activity (Ching et al., 2010). This model is then augmented with a slow adenosine triphosphate (ATP) gated potassium membrane current, which is hence regulated by the activity-dependent metabolic production rate of ATP. By assuming that propofol down-regulates neuronal firing through enhanced synaptic inhibition, thus leading to an autoregulatory decrease in cerebral metabolism and hence ATP production, the modulatory effect of this potassium current is magnified such that bursting emerges. In contradistinction to this model, in which bursting arises due to essentially intrinsic changes of neuronal excitability, Liley and Walsh (2013) developed a model in which bursting arises as a consequence of the slow activity-dependent modulation of synaptic efficacy. In this model the effects of synaptic resource depletion (receptor desensitization and synaptic vesicle depletion) and recovery during periods of sustained neuronal population activity act to slowly modulate neuronal population excitability. This mechanism comes to the fore in anesthesia because the general reduction of cortical activity allows the synaptic neurotransmitter reservoirs to fill up, potentiating excitation until it is sufficiently strong to induce feedback bursts of excitation, followed by suppression as the thereby depleted reservoirs refill. In support of this mechanism are the activity-dependent alterations in synaptic efficacy that have been observed *in vivo* in recordings in cats during burst suppression induced with isoflurane (Kroeger and Amzica, 2007).

1.2. SPATIO-TEMPORAL FEATURES OF BURST SUPPRESSION

Because burst suppression is classically characterized as being a spatially homogeneous phenomenon (Brenner, 1985; An et al., 1996; Lewis et al., 2013), on the basis of near simultaneous burst onset and offset across scalp electrode derivations, little attention has been paid to its spatio-temporal features until recently. Motivated by the inability of scalp electroencephalography to reveal the fine structure of cortical dynamics, due to the spatial blurring induced by volume conduction, Lewis et al. (2013) chose to investigate the spatiotemporal features of burst suppression using intracranial electrocortigraphy (ECoG) in medically intractable epilepsy patients. Five patients, implanted with a range of subdural strip, grid and depth electrodes as part of a standard clinical monitoring procedure, had recordings collected throughout the induction of anesthesia with propofol, during explantation surgery. Burst onset and offset was observed to be visibly asynchronous across recording electrodes, with the absolute difference in burst onset time in general an increasing function of inter-electrode distance. Interestingly, not all recording electrodes would participate in such asynchronous bursting. It was found that burst onsets were visibly clustered across channels such that bursting could either be confined to a small subset of nearby electrodes ("local" bursting) or spread to involve the whole electrode grid ("global" bursting), with more distantly separated electrode pairs less likely to share a burst (based on burst onset within some time window).

It has been speculated that the appearance of spatially inhomogeneous bursting might be a reflection of the differential sensitivity of specific thalamo-cortical networks to anesthetic action. However, another possibility is that the spatially heterogeneous nature of this bursting arises as a feature of the axonal propagation of activity through cortex. In support of such a speculation

[1]For propofol anesthesia this means that alpha activity present prior to the onset of burst suppression is retained within the bursts (Ching et al., 2012). In contrast, during isoflurane anesthesia slow-wave and delta activity persists during bursts (Kroeger and Amzica, 2007).

is the developmental emergence of isoflurane-induced burst suppression in rats. It is conjectured that it is the development of short- and long-range horizontal connections between pyramidal neurons in infra-granular cortical layers, which is the critical factor in determining the appearance of isoflurane-induced burst suppression in the second postnatal week (Sitdikova et al., 2014). Further implicating the role that altered propagation may have in determining the physiological features of anesthetic action are reports that document the effects anesthetics have on nerve conduction—both centrally and peripherally. While peripherally it is generally assumed that anesthetics principally depress spinal motoneuron excitability, as assessed by reductions in F-wave amplitudes (Friedman et al., 1996; Rampil and King, 1996), there are a number of reports documenting the significant effects of anesthetic agents in either increasing (cyclopropane, nitrous oxide, diethyl ether) (Rosner et al., 1971) or reducing (pentobarbital, desflurane, enflurane, halothane) (Rampil and King, 1996; Oh et al., 2010; Nowicki et al., 2013) nerve conduction velocity at clinical levels, as assessed by increases in F-wave latency. Centrally, there is some evidence that volatile anesthetics may preferentially depress nerve conduction in unmyelinated axons (Berg-Johnsen and Langmoen, 1986; Mikulec et al., 1998). For instance, isoflurane was found to induce a conduction block in 20–30% of the unmyelinated fibers in the CA1 region of the rat hippocampus at clinical concentrations, as well as having a 1% effect on the actual conduction velocity (Berg-Johnsen and Langmoen, 1986). On the basis of empirical evidence indicating that the cortico-cortical fiber system is comprised of a mixture of myelinated and unmyelinated fibers, cf. Bojak and Liley (2010) and references therein, we hence expect mean cortical axonal conduction velocity to increase slightly, due to the reduction in the proportion of low conduction velocity unmyelinated fibers, but nevertheless anticipate cortico-cortical synaptic connectivity to be attenuated.

1.3. NECESSITY OF LARGE-SCALE CORTICAL MODELS

Regardless of the specific changes in cortical axonal conduction induced by anesthetics, it is clear that any theoretical attempt to account for burst suppression and its spatial inhomogeneity must explicitly incorporate the spatial extent of cortex. While the construction of a biophysically-based neuronal network model might seem an obvious starting point, numerical tractability and parametric uncertainties militates against the utility of this approach both from a descriptive and an explanatory perspective. For example, to meaningfully accommodate the extent of the spatially heterogeneous burst suppression seen in Lewis et al. (2013), we would need to model $\sim 10^9$ neurons and $\sim 10^{12}$ synapses. While computations at this scale may be at the edge of feasibility for the largest supercomputers, we cannot reasonably expect such massive computations to be used for all the myriad specific research agendas in computational neuroscience any time soon. Even if such resources were readily available we would still be unable to specify the microcircuitry realistically at this level of detail for such a sizeable part of cortex. Such a problem will persist even if our computational capabilities continue to grow exponentially.

Fortunately, by considering the behavior of *populations* of neurons at mesoscopic scales, a variety of numerically tractable modeling approaches can be motivated physiologically and anatomically, cf. the reviews of Deco et al. (2008), Coombes (2010), Liley et al. (2012), and Liley (2013). These *neural population models*, referred to as neural mass models if localized and neural field or mean field models if spatially continuous and extensive, usually aim to describe the dynamical evolution of mean quantities (such as soma membrane potential or firing rate) defined over some suitable spatial domain or scale. Because these models average the activity of many thousands of neurons, they are well-suited as frameworks for understanding the meso- and macroscopic neural activity recorded, or inferred by, ECoG, EEG, magnetoencephalography (MEG) and the blood-oxygen level dependent (BOLD) contrast of functional magnetic resonance imaging (fMRI) (Bojak and Breakspear, 2013). Since the pioneering work of Walter Freeman (Freeman, 1975), this approach has flourished and has resulted in a number of important neural field models aimed at explaining the dynamical genesis of the mammalian EEG (Wilson and Cowan, 1973; Lopes da Silva et al., 1974; Nunez, 1974; Liley et al., 2002; Robinson et al., 2004). Broadly speaking, all these models are able to generate oscillatory activity through reverberant feedforward and feedback synaptic activity between excitatory and inhibitory neuronal populations. We choose to utilize the neural field model of Liley et al. (2002) as a framework for better understanding the spatial heterogeneity of bursting during anesthesia because (i) it has been previously employed to account for a number of anesthetic induced EEG changes (Steyn-Ross et al., 1999; Bojak and Liley, 2005), and (ii) a spatially homogeneous version of the theory has been shown to burst when modified to include a slow modulatory system (Liley and Walsh, 2013).

2. NEURAL FIELD MODEL FOR SPATIOTEMPORAL BURST SUPPRESSION

Here we detail how a neural field model (Liley et al., 2002), subsequently extended to account for the dynamical genesis of the resting EEG and its modulation by anesthesia (Bojak et al., 2004; Bojak and Liley, 2005; Liley and Bojak, 2005; Frascoli et al., 2011; Liley et al., 2011; Bojak et al., 2013), can be plausibly modified to produce bursting-like behavior (Liley and Walsh, 2013), and thus serve as a basis for understanding the emergence of spatially heterogeneous burst suppression seen in cortex. The main advance in this work is that we combine the realistic modeling of isoflurane effects and the extension to a two-dimensional spatial sheet of Bojak and Liley (2005) with an updated version of the slow modulatory system proposed in Liley and Walsh (2013) in order to obtain spatiotemporal activity predictions.

It is perhaps useful to discuss two fundamental limitations of our current approach in advance. First, we are limiting ourselves here to a two-dimensional (toroidal) cortical sheet and use "background" (isotropic and homogeneous) connectivity in order to use computationally efficient activity propagation with partial differential equations (PDEs). Currently there exist a range of mesoscopic approaches available that can incorporate more realistic cortical geometry as well as including "specific" (anisotropic and sparse) connectivity, see for example (Bojak et al., 2010, 2011; Deco et al., 2011; Bojak and Breakspear, 2013; Sanz Leon et al., 2013) and references therein. These typically involve constructing meshes of neural masses and tracking their

information exchanges individually. However, such approaches are computationally about an order of magnitude more expensive. Furthermore, to effectively display spatiotemporal pattern formation on a realistically folded cortex is a graphical challenge. We will show here that spatial differentiation of activity emerges even if one uses a simple toroidal cortical geometry with isotropic and homogeneous connectivity. The additional complexity introduced by anatomical folding structures and patchy connectivity are expected to break up long-range coherence further, but should not qualitatively change our results more locally (where the "background" connectivity is a good approximation) and between well-connected but separated regions (where we would expect emergent differentiation). In addition, we use here the well-known "damped wave" propagation PDEs that have been the mainstay of the field since their initial introduction by Jirsa and Haken (1996). It is by now known that one can use "dispersive" propagation PDEs that are more faithful to the actual distribution of axonal fiber velocities (Bojak and Liley, 2010). However, we are using here a parameter set of Bojak and Liley (2005) that delivers realistic EEG activity under the assumption of "damped wave" propagation. Furthermore, the better "dispersive" propagation is also computationally considerably more expensive and technically difficult to implement. Finally, one of the key results of Bojak and Liley (2010) was that more realistic "dispersive" propagation lead to easier spatiotemporal pattern formation. Thus, we expect that the results here would carry over qualitatively to more realistic propagation models, likely showing spatial differentiation earlier on in the burst phase. In summary, we will show here with the computationally simplest model that spatial differentiation in the burst phase can emerge in qualitative agreement with the experimental observation, and we expect that even more realistic modeling will only enhance these emergent effects.

2.1. THE (EXTENDED) LILEY MODEL

The electrocortical model of Liley et al. (2002) is constructed at the scale of the cortical macrocolumn. Within each macrocolumn, and extending across all cortical layers, distributed populations of excitatory and inhibitory neurons interact with each other by all possible feedforward and feedback intracortical (local) axodendritic connections. Macrocolumns then interact with each other by the exclusively excitatory cortico-cortical (long-range) axonal fibers. The topological organization of this model is well-known, and depicted in **Figure 1**. In this model cortical activity is described by the spatiotemporal evolution of the mean excitatory $h_e(\vec{x}, t)$ and inhibitory $h_i(\vec{x}, t)$ soma membrane potentials. The connection with electrophysiological measurement is through h_e, which is assumed to be linearly related to the EEG, cf. Bojak and Breakspear (2013). Excitatory and inhibitory neuronal populations are modeled as spatially averaged *conductance-based* neurons:

$$\tau_k \frac{\partial h_k(\vec{x}, t)}{\partial t} = h_k^{\mathrm{r}} - h_k(\vec{x}, t) + \sum_{l=e,i} \frac{h_{lk}^{\mathrm{eq}} - h_k(\vec{x}, t)}{|h_{lk}^{\mathrm{eq}} - h_k^{\mathrm{r}}|} I_{lk}(\vec{x}, t) \ , \quad (1)$$

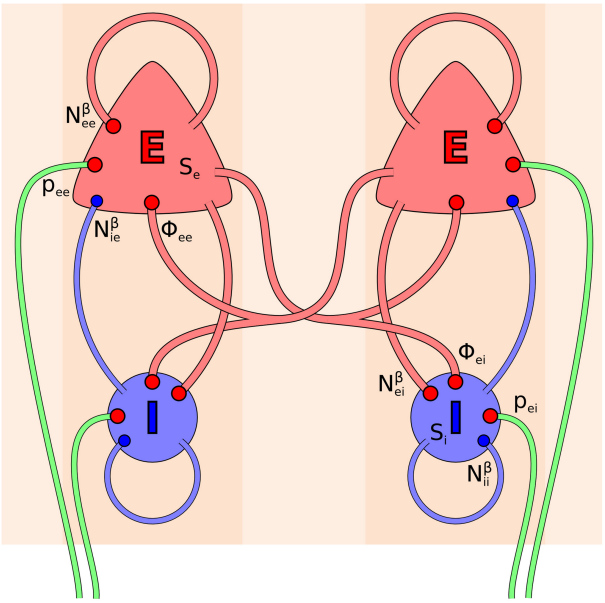

FIGURE 1 | Topology of the Liley model (Liley et al., 2002; Bojak and Liley, 2005). Its two distinct neural populations (E = excitatory, I = inhibitory) are shown for two separate positions on the cortical sheet. Each one can be considered as representing a single macrocolumn. All synaptic connections that occur in the model are shown by red (excitatory) and blue (inhibitory) disks, respectively. Extracortical inputs to the cortical populations are shown by green fibers. Symbols illustrate the various inputs to the excitatory population in the left macrocolumn and to the inhibitory population in the right macrocolumn, respectively, according to Equations (3, 4).

where $\vec{x} \in \mathbb{R}^2$ is position on the cortical sheet, subscripts $l, k \in \{e, i\}$ indicate excitatory and inhibitory subpopulations, respectively, and double subscripts represent first the pre-synaptic source and then the post-synaptic target. The parameters h_k^{r} are the mean resting membrane potentials to which the h_k decay exponentially with characteristic time scales τ_k in the absence of inputs I_{lk}. The fraction in front of the I_{lk} weighs these inputs, so that the depolarizing effect of additional excitation diminishes linearly and then even becomes hyperpolarizing past the reversal potentials h_{ek}^{eq}, and similarly for the hyperpolarization due to inhibition depending on h_{ik}^{eq}. The weight at the resting potentials is $+1$ for excitatory and -1 for inhibitory inputs, respectively.

The dynamics of the post-synaptic potentials (PSPs) I_{lk} are described by critically damped oscillators driven by the mean rate of incoming excitatory or inhibitory axonal pulses A_{lk}, originally defined as follows (Liley et al., 2002):

$$\left(\frac{1}{\gamma_{lk}}\frac{\partial}{\partial t} + 1\right)^2 I_{lk}(\vec{x}, t) = \frac{e\Gamma_{lk}}{\gamma_{lk}} A_{lk}(\vec{x}, t) \ , \quad (2)$$

$$A_{ek}(\vec{x}, t) = N_{ek}^{\beta} S_e[h_e(\vec{x}, t)] + N_{ek}^{\alpha} \Phi_{ek}(\vec{x}, t) + p_{ek}(\vec{x}, t) \ , \quad (3)$$

$$A_{ik}(\vec{x}, t) = N_{ik}^{\beta} S_i[h_i(\vec{x}, t)] \ . \quad (4)$$

For excitatory post-synaptic conductances there are three sources of axonal pulses—local (S_e), cortico-cortical (Φ_{ek}), and subcortical (p_{ek})—whereas for inhibitory post-synaptic conductances the only source of axonal pulses is local (S_i), because thalamic and cortical inhibitory axons are essentially short-range on the basis of existing neuroanatomical evidence. For these equations, at a given location a single pre-synaptic (Dirac delta) spike $A_{lk}(t) = \delta(t)$ would produce a so-called "alpha function" response

$$I_{lk}(t) = \frac{e\Gamma_{lk}}{\gamma_{lk}}\alpha_{lk}(t)\,, \tag{5}$$

$$\alpha_{lk}(t) = \gamma_{lk}^2 t e^{-\gamma_{lk}t}\Theta(t)\,, \tag{6}$$

with the Heaviside step function $\Theta(t)$. The alpha function α_{lk} is normed to one for integration over time, hence the pre-factor in Equation (5) is proportional to the charge transfer of the induced PSP. Furthermore, $\delta_{lk} = 1/\gamma_{lk}$ is the characteristic time scale of the PSP's exponential decay. Since $I_{lk}\,(t = \delta_{lk}) = \Gamma_{lk}$ is the maximum amplitude of the PSP, δ_{lk} is also the rise time to peak amplitude. Note that since we have collapsed all cortical layers into one sheet without radial extension, this rise time is that of the PSP conducted to the soma rather than at the synapse in the dendritic tree. Conduction through a passive dendritic cable effectively leads to a "flattened" PSP at the soma with lower maximum amplitude and prolonged rise and decay times.

The S_e and S_i are respectively the local mean excitatory and inhibitory firing rates, and are assumed to be instantaneous sigmoidal functions of the h_k of the form

$$S_k\left[h_k\left(\vec{x},\,t\right)\right] = S_k^{\max}/\left\{1+\exp\left[-\sqrt{2}\frac{h_k\left(\vec{x},\,t\right)-\mu_k}{\sigma_k}\right]\right\}\,, \tag{7}$$

and the N_{ek}^{α} and N_{lk}^{β} factors in the A_{lk} above multiply these local firing rates by the number of synaptic connections formed with the target populations. The $S_k^{\max}$ are the maximum mean firing rates, and the μ_k and σ_k can be understood as the mean and standard deviation, respectively, of the firing thresholds of the populations, which are taken to be roughly normally distributed. The propagation of axonal pulses by the excitatory cortico-cortical fiber system Φ_{ek} is described here by the following well-known "damped wave" equation[2] (Jirsa and Haken, 1996; Robinson et al., 1997; Liley et al., 2002; Bojak and Liley, 2010):

$$\left[\left(\frac{1}{v_{ek}}\frac{\partial}{\partial t}+\frac{1}{\lambda_{ek}}\right)^2-\nabla^2\right]\Phi_{ek}\left(\vec{x},\,t\right) = \frac{1}{\lambda_{ek}^2}S_e\left[h_e\left(\vec{x},\,t\right)\right]\,. \tag{8}$$

But for the λ_{ek} terms, this would be an inhomogeneous wave equation with conduction velocity v_{ek}, propagating the local excitatory firing rate S_e. However, due to these terms the wave gets suppressed roughly exponentially with distance with a characteristic spatial scale λ_{ek}.

[2]We note that as compared to Bojak and Liley (2005), we have here rescaled v_{ek} and λ_{ek} as in Bojak and Liley (2010), so as to remove a factor 3/2, which technically arises from an expansion of an ansatz for the corresponding Green's function.

Finally, there is also extracortical synaptic input in the form of the p_{ek}. These inputs can be considered to be mainly due to thalamic afferents. If the p_{ek} were constant, then for the model parameters chosen here the system would quickly converge to a static equilibrium point. It is hence the imposition of noise on these inputs which effectively drives the neural activity. This noise is taken to represent the average over the varied extracortical synaptic input to the many thousands of neurons in a neural population, for the case in which there is no strong external (sensory) drive that would lead to clear correlations of the synaptic inputs to the individual neurons. We follow here essentially the approach of Bojak and Liley (2005) for noise generation. Thus, for the sake of computational simplicity noise is imposed only on p_{ee}, whereas p_{ei} is taken to be constant. At every grid point of the two-dimensional cortical sheet normally distributed noise is generated independently, but with the same mean p_{ee}, and a standard deviation that is 10% of this mean. However, we filter this noise spatiotemporally, both to achieve more biological realism and to make it easier to achieve numerical stability. We follow the Fourier space procedure of Bojak and Liley (2005) for the spatial filtering, but use the Catmull-Rom spline procedure detailed in Bojak et al. (2011) for the temporal filtering, with lowpass −3 dB points at 75 Hz and 2/cm, respectively (Bojak and Liley, 2005). Thus, the noisy input oscillates equally at all frequencies, but only up to about 75 Hz, and is identical for neighboring grid points, but becomes uncorrelated at cortical distances greater than about 0.5 cm. The spatiotemporal p_{ee} noise breaks the otherwise perfect homogeneity and isotropy of the system, and consequently acts as seed for the heterogeneities observed in the burst suppression phase. However, the characteristics of the spatiotemporal structures that emerge in the burst suppression phase do not otherwise depend on the noise; hence in particular they do not depend on the details of the noise filtering, and can be elicited with white noise driving.

The model we have described so far has to be extended for a realistic description of the effect of general anesthetic action. In particular, the effect of isoflurane on the rise time δ_{lk} of the PSPs from zero to maximum amplitude Γ_{lk}, and on the subsequent decay time ζ_{lk} back to Γ_{lk}/e (measured here from the start of the PSP, not from the peak) can be parameterized as follows in the form of a Hill equation (Bojak and Liley, 2005):

$$\delta_{lk}(c) \simeq \delta_{lk}\ (\text{constant})\,, \tag{9}$$

$$\zeta_{ek}(c) \equiv \zeta_{ek}^0\kappa_{ek}(c) \simeq \zeta_{ek}^0\ (\text{constant})\,, \tag{10}$$

$$\zeta_{ik}(c) \equiv \zeta_{ik}^0\kappa_{ik}(c) \simeq \zeta_{ik}^0\frac{0.32^{2.7}+4.7c^{2.7}}{0.32^{2.7}+c^{2.7}}\,, \tag{11}$$

where c is the aqueous concentration in mM. Thus, the main effect is a prolongation of the decay of the inhibitory PSPs. In addition, the maximum amplitudes of the PSPs also diminish with increased isoflurane concentration, which is also the case for excitatory PSPs:

$$\Gamma_{ek}(c) \equiv \Gamma_{ek}^0 H_e(c) \simeq \Gamma_{ek}^0\frac{0.707^{2.22}}{0.707^{2.22}+c^{2.22}}\,, \tag{12}$$

$$\Gamma_{ik}(c) \equiv \Gamma_{ik}^0 H_i(c) \simeq \Gamma_{ik}^0\frac{0.79^{2.6}+0.56c^{2.6}}{0.79^{2.6}+c^{2.6}}\,. \tag{13}$$

While for consistency with laboratory based estimates we choose to parameterize isoflurane level in terms of its aqueous concentration, it is important to appreciate that because isoflurane is a volatile gas, clinically its level is typically reported in terms of its concentration in the expired air (which is assumed to be in equilibrium with the blood and hence the extracellular fluid of cortical neurons). At normal body temperature 1.3% isoflurane are equivalent to an aqueous concentration of about $c \simeq 0.27$ mM (Franks and Lieb, 1996). Typical isoflurane concentrations encountered in clinical anesthetic practice range from 0 to 2% of the expired air, equivalent to aqueous concentrations $0 - 0.42$ mM (Mapleson, 1996). A measure commonly employed in anesthetic practice is the minimum alveolar concentration or MAC of an anesthetic agent. It is essentially defined as the concentration of gas in the lungs required to prevent movement in 50% of subjects in response to a painful surgical stimulus. In the case of isoflurane 1 MAC $\simeq 1.17\% \simeq 0.243$ mM for an adult at normal body temperature (Mapleson, 1996). It should be noted that in combination with other anesthetic agents like nitrous oxide, less than 1 MAC of isoflurane will be required to reach the 50% end-point.

It is straightforward to introduce Equations (12, 13) to the Liley model by changing the Γ_{lk} according to isoflurane concentration, i.e., $\Gamma_{lk} \to \Gamma_{lk}(c) = \Gamma^0_{lk} H_l(c)$ with the Γ^0_{lk} now having the same values as the Γ_{lk} had in the standard Liley model. However, Equations (9–11) are more problematic. The decay time of the alpha function in Equation (5) changes linearly with its rise time, thus one cannot match the experimental result that only the decay time is prolonged under anesthesia. Consequently, the following modification of Equation (2) was introduced (Bojak and Liley, 2005)

$$\left[\frac{1}{\gamma_{lk}(c)}\frac{\partial}{\partial t} + 1\right]\left[\frac{1}{\tilde{\gamma}_{lk}(c)}\frac{\partial}{\partial t} + 1\right] I_{lk}(\vec{x}, t) = \frac{e^{\gamma_{lk}(c)\delta_{lk}}\Gamma_{lk}(c)}{\gamma_{lk}(c)} A_{lk}(\vec{x}, t) \ , \tag{14}$$

$$\gamma_{lk}(c) = \frac{\varepsilon_{lk}(c)}{e^{\varepsilon_{lk}(c)} - 1}\frac{1}{\delta_{lk}} \ , \quad \tilde{\gamma}_{lk}(c) = e^{\varepsilon_{lk}(c)}\gamma_{lk}(c) \ . \tag{15}$$

Notably, for $\varepsilon_{lk} \to 0$ one finds that $\tilde{\gamma}_{lk} \to \gamma_{lk}$, and $\gamma_{lk} \to 1/\delta_{lk}$ with a removable discontinuity. Defining these variables as continuous with the limit, the new Equation (14) then becomes identical with the old Equation (2) in this limit. The corresponding response to a single pre-synaptic spike $A_{lk}(t) = \delta(t)$ now becomes a bi-exponential function

$$I_{lk}(t) = \frac{e^{\gamma_{lk}\delta_{lk}}\Gamma_{lk}}{\gamma_{lk}}\beta_{lk}(t) \ , \tag{16}$$

$$\beta_{lk}(t) = \gamma_{lk}\tilde{\gamma}_{lk}\frac{e^{-\gamma_{lk}t} - e^{-\tilde{\gamma}_{lk}t}}{\tilde{\gamma}_{lk} - \gamma_{lk}}\Theta(t) \ , \tag{17}$$

where we have suppressed the concentration dependence. Again the pre-factor in Equation (16) is proportional to the charge transferred, since $\beta_{lk}(t)$ is normed to one for integration over time. Note that now $I_{lk}(t = \delta_{lk}) = \Gamma_{lk}$, which for $\varepsilon_{lk} = 0$ becomes the previous result since in this limit again $\delta_{lk} = 1/\gamma_{lk}$. More generally, for $\varepsilon_{lk} \to 0$ we have $\beta_{lk}(t) \to \alpha_{lk}(t)$ at all times and the alpha function is the "sharpest" response $\beta_{lk}(t) \geq \alpha_{lk}(t)$. Clearly with this new form we can keep the rise time parameter δ_{lk} constant, while changing the ε_{lk} so as to achieve a desired decay time ζ_{lk}. Given the changes imposed by isoflurane in Equations (9–11), one can solve for the appropriate ε_{lk} numerically in dependence on the concentration c. However, here we will use the excellent approximation formula presented in Liley et al. (2011), which can be written as[3]

$$\varepsilon_{lk}(c) \simeq e^{2.5466 - 1.3394\kappa_{lk}(c)}\sqrt{\kappa_{lk}(c) - 1} + \left(e^{-1.2699[\kappa_{lk}(c)-1]} - 1\right) \cdot \left[\frac{1}{\kappa^2_{lk}(c)} + \mathrm{W}_{-1}\left(\frac{e^{-0.23630/\kappa^2_{lk}(c)}}{1 - 3.1462\kappa_{lk}(c)}\right)\right] , \tag{18}$$

where W_{-1} is the -1 branch of the Lambert-W function. Here we assume that $\kappa_{ek} = 1$, thus $\varepsilon_{ek} = 0$, and only the inhibitory decay time is affected.

Equations (1–4, 7–8) represent a system of eight coupled nonlinear PDEs that define the standard Liley model. Changing the PSPs of Equation (2) to those of Equations (14, 15) defines the extended Liley model. It is therein understood that $1/\delta_{lk}$ of the extended Liley model equals γ_{lk} of the standard one, so that for $\varepsilon_{lk} \to 0$ both become identical. Finally, Equations (9–13) parameterize the effect of isoflurane on the extended Liley system. Here Equations (12, 13) can be used straightforwardly as determining $\Gamma_{lk}(c)$, but in order to use Equations (10–11) one additionally needs Equation (18) to translate them into changes of the $\gamma_{lk}(c)$ and $\tilde{\gamma}_{lk}(c)$ parameters. In Bojak and Liley (2005) extensive parameter searches were performed. All selected parameter sets gave rise to a plausible resting EEG power spectrum ('$1/f$' low frequency activity with an alpha peak in the 8–13 Hz range) under noise driving, retained a stable equilibrium point for increasing isoflurane concentration and hence remained in a quasi-linear dynamical regime, and showed the experimentally observed drop of the alpha peak to low frequencies for increasing isoflurane concentration. Some parameter sets furthermore exhibited a so-called "bi-phasic" transient surge in total power during simulated anesthesia induction, as observed in several experiments (Kuizenga et al., 1998, 2001). The parameter values used in this paper correspond to one of these "bi-phasic" parameter sets, and are listed in **Table 1**.

2.2. SLOW AND ACTIVITY-DEPENDENT SYNAPTIC BURSTING MECHANISM

In this work we consider receptor desensitization and synaptic vesicle depletion during periods of high neuronal population activity, and the homeostatic recovery of synaptic readiness during periods of low neuronal activity, as the slow mechanism that can modulate the excitability of cortical tissue. Such activity-dependence of synaptic efficacy has been observed during burst suppression induced with isoflurane (Kroeger and Amzica, 2007).

[3]The last term $\mathrm{W}_{-1}[\exp(a/\kappa^2)/(1 - b\kappa)]$ actually has $b = -\mathrm{W}_{-1}(-1/e^2)$ and $a = -1 + \ln(-1 + b)$. It is real for $\kappa \geq 1$ and for $\kappa = 1$ becomes -1. To avoid spurious imaginary terms one can set $a = -0.23630117$ for a $b = 3.1462$ of limited accuracy.

Table 1 | Mean population parameter values used to obtain bursting in the Liley model.

Definition		Excitatory (target)		Inhibitory (target)
Passive membrane decay times	τ_e	65.815 ms	τ_i	130.13 ms
Resting membrane potentials	h_e^{r}	−78.422 mV	h_i^{r}	−72.959 mV
Maximum firing rates	$S_e^{\max}$	0.39535/ms	$S_i^{\max}$	0.15439/ms
Firing thresholds (FTs)	μ_e	−51.656 mV	μ_i	−47.267 mV
Standard deviations of FTs	σ_e	2.8669 mV	σ_i	4.3250 mV
Synaptic recovery times	τ_e^{rec}	800.00 ms	τ_i^{rec}	600.00 ms
Synaptic depletion factor	f_e	1.2500	f_i	0.17500
EXCITATORY SOURCE				
Reversal potentials	h_{ee}^{eq}	−5.7891 mV	h_{ei}^{eq}	−1.6566 mV
PSP peak amplitudes	Γ_{ee}	0.18424 mV	Γ_{ei}	1.8771 mV
PSP rise times to peak	δ_{ee}	9.1059 ms	δ_{ei}	1.2103 ms
Number of intracortical synapses	N_{ee}^{β}	3410.8	N_{ei}^{β}	2738.9
Number of cortico-cortical synapses	N_{ee}^{α}	3616.3	N_{ei}^{α}	2905.1
Cortico-cortical decay scale	λ_{ee}	24.000 mm	λ_{ei}	24.000 mm
Cortico-cortical conduction velocity	v_{ee}	2.1042 mm/ms	v_{ei}	2.1042 mm/ms
Rate of extracortical input	p_{ee}	9.3193/ms	p_{ei}	3.1563/ms
INHIBITORY SOURCE				
Reversal potentials	h_{ie}^{eq}	−86.675 mV	h_{ii}^{eq}	−84.596 mV
PSP peak amplitudes	Γ_{ie}	1.5969 mV	Γ_{ii}	1.0838 mV
PSP rise times to peak	δ_{ie}	2.5985 ms	δ_{ii}	9.6946 ms
Number of intracortical synapses	N_{ie}^{β}	863.89	N_{ii}^{β}	267.92

In practice, we will modify the maximum PSP amplitudes Γ_{lk} that can be obtained, which directly depend on the available pre-synaptic amount and post-synaptic impact of neurotransmitter. Instead of considering these quantities as parameters as in the extended Liley model (where they act as control parameters that can be changed according to the concentration of an anesthetic agent), we now consider them as variables with their own slow dynamics coupled to the neural activity. Our ansatz is a common phenomenological model for activity-dependent synaptic depression (Bressloff, 2012). It represents a rate-based version of the model proposed by Tsodyks and Markram (1997), under the assumption that the processes responsible for the recovery of synaptic efficacy evolve on a time scale much slower than those associated with that of synaptic depletion (e.g., receptor desensitization and synaptic vesicle depletion):

$$\frac{\partial \Gamma_{lk}\left(\vec{x},\,t\right)}{\partial t} = \frac{\Gamma_{lk}^{\mathrm{r}} - \Gamma_{lk}\left(\vec{x},\,t\right)}{\tau_l^{\mathrm{rec}}} - \rho_l^{\mathrm{dep}} S_l\left[h_l\left(\vec{x},\,t\right)\right]\Gamma_{lk}\left(\vec{x},\,t\right)\ , \tag{19}$$

with $l, k \in \{e, i\}$ indicating the excitatory and inhibitory subpopulations and $S_l(h_l)$ is the local population firing rate of Equation (7), as before. Local neurotransmitter depletion is here considered to be directly proportional both to the strength of the PSPs, represented by Γ_{lk} itself, and to their frequency, represented by S_l. In the absence of neural activity $S_l = 0$/s, there will be an exponential return of Γ_{lk} to the resting value Γ_{lk}^{r} with a characteristic recovery time τ_l^{rec}. However, if there is no recovery $\tau_l^{\mathrm{rec}} \to \infty$ and we have constant neural activity $S_l > 0$/s, then Γ_{lk} will exponentially decay to zero with a characteristic depletion time $1/(\rho_l^{\mathrm{dep}} S_l)$. Note that we have assumed that in the *pre-synaptic* recovery and decay there is no dependence on the target (on the index k), since these processes will be determined by the activity of the source. However, in the *post-synaptic* impact on the maximum amplitude of the PSP, we allow a dependence on the target, since the response will depend on the morphology and physiology of the receiving neurons.

Now consider the case where we have both depletion and recovery. We will choose some homogeneous $h_l\left(\vec{x},\,t\right) \equiv h_l^0$ so that $S_l(h_l^0) > 0$/s. The synaptic system will then converge everywhere to an equilibrium value easily calculated by setting the left hand side of Equation (19) to zero:

$$\Gamma_{lk}\left(\vec{x},\,t\right) \ \to\ \Gamma_{lk}^0 = \frac{\Gamma_{lk}^{\mathrm{r}}}{1 + \tau_l^{\mathrm{rec}}\rho_l^{\mathrm{dep}} S_l\left(h_l^0\right)} \equiv \frac{\Gamma_{lk}^{\mathrm{r}}}{1 + f_l}\ , \tag{20}$$

$$f_l \ \equiv \tau_l^{\mathrm{rec}}\rho_l^{\mathrm{dep}} S_l(h_l^0) = \frac{\Gamma_{lk}^{\mathrm{r}}}{\Gamma_{lk}^0} - 1\ . \tag{21}$$

This equilibrium value is always smaller than the resting one, i.e., $f_l > 0$. We can scale our ansatz in terms of this equilibrium value and then obtain

$$\Gamma_{lk}\left(\vec{x},\,t\right) \equiv \Gamma_{lk}^0 C_l\left(\vec{x},\,t\right)\ , \tag{22}$$

$$\tau_l^{\mathrm{rec}}\frac{\partial C_l\left(\vec{x},\,t\right)}{\partial t} = 1 + f_l - \left(1 + \frac{S_l\left[h_l\left(\vec{x},\,t\right)\right]}{S_l\left(h_l^0\right)} f_l\right) C_l\left(\vec{x},\,t\right). \tag{23}$$

This scaling conveniently removes the post-synaptic dependence from the dynamical equations. Hence if we assume that the scaled initial conditions are identical $\Gamma_{le}\left(\vec{x},\,t=0\right)/\Gamma_{le}^0 = \Gamma_{li}\left(\vec{x},\,t=0\right)/\Gamma_{li}^0$, then in practice we only have to solve the two equations of Equation (23) instead of the four of Equation (19),

obtaining the four potentially different peak amplitudes via the scaling in Equation (22). Our choice for the initial conditions is to start them all at equilibrium $\Gamma_{lk}(\vec{x}, t=0) = \Gamma^0_{lk}$, thus $C_e(\vec{x}, t=0) = C_i(\vec{x}, t=0) = 1$, and then we can use these reduced computations with subsequent scaling. The only constraint we have imposed on the mean membrane potentials h^0_l here is that they should lead to non-zero population firing rates, which however is always the case unless one assumes unphysiological infinite polarization. The depletion coupling constants between the neural activity and the peak amplitude ρ^{dep}_l are empirically unknown, and would have to be determined laboriously from observations of dynamical changes of synaptic efficacy. However, in terms of the model proposed here, if one specifies the equilibrium values of the soma membrane potentials h^0_l and how much the neurotransmitter reservoir is depleted at the corresponding activity levels (Γ^0_{lk} vs. Γ^{r}_{lk}), then this in turn determines the depletion coupling constants

$$\rho^{\text{dep}}_l = \frac{f_l}{\tau^{\text{rec}}_l S_l\left(h^0_l\right)} = \frac{\Gamma^{\text{r}}_{lk}/\Gamma^0_{lk} - 1}{\tau^{\text{rec}}_l S_l\left(h^0_l\right)} \,. \tag{24}$$

In practice we make an implicit choice of the coupling constants by choosing the f_l for the system.

Now we wish to combine this synaptic system with the extended Liley model for anesthesia. For the parameter sets provided by Bojak and Liley (2005), that model has stable equilibrium points. That is to say, if we re-write the extended Liley model in the abstract form

$$\vec{s}(\vec{x}, t) \equiv (h_e,\ h_i,\ I_{ee},\ I_{ei},\ I_{i.e.},\ I_{ii},\ \Phi_{ee},\ \Phi_{ei})^T(\vec{x}, t) \,, \tag{25}$$

$$\mathcal{D}\vec{s}(\vec{x}, t) = \text{F}[\vec{s}(\vec{x}, t)] + \text{P}(\vec{x}, t) \,, \tag{26}$$

with a suitable differential operator $\mathcal{D}$, a function F and a noise drive P, then there exists a solution

$$F[\vec{s}^{\,*}] = 0 \,, \tag{27}$$

so that for $\text{P}(\vec{x}, t) = 0$ the system is static. Furthermore, since this equilibrium is stable, after small and transient disturbances the system will return dynamically to $\vec{s}^{\,*}$. We now make the following replacements in the extended Liley system

$$\Gamma_{lk} \ \rightarrow \ \Gamma_{lk}(\vec{x}, t) \,, \tag{28}$$

i.e., we replace the parameter values Γ_{lk} of the extended Liley model with the variables $\Gamma_{lk}(\vec{x}, t)$ of the synaptic system that we have just described. Together with the coupling to the neural activity explicit in Equation (23) this closes the combined system, which we will call the bursting Liley model henceforth. We now make the following convenient choices

$$\vec{s}(\vec{x}, t=0) = \vec{s}^{\,*}, \quad C_l(\vec{x}, t=0) = 1, \quad h^0_l = h^*_l, \quad \Gamma^0_{lk} = \Gamma_{lk}, \tag{29}$$

This homogeneous initial state of the bursting Liley model must now be an equilibrium point by construction: while Equation (27) is calculated with the parameters Γ_{lk}, we have arranged it so that the equilibrium value Γ^0_{lk} of the synaptic system at the resulting mean soma membrane potentials has the same value as that parameter. This is simply achieved by fixing the Γ^{r}_{lk} for a given f_l according to Equation (20), i.e., $\Gamma^{\text{r}}_{lk} = \Gamma^0_{lk}(1 + f_l)$. Hence the equilibrium of one system is compatible with that of the other, and if we start them off in their respective equilibrium states nothing will change. However, there is no guarantee that this constructed equilibrium point of the bursting Liley model will be stable.

Previously, we had incorporated the effects of isoflurane into the extended Liley model in part by replacing the standard parameter Γ^0_{lk} according to Equations (12, 13) with the anesthesia-dependent $\Gamma_{lk}(c) = \Gamma^0_{lk} H_l(c)$. In the bursting Liley model these parameters have become state variables with their own dynamics due to synaptic depletion and recovery. Hence the synaptic dynamics pertaining to the (pre-synaptic) source likewise must be multiplied by the anesthesia-dependent $H_l(c)$ to compute the (post-synaptic) amplitude induced at the target:

$$\begin{aligned}\Gamma_{lk}(\vec{x}, t, c) &\equiv \Gamma_{lk}(\vec{x}, t)\, H_l(c) = \Gamma^0_{lk} C_l(\vec{x}, t)\, H_l(c) \\ &= \Gamma_{lk}(c) C_l(\vec{x}, t) \,.\end{aligned} \tag{30}$$

However, since the synaptic dynamics are now coupled to the spatially variable cortical activity, we need to adjust our synaptic inputs to Equation (14):

$$\begin{aligned}A_{ek}(\vec{x}, t) = N^{\beta}_{ek} C_e(\vec{x}, t)\, S_e[h_e(\vec{x}, t)] + N^{\alpha}_{ek} \Phi_{ek}(\vec{x}, t) \\ + p_{ek}(\vec{x}, t),\end{aligned} \tag{31}$$

$$A_{ik}(\vec{x}, t) = N^{\beta}_{ik} C_i(\vec{x}, t)\, S_i[h_i(\vec{x}, t)] \,, \tag{32}$$

$$\left[\left(\frac{1}{v_{ek}}\frac{\partial}{\partial t} + \frac{1}{\lambda_{ek}}\right)^2 - \nabla^2\right]\Phi_{ek}(\vec{x}, t) = \frac{1}{\lambda^2_{ek}} C_e(\vec{x}, t)\, S_e[h_e(\vec{x}, t)]. \tag{33}$$

Here the first term in A_{lk} is multiplied with $C_l(\vec{x}, t)$ at the same time and position, since it represents local and quasi-instantaneous synaptic input. For the second term of A_{ek}, the $C_e(\vec{x}, t)$ term is instead included through Equation (33). The right hand side of this propagation equation, while written in terms of the $(\vec{x}, t)$, effectively encodes the signal at a distance location $\vec{x}\,'$, sampled there at time t', and then transported with velocity v_{ek} to the local position $\vec{x}$ with a conduction delay $t - t'$; see for example (Bojak and Liley, 2010) for an explanation in terms of Green's functions. Thus, we now propagate the firing rate as scaled by the pre-synaptic efficacy of the neural populations at a distant position $\vec{x}\,'$ at the time t'. We note that this is not quite physiologically accurate either, since the synaptic dynamics should be evaluated at $(\vec{x}, t)$, not $(\vec{x}\,', t')$, albeit driven with the firing rates from $\vec{x}\,'$ delayed by $t - t'$. This could be achieved by setting $N^{\beta}_{ek} C_e \rightarrow N^{\beta}_{ek} C^S_e$ and $N^{\alpha}_{ek} \Phi_{ek} \rightarrow N^{\alpha}_{ek} C^{\Phi}_{ek} \Phi_{ek}$ in Equation (31), removing C_e in Equation (33), and then tracking separately the spatiotemporal dynamics of C^S_e and C^{Φ}_{ek}, respectively, where the latter would have Φ_{ek} instead of S_e in Equation (23). However, this would double the effort for computing the synaptic dynamics and could have potentially undesirable consequences for the

separation of distant sources, see the Discussion for further detail. Finally, for simplicity we have assumed here that the extracortical input p_{ek} remains unchanged. This assumption will likely need to be improved upon for greater physiological realism, i.e., we do expect that in particular thalamic activity will also be modified by anesthesia. However, our current focus on only the cortical side allows us to highlight the proposed bursting mechanism without potential interference from complex interactions between extracortical and cortical structures. Given the assumption that p_{ek} is constant (or in the case of p_{ee}, that its mean is constant), we would not expect the pre-synaptic efficacy to change. Overall, if we switch off the synaptic dynamics $C_l \equiv 1$, we recover exactly the extended Liley model of Bojak and Liley (2005).

The bursting Liley model hence consists of Equations (1, 7, 14, 15, 21–23, 30–33), with the influence of isoflurane anesthesia being parameterized by Equations (9–13, 18). In practice we choose the $f_l > 0$, and as before use the "combined fixed point" initial state of Equation (29). The parameter values we have chosen are listed in **Table 1**. For the synaptic system, we have followed qualitatively the work of Tsodyks and Markram (1997) in assuming a possible range of about 250 ms to 1000 ms for τ_l^{rec}, and values between 0.1 and 2.0 for f_l. The values used in this paper were chosen after computational experimentation with various settings, and were selected because they lead to bursting only for relatively large concentrations of isoflurane. Clearly, more systematic and comprehensive scans of the available parameter space and better understanding of the dependence of the observed dynamics on these parameter values are needed in order to elucidate the mechanisms proposed here. However, it takes considerable computing time to simulate such large spatial systems. In order to accomplish a proper analysis of the parametric dependencies, one will likely need to find approximate but rapid evaluation methods, similar to replacing the full simulation with an eigenvalue calculation as in Bojak and Liley (2005). The development of such methods is beyond the scope of this article, here we want to demonstrate in a pilot study that we can qualitatively reproduce the spatial differentiation in burst suppression that has been observed experimentally.

2.3. NUMERICAL SIMULATIONS

All our simulations are performed on a two-dimensional cortical sheet discretized by a 512×512 numerical grid, where we assume a grid spacing of $\Delta x = \Delta y = 1$ mm. The effective simulation area of $2,621.44$ cm^2 corresponds roughly to the size of an entire human cortex (Im et al., 2008). Smaller grids, with or without larger grid spacing, have been used to investigate parameter dependencies more rapidly, but the results presented in this paper were all obtained on this standard grid. In order to avoid boundary effects we have made the numerical grid toroidal, i.e., if we number the grid points 0–511 along one dimension from left to right, then the grid point to the left of 0 is 511, and the grid point to the right of 511 is 0, and this is true for both dimensions. Obviously such a geometry is artificial as compared to the real brain. However, since it leaves all numerical grid points entirely equivalent, this together with the isotropic and homogeneous "background" connectivity implicit in the PDE propagation makes minimal assumptions about the actual geometry and specific connectivity of the brain. Basically, it represents a kind of anatomical "null hypothesis" from which any anatomical detail will deviate; and the more homogeneous the brain turns out to be in an effective sense, the better this approximation will represent its activity. As argued above, at significantly increased computational costs one can improve this description with neural mass meshes, but this is not expected to change the results obtained here at least qualitatively.

The only dependence on space is found in the propagation PDE of Equation (33). Hence the other dynamics are effectively described by a set of independent ordinary differential equations (ODEs) in time at every grid point. We solve all these ODEs with the following simple method: First, any higher time derivatives are turned into first derivatives by defining auxiliary variables, e.g., $d^2g/dt^2 = f(g)$ becomes $dg/dt = \tilde{g}$ and $d\tilde{g}/dt = f(g)$. Next, we solve these first order ODE systems with the forward Euler method. Obviously many more efficient numerical schemes exist. But in our experience they occasionally fail for specific parameter settings with the Liley model, whereas the forward Euler method always remains stable. Thus, we trade speed for guaranteed stability here. In the propagation PDE, the Laplacian is approximated by a five point stencil, i.e., to estimate the Laplacian at a grid point, we use the value at that point and those of its four horizontal and vertical nearest grid neighbors. We find that numerical stability is increased, if in this PDE we likewise estimate the second derivative in time directly by considering the current, previous and future values (and solving for the future one), rather than first rewriting them into first order derivatives as for the other dynamics. We use MPI-C to parallelize the computation across multiple nodes (threads and/or cores). This involves splitting up the grid into patches assigned to the individual nodes. We note that since the only spatial dependence in the dynamics arises from the Laplacian, and since we approximate it with a five point stencil, the only required communication between these nodes is that of the proximate part of the one grid point deep boundary of the local patch to the nodes working on the adjacent patches. This limited need for communication between nodes allows for very efficient parallel computation.

How the noise driving the system is generated and filtered in a mathematical sense has been described above, here we will add the following technical comments: The temporal Catmull-Rom spline filter is obviously local in space, and hence in a parallel setting can be performed by every individual compute node on the grid points assigned to it. However, the initial noise generation is done in Fourier space, to allow spatial filtering by a simple multiplication at every (Fourier space) grid point, followed by an inverse Fourier transformation. We use FFTW (Frigo and Johnson, 2005) to perform the inverse Fourier transform in parallel across the available compute nodes. This means that the random number generation and the Fourier space filtering can be done local in each node on its part of the Fourier grid, while FFTW organizes the communications between the nodes involved in the inverse Fourier transform.

The time step used in our simulations is $\Delta t = 5 \cdot 10^{-5}$ s, which for our chosen grid spacing is sufficient to achieve stable and convergent results. However, we save the simulation results neither at every time step, nor the entire system state, nor at the

internal double floating point precision (8 Bytes). The reason is that the 10 state variables of the bursting Liley model saved for 512×512 grid points at 8 bytes per point already would require 20 MB of hard disk space per time step, and thus at full time resolution a mere 3 s of run time would generate more than 1 TB of data. In practice, we typically save between one and four selected state variables with 250 Hz, converting to single floating point precision (4 Bytes) in the output. This still generates data files of many GB for our longest runs. Finally, even this data reduction is not sufficient to generate suitably sized animations of our results. Basically, the fine detail of a 512×512 grid leads to low compression efficiency of the employed (H. 264) movie codec. For producing animations we hence tile the output grid into squares of 4×4 grid points and average over these to obtain an effective 128×128 grid with smoother values that compress better. This explains the mild visual disparity between our figures (at full 512×512 resolution) and the animations, even though they are produced from the same underlying data set. We also produce video frames at an even lower sampling rate in time, and we use variable sampling rates to selectively speed up uneventful parts of the video. A time counter in the videos keeps track of the sampling rate, and occasional choppiness and blurriness in the videos does not reflect actual discontinuities in the simulations but merely low sampling rates and aggressive video compression.

3. RESULTS

We explore the influence of isoflurane on the model in a long simulation run presented in **Figure 2**. The entire simulation also has been animated as **Movie 1**, included in the Supplementary Material. In **Figure 2A** we show the time course of the isoflurane concentration that we have imposed. First the system is run free of anesthesia (0 MAC) for 10 s. We call this the first plateau in the following. The equilibrium values of the system are used as initial conditions. Hence there are no transient dynamics, which allows us to estimate a power spectral density (PSD) from the h_e time series. Then we increase the concentration linearly to 0.5 MAC (equivalent to 0.1215 mM or 0.585% inspired at normal body temperature) over 10 s, and keep the system at this concentration for another 10 s. This second plateau corresponds to a light anesthesia state, without burst suppression, and again we can estimate a PSD here. Next we increase the concentration linearly to 1.0 MAC (equivalent to 0.243 mM or 1.17% inspired), and keep the system there for 40 s. This third plateau corresponds to a state of deep anesthesia, with burst suppression, and we can estimate a PSD here as well. After that, we increase the isoflurane concentration again for 10 s to 1.5 MAC (equivalent to 0.3645 mM or 1.755% inspired), and maintain it at this value for 10 s. Bursting is abolished at this fourth plateau, and we compute another PSD here. Finally, we raise the concentration for another 20 s up to 2.5 MAC (equivalent to 0.6075 mM or 2.925% inspired). This demonstrates that the system has finally returned to a regime without bursting.

In **Figure 2B**, we see PSDs estimated over these plateaus. At each concentration, we have calculated PSDs for every individual grid point from the h_e time series for the entire duration of the plateau, using a Welch estimate with a 2.5 s window and 50% overlap, and then have averaged the resulting 262,144 PSDs. We have normed these average PSDs to have unit area, i.e., their total power over all frequencies is one. This makes it easier to compare them visually. Please note that the parameter set used here is a "bi-phasic" one, see the discussion in Bojak and Liley (2005). Consequently, the total power at the second plateau is actually increased over that at the first plateau by a factor of 1.26. We see the characteristic shift of the alpha resonance to lower frequencies, in this case initially accompanied by a sharpening of the peak. Without the slow synaptic system as in Bojak and Liley (2005), a further increase of the isoflurane concentration would move the former alpha peak to ever lower frequencies, accompanied eventually by strong damping of the peak and a reduction of the total power, completing the bi-phasic power change. However, with the introduction of the slow synaptic system we see a burst suppression pattern emerge, and the large amplitude oscillations imply a drastic increase in total power by a factor 131 over the resting values. Yet we see that the PSD obtained from the third plateau—as far as frequency content is concerned—roughly follows what is expected without the synaptic system: The majority of the power, which is generated by the large bursts, is located where one would expect to see the former alpha resonance in the previous model of Bojak and Liley (2005). In other words, the bursts roughly conserve the regular dynamics of the system, in particular of the former alpha resonance. At the fourth plateau the system has ceased to burst but still shows elevated total power 1.44 times larger than at rest.

In **Figure 2C1** we see the system at rest under noise drive. The visible structure is hence basically that of the spatial correlations we have included in the noise. The corresponding time series in **Figure 2C2** shows the typical waxing and waning of a resting alpha rhythm in h_e. Unsurprisingly, Γ_{ee} oscillates slowly at values about the equilibrium value of the slow synaptic system Γ_{ee}^0, cf. **Table 1**. In **Figures 2D1,D2** we see the corresponding state at light anesthesia. The overall h_e is now lower across the grid, indicating smaller firing rates on average. However, as we can see in the time series the amplitude of the oscillations has increased, corresponding to the power increase expected for this "bi-phasic" parameter set. The oscillation frequency also has become lower, though this is easier to see in the PSDs of **Figure 2B**. We see that Γ_{ee} is still oscillating slowly, but around values somewhat higher than Γ_{ee}^0, because the synaptic resources are not as rapidly depleted by the reduced excitatory firing rate of the depressed h_e.

In **Figure 2E1** burst suppression patterns have emerged. These patterns are clearly independent of the noise drive. In the **Movie 1**, included in the Supplementary Material, one can see how this is a snapshot of "burst waves" moving across cortex, with centers of burst activity spontaneously forming and disappearing. The geometry of these excitations is complex and constantly changing. We see in **Figure 2E2** that the strongest oscillations in h_e are associated with a rapid drop in Γ_{ee} due to the synaptic depletion during these periods of high firing. This lowering of Γ_{ee} quickly suppresses the burst by reducing the self-excitation of cortex. This is then followed by a recovery to values of Γ_{ee} that are large compared to those at rest or light anesthesia. This recovery to high values of Γ_{ee} is driven by the isoflurane-induced reduction in the mean excitatory firing rate during the suppressed periods. In turn, these strong PSPs eventually destabilize the neural system,

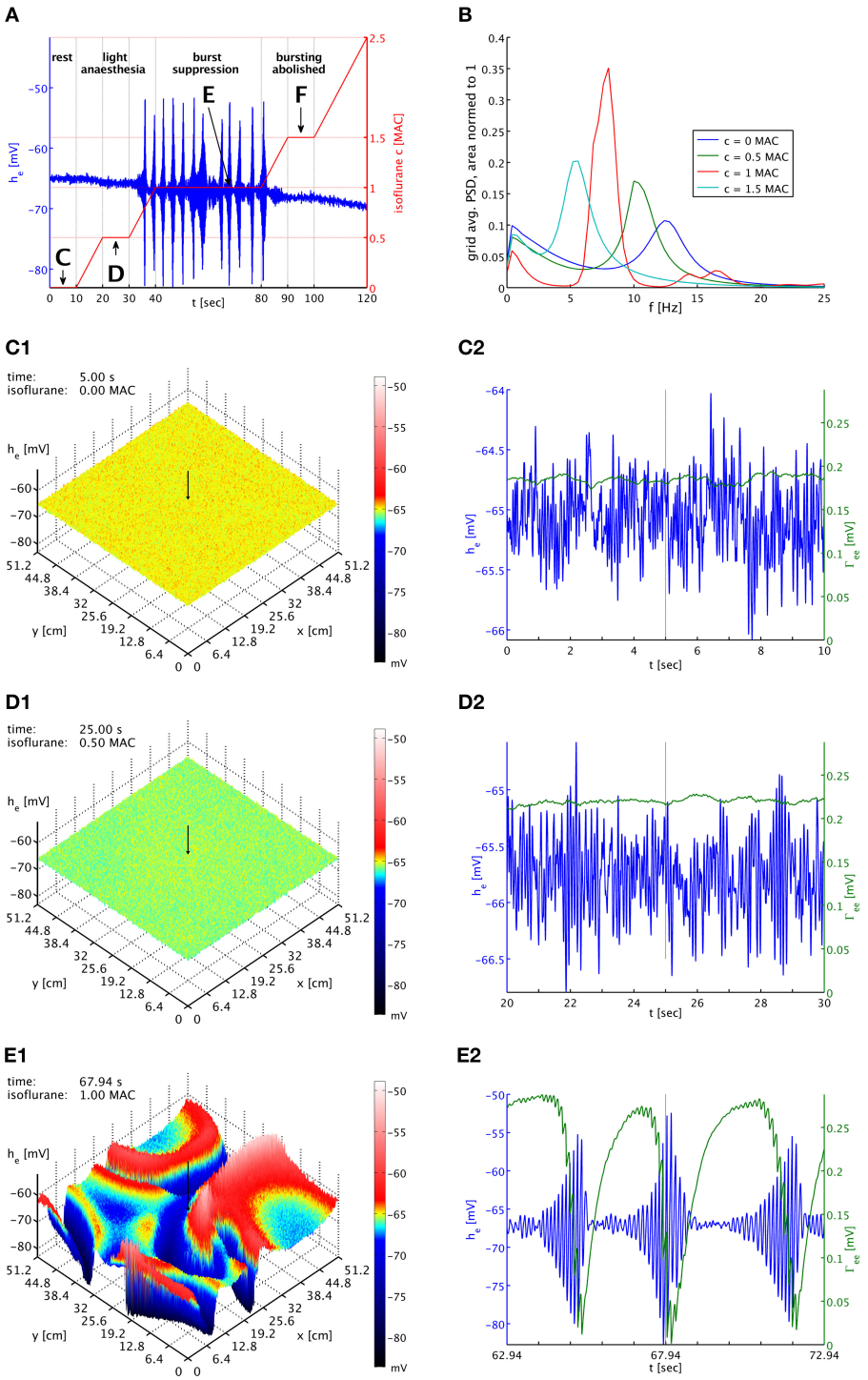

FIGURE 2 | (A) Imposed concentration of isoflurane (red curve), and the h_e response (blue curve) at the cortical location indicated by black arrows in the snapshot panels below. Different plateaus of concentration are labeled "C," "D," "E," and "F." Arrows point to the central times of the corresponding time series shown below. **(B)** PSDs of h_e averaged over the entire grid and normed to unit area for plateaus "C" (blue), "D" (green), "E" (red), and "F" (cyan). The motion of the alpha peak to lower frequencies persists qualitatively into the burst suppression phase "E" at much increased power. **(C1)** Snapshot of the h_e activity of the cortical surface at 0 MAC isoflurane. The size of h_e is indicated by both height and color, cf. the color bar. A black arrow shows the position from which the corresponding time series were recorded. **(C2)** Time series of h_e (blue) and Γ_{ee} (green) over the 10 s of the "C" plateau. Regular alpha rhythms in h_e and slow Γ_{ee} oscillations around the standard value Γ^0_{ee} can be seen. **(D1)** Snapshot at 0.5 MAC. **(D2)** Time series of the "D" plateau. The oscillations of h_e have larger amplitude at a lower average. The slow Γ_{ee} oscillations now occur at an elevated level. **(E1)** Snapshot at 1 MAC. Burst suppression patterns have emerged and move across the cortical surface. **(E2)** Time series of the "E" plateau. Burst suppression is apparent both in h_e and Γ_{ee}, with a rapid drop in Γ_{ee} caused by the strongest h_e oscillations. An animation of this simulation is provided as **Movie 1** in the Supplementary Material.

leading to another burst. The burst suppression pattern persists as the anesthesia concentration is being increased again, up to quite high concentrations. In **Movie 1**, one can see that the amplitudes of the "burst waves" eventually become smaller and smaller until the burst activity fades away into regular noise driven activity. We do not show here corresponding plots for the fourth plateau with abolished bursting, but they would look similar to **Figures 2D1,D2** with a further reduced mean value h_e, even lower oscillation frequency, and a Γ_{ee} that is on average even higher.

The burst suppression phase shown in **Movie 1** of the Supplementary Material makes obvious that one cannot expect global synchrony of the burst suppression across cortex. A multitude of transient spatiotemporal patterns emerge, travel across cortex, and dissolve. This is also shown in **Figure 3**, which shows time series from three well-separated locations on the simulated cortex at a specific point in time. There is little evidence of strong systematic correlations. While one might expect that the propagation of "burst waves" should lead to correlations with temporal delay at these distances, other burst features emerge across these spatial scales and interfere with the burst timing. Without observing spatiotemporal pattern globally, it hence will be difficult to find systematic correlations of the bursts at large distances. However, locally it may be possible to track the regular motion of burst patterns, e.g., at a point close to the one labeled "a" one might see bursting appear with a delay, characteristic for the "burst wave" passing through these two points sequentially. Overall, we expect stronger synchronization—or at least consistent phase differences from traveling patterns—at shorter distances, whereas at longer distances such correlations will be basically accidental. Thus, one would expect to see considerable spatial differentiation if one records from several spatial locations, as in Lewis et al. (2013). How many electrodes would be seen to burst at the same time would depend on the size and motion of the emerging spatiotemporal burst patterns.

Local variation of cortical tissue properties, reflected in the model evaluation by a change in the parameters, may also affect the ability of some part of cortex to participate (fully) in the spatiotemporal burst suppression dynamics. Such variation of tissue properties can be natural and develop intrinsically, or could be induced extrinsically by physical insult or the application of drugs. We have seen that bursts are associated with slow but large oscillations in the excitatory peak amplitudes of the PSPs. It is important to note that there are two different effects determining the general size of the Γ_{ek}. On one hand, anesthesia is reducing Γ_{ek} directly as parameterized by the Hill factor $H_e(c)$, cf. Equation (30). On the other hand, the reduction in the average h_e, mostly due to the strong prolongation of the inhibitory PSPs with anesthesia, means that the average excitatory firing rate S_e decreases. This in turn leads to less synaptic depletion and hence actually a rise in Γ_{ek}, cf. Equation (19). The net effect with increasing concentration is actually an increase of Γ_{ek}, and this is crucial for the onset of bursting. If one increases anesthesia further, eventually the Hill factor begins to dominate and Γ_{ek} decreases again.

The same can be said for the Γ_{ik}, and the corresponding balance between the Hill factor $H_i(c)$ and the reduction in S_i for increasing anesthesia. However, we see that in the standard parameters the excitatory synaptic depletion factor $f_e = 1.25$ is much larger than the inhibitory one $f_i = 0.175$. This means that there is much less room for Γ_{ik} to grow, since the steady maximum is $\Gamma^{\mathrm{r}}_{lk}(c) = \Gamma^{0}_{lk}(1 + f_l)H_l(c)$. One simple idea for reducing the ability of cortical tissue to participate in burst suppression is hence to increase the growth of inhibition with anesthesia by raising f_i. What do we expect to be the effect of this increased inhibition, in particular concerning the excitatory Γ_{ek}? In general we expect h_e and h_i to decrease even more rapidly with increasing concentration of anesthesia, due to the boosted inhibition. But silencing the cortex also decreases synaptic depletion,

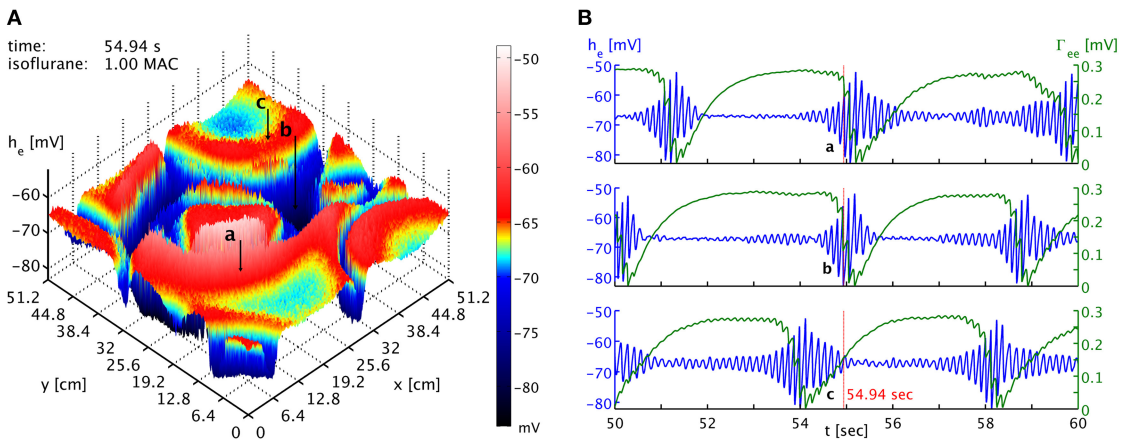

FIGURE 3 | (A) Snapshot of the h_e activity of the cortical surface at simulation time 54.94 s under the influence of 1 MAC isoflurane. Black arrows with labels "a," "b," and "c" point to the cortical locations of the time series shown in the other panel. Note the toroidal boundaries, e.g., the circular burst front that appears cut off around $(x, y) = (44.8,\ 0)$ cm continues at $x = (44.8,\ 51.2)$ cm. **(B)** Time series of h_e (blue) and Γ_{ee} (green) taken from the three different positions marked as "a," "b," and "c" in the other panel. It is obvious that bursts are not generally synchronized in time at the different positions. Spatiotemporal correlations from propagating "burst waves" can occur, but are removed at larger distances by the interference from other emergent patterns. An animation of this simulation is provided as **Movie 1** in the Supplementary Material.

so we actually expect a stronger initial Γ_{ek} growth for increasing anesthesia. It is hence not a priori clear whether the more rapid decrease in h_e or the more rapid increase in Γ_{ek} dominates, and in consequence whether bursting is abolished or maintained, respectively. We note that for our regular parameter set bursting is abolished at higher concentrations even though Γ_{ek} is still increasing, because h_e has then decreased too much. We may hence expect that an increase of f_i alone can stop the bursting.

To test this, we use a typical simulation at 0.25 mM isoflurane. However, in a circular patch of tissue we set $f_i = 1.25$ instead of the standard $f_i = 0.175$, while leaving this parameter at $f_i = 0.175$ across the rest of the cortical sheet. Using $\Gamma^{\mathrm{r}}_{lk}(c) = \Gamma^{0}_{lk}(1 + f_l)H_l(c)$, we have inside this patch $\Gamma^{\mathrm{r}}_{ie,ii}(0.25) = (3.5174,\ 2.3872)$ mV and outside $\Gamma^{\mathrm{r}}_{ie,ii}(0.25) = (1.8369,\ 1.2467)$ mV, respectively, while everywhere $\Gamma^{\mathrm{r}}_{ee,ei}(0.25) = (0.37703,\ 3.8414)$ mV. As shown in **Figure 4**, outside of the circular patch burst suppression patterns emerge as usual, see **Figures 4A,B**, while in the dead center of the circular patch there is no sign of such activity, see **Figures 4A,D**. Hence inside the patch the greater decrease in h_e was more effective than the greater increase in Γ_{ek}, compare **Figures 4B,D**. Interestingly, at the border of the circular patch, see **Figures 4A,C**, we see largely the same state as for the center, but there appear to be some "quasi-bursts". Actually, this is activity spilling into the circular patch from the outside through the propagation with Equation (33). The characteristic spatial decay scale of this propagation is $\lambda_{ek} = 2.4$ cm. Given a radius of 9.6 cm of the circular patch, we expect a signal from the outside to have fallen to less than 2% of its original value at the center. So it is unsurprising that any outside influence on the center is not obvious to the eye, but that close to the rim we see stronger echoes of the surrounding burst activity. In **Movie 2** in the Supplementary Material h_e (top panel) and Γ_{ee} (bottom panel) animations are shown. Here one can observe the bursting waves collide with the circular patch, and then fade as they penetrate deeper. We note that an increase to for example $f_i = 0.5$ in the patch is not sufficient to abolish bursting in this manner, illustrating that it is the balance between the decrease in h_e and the increase in Γ_{ee} which determines whether self-excitation is possible.

The dynamics of Γ_{ee} are of course much slower than those of h_e, and we can track the h_e burst fronts by the progression of the lowest dips and valleys in Γ_{ee}. This corresponds to rapid synaptic depletion in high firing regions. The extent of "spill-in" from the outside into the circular patch is also easier to discern

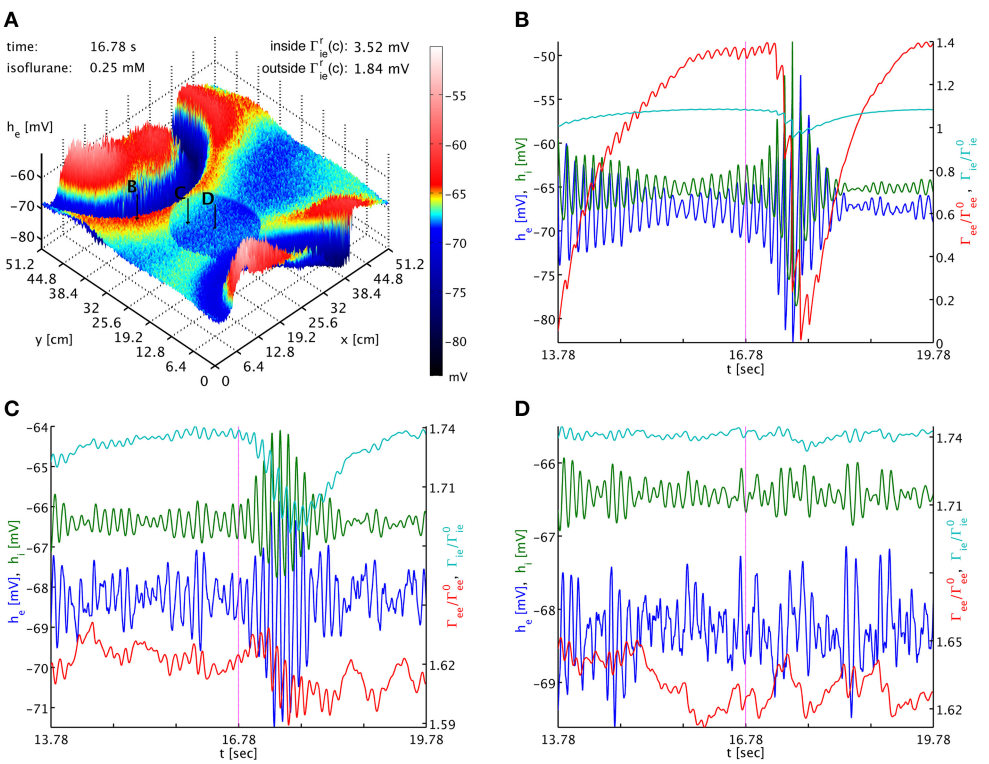

FIGURE 4 | (A) Snapshot of the h_e activity of the cortical surface at simulation time 16.78 s under the influence of 0.25 mM isoflurane, where in a circular patch (center $(x, y) = (20.0, 20.0)$ cm, radius 9.6 cm) the inhibitory synaptic depletion factor f_i has been increased from 0.175 to 1.25, leading to an increase of $\Gamma^{\mathrm{r}}_{ie,ii}$ there by a factor 1.91. The size of h_e is indicated by both height and color, cf. the color bar. One can see that the circular patch does not participate in the burst suppression pattern. Black arrows with labels "B," "C," and "D" point to the cortical locations used in the other panels. **(B)** Six seconds long time series of h_e (blue), h_i (green), $\Gamma_{ee}/\Gamma^0_{ee}$ (red), and $\Gamma_{ie}/\Gamma^0_{ie}$ (cyan) around the time of the snapshot from a point outside of the circular patch. Burst suppression is clearly visible in all variables. **(C)** Time series from just inside the circular patch. There is no local burst suppression, but some of the outside burst activity spills in. **(D)** Time series taken from the center of the circular patch. There is neither local burst suppression nor spill-in. Animations of this simulation are provided as **Movie 2** in the Supplementary Material.

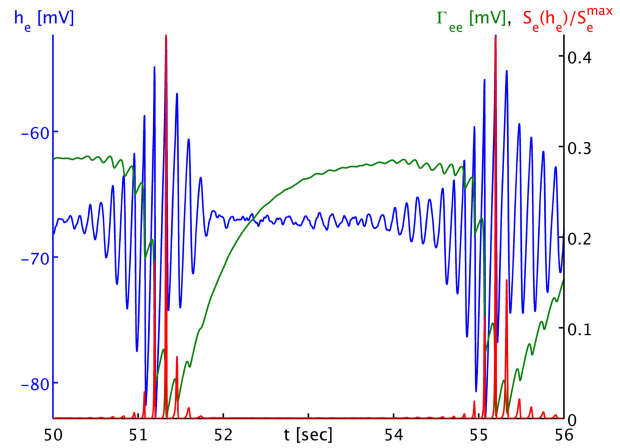

FIGURE 5 | Time series of the mean excitatory soma membrane potential h_e (blue), the excitatory post-synaptic peak amplitude Γ_{ee} (green) and the average excitatory firing rate normed to the maximum attainable rate $S_e(h_e)/S_e^{\max}$ (red). Note that both Γ_{ee} and $S_e(h_e)/S_e^{\max}$ map by value to the black ordinate on the right, though with different units. The time series shown here is part of the times series labeled "a" in **Figure 3B**. One sees that the strongly non-linear relationship between h_e and S_e in the anesthetic regime transforms the "symmetric" h_e oscillation that would be visible in local field potentials and the EEG during the burst phase into strong "spikes" in the firing rate S_e, and consequently to a "jagged" appearance of the synaptic depletion of Γ_{ee}.

in Γ_{ee}: the center of the patch remains at roughly constant values, while at the rim Γ_{ee} drops when high firing propagates into the patch. We note that the strong oscillations that one can see as Γ_{ee} drops rapidly in **Figure 4C** show up in the movie as a kind of "bouncing" rather than a smooth advance of the burst fronts. To understand this better, we provide **Figure 5**. It shows part of the time series labeled "a" in **Figure 2B**. However, in addition to h_e (blue curve) and Γ_{ee} (green curve), it also shows the mean excitatory firing rate $S_e(h_e)$ as red curve. So that one ordinate can be used for both Γ_{ee} and $S_e(h_e)$, we have normalized the latter by the maximum excitatory firing rate $S_e(h_e)/S_e^{\max}$. The basically symmetric oscillations of the mean membrane potential h_e around an average value translate into strong "spikes" in the mean firing rate $S_e(h_e)$. This is due to the sigmoidal nature of Equation (7), combined with the fact that the average h_e is about 5.5 standard deviations $\sigma_e = 2.8669$ mV below the average firing threshold $\mu_e = -51.656$ mV, leading to low firing rates. Only the strongest depolarizations in the burst come close to this threshold—though even they do not quite reach it here, as we can see, since $S_e(\mu_e)/S_e^{\max} = 0.5$ by definition. Thus, the relationship between h_e (local field potentials and EEG) with firing rates is highly non-linear in the anesthetic regime. It is obvious from **Figure 5** that the jagged drop of Γ_{ee} is simply caused by strong synaptic depletion induced by "spikes" in the mean excitatory firing rate.

Finally, we also considered the influence of the spatial scale of brain connectivity on the spatiotemporal expression of burst suppression. As mentioned above, in this simplified model it is represented by the parameter λ_{ek}, the characteristic length scale of the exponential decay of activity propagated with Equation (33). Its regular value according to **Table 1** is $\lambda_{ek} = \lambda_2 = 2.4$ cm. This is a length scale one might associate with a brain region and cortico-cortical connections, in particular since the influence of activity at a point would be felt across a distance of several λ_{ek}. We vary this length scale up $\lambda_{ek} = \lambda_1 = 2.7$ cm and down $\lambda_{ek} = \lambda_3 = 2.1$ cm to investigate the impact of brain connectivity on the dynamics. In **Figure 6** we see the dependence of the spatiotemporal activity on adjusting this parameter. The spatial extent of the emerging burst patterns clearly becomes smaller as λ_{ek} is being decreased, cf. **Figures 6A–C**. This is particularly obvious in the corresponding animations for the different λ_{ek} values, **Movies 3–5** of the Supplementary Material, where we can see that at λ_1 large parts of cortex are recruited in the bursts, whereas for λ_3 bursting is much more localized. Our standard λ_2 represents an intermediate case. However, the time interval between bursts for these different λ_{ek} appears at first sight comparable, see **Figure 6D**. To be more quantitative, one can use the point where Γ_{ee} drops lowest as a convenient marker for the time of a burst peak. To carry out automatic computations for 50 s time series for every grid point, we select the deepest minimum within a specific continuous "burst peak region" defined by $\Gamma_{ee} \leq 0.05$ as burst peak time, and we remove inter-burst intervals with $\Delta t_{\mathrm{IBI}} < 1.0$ s as not representative for single burst behavior. This cut removes "double-dipping" below our Γ_{ee} threshold, caused for example by two subsequent activity "spikes" in the same burst with just enough recovery in between to get above threshold (very small Δt_{IBI}) or the interference of two burst waves (small Δt_{IBI}). We find the following grid averages: $\langle \Delta t_{\mathrm{IBI}} \rangle_{\lambda_1} = (4.44 \pm 0.26)$ s, $\langle \Delta t_{\mathrm{IBI}} \rangle_{\lambda_2} = (4.0 \pm 1.1)$ s, and $\langle \Delta t_{\mathrm{IBI}} \rangle_{\lambda_3} = (3.5 \pm 1.5)$ s. We see that the mean of Δt_{IBI} is decreasing roughly by 0.5 s per 3 mm reduction of λ_{ek}; whereas the standard deviation increases considerably with decreasing λ_{ek}, reflecting the more diverse spatial distribution of the burst patterns. According to these simulations, we can expect that spatial differentiation—the size of the burst suppression patterns and their timing—is intimately linked to the effective extent of the brain connectivity propagating the burst activity.

4. DISCUSSION

We find that the simulation of isoflurane induction with the model proposed here reproduces at least qualitatively the electrophysiological response that one can measure in the EEG (Foster et al., 2008). At light anesthesia there is an oscillatory shift to lower frequencies with higher amplitudes, then in deep anesthesia we find burst suppression patterns, and finally for even higher concentrations these bursts are abolished as cortex slowly heads toward electrotonic death. Significantly, in the burst suppression phase the prior regular activity of cortex is roughly "echoed" in the frequency content of the burst (Kroeger and Amzica, 2007; Ching et al., 2012), though of course the amplitude of the oscillations is much increased. We find that burst suppression results in dynamic and complex burst patterns that travel across cortex in waves, rather than remaining statically in place. The burst suppression phase is foreshadowed by the continuous elevation of peak PSP amplitudes, until finally these strong inputs destabilize the neural system into bursting. At maximum oscillation of the mean soma membrane of the neural population, strong

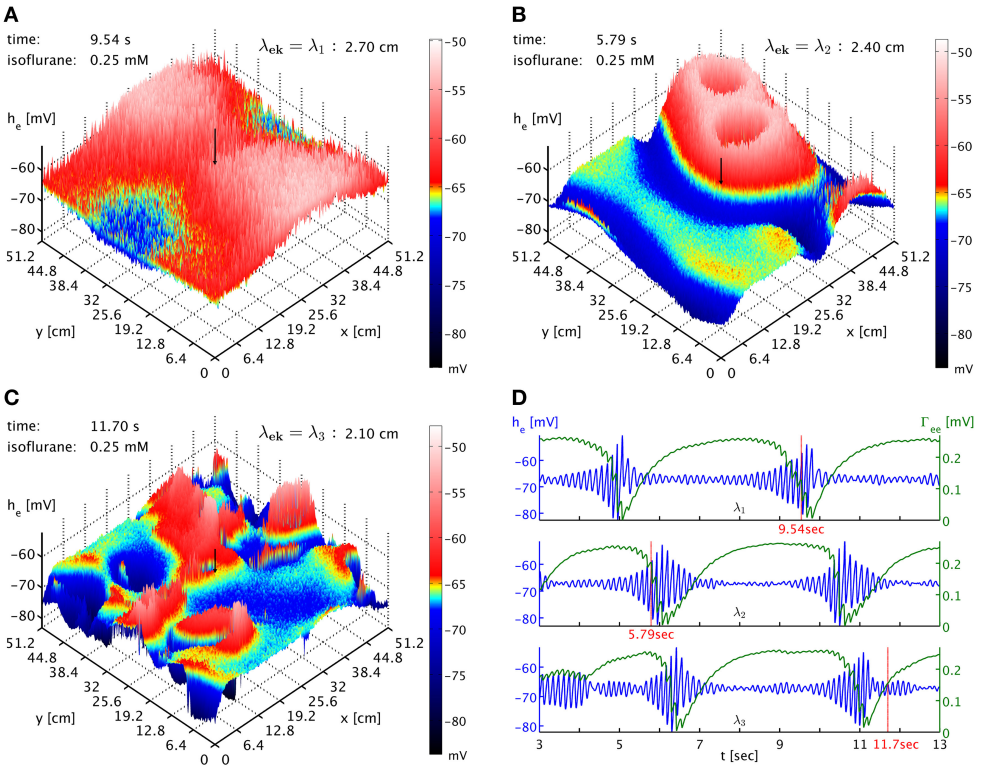

FIGURE 6 | (A) Snapshot of the h_e activity of cortex at simulation time 9.54 s at 0.25 mM isoflurane with $\lambda_{ek} = \lambda_1 = 2.7$ cm. A black arrow shows the cortical location at which the corresponding time was recorded. An animation is provided as **Movie 3** in the Supplementary Material **(B)** Snapshot at simulation time 5.79 s with $\lambda_{ek} = \lambda_2 = 2.4$ cm, the standard value. An animation is provided as **Movie 4** in the Supplementary Material. The characteristic size of the burst patterns is reduced. **(C)** Snapshot at simulation time 11.70 s with $\lambda_{ek} = \lambda_3 = 2.1$ cm. An animation is provided as **Movie 5** in the Supplementary Material. The characteristic size of the burst patterns is reduced even further. **(D)** Time series of h_e (blue) and Γ_{ee} (green) taken from these three simulations, marked as "λ_1," "λ_2," and "λ_3." We see that inter-burst interval remains roughly the same.

depletion of the synaptic system leads to a sudden drop of the PSP peak amplitude, which suppresses the burst until the synaptic system is able to recover again. The relatively slow time scale of this recovery is what governs the periodicity of the bursts in the burst suppression regime in this model.

While we are mostly interested here in investigating the spatial differentiation of burst suppression qualitatively, the emergence of burst suppression in our simulations is also in rough quantitative agreement with what has been observed clinically. Because the emergence of burst suppression in the EEG represents a distinct endpoint, it has been proposed that it may be a suitable measure by which to titrate the administration of anesthesia to ensure optimal hypnosis. On this basis a variety of efforts have been made to estimate the concentration dependent emergence of burst suppression during anesthesia. It has been found that during sole agent isoflurane anesthesia, the burst suppression pattern can emerge at end-tidal concentrations as low as 1.2% (Hoffman and Edelman, 1995; Pilge et al., 2014), i.e., aqueous concentrations of $\simeq 0.25$ mM at 37°C. However when arterial blood concentrations of isoflurane have been measured the onset of burst suppression has been reported for levels as low as 34.9 μg/ml or $\simeq 0.19$ mM (Loomis et al., 1986) – close to the value at which we observed the onset of burst suppression in our model.

However, more importantly our model predicts the appearance of large-scale spatial burst patterns across cortex, which emerge, travel and disappear over time. In consequence, coherence of burst timing is mostly local, though one can expect to see characteristic burst onset time shifts in the case of burst patterns traveling across neighboring recording sites. Some of the simulated patterns become large in size intermittently, recruiting large parts of cortex and thus leading to more "global" correlations of burst timing. However, for the most part the complex spatiotemporal dynamics will lead to "local" correlations, with synchronization over large distances being mostly accidental. These predictions are at least qualitatively in line with the experimental observations of Lewis et al. (2013), see in particular their **Figures 3**, **4**. We suggest that spatially dense experimental recordings may allow one to track such spatiotemporal burst patterns in detail. At least in principle it should be possible to reconstruct the underlying cortical state in terms of our model from such recordings, in particular if one tracks the activity over some length of time. The relatively slow spatiotemporal dynamics of the bursts may help in this regard.

We have shown here as well that increasing the inhibitory depletion factor f_i, or equivalently the resting values Γ_{ie}^r and Γ_{ii}^r of the inhibitory peak amplitudes, can abolish bursting in the model

in a localized manner (in a patch of simulated cortical tissue). This is due to affecting the balance of two competing effects: the decrease of h_e reduces, whereas the increase of Γ_{ee} increases, the capacity of cortex for self-excitation. For large enough increases of inhibition the former dominates the latter. This provides further possibilities for spatial differentiation in cortex as some tissue may have naturally higher inhibitory peak amplitude resting values, and hence be less capable of participating in burst suppression. In addition, it is expected that spatial heterogeneity in the cortical actions of anesthetics will contribute to the spatial differentiation of burst suppression. Most anesthetics that induce burst suppression are GABAergic agents, which in addition to enhancing inhibitory PSP action also produce increases in tonic inhibition, as well as reductions in tonic excitation by altering the activity of a variety of membrane bound channels that include two pore potassium channels, extrasynaptic $GABA_A$ and nicotinic acetylcholinergic ionotropic receptors. However, these synaptic and extra-synaptic channels, which exist in multiple isoforms that are variably affected by the same anesthetic agent, are not distributed uniformly throughout cortex. Thus, we would expect no two regions of cortex to share exactly the same propensity to burst for a given anesthetic level. This is not reflected in the current work, but left for future studies.

The hypothesized synaptic basis for spatially heterogeneous burst suppression suggests that if one can accordingly manipulate the cortical tissue, then one can artificially suppress, abolish or even enhance its participation in bursts. Importantly, our model predicts that drugs increasing inhibition could have the paradoxical effect of increasing burst activity, depending on the precise balance of the h_e decrease and Γ_{ee} increase that they induce. In particular, one would typically expect that any paradoxical effects would occur at lower doses, since strongly increasing inhibition should eventually see the h_e decrease win over the Γ_{ee} increase. It is interesting to note that a wide variety of $GABA_A$ modulators appear to have paradoxical effects at low doses, see for example (Bäckström et al., 2011) and references therein. Furthermore, our spatial model predicts that bursting activity of surrounding tissue can propagate into tissue that is incapable of bursting itself, to a depth depending on the density of synaptic connectivity, and lead there to "quasi-bursts" which simply reflect the dramatic variation of the synaptic input. However, if bursts are abolished by the mechanism suggested here, namely an increase in the inhibitory synaptic depletion factor f_i, then this tissue would show particularly large inhibitory PSP amplitudes and largely constant (rather than strongly varying) excitatory ones . This suggests that one could experimentally distinguish between bursting and "quasi-bursting" tissue by monitoring the size of the PSPs.

Furthermore, we have shown that both the spatial extent of the burst patterns, and the timing of the bursts (in particular the interval between bursts) depend on the characteristic scale of the brain connectivity effectively involved in propagating this activity: the shorter range these connections, the smaller the regions of coherent burst activity, and the more rapidly one burst follows on after the other. While at present this constitutes a qualitative finding, and while the implementation of brain connectivity in our model (homogeneous, isotropic and exponentially reducing with distance) is too simplistic to speak directly to the complexity of actual cortico-cortical connectivity, this nevertheless suggests that there is an intimate link between the spatiotemporal profile of burst suppression and the underlying brain connectivity. This will have to be taken into account when trying to improve the realism of such simulations. Thus, by being more specific about the anatomical structure of our mesoscopic model it may become possible that observations of burst suppression patterns will enable estimation of the effective connectivity of the bursting tissue. This would provide a new window on a difficult to access but key property of the brain.

Our present simulation has been restricted to studying the role that one slow modulatory system might have in the genesis of the burst suppression pattern. However, given the feedback inherent in the physiological and anatomical organization of cortex it is certainly only one of many systems that are capable of modulating cortical excitability, and hence the emergence of fast-slow bursting activity. Indeed we might hypothesize that such slow modulatory systems will span a number of functional scales in the brain—from perturbations in the autoregulatory coupling of neuronal and metabolic activity to alterations in the dynamics of cortico-thalamic and cortico-cortical feedback, to mention only the most obvious. However, regardless of the specifics of the slow system it is clear that any theory purporting to account for the genesis and features of cortical electrodynamics must be able to account for the reversible emergence of burst suppression in response to the action of anesthetic agents. In this respect both our model and the model of Ching et al. (2012) may be seen as meeting this requirement, even though they take as their starting points neuronal activity modeled at different spatial scales. A possible advantage of our approach, besides being able to deal easily with a spatially extended cortex, is that the modeled action of anesthesia is directly coupled to the emergence, and subsequent disappearance, of bursting. In contrast, in Ching et al. (2012) the parameters defining anesthetic action (τ_{GABA} and g_{GABA}) are not directly related to the parameter J_{ATP} (the metabolic production rate of ATP) that defines the emergence of bursting.

Our model of synaptic depression is driven by pre-synaptic firing rates. This is unproblematic for the quasi-instantaneous local activity. However, an issue arises due to the propagation of action potentials from distant sources with finite velocities along cortico-cortical fibers. The current formulation of Equations (31, 33) as to how such distant inputs drive local PSPs is not entirely faithful to the actual physiology: the pre-synaptic firing rate is now modulated with the concurrent synaptic dynamics at the *distant* pre-synaptic site, which is then propagated with conduction delay; whereas it would be more physiologically accurate to propagate the pre-synaptic firing rates, and then modulate these conduction-delayed inputs with *local* synaptic dynamics. However, this would mean tracking separately local synaptic dynamics driven by quasi-instantaneous local (C_l^S) and delayed distant (C_{ek}^Φ) pre-synaptic firing rates, respectively. Our current model requires only one local synaptic dynamics (C_l), making it computationally simpler. Furthermore, one can argue that the current formulation better separates distant sources: If there are two distant sources, but only one of them begins to fire at higher rates, then only its signal would become depressed by the resulting synaptic dynamics, but not that of the other. Whereas if we were to

drive a local C_{ek}^{Φ} directly with the sum of the delayed signals, then the higher firing of one would lead to synaptic depression also of the other. Yet one can argue to the contrary that such a conflation of distant inputs is simply part of the averaging approximation involved in considering neural populations rather than individual cells. We have made here a choice of convenience, but this may not always be possible. The parameters characterizing the (excitatory) synaptic dynamics are in this work taken to be spatially homogeneous. We are not aware of any extant empirical evidence that would require a significant deviation from homogeneity, but the alternative method mentioned above would be more suited for this case. For as currently formulated, the synaptic dynamics will be determined by parameters located at the origin of such activity and not, as must be physiologically the case, its pre-synaptic termination. A further possibility that we have not considered, due to the lack of any clear empirical data, is that these parameters themselves depend systematically on anesthetic concentration. If such a relationship is demonstrated, then this could act as a possible source of spatial inhomogeneity in the parameters of the synaptic dynamics, under the assumption that anaesthetic action shows spatial variability.

Finally, there are obvious extensions to this work that should be considered, but were beyond the scope of this initial investigation. The most obvious extension is to more systematically consider the effects of variations in the neural field model parameters defining the resting (unperturbed) EEG, and to study the resulting dynamics for spatially homogeneous models of synaptic resource depletion and anesthetic action. Furthermore, the neural field model used here can be extended to an equivalent neural mass mesh constrained by a real cortical head model based on MRI data (Bojak et al., 2010, 2011). Then one could investigate regional variations of the neural mass parameters with areal boundaries defined according to any of the available cortical structural/anatomical atlases [e.g., the Harvard-Oxford cortical and subcortical structural atlas (Desikan et al., 2006), or the Jülich histological atlas (Eickhoff et al., 2005)]. For example, each region could be assigned a distinct parameter set identified as producing physiologically plausible EEG within the physiologically admissible/plausible parameter space (Bojak and Liley, 2005). One could then additionally study regional variations in the synaptic resource depletion and/or anesthetic action parts of the model, as well as the interactions of heterogeneities in the component systems.

A perhaps less immediately obvious development, which however will be necessary to obtain a deeper understanding of the dynamical mechanisms responsible for the emergence of burst-suppression, would be some form of systematic bifurcation analysis. In such an analysis, the slow system would be "frozen", i.e., one would set the synaptic $\partial C_l/\partial t \equiv 0$, and a bifurcation analysis of the remaining "fast" subsystem would be performed by treating the C_l as bifurcation parameters. Such a bifurcation analysis, known as a fast-slow analysis, was pioneered by Rinzel (1985) in his formal analysis of bursting in biophysical models of the neuronal action potential. While such a bifurcation analysis is relatively straightforward for the temporal dynamics of non-linear ODE systems, using a variety of available bifurcation software tools like AUTO, Content, and MatCont (Meijer et al., 2013), it is considerably more challenging in systems of non-linear PDEs of the type we have studied here. A fast-slow bifurcation analysis of the spatiotemporal dynamics of burst suppression will require the development of new numerical methods and tools, which are only just beginning to emerge (Green and van Veen, 2014).

Our work then represents only a first step toward a deeper understanding of the spatiotemporal dynamics of burst suppression, in particular as induced by anesthesia. Yet it is already clear from the theoretical results obtained here, which were motivated by the recent experimental results of Lewis et al. (2013), that the classical understanding of burst suppression as spatially homogeneous phenomenon has become outdated. This can only add to the importance of burst suppression as a dynamical probe to investigate the properties and function of cortical tissue, whether in a theoretical modeling or an applied clinical setting. We expect that in the near future theory will be further challenged by the rapid technological advances in electrophysiology and neuroimaging, which are producing increasingly accurate and dense measurements of neuronal activity and cortical dynamics. This hopefully will allow us to test to what extent the synaptic resource depletion mechanism proposed here is indeed the driver of the observed burst suppression dynamics.

AUTHOR CONTRIBUTIONS

IB and DTJL developed the model. IB and ZVS programmed the simulation software, analyzed the generated data, and produced the figures and movies. IB and DTJL wrote the paper. All authors have approved the final version of the paper and the Supplementary Material.

ACKNOWLEDGMENT

We would like to thank the University of Reading for supporting ZVS with RETF grant E3470200. ZVS is thankful to Dr Garry Smith, School of Systems Engineering, University of Reading, for providing computing resources and support. The authors would like to thank one of the reviewers for comments that led to a significant improvement of the synaptic model.

SUPPLEMENTARY MATERIAL

The Supplementary Material for this article can be found online at: http://www.frontiersin.org/journal/10.3389/fnsys.2015.00018/abstract

We include the animations below to illustrate the results described in this work. In all cases the 512 × 512 grid for numerical evaluation has been averaged over 4 × 4 patches, and strong compression and low time sampling may limit the movie quality, see the discussion in Section 2.3.

Movie 1 | Animation showing the h_e dynamics for variations in the isoflurane concentration, for details see Figures 2, 3. Note that the parts prior and after the emergent burst suppression have been sped up by increasing the time step between the movie frames.

Movie 2 | Animation showing h_e (top panel) and Γ_{ee} (bottom panel), respectively, at 0.25 mM isoflurane with an increased $f_i = 1.25$ inside a circular patch—preventing burst suppression there—while the regular f_i=0.175 is kept elsewhere. For further detail see **Figure 4** and the text. Note that the induction phase is not shown.

Movie 3 | Animation showing the h_e dynamics at 0.25 mM isoflurane with regular $\lambda_{ek} = \lambda_1 = 2.7$ cm, for detail see Figure 6. Note that the induction phase is not shown.

Movie 4 | Like Movie 3 but with $\lambda_{ek} = \lambda_2 = 2.4$ cm.

Movie 5 | Like Movie 3 but with $\lambda_{ek} = \lambda_3 = 2.1$ cm.

REFERENCES

Adrian, E. D., and Matthews, B. H. C. (1934). The Berger rhythm, potential changes from the occipital lobe in man. *Brain* 57, 355–385. doi: 10.1093/brain/57.4.355

Akrawi, W. P., Drummond, J. C., Kalkman, C. J., and Patel, P. M. (1996). A comparison of the electrophysiologic characteristics of EEG burst-suppression as produced by isoflurane, thiopental, etomidate, and propofol. *J. Neurosurg. Anesthesiol.* 8, 40–46. doi: 10.1097/00008506-199601000-00010

An, D. S., Straumann, D., and Wieser, H. G. (1996). One-way asynchrony' of burst-suppression activity. *Neurophysiol. Clin.* 26, 329–334. doi: 10.1016/S0987-7053(97)85100-3

Bäckström, T., Haage, D., Löfgren, M., Johansson, I., Strömberg, J., Nyberg, S., et al. (2011). Paradoxical effects of GABA-A modulators may explain sex steroid induced negative mood symptoms in some persons. *Neuroscience* 191, 46–54. doi: 10.1016/j.neuroscience.2011.03.061

Bauer, G., Trinka, E., and Kaplan, P. W. (2013). EEG patterns in hypoxic encephalopathies (post-cardiac arrest syndrome): fluctuations, transitions, and reactions. *J. Clin. Neurophysiol.* 30, 477–489. doi: 10.1097/WNP.0b013e3182a73e47

Berger, H. (1929). Über das Elektrenkephalogramm des Menschen. *Arch. Psychiatr. Nervenkr.* 87, 527–570. doi: 10.1007/BF01797193

Berger, H. (1930). Über das Elektrenkephalogramm des Menschen. Zweite Mitteilung. *J. Psychol. Neurol.* 40, 160–179.

Berg-Johnsen, J., and Langmoen, I. A. (1986). The effect of isoflurane on unmyelinated and myelinated fibres in the rat brain. *Acta Physiol. Scand.* 127, 87–93. doi: 10.1111/j.1748-1716.1986.tb07879.x

Bojak, I., and Breakspear, M. (2013). "Neuroimaging, neural population models for" in *Encyclopedia of Computational Neuroscience*, eds D. Jaeger and R. Jung (New York, NY: Springer), 348135.

Bojak, I., and Liley, D. T. J. (2005). Modeling the effects of anesthesia on the electroencephalogram. *Phys. Rev. E Stat. Nonlin. Soft. Matter. Phys.* 71:041902. doi: 10.1103/PhysRevE.71.041902

Bojak, I., and Liley, D. T. J. (2010). Axonal velocity distributions in neural field equations. *PLoS Comput. Biol.* 6:e1000653. doi: 10.1371/journal.pcbi.1000653

Bojak, I., Liley, D. T. J., Cadusch, P. J., and Cheng, K. (2004). Electrorhythmogenesis and anaesthesia in a physiological mean field theory. *Neurocomputing* 58-60, 1197–1202. doi: 10.1016/j.neucom.2004.01.185

Bojak, I., Oostendorp, T. F., Reid, A. T., and Kötter, R. (2010). Connecting mean field models of neural activity to EEG and fMRI data. *Brain Topogr.* 23, 139–149. doi: 10.1007/s10548-010-0140-3

Bojak, I., Oostendorp, T. F., Reid, A. T., and Kötter, R. (2011). Towards a model-based integration of co-registered electroencephalography/functional magnetic resonance imaging data with realistic neural population meshes. *Philos. Trans. A Math. Phys. Eng. Sci.* 369, 3785–3801. doi: 10.1098/rsta.2011.0080

Bojak, I., Day, H. C., and Liley, D. T. J. (2013). Ketamine, propofol, and the EEG: a neural field analysis of HCN1-mediated interactions. *Front. Comput. Neurosci.* 7:22. doi: 10.3389/fncom.2013.00022

Brenner, R. P. (1985). The electroencephalogram in altered states of consciousness. *Neurol. Clin.* 3, 615–631.

Bressloff, P. C. (2012). Spatiotemporal dynamics of continuum neural fields. *J. Phys. A Math. Theor.* 45:0331001. doi: 10.1088/1751-8113/45/3/033001

Ching, S., Cimenser, A., Purdon, P. L., Brown, E. N., and Kopell, N. J. (2010). Thalamocortical model for a propofol-induced alpha-rhythm associated with loss of consciousness. *Proc. Natl. Acad. Sci. U.S.A.* 107, 22665–22670. doi: 10.1073/pnas.1017069108

Ching, S., Purdon, P. L., Vijayan, S., Kopell, N. J., and Brown, E. N. (2012). A neurophysiological-metabolic model for burst suppression. *Proc. Natl. Acad. Sci. U.S.A.* 109, 3095–3100. doi: 10.1073/pnas.1121461109

Coombes, S. (2010). Large-scale neural dynamics: simple and complex. *Neuroimage* 52, 731–739. doi: 10.1016/j.neuroimage.2010.01.045

Deco, G., Jirsa, V., Robinson, P., Breakspear, M., and Friston, K. (2008). The dynamic brain: from spiking neurons to neural masses and cortical fields. *PLoS Comput. Biol.* 4:e1000092. doi: 10.1371/journal.pcbi.1000092

Deco, G., Jirsa, V. K., and McIntosh, A. R. (2011). Emerging concepts for the dynamical organization of resting-state activity in the brain. *Nat. Rev. Neurosci.* 12, 43–56. doi: 10.1038/nrn2961

Desikan, R. S., Segonne, F., Fischl, B., Quinn, B. T., Dickerson, B. C., Blacker, D., et al. (2006). An automated labeling system for subdividing the human cerebral cortex on MRI scans into gyral based regions of interest. *Neuroimage* 31, 968–980. doi: 10.1016/j.neuroimage.2006.01.021

Detsch, O., Kochs, E., Siemers, M., Bromm, B., and Vahle-Hinz, C. (2002). Increased responsiveness of cortical neurons in contrast to thalamic neurons during isoflurane-induced EEG bursts in rats. *Neurosci. Lett.* 317, 9–12. doi: 10.1016/S0304-3940(01)02419-3

Doyle, P. W., and Matta, B. F. (1999). Burst suppression or isoelectric encephalogram for cerebral protection: evidence from metabolic suppression studies. *Br. J. Anaesth.* 83, 580–584. doi: 10.1093/bja/83.4.580

Eickhoff, S. B., Stephan, K. E., Mohlberg, H., Grefkes, C., Fink, G. R., Amunts, K., et al. (2005). A new SPM toolbox for combining probabilistic cytoarchitectonic maps and functional imaging data. *Neuroimage* 25, 1325–1335. doi: 10.1016/j.neuroimage.2004.12.034

Ferron, J. F., Kroeger, D., Chever, O., and Amzica, F. (2009). Cortical inhibition during burst suppression induced with isoflurane anesthesia. *J. Neurosci.* 29, 9850–9860. doi: 10.1523/JNEUROSCI.5176-08.2009

Foster, B. L., Bojak, I., and Liley, D. T. J. (2008). Population based models of cortical drug response: insights from anaesthesia. *Cogn. Neurodyn.* 2, 283–296. doi: 10.1007/s11571-008-9063-z

Franks, N. P., and Lieb, W. R. (1996). Temperature dependence of the potency of volatile general anesthetics: implications for *in vitro* experiments. *Anesthesiology* 84, 716–720. doi: 10.1097/00000542-199603000-00027

Frascoli, F., van Veen, L., Bojak, I., and Liley, D. (2011). Metabifurcation analysis of a mean field model of the cortex. *Physica D.* 240, 949–962. doi: 10.1016/j.physd.2011.02.002

Freeman, W. (1975). *Mass Action in the Nervous System: Examination of the Neurophysiological Basis of Adaptive Behavior Through the EEG, 1st Edn.* New York, NY: Academic Press. Available online at: http://sulcus.berkeley.edu/MANSWWW/MANSWWW.html.

Friedman, Y., King, B. S., and Rampil, I. J. (1996). Nitrous oxide depresses spinal F waves in rats. *Anesthesiology* 85, 135–141. doi: 10.1097/00000542-199607000-00019

Frigo, M., and Johnson, S. G. (2005). The design and implementation of FFTW3. *Proc. IEEE* 93, 216–231. doi: 10.1109/JPROC.2004.840301

Green, K. R., and van Veen, L. (2014). Open-source tools for dynamical analysis of Liley's mean-field cortex model. *J. Comput. Sci.* 5, 507–516. doi: 10.1016/j.jocs.2013.06.001

Grigg-Damberger, M., Coker, S., Halsey, C., and Anderson, C. (1989). Neonatal burst suppression: its developmental significance. *Pediatr. Neurol.* 5, 84–92. doi: 10.1016/0887-8994(89)90032-5

Hartikainen, K. M., Rorarius, M., Perakyla, J. J., Laippala, P. J., and Jantti, V. (1995). Cortical reactivity during isoflurane burst-suppression anesthesia. *Anesth. Analg.* 81, 1223–1228.

Henry, C., and Scoville, W. (1952). Suppression-burst activity from isolated cerebral cortex in man. *Electroencephalogr. Clin. Neurophysiol.* 4, 1–22. doi: 10.1016/0013-4694(52)90027-8

Hoffman, W. E., and Edelman, G. (1995). Comparison of isoflurane and desflurane anesthetic depth using burst suppression of the electroencephalogram in neurosurgical patients. *Anesth. Analg.* 81, 811–816.

Hudetz, A. G., and Imas, O. A. (2007). Burst activation of the cerebral cortex by flash stimuli during isoflurane anesthesia in rats. *Anesthesiology* 107, 983–991. doi: 10.1097/01.anes.0000291471.80659.55

Huotari, A. M., Koskinen, M., Suominen, K., Alahuhta, S., Remes, R., Hartikainen, K. M., et al. (2004). Evoked EEG patterns during burst suppression with propofol. *Br. J. Anaesth.* 92, 18–24. doi: 10.1093/bja/aeh022

Im, K., Lee, J. M., Lyttelton, O., Kim, S. H., Evans, A. C., and Kim, S. I. (2008). Brain size and cortical structure in the adult human brain. *Cereb. Cortex* 18, 2181–2191. doi: 10.1093/cercor/bhm244

Jantti, V., Sonkajarvi, E., Mustola, S., Rytky, S., Kiiski, P., and Suominen, K. (1998). Single-sweep cortical somatosensory evoked potentials: N20 and evoked bursts in sevoflurane anaesthesia. *Electroencephalogr. Clin. Neurophysiol.* 108, 320–324. doi: 10.1016/S0168-5597(98)00005-7

Jirsa, V. K., and Haken, H. (1996). Field theory of electromagnetic brain activity. *Phys. Rev. Lett.* 77, 960–963. doi: 10.1103/PhysRevLett.77.960

Kalviainen, R., Eriksson, K., and Parviainen, I. (2005). Refractory generalised convulsive status epilepticus : a guide to treatment. *CNS Drugs* 19, 759–768. doi: 10.2165/00023210-200519090-00003

Kellaway, P., Gol, A., and Proler, M. (1966). Electrical activity of the isolated cerebral hemisphere and isolated thalamus. *Exp. Neurol.* 14, 281–304. doi: 10.1016/0014-4886(66)90115-4

Kroeger, D., and Amzica, F. (2007). Hypersensitivity of the anesthesia-induced comatose brain. *J. Neurosci.* 27, 10597–10607. doi: 10.1523/JNEUROSCI.3440-07.2007

Kuizenga, K., Kalkman, C. J., and Hennis, P. J. (1998). Quantitative electroencephalographic analysis of the biphasic concentration-effect relationship of propofol in surgical patients during extradural analgesia. *Br. J. Anaesth.* 80, 725–732. doi: 10.1093/bja/80.6.725

Kuizenga, K., Wierda, J. M. K. H., and Kalkman, C. J. (2001). Biphasic EEG changes in relation to loss of consciousness during induction with thiopental, propofol, etomidate, midazolam or sevoflurane. *Br. J. Anaesth.* 86, 354–360. doi: 10.1093/bja/86.3.354

Lamblin, M. D., Walls Esquivel, E., and Andre, M. (2013). The electroencephalogram of the full-term newborn: review of normal features and hypoxic-ischemic encephalopathy patterns. *Neurophysiol. Clin.* 43, 267–287. doi: 10.1016/j.neucli.2013.07.001

Land, R., Engler, G., Kral, A., and Engel, A. K. (2012). Auditory evoked bursts in mouse visual cortex during isoflurane anesthesia. *PLoS ONE* 7:e49855. doi: 10.1371/journal.pone.0049855

Lewis, L. D., Ching, S., Weiner, V. S., Peterfreund, R. A., Eskandar, E. N., Cash, S. S., et al. (2013). Local cortical dynamics of burst suppression in the anaesthetized brain. *Brain* 136(Pt 9), 2727–2737. doi: 10.1093/brain/awt174

Liley, D. T. J., and Bojak, I. (2005). Understanding the transition to seizure by modeling the epileptiform activity of general anesthetic agents. *J. Clin. Neurophysiol.* 22, 300–313.

Liley, D. T., and Walsh, M. (2013). The mesoscopic modeling of burst suppression during anesthesia. *Front. Comput. Neurosci.* 7:46. doi: 10.3389/fncom.2013.00046

Liley, D., Cadusch, P., and Dafilis, M. (2002). A spatially continuous mean field theory of electrocortical activity. *Netw. Comput. Neural Syst.* 13, 67–113. doi: 10.1080/net.13.1.67.113

Liley, D., Foster, B., and Bojak, I. (2011). "A mesoscopic modelling approach to characterising anaesthetic action on brain electrical activity," in *Sleep and Anesthesia: Neural Correlates in Theory and Experiment, Springer Series in Computational Neuroscience*, ed A. Hutt (New York, NY: Springer), 139–166.

Liley, D. T. J., Foster, B. L., and Bojak, I. (2012). "Co-operative populations of neurons: mean field models of mesoscopic brain activity," in *Computational Systems Neurobiology*, ed N. L. Novère (Berlin: Springer), 317–364.

Liley, D. T. J. (2013). "Neural population model," in *Encyclopedia of Computational Neuroscience*, eds D. Jaeger and R. Jung (New York, NY: Springer), 348134.

Loomis, C. W., Brunet, D., Milne, B., Cervenko, F. W., and Johnson, G. D. (1986). Arterial isoflurane concentration and EEG burst suppression during cardiopulmonary bypass. *Clin. Pharmacol. Ther.* 40, 304–313. doi: 10.1038/clpt.1986.181

Lopes da Silva, F., Hoeks, A., Smits, H., and Zetterberg, L. (1974). Model of brain rhythmic activity: the alpha-rhythm of the thalamus. *Kybernetik* 15, 27–37. doi: 10.1007/BF00270757

Lukatch, H. S., and MacIver, M. B. (1996). Synaptic mechanisms of thiopental-induced alterations in synchronized cortical activity. *Anesthesiology* 84, 1425–1434. doi: 10.1097/00000542-199606000-00019

Mapleson, W. W. (1996). Effect of age on MAC in humans: a meta-analysis. *Br. J. Anaesth.* 76, 179–185. doi: 10.1093/bja/76.2.179

Meijer, H., Dercole, F., and Oldeman, B. (2013). "Numerical bifurcation analysis," in *Encyclopedia of Complexity and Systems Science*, ed R. A. Meyers (Berlin; Heidelberg: Springer-Verlag), 60545.

Mikulec, A. A., Pittson, S., Amagasu, S. M., Monroe, F. A., and MacIver, M. B. (1998). Halothane depresses action potential conduction in hippocampal axons. *Brain Res.* 796, 231–238. doi: 10.1016/S0006-8993(98)00348-5

Niedermeyer, E. (2009). The burst-suppression electroencephalogram. *Am. J. Electroneurodiagnostic. Technol.* 49, 333–341. doi: 10.1080/1086508X.2009.11079736

Nowicki, M., Baum, P., Kosacka, J., Stockinger, M., Kloting, N., Bluher, M., et al. (2013). Effects of isoflurane anesthesia on F-waves in the sciatic nerve of the adult rat. *Muscle Nerve* 50, 257–261. doi: 10.1002/mus.24150

Nunez, P. (1974). The brain wave equation: a model for the EEG. *Math. Biosci.* 21, 279–297. doi: 10.1016/0025-5564(74)90020-0

Oh, S. S., Hayes, J. M., Sims-Robinson, C., Sullivan, K. A., and Feldman, E. L. (2010). The effects of anesthesia on measures of nerve conduction velocity in male C57Bl6/J mice. *Neurosci. Lett.* 483, 127–131. doi: 10.1016/j.neulet.2010.07.076

Pilge, S., Jordan, D., Kreuzer, M., Kochs, E. F., and Schneider, G. (2014). Burst suppression-MAC and burst suppression-CP_{50} as measures of cerebral effects of anaesthetics. *Br. J. Anaesth.* 112, 1067–1074. doi: 10.1093/bja/aeu016

Rampil, I. J., and King, B. S. (1996). Volatile anesthetics depress spinal motor neurons. *Anesthesiology* 85, 129–134. doi: 10.1097/00000542-199607000-00018

Rinzel, J. (1985). "Bursting oscillations in an excitable membrane model," in *Ordinary and Partial Differential Equations: Proceedings of the 8th Dundee Conference Number 1151 in Lecture Notes in Mathematics*, eds B. Sleeman and R. Jarvis (Berlin: Springer), 304–316.

Robinson, P. A., Rennie, C. J., and Wright, J. J. (1997). Propagation and stability of waves of electrical activity in the cerebral cortex. *Phys. Rev. E* 56, 826–840. doi: 10.1103/PhysRevE.56.826

Robinson, P. A., Rennie, C. J., Rowe, D. L., and O'Connor, S. C. (2004). Estimation of multiscale neurophysiologic parameters by electroencephalographic means. *Hum. Brain Mapp.* 23, 53–72. doi: 10.1002/hbm.20032

Rosner, B. S., Clark, D. L., and Beck, C. (1971). Inhalational anesthetics and conduction velocity of human peripheral nerve. *Electroencephalogr. Clin. Neurophysiol.* 31, 109–114. doi: 10.1016/0013-4694(71)90179-9

Sanz Leon, P., Knock, S. A., Woodman, M. M., Domide, L., Mersmann, J., McIntosh, A. R., et al. (2013). The virtual brain: a simulator of primate brain network dynamics. *Front. Neuroinform.* 7:10. doi: 10.3389/fninf.2013.00010

Schomer, D., and Lopes da Silva, F. (eds.). (2010). *Niedermeyer's Electroencephalography: Basic Principles, Clinical Applications, and Related Fields*. Philadelphia, PA: Lippincott.

Schwartz, A., Tuttle, R., and Poppers, P. (1989). Electroencephalographic burst suppression in elderly and young patients anesthetized with isoflurane. *Anesth. Analg.* 68, 9–12. doi: 10.1213/00000539-198901000-00003

Sitdikova, G., Zakharov, A., Janackova, S., Gerasimova, E., Lebedeva, J., Inacio, A. R., et al. (2014). Isoflurane suppresses early cortical activity. *Ann. Clin. Trans. Neurol.* 1, 15–26. doi: 10.1002/acn3.16

Stecker, M. M., Cheung, A. T., Pochettino, A., Kent, G. P., Patterson, T., Weiss, S. J., et al. (2001). Deep hypothermic circulatory arrest: I. Effects of cooling on electroencephalogram and evoked potentials. *Ann. Thorac. Surg.* 71, 14–21. doi: 10.1016/S0003-4975(00)01592-7

Steriade, M., Amzica, F., and Contreras, D. (1994). Cortical and thalamic cellular correlates of electroencephalographic burst-suppression. *Electroencephalogr. Clin. Neurophysiol.* 90, 1–16. doi: 10.1016/0013-4694(94)90108-2

Steyn-Ross, M. L., Steyn-Ross, D. A., Sleigh, J. W., and Liley, D. T. J. (1999). Theoretical electroencephalogram stationary spectrum for a white-noise-driven cortex: evidence for a general anesthetic-induced phase transition. *Phys. Rev. E* 60, 7299–7311. doi: 10.1103/PhysRevE.60.7299

Treiman, D., Walton, N., and Kendrick, C. (1990). A progressive sequence of electroencephalographic changes during generalized convulsive status epilepticus. *Epilepsy Res.* 5, 49–60. doi: 10.1016/0920-1211(90)90065-4

Tsodyks, M. V., and Markram, H. (1997). The neural code between neocortical pyramidal neurons depends on neurotransmitter release probability. *Proc. Natl. Acad. Sci. U.S.A.* 94, 719–723. doi: 10.1073/pnas.94.2.719

Wilson, H., and Cowan, J. (1973). A mathematical theory of the functional dynamics of cortical and thalamic nervous tissue. *Kybernetik* 13, 55–80. doi: 10.1007/BF00288786

Yli-Hankala, A., Jantti, V., Pyykko, I., and Lindgren, L. (1993). Vibration stimulus induced EEG bursts in isoflurane anaesthesia.

Electroencephalogr. Clin. Neurophysiol. 87, 215–220. doi: 10.1016/0013-4694(93)90021-M

Young, G. B. (2000). The EEG in coma. *J. Clin. Neurophysiol.* 17, 473–485. doi: 10.1097/00004691-200009000-00006

Conflict of Interest Statement: The authors declare that the research was conducted in the absence of any commercial or financial relationships that could be construed as a potential conflict of interest.

Received: 15 October 2014; accepted: 02 February 2015; published online: 26 February 2015.

Citation: Bojak I, Stoyanov ZV and Liley DTJ (2015) Emergence of spatially heterogeneous burst suppression in a neural field model of electrocortical activity. Front. Syst. Neurosci. ***9****:18. doi: 10.3389/fnsys.2015.00018*

This article was submitted to the journal Frontiers in Systems Neuroscience.